Politecnico di Milano
School of Industrial and Information Engineering
Master of Science in Energy Engineering
Power Production

POLITECNICO
MILANO 1863

Techno-Economic Analysis of Molten Carbonate Fuel Cell Plants for Carbon Capture in Steam Methane Reformers

Advisor:
Prof. Matteo Carmelo ROMANO

Candidates:
Davide Elia LATTUADA ID 918261
Davide MASUELLI ID 905757

Academic Year 2019-2020
Energy Department of Politecnico di Milano
Milano Italy

Ringraziamenti

Desidero ringraziare prima di tutti il professor Romano per la possibilità di sviluppare la tesi e approfondire un argomento su cui nutro profondo interesse. Indispensabili sono stati i suoi consigli, il suo supporto tecnico e la costante disponibilità. Riuscire in questi quattro mesi a sostenere l'ultimo esame, imparare ad utilizzare Aspen Plus e redigere una tesi non sarebbe stato possibile senza il suo sostegno.

Il secondo doveroso ringraziamento è per Davide, amico, collega di studi e di tesi. Ho provato, come lui, tutta la frustrazione di dover cambiare relatore e tesi a giugno causa covid-19. Arrivati a questo punto possiamo dire che ce l'abbiamo fatta.

Il più profondo e sentito ringraziamento va a Deborah, con la quale condivido da sette anni i successi, le delusioni, le nuove sfide ed avventure della vita. Grazie perché ci sei sempre stata, hai reso piccole le difficoltà e grandi i successi. Senza di te niente di tutto ciò sarebbe possibile.

Un particolare ringraziamento va agli amici e compagni di università con i quali ho condiviso momenti indelebili dentro e fuori dalle mura dell'ateneo. Grazie a Beno, Seba, Bea, Ale, Suliman, Alessandro e tanti altri.

Non posso non ringraziare il PoliMi che mi ha fatto crescere non solo come ingegnere ma soprattutto come persona. Il mio percorso non è stato lineare. Cambiare corso di ingegneria al terzo anno di triennale, consapevole del fatto di dover sostenere ulteriori esami che il vecchio indirizzo non prevedeva, ha reso tutto più lungo. Ora, guardando al passato, ritengo quella scelta la più felice della mia vita. Grazie soprattutto per permettermi di osservare la realtà da un altro punto di vista. Ritengo quest'ultima caratteristica la chiave di ogni successo: cambiare prospettiva da cui si osserva la vita. È come se posti fisicamente davanti ad un punto di domanda, lo iniziassimo ad osservare lateralmente al posto che frontalmente. Ci accorgeremmo che invece di quello che è sempre stato in apparenza, esso si trasformerà in un punto esclamativo, ribaltandone completamente il significato. È questo l'insegnamento più grande che ho fatto mio. Essere fedeli a sé stessi ed alle proprie idee senza però permettere che esse ci rendano ciechi, consci del fatto che la realtà, in fondo, è un po' come un panorama: interpretabile in relazione all'angolazione dalla quale lo si guardi ma comunque bellissimo.

Infine, ringrazio la mia famiglia, gli amici e tutti coloro che mi hanno supportato in questi anni.

Davide Elia Lattuada

Ringraziamenti

6/11/2020

Eccomi giunto alla conclusione di questo percorso. Questi anni passati sono stati piuttosto impegnativi e faticosi ma anche pieni di numerosi momenti belli e di soddisfazioni. Non è stato facile ma alla fine passo dopo passo, esame dopo esame sono riuscito ad arrivare in "vetta". Grazie al percorso fatto ho avuto l'opportunità di conoscere maggiormente me stesso, di cimentarmi in nuove sfide, di crescere come ingegnere e come persona.

Ringrazio il Politecnico di Milano per tutto quello che mi ha trasmesso ed insegnato e tutte le fantastiche persone incontrate sempre pronte ad aiutare gli altri e con cui ho condiviso una parte di questo percorso.

Ringrazio molto Matteo Romano per avermi dato la possibilità di fare questa tesi, di imparare l'utilizzo di un software nuovo, per avere supportato sempre il nostro lavoro e seguito con costanza.

Ringrazio Davide Lattuada, amico e collega di tesi per tutte le giornate di studio passate soprattutto durante la quarantena e compagno di "sventure" poiché abbiamo dovuto cambiare tesi a causa della pandemia; nonostante lo sconforto iniziale però non ci siamo persi d'animo e con impegno siamo riusciti a scrivere questa tesi in quattro mesi di lavoro.

Ringrazio la mia famiglia per avermi sempre supportato, aiutato nei momenti difficili e per avermi dato tutto il necessario per concludere il mio percorso.

Ringrazio Marco Benini, amico con cui ho preparato molti esami della magistrale e della triennale e per aver allietato le pause caffè rendendo divertenti anche le lunghe giornate di studio.

Infine, volevo ringraziare tutte quelle persone che ho conosciuto anche solo di passaggio e che sarebbe troppo lungo elencare ma non per questo meno importanti.

Masuelli Davide

.

Sommario

In futuro l'idrogeno avrà un ruolo più importante e la sua produzione sarà realizzata in parte attraverso fonti rinnovabili, in parte attraverso tecnologie convenzionali con l'uso della CCS. Lo scopo è quello di studiare un sistema di retrofit per effettuare la cattura di CO_2 dai gas esausti del SMR; inoltre, viene potenziata la produzione di H_2 blu e di energia elettrica. Viene proposto un sistema di cattura che utilizza MCFC per la separazione della CO_2 e una sezione criogenica per la cattura. Sono in esame tre diversi layout di impianto: il primo alimenta la cella con gas naturale, mentre il secondo usa gli offgas del SMR come combustibile e l'ultimo, alimentato con gas naturale, permette un ricircolo di combustibile al lato anodo. Tutti gli impianti sono stati modellizzati per mezzo del software Aspen Plus®. I principali indici di prestazione sono calcolati per le tre configurazioni e viene eseguita un'analisi di sensibilità tecnico-economica sul funzionamento della cella, al fine di valutare la migliore configurazione on-design. Solo per il caso che garantisce una maggiore flessibilità, viene effettuata una valutazione tecnico-economica fuori progetto per studiare come il sistema di retrofit possa essere usato al fine di produrre H_2 per la vendita. La MCFC è più conveniente rispetto alla cattura MEA poiché consente un notevole aumento sia della produzione di energia elettrica che di idrogeno. Per quanto riguarda la cattura di CO_2, si verifica un leggero aumento di richiesta di gas naturale. Dal punto di vista tecnico ogni impianto considerato presenta vantaggi e svantaggi. Il migliore dipende dallo scopo principale per il quale è progettato e da parametri esterni come le condizioni di mercato. Oggi, dato il costo della MCFC e il valore della carbon tax, questo retrofit non è conveniente per nessuna delle configurazioni proposte. In futuro potrebbe essere redditizio con una politica energetica che promuove tecnologie a basse emissioni di carbonio.

Parole chiave: Reforming del metano, Idrogeno, Retrofit, Cattura della CO_2, Cella combustibile a carbonati fusi, Analisi tecnico-economica

Abstract

In future hydrogen will play a more important role and its production will be made partly through renewable sources, partly through conventional thermochemical technologies with the use of CCS. The purpose is to study a retrofit system in order to perform CO_2 capture from SMR flue gas that is one of the main causes of emissions in oil industry; in addition, the production of blue hydrogen and power is enhanced. A capture system that use MCFC for carbon dioxide separation and a cryogenic section for the capture is proposed. Three different plant layout are under examination: the first assume to feed the cell with natural gas, while the second has offgas of FTR as fuel in anode side and the last, feeding it with natural gas, has fuel recirculation at anode side. All the plants are modelled using the software Aspen Plus®. Main performance indexes are calculated for the three configuration and a techno-economic sensitivity analysis on cell operating condition is performed to assess the best on-design configuration. At the end, only for the case that guarantee more flexibility a technoeconomic off-design evaluation of retrofit section is made to simulate its flexible operation in the production of variable quantities of H_2 for market purpose. The MCFC technology is more convenient compared to MEA capture, allowing a considerable increase both in the electric and hydrogen production. Concerning CO_2 capture, only a slightly increase of natural gas input takes place. From the technical point of view every plant considered have advantages and disadvantages. The best one depends on the main project purpose and on external parameters such as market conditions. Today, given the cost of the MCFC and the value of the carbon tax, this retrofit is not convenient for any of the proposed configurations. In the future it could be a valid alternative if an energy policy promotes low carbon technologies.

Keywords: Steam Methane Reforming, Hydrogen, Retrofit, CO_2 Capture, Molten Carbonate Fuel Cell, Techno-Economic Analysis

Extended abstract

Keywords	Scope of work
Hydrogen SMR Retrofit CO_2 Capture MCFC Techno Economic Analysis	The purposes of this work are the followings: • To study the application of MCFC for CO_2 capture from gas of reformer, using MCFC as an additional reforming system to increase H_2 production of the plant • To study the operation of the system with different fuels (natural gas and PSA off-gas of SMR) and the variation of the most significant process parameters (eg: ΔV and FU) • To study the operation in off-design condition at different FU, to simulate its flexible operation in the production of variable quantities of H_2. The scope is to analyse how this system can be used in order to produce blue hydrogen for sale purpose in variable quantities depending on the demand that may have seasonal fluctuations.

1. Introduction

Nowadays special emphasis is focused on the problem of environmental impact and the greenhouse effect. Industrial sector is responsible for 24% of the world's GHG emissions. In particular, the refinery sector generates 7% of total emissions worldwide (2017) [8].

In Europe most of the oil refining plants are of average size of about 250 000 bbl/d [6] and it necessary to have a conspicuous production of H_2 for some treatments and therefore the plant is supported by an steam methane reforming (SMR). SMR is a thermochemical process using energy of natural gas to release hydrogen from its molecular structure. It is considered the reference process because it has the lowest costs and the highest reliability [10]. The hydrogen production process is one of the main causes of CO_2 emissions in a refinery.

The refining industry has started an evolution [4] in order to mitigate its climate impact but at the same time this industry must continue to satisfy needs of consumers. Several solutions are considered, which include CCS (Carbon Capture and Storage) and CCU (Carbon Capture and Use) applied to refinery flue gas. They are valid methods in order to mitigate carbon footprint of sector.

Regarding CO_2 capture, MCFC has a rather unique feature among the conventional technologies with chemical solvent. Fuel cell allows, in addition to capture, to generate electricity and blue hydrogen (which requires a moderate fuel utilization factor); they represent useful products in a refinery. The use of MCFCs for CCS applications in the energy sector (*Chiesa et al.* 2010 [16]), in the cement sector (*Romano et al.* 2014 [2]) and in the steel sector (*Mastropasqua et al.* 2019 [14]) has already been discussed in previous work carried out by the *GECoS* research group [17]. There are not any detailed studies on CCS from SMR fluegas with this system.

2. Plant configuration

Three different capture section configurations have been studied (figure 1).

- Case A: fuel cell is fed with natural gas. The capture section produces electric power and hydrogen.
- Case B: fuel cell is fed with PSA-offgas of FTR. The capture section produces W_{el}, H_2 and LP steam.
- Case C: fuel cell is fed with natural gas and anodic recirculation. Capture section produces electric power and LP steam but without hydrogen production.

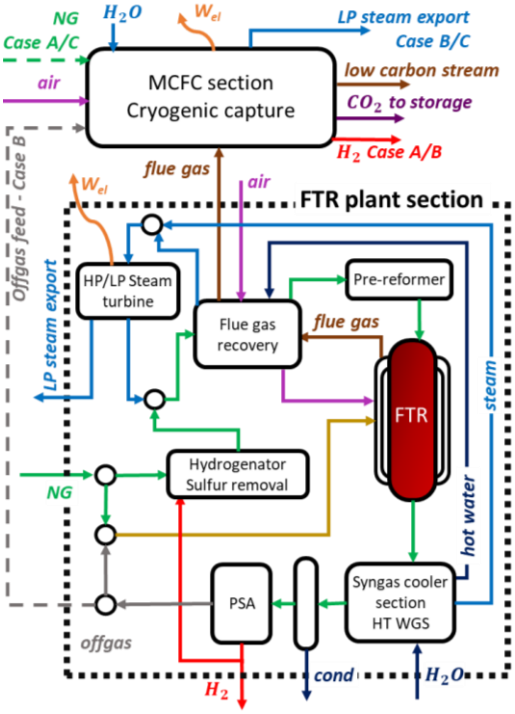

Fig. 1 Block diagram of SMR + capture section

All the systems have been modelled in *Aspen Plus* with a Peng-Robinson as equation state and all chemical reactor are imposed to equilibrium.

2.1 SMR configuration

As regards SMR, the reference it is FTR Base Case in *Demoys* assessment [12]. The fired tubular reforming proposed reproduces a conventional plant based on the production of 30 000 Nm^3/h of H_2.

Natural gas is introduced into the plant at 70 bar. A part of it is splitted to feed, together with PSA offgas, the

combustor of reforming in order to have the necessary heat to support the endothermic reaction.

The desulphurised charge before entering the main reforming reactor is mixed with steam from the HP steam turbine to obtain correct steam to carbon ratio of 3.4. Then it is pre-reformed by an adiabatic pre-reforming at 490 °C. The syngas exits FTR at 890 °C (table 1) and it is introduced into a syngas cooler section to cool it by producing steam/hot water and reach the correct temperature (330 °C) for the water gas shift reaction. The H_2-rich flow is then cooled and, after removing the condensed water, it is sent to a PSA for H_2 separation under pressure of 29.5 bar. The offgas from bed regeneration (at 1.3 bar) is sent into the burner.

The water required for the steam to carbon ratio and to run two steam turbines is taken from a refinery boiler at 150.8 °C and 6 bar. This flow is economized and evaporated in the syngas cooler section using the heat of syngas and superheated in flue gas recovery using heat of exhaust gas. Finally, all the steam produced is sent directly to the turbine group that generate 1.74 $MW_{el,net}$. The steam coming out from low-pressure turbine is sent in export for refinery use. The air required for combustion is taken at ambient conditions (15 °C, 1 bar), pressurised through a fan and heated (425 °C) through regenerative heat exchangers exploiting the heat of exhaust gas. The exhaust flue gases are sent to the retrofit capture plant.

Tab. 1 Main operative assumptions and parameters of FTR

Parameter	Unit	Value
Adiabatic pre reformer		
Inlet temperature	°C	490
S/C ratio	-	3.4
Fired Tubular Reformer		
Inlet/Outlet temperature	°C/°C	620/890
Outlet pressure	bar	32.7
Combustor		
Exhaust gas outlet temperature	°C	1010
Air inlet temperature	°C	425
High temperature WGS		
Inlet temperature	°C	330
PSA		
H_2 sep. efficiency	%	89

2.2 MCFC capture section configuration

In figure 2 the scheme of plant for base case A is presented; in the next paragraph the differences in cases B and C are explained. The main assumptions for all cases are reported in table 2. The process exhaust gases (# 25) are used directly as a supply to the cathode of the cell, where CO_2 permeates through the electrolyte to the anode, concentrating the carbon dioxide to the anodic exhaust gas (# A-16). Before entering in the fuel cell, flue gas of FTR are mixed with ambient air to provide sufficient O_2 for cathodic reactions and to control the cell temperature. This mixture then enters a Ljungstrom heat exchanger where it heats up, cooling hot cathodic residue (# A-8B), until cold stream reaches a temperature of 530 °C; in this way it is possible to use less fuel at the burner and to reduce the second principle losses at the stack due to outlet exhaust gases. The oxidant mixture enters a catalytic burner fed by flow coming out to the cryogenic section (# A-41) and by the PSA offgas (# A-31). This mixture is preheated in the exchanger *A-H7* to 300 °C cooling the hot anodic residue. Combustor, in addition to providing necessary heat for the correct cathode inlet temperature (set at 575 °C), oxidises CO present in the offgas flow, increasing CO_2 concentration at the inlet. The external pre-reformer (which requires an input temperature of 450 °C, table 2) converts all hydrocarbons above methane and part of it. As the endothermic reaction, this component lowers the exit temperature (# A-14), thus requiring an additional heat exchanger to reach an inlet temperature of 450 °C at the anode side (# A-15A). The discharge flow from anode (# A-16) at 645 °C is cooled by preheating the charge, producing the steam necessary to obtain the correct steam to carbon ratio: the quantity of water needs by process (# A-34A) enters in ambient conditions. It is first pumped up to 2 bar by means of a centrifugal pump to overcome the pressure drops and allow optimum heat recovery thanks to a higher evaporation temperature. The water is first preheated to 107 °C in an economiser that uses the heat from the hot cathodic residue. This sub-cooling ΔT (15 °C) is chosen to have enough flexibility in off-design condition. In case B the anodic residue is used to economise water but in the basic case proposed here, this solution cannot be pursued in order to respect the minimum ΔT in the subsequent exchangers; moreover, decreasing the temperature of the stream A-9B allows lower second principle losses to the stack.

Tab. 2 Main operative assumptions and parameters MCFC

Parameter	Unit	Value
Reactor		
HT-WGS inlet T	°C	330
Pre-ref./ Internal ref. inlet T	°C / °C	450 / 450
Adiabatic pre-ref. S/C ratio	-	2.1
Molten carbonate fuel cell		
Anode / Cathode inlet T	°C / °C	600 / 575
Outlet T	°C	645
Anode / Cathode inlet P	bar / bar	1.07/1.12
Max ΔT across cell	°C	70
Min xO2, out / xCO2, out cathode	% / %	2.5 / 1.0
Min ΔV	mV	600
DC/AC efficiency	%	94

The water evaporation process is divided between two evaporators that recover the available heat in the anodic exhausts. The saturated steam produced at T_{sat} = 122 °C (streams A-36 and A-38 mixed in the mixer *A-MIX4*) is mixed with natural gas (# A-11) in the mixer. The fuel (# A-10) is preheated in heat exchangers up to a sufficient temperature so as not to cause condensation of the steam flow during mixing.

The presence of the WGS reactor is necessary in order to allocate the calorific value from CO to H_2 and increase the concentration of CO_2 before the cryogenic section. In this study it is assessed whether a low-temperature shift reactor is also required. Since the concentration of CO exiting the HT reactor is very low

(0.77% for case A, but also in other case it is always around 1%) the additional cost of this component does not justify the advantages that can be obtained. The anodic flow out of the last heat exchanger is processed in the GPU which separates a stream of pure CO_2 for storage and a stream of H_2-rich to be purified in a PSA.

The fuel cell operates at approximately atmospheric pressure. We have chosen to use a single MCFC and not two FC stacks in series because the CO_2 concentration coming out of the SMR is not too high. The CO_2 concentration at the exit from the cathode is set at the minimum possible value in order to maximize the separation efficiency of the cell as reported by *Spinelli et al* [18]. The minimum value is 0.5 – 1 %. For oxygen exit from the cathode a concentration higher than 2.5 % is also required. These limits are to avoid polarization for concentration. The cell voltage is imposed at the value of 0.7 V even if it does not coincide with the point of maximum power density. As will be clear in the sensitivity analysis on ΔV, a higher value of it guarantees a higher capture efficiency but a lower power density with, therefore, a larger area with the same power. In our opinion, 0.7 V is a good compromise value for base case.

In *Aspen Plus* there is no fuel cell model and so it is modelled through a series of unitary operations. The cathode side is design with a separator to model the reaction $CO_2 + \frac{1}{2}O_2 + 2e^- \rightarrow CO_3^=$ and the permeate to anode side. A heater is chosen to model ΔT across the section. Instead in anode side a RGibbs (reactor to equilibrium) model unit operation for internal reforming is used and another one is adopted for hydrogen reaction: $H_2 + CO_3^= \rightarrow CO_2 + H_2O$. All the heat fluxes of the cell are combined in heat mixer to model heat exchange in the component. Air flow rate at cathode is imposed by a Design Spec in order to control ΔV and so T_{cell}.

The polarization curve is developed using a simplified lumped parameter approach proposed by *Lukas et al.* [19]. It is known that the potential decreases as the current density increases from an initial value, the Nernst Voltage (E_{rev}), according to the following relationship $\Delta V = E_{rev} - \eta_{act} - j\,R_{ohm} - \eta_{conc}$. All this parameters are function of cathode and anode compositions at inlet and outlet, avarage temperature across cathode and pressures of cell.

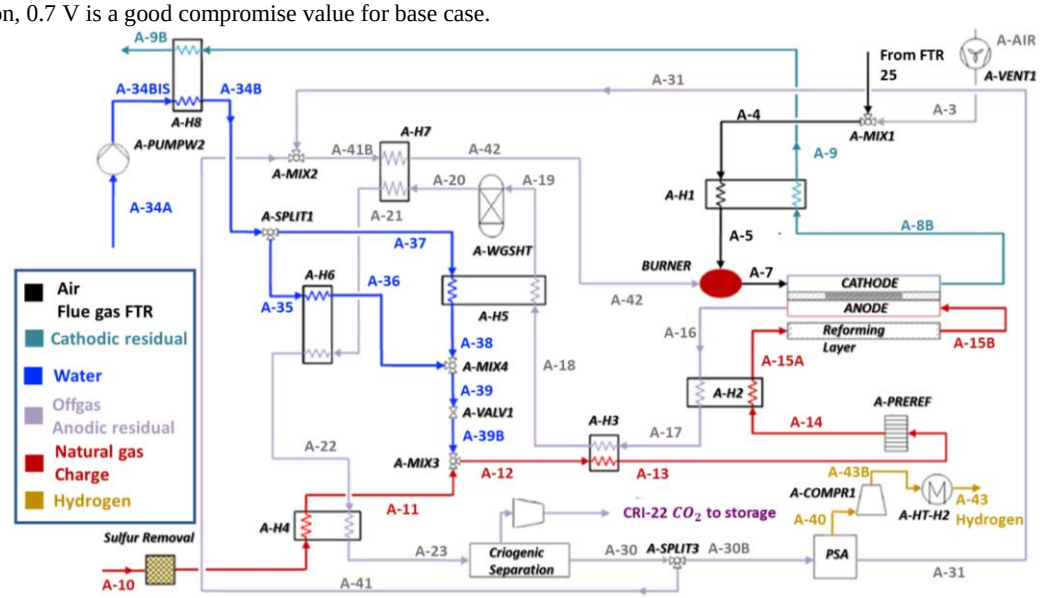

Fig. 2 MCFC plant with natural gas alimentation - Base case A

2.3 Cryogenic section configuration

The discharge from the shift reactor has a CO_2 concentration (about 80 % on a dry molar basis) that does not allow a purity corresponding to the standards required for transport and pipeline storage (CO_2 purity greater than 96 % [15]). In addition, the exhaust gas from the anode contains a significant amount of unreacted H_2 and CO. This requires a gas processing unit (GPU) to generate high purity CO_2 and pure H_2 (figure 3). This separation is carried out by cryogenic techniques, where the temperature is made low enough so most of CO_2 is condensed and separated by gravity from the other gaseous species included in the mixture. A self-cooled cycle is adopted for reaching cryogenic temperature.

The modelling starts from the one proposed by *Chiesa el al.* [16] and is readapted for this work.

The anodic residue is first compressed in an intercooled compressor at the pressure required to guarantee a CO_2 purity over 99%; this condition is achieved through a DS. Discharge stream is cooled in a regenerative heat exchanger and enters a separator that removes all the water present. The temperature inlet the knockout drum is an important parameter for the operation of process. Lowering this temperature facilitates condensation and reduces the mass flow rate sent to the second drum and therefore the mass flow rate condensate by it circulated to the CO_2 booster compressor. On the other hand, lowering this temperature increases the duty of heat exchanger, requiring a greater pressure drop of separated liquid in the valve to maintain

a given minimum temperature difference; this reduces the pressure at second intercooled compressor. In order to find a compromise between these opposite effects, a sensitivity analysis is carried out on the temperature to minimize the compression work demand of the cryogenic section, that is about -33 °C.

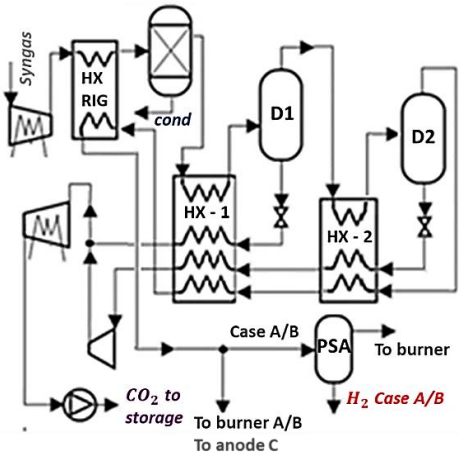

Fig. 3 Block diagram of GPU section

A second knockout drum, working at temperatures (equal to -53 °C) close to those of the triple point (-56.6 °C, table 3), permits to reach high separation efficiency because it increases monotonically as the temperature decreases. As a result, the steam fraction coming out of the first knockout drum is further cooled to -53 °C by another heat exchanger. This value is chosen to ensure that the inlet temperature of cold side flow of heat exchangers is slightly above the CO_2 freezing point after being throttled by a valve which requires a cooling of - 3 °C. The liquid separated in the first knockout drum, is throttled through a valve and introduced into the cold side of a heat exchanger where it is heated and evaporated. The pressure drop in valve is set to guarantee a ΔT_{min} of 3 °C (table 3).

Tab. 3 Main assumption for cryogenic section

Parameter	Unit	Value
CO_2 liquid pump		
Hydraulic/Mech./Elect. efficiency	%	80/84/ 98.5
Liq CO_2 conditions at pump inlet	°C / bar	25 / 80
Outlet pressure	bar	150
Compressor / Intercooled compressor		
Iso./Mech./Elect. efficiency	%	84/ 94/ 98.5
Stage pressure ratio	-	2.5
Inter-coolers outlet T/ $\Delta P/P_{in}$	°C / %	30 / 2
Heat exchangers		
Min separation T	°C	-56
Min ΔT in exchangers	°C	3

The booster compressor is used to send the liquid coming out from the second knockout drum at the same pressure as the liquid coming out from the first knockout drum. In this way less duty is required to the next intercooled compressor. This compressor brings the pressure of the storage flow up to 80 bar, which is then pumped in the liquid phase up to 150 bar for long-range transport. According to the calculation made, the process achieves CO_2 separation efficiencies around 89% (case A) and provides a storage flow whose purity is close to 99.5% (molar base).

2.4 Comparison between case A and MEA capture

Concerning case A, almost all of the carbon (99.6%) in the system is due to the natural gas feeding FC and the SMR. Of this, about 88% is captured by the cryogenic section and sent to storage, while the remain part is released to the plant stack, representing the only source of GHG. Consider a study conducted by *IEAGHG* commissioned by *Foster Wheeler* [11] (table 4) on the capture of CO_2 from the flue gas of a FTR stand-alone (i.e. operating in merchant plant mode) by means of a passive process using a MEA type chemical solvent. In this case it is possible to achieve CO_2 capture efficiencies up to 90% but decreasing the performance of the plant as the efficiency of H_2 equivalent produced and net electrical power produced. Carbon capture ratio is defined as $CCR = \frac{N_{C,storage}}{N_{C,in}}$ and CO_2 avoided with respect no capture case as $CA = \frac{E^{conv}_{CO_2,eq} - E^{ccs}_{CO_2,eq}}{E^{conv}_{CO_2,eq}}$. Equivalent H_2 efficiency is defined as $\eta_{H_2,eq} = \frac{m^{out}_{H_2} LHV_{H_2}}{m^{in}_{NG} LHV_{NG} - \frac{Q^{export}_{steam}}{\eta_{th}} - \frac{W_{el}}{\eta_{el}}}$ where $\eta_{th} = 90\%$ is the reference thermal efficiency of a conventional industrial boiler [12], while $\eta_{el} = \frac{W_{el,net}}{m^{in}_{NG} LHV_{NG}} = 58.33\,\%$ is the electric efficiency of a conventional natural gas fired power plant [12]. SPECCA is defined as $\frac{\frac{1}{\eta^{ccs}_{H_2}} - \frac{1}{\eta^{conv}_{H_2}}}{E^{conv}_{CO_2,eq} - E^{ccs}_{CO_2,eq}}$ and it is the Specific Primary Energy Consumption for CO_2 Avoided. This coefficient is used only for plant with CCS and measures the amount of thermal fuel input in terms of primary energy to avoid emission of one kg of CO_2. [12]

In the case of amine capture (table 4) there is a strong decrease in the W_{el} and a slight increase in the natural gas required, while H_2 production remains the same.

Tab. 4 Comparison CCS using MEA [11] and MCFC section.

IEAGHG - Case 3 [48]		
	FTR base case	FTR+MEA
η_{el} [%]	2.5	0.1
$\eta_{H_2,eq}$ [%]	79.3	69.2
Feed+fuel [MJ/Nm^{3}H$_2$]	14.2	15.6
CA [%]	-	89.2
CCR [%]	-	90
SPECCA [MJ/kg$_{CO2}$]	-	2.74
Case A - FU = 0.75		
	FTR base case	FTR with capture
η_{el} [%]	1.4	9.1
$\eta_{H_2,eq}$ [%]	80.6	74.7
$\eta^{MCFC}_{H_2,eq}$ [%]	-	40.8
Feed+fuel [MJ/Nm^{3}H$_2$]	14.6	18.0
CA [%]	-	84.8
CCR [%]	-	88.0
SPECCA [MJ/kg$_{CO2}$]	-	1.50

In the case of FC capture, the production of H_2 increases slightly compared to the initial value; in this

case, the necessary input of NG is greater than the previous retrofit, while the CO_2 avoided and the CCR are slightly lower, even if they remain at high values. The advantage of a capture with MCFC is the production both W_{el} and H_2. The first is useful to self-power the auxiliaries and GPU and feed energy into the grid, while the latter allows to increase H_2 production of plant. Finally, MEA capture leads to a lower $\eta_{H_2}^{eq}$ and a higher SPECCA especially since the system is "passive". Instead, capture with MCFC is an "active" system with an $\eta_{H_2}^{eq}$ equal to 40.8 %. Finally, $W_{el,net}/Q_{LHV,in}$ increases using MCFC and decreases using MEA.

2.5 Case B

The second configuration analysed assumes that MCFC is no longer fed with NG but with the offgas produced by the PSA of FTR. This configuration avoids the supply of NG to fuel cell; offgas are hydrocarbons C_{2+} free, so pre-reforming is no necessary. This last advantage is important because in this case the anodic residue coming out of the cell is no longer strongly cooled to heat the charge coming out from endothermic pre-reforming and it is possible to use that heat to produce steam export at the same condition of the one of FTR. Then in this case the economization of water is performed using exhausted anodic gases and not exhausted cathodic gases as in case A, because the higher evaporation temperature (160 °C, 6 bar) requires a higher temperature at economizer outlet. The hot cathodic gas is no more sufficient to permit the minimum quantity of H_2O feeding to match the S/C ratio. This solution also has disadvantages mainly due to the FTR section. Decreasing the share of offgas at the FTR combustor, this flow is replaced by NG. This means that flue gas mass flow rate is less (due to high LHV of NG) and lower quantity of carbon molar basis and higher N_2 share. So, the thermal capacity of this flow decreases and less steam is produced in SMR section, as well as power from steam turbine. Finally, the total NG inlet (i.e. the FTR + capture section) is lower than in case A.

2.6 Case C

Case C considers a cell feeding with NG but without H_2 production. The main advantage is related to the recirculation of offgas flow rate from the outlet of the cryogenic section to anode inlet. This flow is rich in H_2 and allows, at the same FU at single passage (0.75), to decrease the flow rate of incoming natural gas. We obtain a global FU equal to 0.88. Less NG at inlet means a lower duty to internal pre-reforming: in fact, a charge richer in offgas and less in NG implies a higher H/C ratio. This permit, as well as in case B, steam production in MCFC section at the same condition of case B. In this case FTR remains equal, so this means that the total amount of steam export is greater than base case A.

2.7 Results and comparison

For each case, a polarization curve has been created using the procedure described but they are not comparable because U_{CO2} and U_{O2} is not the same. In table 5 fuel cell performances are reported. The amount of CO_2 input with fluegas in case B is reduced by 50% compared to case A. Therefore, the permeated CO_2 is lower considering that the contribution of air and offgas to burner is less important. ΔV is constant so the power decreases. Also, the active area of MCFC decreases because CO_2 permeation is less. The H_2 production by fuel cell in case B is less with respect case A because, considering the same FU, if $N_{CO_3^=}$ decreases the equivalent H_2 in input decreases.

Different is the situation in case C where the CO_2 flow rate to cathode can be considered almost constant because FTR system does not change. $N_{CO_3^=}$ depends almost on air flow rate. The fuel feeding fuel cell is no more only NG, but a mixture of natural gas and retentate of cryogenic section. This last stream is H_2 rich. So, the ratio CH_4/CO_2 feeding to fuel cell is less and this fact implies less heat absorbed by reforming reaction. If the reforming absorbs less heat, this means that for control the temperature, more air has to be fed at the cathode side. $N_{CO_3^=}$ decreases and, at the same ΔV, also cell power decreases. Stack active area decreases, driving by the less cell power while current density remains almost constant. Instead, electrical efficiency of MCFC increases thanks to offgas recirculation that permits less input of NG.

Tab. 5 Overview and comparison of fuel cell performances for three different cases

Case	ΔV V	j A/m²	A_{stack} m²	U_{CO_2} %	U_{O_2} %	$x_{O_2,in}^{cathode}$ %	$N_{CO_2,in}^{flue\ gas}$ kmol/s	$Offgas_{in}$ kg/s	NG_{in} kg/s	$H_{2,out}$ Nm³/h	Q_{steam} MW	$W_{cell\ DC}$ MW	$W_{el,net}$ MW	η_{el} %
A	0.7	1733	17533	85.7	18.74	13.07	0.159	-	0.9	2677.4	-	21.3	18.6	44.2
B	0.7	1475	10292	82.1	16.54	11.68	0.078	4.1	-	1109.3	0.7	10.5	9.2	39.3
C	0.7	1730	15667	83.4	15.58	13.73	0.159	-	0.7	-	1.0	19.0	16.5	51.1

Considering SPECCA (table 6), it is clear how case B is the case that require less primary energy for CO_2 capture with respect the two other cases. Moreover, B has a higher $\eta_{H_2}^{eq}$ with respect the other cases, mainly due to lower inlet flow of NG despite the quantity of H_2 produced is lower than in case A and the heat in export is lower than in case C. This last case is the one characterized by a higher steam production but despite this, the absence of H_2 produced by the FC penalizes the retrofit in terms of SPECCA and $\eta_{H_2}^{eq}$. Indeed, the amount of H_2 produced is the same compared to the case without capture but with a higher demand of NG to feed the MCFC. In terms of carbon capture, case B is the best thanks mainly to offgas feeding of FC that gives two main advantages: the flue gas of the FTR is less CO_2 rich and supply the cell with offgas avoids the necessity to feed NG to the capture section.

Tab. 6 Overview and comparison of overall plant performances for different cases

Case	NG_{in} kg/s	$H_{2,out}$ Nm³/h	CO_2^{out} kg/s	CCR %	CCA %	E_{CO_2} $\frac{g_{CO_2}}{MJ_{H_2}}$	$W_{el,net}$ MW	Q_{steam} MW	$\eta_{H_2}^{eq}$ %	SPECCA $\frac{MJ}{kg_{CO_2}}$
No capt.	2.63	30258.9	6.98	-	-	77.61	1.77	6.99	80.60	-
A	3.54	32936.4	1.158	88.0	84.8	11.8	15.01	6.99	74.67	1.50
B	3.02	31368.2	0.745	90.9	89.7	8.0	6.69	3.98	74.89	1.36
C	3.33	30258.9	1.231	86.4	82.4	13.7	13.33	8.03	73.21	1.96

3. Sensitivity analysis

A sensitivity on-design analysis on FU for case A is performed (table 7). The range of variation is between 0.67 and 0.75. Below the lower limit the anodic and cathodic cooling section should be further revisited; a lower FU leads to a higher input fuel flow rate and, an equal S/C ratio, a higher water content to evaporate. Moreover, the pre-reforming would absorb more heat for the reaction with a consequent further cooling of the anodic exhaust in order to obtain the correct temperature at the cell inlet. As the FU decreases, the input air decreases due to the fact that the internal reforming absorbs more heat at the same CO_2 amount from the flue gas. The flow rate of $N_{CO_3^=}$ increases to obtain an output CO_2 concentration equal to 1%. This implies not only a higher cell power but also a higher active area and a higher cost. By decreasing the FU, the CO_2 capture performance and also the net power of the system increase due to the higher quantity of permeated ion.

Tab. 7 FU sensitivity analysis on overall plant performance – Case A

MCFC section only				Overall plant								
FU	j A/m²	A_{stack} m²	$W_{density}^{FC}$ W/m²	NG_{in} kg/s	$H_{2.out}$ Nm³/h	CO_2^{out} kg/s	CCR %	CA %	E_{CO_2} $\frac{g_{CO_2}}{MJ_{H_2}}$	$W_{el.net}$ MW	η_{H_2} %	SPECCA $\frac{MJ}{kg_{CO_2}}$
No capt.	-	-	-	2.63	30258.9	6.98	-	-	77.61	1.77	80.60	-
0.67	1720	20092	1204	3.79	35995	0.978	90.55	88.23	9.14	16.73	76.59	0.95
0.71	1730	18570	1212	3.65	34261	1.082	89.14	86.32	10.62	15.71	75.49	1.25
0.75	1733	17533	1213	3.54	32936	1.158	88.02	84.76	11.83	15.01	74.67	1.50

Referring to table 8, a sensitivity analysis is performed by varying the ΔV between 0.67 and 0.73 and keeping a constant utilization factor equal to the base case of 0.75. By decreasing the ΔV, the current density becomes higher leading to a high ohmic resistance that penalises the net electrical efficiency of the fuel cell module and therefore that of the MCFC system. Due to the increased heat emitted by the electrochemical process, a higher input air flow rate is required. This additional air flow is also due to a lower thermal power absorbed by the internal reforming. However, it increases the power density because the nominal operating point of the cell is not set for a voltage that maximises the power density but for a higher one to promote the CO_2 capture by the MCFC. A higher ΔV results in a lower air flow with a higher $CO_3^=$ permeation in order to achieve at cathode outlet CO_2 concentration equal to 1%; this leads to a higher cell power and a higher U_{CO2}. CO_2 emission at the output is lower. The H_2 produced increases only slightly because of the slight increase in NG. The electrical power increases, despite the lower power density of the FC because this decrease is determined by the greater cell area. Finally, the SPECCA decreases due to lower CO_2 emissions.

Tab. 8 ΔV sensitivity analysis on MCFC and overall plant performance – Case A

MCFC section only												Overall plant				
ΔV V	j A/m²	A_{stack} m²	$N_{CO_3^=}$ kmol/s	U_{CO_2} %	GN_{in} kg/s	m_{aria} kg/s	$H_{2,out}$ Nm³/h	$W_{cell\ DC}$ MW	$W_{density}$ W/m²	$W_{el.net,FC}$ MW	$\eta_{el,FC}$ %	E_{CO_2} $\frac{g_{CO_2}}{MJ_{H_2}}$	CCR %	CA %	η_{H_2} %	SPECCA $\frac{MJ}{kg_{CO_2}}$
0.67	1866	15873	0.153	83.8	0.89	67.5	2415	19.8	1250	17.2	41.7	13.5	86.4	82.7	73.4	1.90
0.70	1733	17533	0.157	85.7	0.91	57.9	2677	21.3	1213	18.6	44.2	11.8	88.0	84.8	74.7	1.50
0.73	1586	19644	0.161	87.6	0.93	48.4	2943	22.8	1158	20.2	46.6	10.2	89.7	86.9	76.1	1.10

4. Economic analysis

For the economic analysis, the bottom-up approach used is the one adopted by *Mastropasqua et al.* [14] and *Spinelli et al.* [18]. The analysis is differential type, considering the revenues and costs of capture section only. Cost of component are calculated following economic of scale, where the parameters of equations used are taken from literature. A resume of CAPEX calculation is in figure 4.

The cost of MCFC, according to *Spinelli et. al* [18], is been evaluated for the two scenario: the first scenario is characterized by a cost of the FC stack about the current one, assumed 1200 €/kWel with an increase about 50% in order to consider both FC stack replacement ever 7 years and maintenance cost. The second scenario represents an achievable future and in this case the total cost including maintenance and FC stack replacement is equal to 610 €/kWel. The investment cost of the plant is intrinsically related to the cost of the fuel cell.

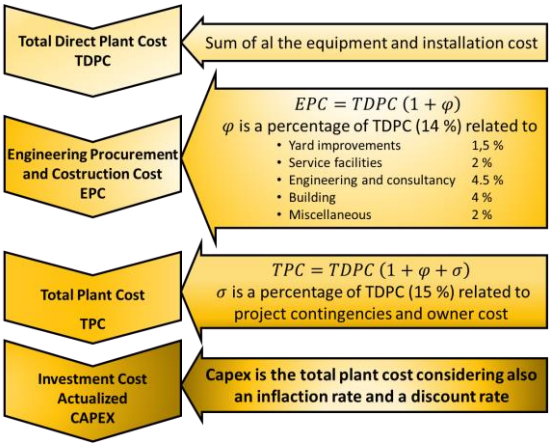

Fig. 4 CAPEX calculation scheme

It is interesting to compare case A and case C (figure 5). Case C allows a lower investment cost due to lower MCFC cost; it has any H_2 production but produces more steam in export. The cost of cryogenic capture, after the cell cost is the most relevant in all types of plants, it may even become more predominant in the second scenario. The case B with the same FU is the most economical one; this is essentially because the FC stack area is about 7345 m^2 smaller with respect case A. Finally, O&M cost are calculated as reported by *Spinelli et al.* [18].

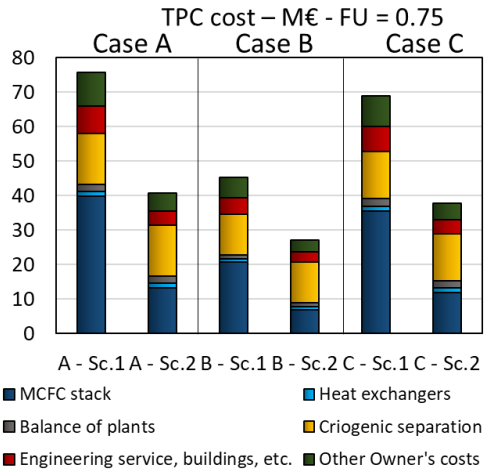

Fig. 5 Breakdown of TPC for case A, B and C with FU 0.75. Balance of plants includes cost of WGS and pre-reforming reactor, pump, fan and all the other component not mentioned.

In the base case the price of NG is set to 6 €/GJLHV, H_2 price to 2 €/kg_{H2}, electricity market price to 50 €/MWh_{el} and carbon tax equal to 20 €/$tonn_{CO2}$. The power plant operating life is equal to 20 years, while construction period is about 3 years. The operating hours are 5700 the first year and 7500 for the followings. The cost is assessed from EBITDA point of view. A discount rate equal to 8% is considered.

Observing only the NPV (table 9), case B would seem the most convenient and characterized by the lower investment cost. This configuration has the disadvantage to produce a lower quantity of H_2 and W_{el}; for this reason, the minimum price of H_2 to obtain a profitable system is higher than the one of case A, although A has higher investment costs. Moreover, supplying the cell with off-gas decreases the steam export and this quantity is replaced in an external boiler which represents another sources of CO_2 emission while in case C happens the contrary. Case C has the disadvantages of no H_2 production so retrofit profitability is not affected by H_2 price. In case A, lower FU leads to higher investment costs, whose driving force is the largest A_{MCFC} (table 7) and therefore the higher FC stack cost but the additional revenues due to the higher H_2 production and higher electricity sales fully compensate the higher plant cost.

Tab. 9 Economic results comparison with FU = 0.75

Minimum value for different case with FU = 0.75						
	Case A		Case B		Case C	
	Sc. 1	Sc. 2	Sc. 1	Sc. 2	Sc. 1	Sc. 2
NPV [M€]	-92.4	-34.3	-57.4	-27.1	-105.2	-53.4
Min €/kg_{H2}	6.9	3.8	9.3	5.5	-	-
Min €/MWh_{el}	138.0	82.7	197.3	119.4	164.8	108.2
Min €/$tonn_{CO2}$	75.5	40.6	53.3	35.7	83.4	52.1

A sensitivity analysis for case A with FU 0.67 in scenario 2 is performed (figure 6.a). Red line represents set of points with NPV equal to zero. Its slope depends on the W_{el} produced and CO_2 avoided while its location in the diagram depends on the quantity of extra H_2 produced at the same price. More is the H_2 produced and more the red curve is lowered making the positive profit zone greater. This is more evident in case B (figure 6.b), where the quantity of H_2 produced is less than in case A and the not profitable area is wider. NPV mostly depends on C_{tax} and less on electricity market price. In figure 6.b there is also a comparison between case A and B in scenario 2 with FU 0.67. Profitability of case B depends less on electric production with respect case A because, with fixed C_{tax}, to reach positive profit a larger variability of the electric price is necessary.

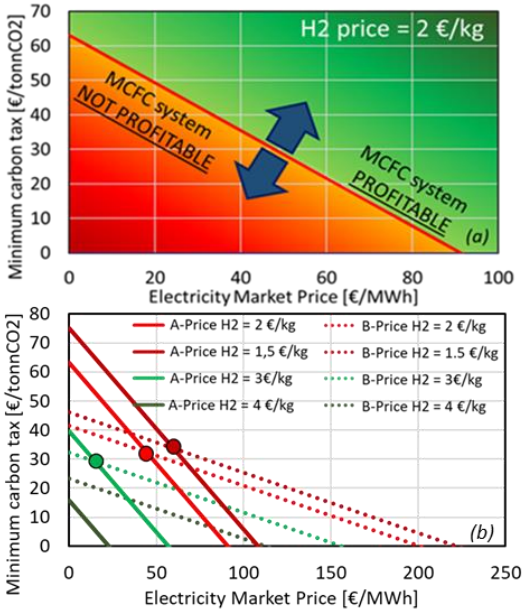

Fig. 6 Profitability of capture section (a); profitability comparison between case A and B varying hydrogen price (b).

At low H_2 price, for low electricity market price case B is more profitable than case A, while for high electricity price case A is more profitable. The electricity market price that decided this, is the one obtained crossing the lines at same H_2 price (points in figure 6.b). This is due to the fact that B produces less electricity but has better CO_2 capture performance compared to case A.

From figure 5 is evident how Case A is characterized by higher TPC than case B but is the one the produces more H_2 and W_{el} (tab. 6). It is useful to perform a non-dimensional analysis using IRR (figure 7). It is preferable respect to NPV because it is independent of the size of the plant. At equal NPV obtained, the economic quality of the project is very different depending on the initial investment required.

Considering only the case in which IRR is greater than discount rate (8 %). From figure 7 it is possible to observe how for low H_2 prices case B is has higher IRR and so it is the preferable one even if it requires a minimum C_{tax} higher than 30 €/tonn$_{CO2}$. At high H_2 prices case A is more convenient up to average C_{tax} values because it produces more H_2.

It is possible to remark how the break-even point of IRR between the two cases moves to higher C_{tax} if the H_2 price increases. This means that, in order to have for case B the same investment return as case A, is necessary to have a C_{tax} and that it is quite penalizing for the higher emitter plant. With a high value of the H_2 produced, it is better to choose the solution that allows a higher production of this, i.e. case A. Instead with low H_2 valorisation case B is preferable because it allows a higher capture, i.e. lower emissions that imply a higher saving for the non-payment of the C_{tax}. At the end, the choice between investment A and B is dictated by the current and future market conditions in which plant operates and how this market will valorise useful products of capture section.

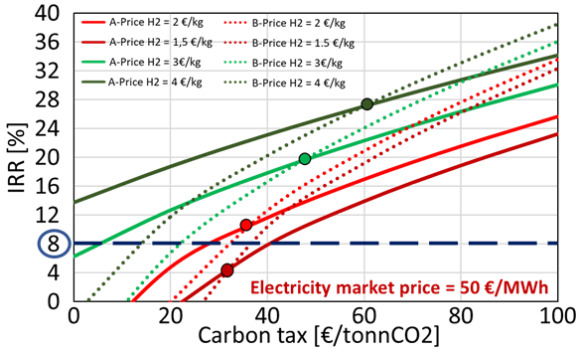

Fig. 7 IRR comparison with respect carbon tax and hydrogen price. Case A Vs. Case B Sc.2 with FU = 0.67

5 Off-design assessment

An assessment about off-design operating condition for MCFC system is performed. This study wants to simulate the situation in which an operator for market reason needs varies the production of H_2. Taking as reference the basic case with FU = 0.71 in which the retrofit plant is fed with NG, FU is changed to simulate the variable H_2 production. The variation has been done in a range from 0.75 (in which it is considered minimum or no H_2 production) to 0.67 (in which H_2 is maximum).

5.1 Method description

Once the basic case of optimized design has defined, it is necessary to investigate the geometries of the most critical components to study their operation more realistically when operating conditions change. The analysis is made only on the heat exchangers, on the stack of MCFC cells, i.e. all those components where the fixed geometry is decisive for the performance of the plant. The cryogenic section, the PSA, the catalytic burner, the WGS, and pre-reforming reactor have not been analysed so in detail because the analysis wants to focus mainly on the fuel cell and its performance.

5.1.1 Heat exchanger modelling

Given the temperature and heat duty values of each heat exchanger, the logarithmic mean temperature equation $Q = US \cdot \Delta T_{mln} \rightarrow S = \frac{Q}{U\ \Delta T_{mln}}$ is used to find their geometry in on design condition. For the determination of global heat transfer coefficient, a simple approach has been used. Convective heat exchange coefficient (h_i) depends on numerous factors such as the motion of the fluid, heat capacity, density, viscosity and geometry of component. Values for h_i are supposed because the previous parameters are unknown. The conductive resistance of material and the fouling of the ducts, considering the wall of the pipes thin enough and the thermal conductivity k quite high, are assumed negligible. Therefore, the overall heat exchange coefficient U can be defined as $U = \left(\frac{1}{h_{inside}} + \frac{1}{h_{outside}}\right)^{-1}$. After U and design surface calculation, in off-design condition the ratio $S_{design,i} = \frac{Q_i}{U_i \cdot \Delta T_{mln,i}}$ is kept constant changing heat duty and ΔT_{mln} of heat exchanger. For the evaporators and economizer two constraints are imposed: the first one is geometry of the heat exchangers. The second one is saturated steam condition set at the evaporator outlet because in any off-design condition it is not admissible to have exit fluid in a two-phase state or that the ΔT_{sub} of the economizer drops so much so water evaporates inside the piping.

The *Aspen Plus* methodology is similar to that used in gas-gas exchangers but, as concerns the economizer, a variation has been set on ΔT_{sub}. Concerning the evaporators, the heat exchanger surface has been set varying the inlet water flow rate at the evaporators while maintaining the saturated steam condition at the outlet. Increasing FU all these components are oversized because less mass flow rate passing.

5.1.2 MCFC active area modelling

Also, active area of FC stack is kept constant as $A_{design} = \frac{W_{cell}}{\Delta V \cdot j}$. For each operating condition variations, an iterative approach is performed in order to change the power, ΔV and j such as the polarization curve. Figure 8 shows the algorithm used.

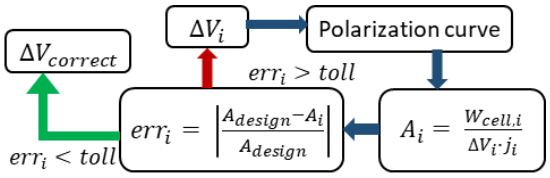

Fig. 8 Iterative process for MCFC active area modelling

A first attempt value for ΔV is assumed, then inlet and outlet conditions of FC are calculated. After that, using the equation proposed by Lukas et. al [19], a new polarization curve is obtained as well as W_{stack}. From it, given ΔV, j and the A_{MCFC} is obtained. The area is compared with the design one and if the difference is less than a certain tolerance (set to 0.5 %), ΔV assumed is correct, otherwise a new value for it must be considered.

5.1.3 Anode inlet temperature modelling

The cathode inlet temperature in off-design condition remains fixed thanks the presence of the burner. The anode inlet temperature depends on the equilibrium temperature of the internal reforming that can varying in off-design conditions. To have a correct modelling of charge heating in the internal reforming, its area has to be constant. Due to reaction there is a variation of the composition and so of the heat capacity. To better modelling, it is necessary to divide the reforming reaction as many reactors as possible: 10 reactors brought to equilibrium are supposed. In on-design condition, considering the same ΔT (15 °C), between one reactor and the others, $UA_{design,i}$ is calculated; then in off-design mode every UA_i is kept constant varying heat duty and ΔT_{mln}. The latter value is calculated considering charge exchange heat between a source at constant temperature equal to the outlet FC one (645 °C). In this way, the equilibrium temperature of the reaction change causing a new equilibrium composition. Decreasing FU, the anode inlet temperature is lower, while outlet temperature is constant (645 °C). Table 10 shows how at low FU the heat exchangers and the internal pre-reforming are undersized because the quantity of fuel fed is greater: flow rate is higher and therefore their efficacy decreases. At high FU, the heat exchangers behaviour is opposed because they are oversized.

Tab. 10 Tin and Tout of internal ref. with respect different FU

FU	T in anode [°C]	T in internal ref. [°C]
0.67	578.6	421.44
0.71 On Design	**600.0**	**450.00**
0.75	610.3	466.81
0.75 no H_2	625.5	480.00

5.2 Performances with different H_2 production

If more H_2 is produced, FU decreases, NG input increases and so cell operating conditions change (table 11). Less ΔV implies higher j and so more power but the heat exchangers are undersized. Also, the thermal power released from the FC increases because of higher current density.

The heat is inversely proportional to ΔV, greater is the heat output and the lower is the ΔV (table 11). At the same A_{MCFC}, if ΔV decreases, the power increases (due to a higher power density) and the current density increases. So $N_{CO_3^=}$ increases but U_{CO2} decreases, as shown in figure 9, because the amount of CO_2 entering the cathode increases by decreasing FU.

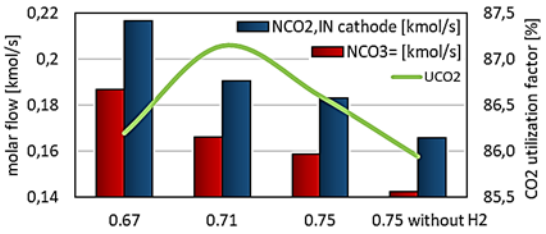

Fig. 9 CO_2 performance of fuel cell

This trend is justified by two aspects. The first is due to the *A-H1* exchanger is undersized at low FU and so T_{in} to the catalytic burner is lower, which leads to a higher demand for retentate offgas (rich in CO which is oxidized to CO_2). The second aspect is due to the constraint to keep constant the molar fraction of CO_2 output to the cathode equal to 1%.

The input air flow rate increases as more cooling is required to the cell. At low FU, S/C ratio decreases but remains at acceptable values. Its decrease, as well as the change in the equilibrium temperatures of the reforming, implies a different composition at anode inlet. Finally, the FC efficiency decreases because the higher input of NG is not proportional to the higher power produced.

Tab. 11 Overview of fuel cell and overall plant performance in different operating condition – Case off design

MCFC section only								Overall plant					
FU	ΔV V	j A/m²	U_{CO2} %	GN kg/s	S/C	H_2 Nm³/h	η_{cell} %	CCR %	CA %	E_{CO2} $\frac{g_{CO_2}}{MJ_{H_2}}$	$W_{el,net}$ MW	η_{H_2} %	SPECCA $\frac{MJ}{kg_{CO_2}}$
0.67	0.655	1934	86.2	1.20	1.98	5251.0	36.67	87.45	83.95	12.45	15.74	73.48	1.84
0.71	**0.70**	**1730**	**87.1**	**1.02**	**2.10**	**4002.0**	**42.01**	**89.14**	**86.32**	**10.62**	**15.71**	**75.49**	**1.25**
0.75	0.719	1642	86.6	0.92	2.20	2837.5	45.67	88.86	85.87	10.97	15.79	75.61	1.23
No H_2	0.752	1475	86.0	0.68	2.75	-	50.50	88.69	85.33	11.39	12.76	72.21	2.18

On design configuration is the one that maximize carbon capture, while the minimum SPECCA and H_2 efficiency is achieved in configuration with low hydrogen production (FU 0.75). H_2 efficiency rises with the increase of FU for two main reasons: the first one is related to the decrease of NG input, while the second is related to the better efficacy of the heat exchangers that allows to obtain better plant performance. For the case without H_2 production, the plant has worse performances. The H_2 production efficiency decreases because the capture section does not produce H_2. Consequently, the SPECCA increases. At the end, the trend of main

performances is linear with respect FU, while total power plant is almost constant in case of H_2 production because higher FC electric power is compensated by more cryogenic electric power request. It is conclusion that for the CO_2 capture it is better on-design condition, for hydrogen production efficiency the operating point with FU equal to 0.75 one, for the quantity of H_2 produced the configuration with the lowest FU while for the lower cost of NG the operating point without H_2 production.

5.3 Economic evaluation

For a correct analysis, the share of equivalent hours for each operating condition must be assumed. To decide how much are the h_{eq} without H_2 production, the generation of vRES is considered. Indeed, in a future scenario [20] the non-dispatchable RES will store energy as H_2 during the production surplus thanks to installed capacity greater than the demand [21]. Our plant has opposite trend with respect vRES in order to compensate lack of H_2 when surplus of vRES is not present. So, two different scenarios (A and B) are evaluated. The first one divides the h_{eq} for different operating mode observing the trend of vRES production during the year, while the second considers only two operating point: one with medium production and the other without H_2 production. Concerning scenario B the parameter that influences the profitability of the plant is the number of hours of operation without H_2 production because in other operating conditions the trends of W_{el}, H_2 production, natural gas request, carbon capture and efficiencies are mostly linear and can be approximated with an average production operation (FU = 0.71). This fact is supported by NPV value that is almost the same, modelling all hours with H_2 production only in medium operating mode (table 12). The small difference is due only to the little different H_2 production efficiency.

Tab. 12 Comparison between Scenario A and Scenario B

Configuration point	Sc. A h_{eq} [%]	Sc. B h_{eq} [%]
Max H_2 production	33	0
Medium H_2 production	42	92
Min H_2 production	17	0
No H_2 production	8	8
NPV [M€]	**-28.0**	**-27.0**

An analysis is performed with basic parameters and scenario 2 for MCFC cost. In scenario A, also an assessment on natural gas price is performed. The case more profitable (with a higher NPV) is the situation with major carbon tax and lower natural gas price. NPV also is strongly dependence on carbon tax.

In the scenario B, analysing the plant production varying the hour without H_2 production the minimum carbon tax to have a plant profitable is 34.13 €/$tonn_{CO2}$ with the other parameters as basic value. For the H_2 price the minimum value for profitability is 2.84 €/kg_{H2} and for electricity price is 71.53 €/MWh. The parameters that most influence the profitability of the plant are the carbon tax and the selling price of the H_2 produced (figure 10). We have not considered cases with value of IRR is negative or it is not possible to calculate. If IRR is lower than cut-off rate we will not realize the expected return on investment. The slope of the lines in figure 10.b is higher with respect the one in figure 10.a because the valorisation of H_2 in the case b is higher and so a decreasing in its production penalize more the plant profitability; in addition comparing the two graphs, at the same condition a higher H_2 price permits a higher IRR and so a better investment return. Moreover, increasing the C_{tax}, the curves are flatter with a lower slope. This is because a better valorisation of CO_2 capture compensates the lower H_2 production. Considering NG price and the P_{el} equal to the base values, only a C_{tax} greater about 60 €/$tonnCO_2$ permits to run MCFC without H_2 production and recirculating fuel at anode side increasing global FU. This means that a retrofit section, in addition to CO_2 capture, has to produce useful products to reach the profitability of plant.

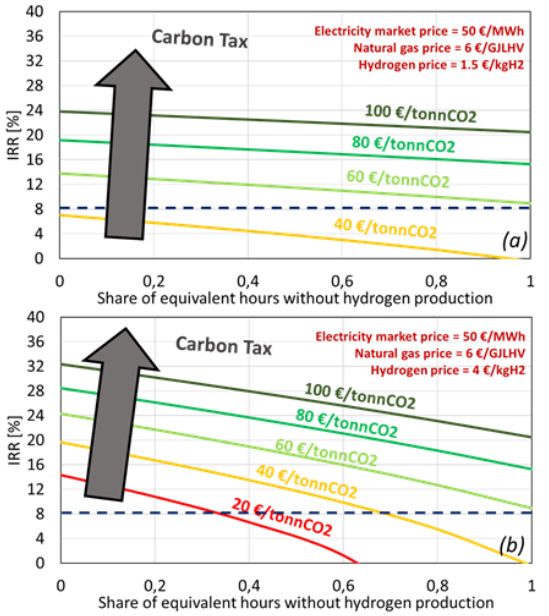

Fig. 10 IRR comparison with respect C_{tax} and share of equivalent hours without H_2 production. (a) with H_2 price equal to 1.5 €/kgH_2; (b) with H_2 price equal to 4 €/kgH_2

6. Conclusion

In future, hydrogen of refineries will play a more important role and its production will be made partly through renewable sources, partly through conventional technologies with CCS. The MCFC technology is more convenient compared to MEA capture, allowing a considerable increase both in the W_{el} and H_2 production. Concerning CO_2 capture, only a slightly increase of NG input takes place. From the technical point of view every plants considered have advantages and disadvantages. The best one depends on the main project purpose and on external parameters such as market conditions. Today, given the cost of the MCFC and the value of the carbon tax, this retrofit is not convenient for any of the proposed configurations. In the future it could be a valid alternative if an energy policy promotes low carbon technologies.

.

Acronyms and abbreviations – Extended abstract

CA	CO2 Avoided
CCR	Carbon Capture Ratio
CCS	Carbon Capture and Storage
CCU	Carbon Capture and Use
C_{tax}	Carbon Tax
FC	Fuel Cell
FTR	Fired Tubular Reformer
FU	Fuel Utilization Factor
GHG	Greenhouse Gas
GPU	Gas Processing Unit
HT	High Temperature
IRR	Internal Rate of Return
j	Current Density
MCFC	Molten Carbonate Fuel Cell
MEA	Mono Ethanol Ammine
NG	Natural gas
NPV	Net Present Value
P_{el}	Electricity Market Price
PSA	Pressure Swing Adsorption
S/C	Steam to Carbon Ratio
SMR	Steam Methane Reforming
SPECCA	Specific Primary Energy Consumption for CO2 Avoided
vRES	Variable Renewables Energy Source
Wel	Electric Power Production
WGS	Water Gas Shift Reaction

References – Extended abstract

[1] IEA - Data and statistics

[2] Application of Molten Carbonate Fuel Cells in Cement Plants for CO_2 Capture and Clean Power Generation. Matteo C. Romano et al.

[3] Global Energy Review 2020. The impacts of the Covid-19 crisis on global energy demand and CO_2 emissions – IEA

[4] Vision 2050 A pathway for the evolution of refining industry and liquid fuels – Concawe and Fuels Europe – 2019

[5] Damien Valdenaire CONCAWE John Gale IEAGHG, Lily Gray CONCAWE. Understanding the cost of retrofitting CO_2 capture in an integrated oil refinery. Technical report, IEAGHG, 2017/TR8, August 2017. Cap 1.1 , pag 104,pag 126,pag 19,pag 25

[6] https://www.fuelseurope.eu/wp-content/uploads/SR_FuelsEurope-_2020-1.pdf pag 1,39,40,41

[7] Pascal Barthe et al. Best available techniques (BAT) reference document for the refining of mineral oil and gas. Technical report, DOE/NETL, 2015. Pag72, cap.8.1.1, cap 8.1.2, cap 8.1.3, cap8.1.4, pag 66

[8] Report European emission refineries Concawe 2017 Rpt_20-4: pag37, pag38

[9] EPA. U.S. - direct GHG emissions of selected gases reported by sector. https://ghgdata.epa.gov/ghgp/main.do# pie sector 2017

[10] Hydrogen and hydrogen-derived fuels through methane decomposition of natural gas – GHG emissions and costs. Sebastian Timmerberg et al.

[11] IEAGHG Technical Report 2017-02 February 2017. Techno-Economic Evaluation of SMR Based Standalone (Merchant) Hydrogen Plant with CCS

[12] Demoys. Assessment of performance and thermal balance of plants based on mixed conducting oxygen and hydrogen separation membranes. collaborative project with Politecnico of Milan. Pag 36 to 41-56

[13] IEA – World Energy Outlook 2020

[14] L. Mastropasqua, L. Pierangelo, M. Spinelli, M.C. Romano, S. Campanari, S. Consonni, Molten Carbonate Fuel Cells retrofits for CO_2 capture and enhanced energy production in the steel industry, International Journal of Greenhouse Gas Control, Volume 88, 2019, Pages 195-208, ISSN 1750-5836, https://doi.org/10.1016/j.ijggc.2019.05.033

[15] Fout. T. Herron. S. 2013. Quality guidelines for energy system guidelines. CO_2 impurity design parameters. NETL Qual. Guidel. Energy Syst. Stud.

[16] CO2 cryogenic separation from combined cycles integrated with molten carbonate fuel cells. Paolo Chiesa et al.

[17] GECoS (Group of Energy Conversion Systems) is a group of researchers of Politecnico di Milano working in the field of environmentally friendly energy conversion technologies

[18] Spinelli, M. et al. Campanari, S., Consonni, S., Romano, M.C., Kreutz, T., Ghezel-Ayagh, H.,Jolly, S., 2018. Molten carbonate fuel cells for retrofitting post combustion CO_2 capture in coal and natural gas power plants. J. Electrochem. Energy Convers. Storage 15, 031001. https://doi.org/10.1115/1.4038601.

[19] M. D. Lukas, K. Y. Lee and H. Ghezel-Ayagh, "An explicit dynamic model for direct reforming carbonate fuel cell stack," in IEEE Transactions on Energy Conversion, vol. 16, no. 3, pp. 289-295, Sept. 2001, doi: 10.1109/60.937210

[20] Erik Wolf, Chapter 9 - Large-Scale Hydrogen Energy Storage, Editor(s): Patrick T. Moseley, Jürgen Garche, Electrochemical Energy Storage for Renewable Sources and Grid Balancing, Elsevier, 2015, Pages 129-142, doi 10.1016

[21] “Is a 100% renewable European power system feasible by 2050?” William Zappa, Martin Junginger, Machteld van den Broek

Table of Contents

Climate change, CO_2 emission and oil refinery

1

The first chapter introduces the issue of anthropogenic carbon dioxide emissions and the correlation with energy consumption. It then focuses on the problem of the greenhouse effect and climate change. Then we will talk about the impact of COVID-19 in the energy and environmental field. In addition, we will describe in detail the refining process, the types of refinery and the emissions that characterize them. Finally, we present a possible future scenario 2050 of a refinery.

1.1 Energy consumption and CO_2 emission

Modern society demands both greater energy (expressed in terms of TPES) and a reduction in greenhouse gas emissions [1]. This seems to lead to an antithesis, since current energy demand is largely met by primary fossil fuels: coal, natural gas and oil. According to *IEA* statistics [2] the global TPES (updated to 2017) is about 13.97 billion toe (tonne of oil equivalent), more than 80% of it satisfied by fossil fuels as shown in figure 1.1(a).

Fossil fuels are molecules composed mainly of carbon and hydrogen and their combustion releases into the environment CO_2 and H_2O. So, in a perspective of decarbonisation of the world system, this 80 % share should decrease in favour of other sources, less climate impacting. In the recent years, after the international climate agreements, we are facing an energy transition that will continue for most of the 21st century. The solution cannot be unique to this complex problem but must be provided by all those technologies that can lead to a reduction in greenhouse gas emissions without sacrificing the current level of welfare. As you can see from the graph in figure 1.1(b), emissions related to the transport sector represent about 1/4 of the total while those related to the industrial sector 1/5. While for the electricity sector, a reduction in emissions can be achieved through the more intensive use of renewable sources and nuclear power, for the sectors mentioned above, based on fossil fuels, it is more complicated to achieve a reduction of their environmental impact.

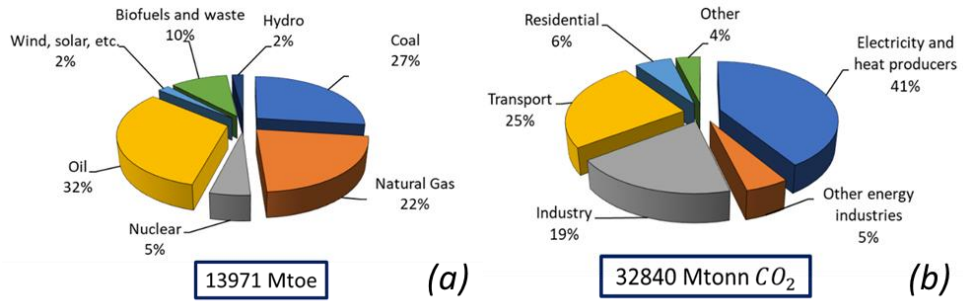

Figure 1.1 Global TPES in 2017 based on resources used (a); CO2 emission by sector in the world (2017) (b) [2]

Consider, for example, the transport sector, which is characterised by many small emitters. As can be seen in figure 1.2, over the years there has been a decrease in specific CO_2 emissions g_{CO2}/km for the road transport sector, driven only by a higher efficiency of the ICE (Internal Combustion Engine) and this is even more evident after the Volkswagen scandal in 2015, where the discrediting of diesel has led to an increase in the market share of the gasoline engine, which is less efficient and more climate-altering. However, total emissions have increased due to more users in this sector.

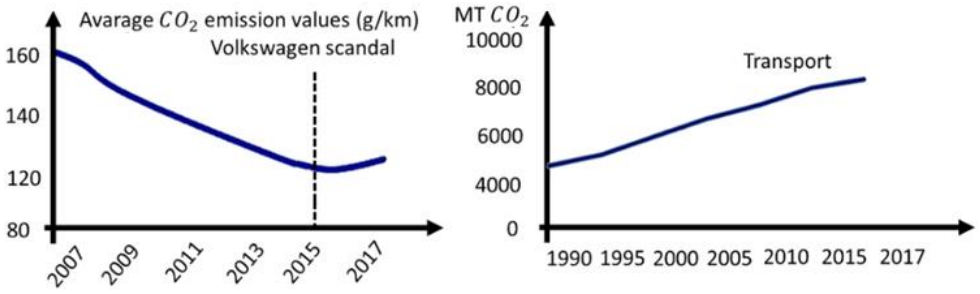

Figure 1.2 Averaged CO2 emission measured in the laboratory [3]

From what has been said, the conclusion can be that the only solution to reduce CO_2 emissions within the transport sector (consider here only the part related to light road vehicles) is to abandon thermal engine technology in favour of electric or hydrogen technology. Concerning this, it is necessary to briefly underline some disadvantages of these two possible alternatives. First of all, battery electric motors (BEV) have the disadvantage of poor autonomy and considerably long charging times, moreover, their extensive use would cause greater demand on the electrical system, which would be covered by fossil fuel technology (combined cycle system). On the other hand, fuel cell electric vehicles (FCEV), in addition to the problems and costs related to PEM fuel cells, have the disadvantage of using hydrogen, which is an energy vector that does not exist pure in nature; in fact, today the majority of hydrogen (> 90%) is produced from fossil fuels (figure 1.3) with consequent CO_2 emissions as a waste of the process.

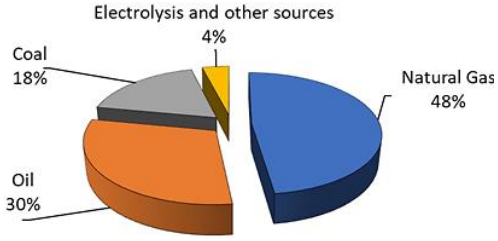

Figure 1.3 Hydrogen Source [4]

Considering it, the current energy transition in the road transport sector will always have thermal engines as a reference technology also in the next few years, as shown in figure 1.4, although their growth will be practically zero or slightly decreasing.

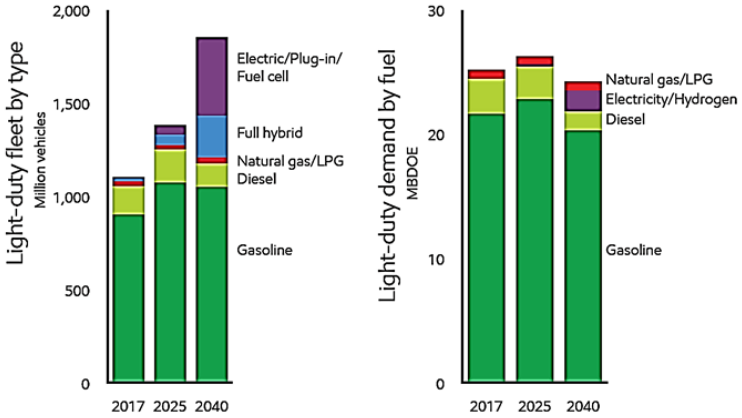

Figure 1.4 Light-Duty projections in transportation field [5]

Similar arguments can be made for the rest of the transport sector (heavy-duty, marine, aviation and rail). Moreover ExxonMobil [5] forecasts a growth in the global transportation energy demand by about 25% in 2040 thanks to heavy duty or commercial activity on wheel, marine, aviation and rail transports.

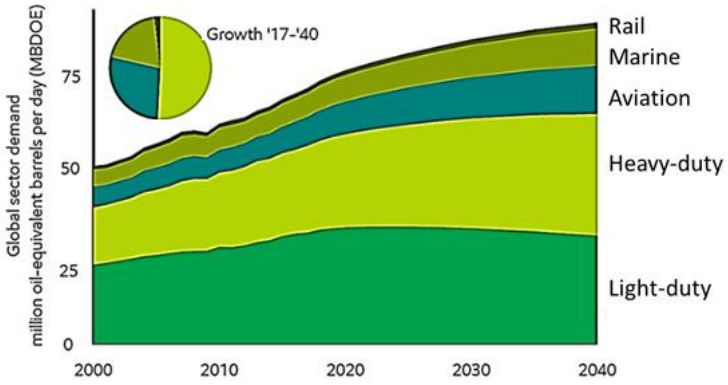

Figure 1.5 Transportation energy demand growth driven by commerce [5]

Figure 1.5 shows a peak in the fuel demand for the vehicle mobility. ExxonMobil explains how the peak depends on the increasing in the light duty vehicles' energy efficiency bringing

fuel demand to a stabilized or decreasing level, despite the larger distribution of this type of vehicles.

BP [6] also shows great growth in global refining activities in 2017. The world oil refining capacity has increased by 1.7 million barrels per day, more than in the last 10 years. Indeed the global consumption of energy from crude oil is constantly growing reaching 92.649 million barrels per day of oil consumed worldwide and 1.464 million barrels per day of oil consumed in the countries of the European Union.

Transport petroleum products are fundamental for the economy of the oil refining sector, however, crude oil products cover a wider class of markets. Solvents produced by aromatic compounds are a product for various industrial applications: development of protective coatings, ink and varnish production industries, etc... Petroleum waxes originate from paraffin compounds and are mainly used as waterproofing agents in the pulp or paper industry and are also sold as electrical insulation. In addition, lubricants are an important source of income for the refining industry. Concerning the use of the heavier fraction, bitumens play a leading role in the road construction industry; while the lighter fraction of the distillate as naphtha is used for the production of ethylene and propylene used as raw material in the plastics industry. It is easy to see how refining products cover different market areas and represent a source of income in each of them. As a result, the growth of the refining industry is driven by the growth of related markets, so it is important to lead the development of the refining industry by introducing advanced technologies to improve energy conversion and reduce environmental impact.

It is also interesting to mention the point of view of the *IEA* [2] (International Energy Agency) which proposes two possible scenarios, based on greater energy sustainability.

The demand for oil in 2018 has increased constantly but less than forecast by *IEA*. The main source of growth in consumption has been the United States despite the continuous increasing in the number of electric vehicles. The main increment in demand for oil products were driven by gasoline and diesel, but also by ethane, liquefied petroleum gas (LPG) and naphtha; this is mainly due to the use of oil in the petrochemical industry as a raw material. It is important, in order to choose the right investment, to predict how the demand for oil will be in the coming years.

The World Energy Outlook [53], a report prepared annually by the *IEA*, defines two possible scenarios considering current energy policies. Many countries, including ten *OPEC* Member Countries, have ratified the Paris Agreement. In the road transportation sector, fuel quality and vehicle emissions standards continue to evolve in major consuming regions. We remember that *OPEC* is a permanent intergovernmental organization of 13 oil-exporting developing nations that coordinates and unifies the petroleum policies of its Member Countries. Although the US is relaxing Corporate Average Fuel Economy (*CAFE*) standards, the European Union, China, and India are continuing to increase fuel economy and vehicle

emissions standards. Also the incentives on electric vehicles are under discussion. This could shift demand against thermal ones.

The World Energy Outlook [53] defines a series of paths. In the stated policies scenario, demand growth is strong until 2025, but slows down until demand reaches 106 mb/d in 2040. In the sustainable development scenario demand reaches peaks quickly and drops to less than 67 mb/d in 2040.

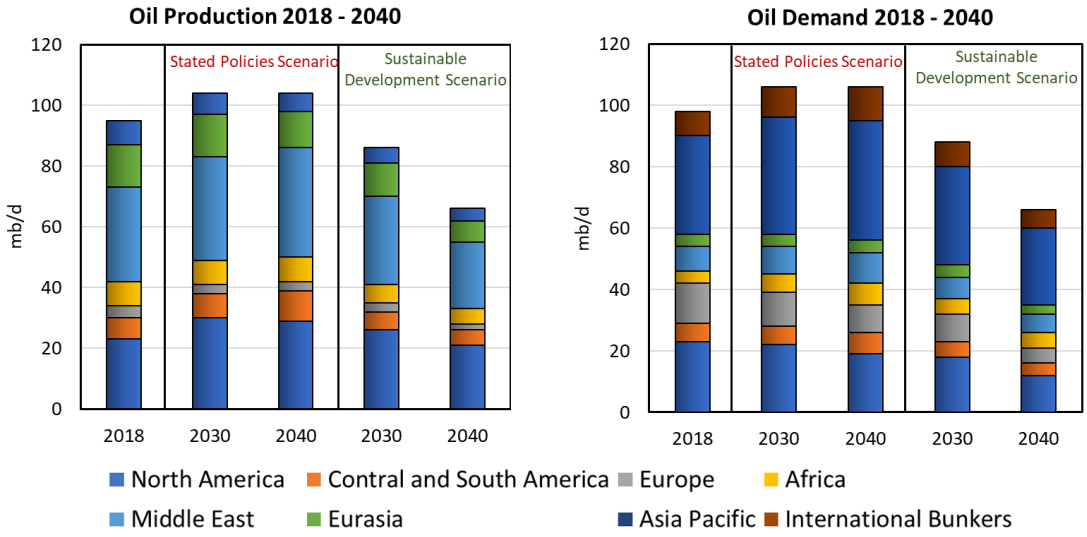

Figure 1.6 Oil production and demand adapted from World Energy Outlook of IEA [53] International bunkers represent consumption of ships and aircraft on international routes.

In the **Stated Policies Scenario** [53], global oil increases by about 1 mb/d on average each year until 2025. Oil use in passenger cars reaches its peak at the end of the 2020-2030 decade and in 2030 demand increases by an average of only 0.1 mb/d per year. Overall, there is no definitive peak in oil use, as there are continuous increases in the petrochemical, heavy duty vehicle, maritime and air transport sectors.

In the **Sustainable Development Scenario** [53], certain policy interventions lead to a peak in global oil demand in the next few years. Demand falls by more than 50% in advanced economies between 2018 and 2040 and 10% in developing economies. Particularly significant is the reduction in the use of oil in road transport. In 2040, 50% of cars are electric like most city buses; nearly 2 million barrels of oil equivalent (mboe) per day are consumed in aviation and shipping and almost 20% of the fuel used by heavy duty vehicles worldwide is low carbon. The only sector to see the growth in demand is the petrochemical sector: while the recycling rate of plastics has more than doubled (from about 15% today to 35% in 2040 [53]), demand for oil as a raw material still increases by almost 3 mb/d until 2040.

1.2 Greenhouse effect and climate change

Carbon dioxide is, together with water, the base product of any oxidation reaction conducted with fossil fuels. This chemical species is not considered as a harmful gas since it is naturally present in the environment without any limitation or damage to humans but is classified as a climate-altering gas. CO_2, in fact, is one of the main authors of the greenhouse effect, i.e. the phenomenon that involves a decrease in heat radiation from the earth's surface to space caused by the presence of gaseous species, such as carbon dioxide, which have a greater capacity to absorb radiation in the infrared spectrum. Part of the energy that the earth reflects and tries to dissipate towards space is therefore captured and contributes to determining the thermal level of the earth. If in itself this phenomenon is indispensable to guarantee conditions suitable for life, with the industrial era and the increasing use of fossil fuels, humans have begun to release more and more important quantities of CO_2 into the environment, which is such as to condition and modify the Earth's temperature control behaviour, with clearly observable consequences. In the international scientific community it is now widely accepted that human influence leads to changes in the climate system; anthropogenic greenhouse gas emissions are the highest ever and this affects the lives of animals including humans and the earth (global warming, rising ocean levels, decrease in perennial snows). Finally, the land-use makes another important but minor contribution to the increase in atmospheric carbon dioxide concentration (figure 1.7).

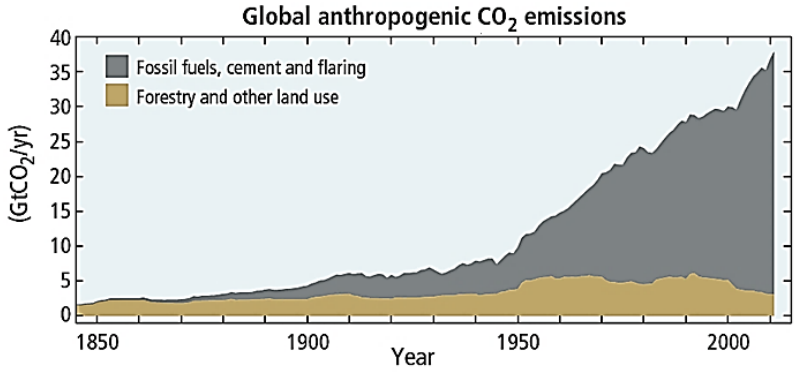

Figure 1.7 Global anthropogenic CO_2 emissions from forestry and other land use as well as from burning of fossil fuel, cement production and flaring [8]

Over time, the amount of CO_2 has changed continuously and cyclically, without ever exceeding 300 ppm. Today (updated to 2019) we have exceeded 400 ppm. In fact, the last time the amount of CO_2 in the atmosphere was so high was more than 3 million years ago, when the temperature was 2-3°C higher than in the pre-industrial era, and the sea level was 15-25 meters (50-80 feet) higher than today[7].

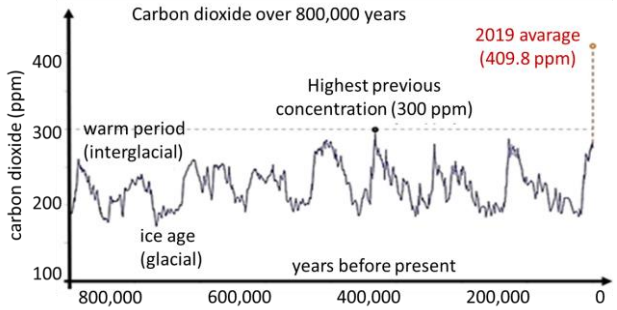

Figure 1.8 Global atmospheric carbon dioxide concentrations in parts per million (ppm) for the past 800 000 years [7]

It is important to underline that carbon dioxide as CO_2 equivalent includes all those gases that are considered to have a greenhouse effect (mainly water vapor, methane, nitrous oxide, hydrofluorocarbons and carbon dioxide). For example, compounds such as CH_4 or N_2O have a higher greenhouse effect than carbon dioxide but have a lower concentration in the atmosphere. According to a research of the IPCC [8], between 1750 and 2011 the cumulative anthropogenic CO_2 emissions into the atmosphere were 2040 ± 310 Gt CO_2. About 40% of these emissions remained in the atmosphere while the rest was removed and stored on land (in plants and soil) and in the ocean. The ocean absorbed about 30% of the anthropic CO_2 emitted, causing its acidification, one of the dangers due to global warming. In the 200 years since the beginning of the industrial revolution, the pH of surface oceanic waters has dropped by 0.1 pH unit; this does not seem much, but the pH scale is logarithmic, so this change represents about 30% increase in acidity. If the CO_2 in the atmosphere increases, then the amount absorbed by the oceans increases and therefore acidification of the water increases: all these facts will lead to damage of the marine ecosystem. There is also other unequivocal evidence that makes climate change visible. The first evidence is the increase in the global average temperature (figure 1.9). As reported by research conducted by the IPCC [8] (Intergovernmental Panel on Climate Change that is the United Nations body for assessing the science related to climate change), each of the last three decades has subsequently been warmer (on the Earth's surface) than any previous decade since 1850. The period from 1983 to 2012 was most likely the hottest 30-year period in the northern hemisphere in the last 800 years, where such an assessment is possible [8].

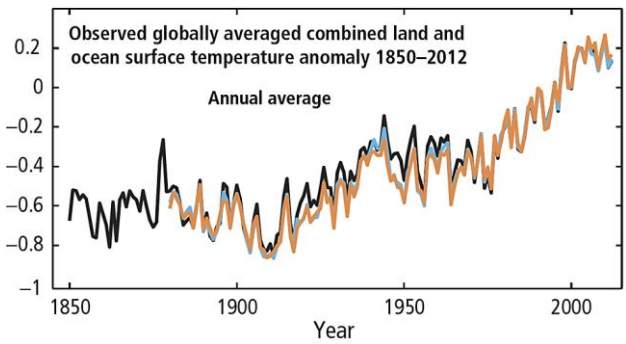

Figure 1.9 Observed globally averaged combined land and ocean surface temperature anomalies [8]

It is very likely that regions of high surface salinity, where evaporation dominates, have become more saline, while regions of low salinity, where precipitation dominates, have become fresher since the 1950s. These regional trends in ocean salinity provide indirect evidence for changes in evaporation and precipitation over the oceans and thus for changes in the global water cycle [8] During the period 1901-2010, the global average sea level increased by about 0.19 meters. The rate of rise in water levels since the mid-19th century has been higher than the average rate of the previous two millennia.[8] In the last two decades, the Greenland and Antarctic ice caps have lost mass. Glaciers have continued to reduce almost all over the world, and the spring snow cover of the northern hemisphere has continued to decrease. [8] In its report, the IPCC presents several possible scenarios on the evolution of CO_2 emissions. Most of them have catastrophic consequences by 2100 if no further mitigation efforts are made beyond the current ones: warming is more likely to exceed pre-industrial levels by 4°C. Risks associated with temperatures of 4°C and above include the extinction of substantial species, global and regional food insecurity and the consequent constraints on common human activities. It is clear that the problem must be taken into account seriously.

1.3 Effect of COVID-19 on energy consumption and CO_2 emissions

The coronavirus pandemic caused an unexpected macroeconomic shock. Today (data update at August 2020), the *World Health Organization* has recorded more than 20 million confirmed cases of the virus. To slow the spread of the virus, governments around the world have imposed restrictions on most social and economic activities in March and April. These include partial or complete isolation, lockdown, closure of educational institutions and non-essential businesses, and a ban on public meetings. As we said, in addition to the immediate impact on health, the current crisis has brought serious implications for the global economy, energy use and CO_2 emissions.

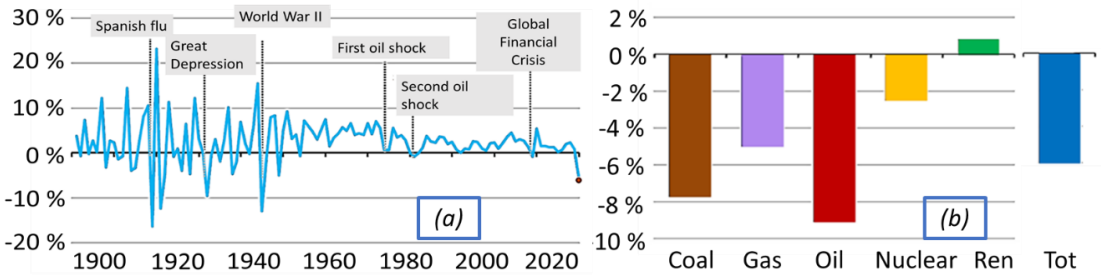

Figure 1.10 (a) Rate of change in global primary energy demand, 1900-2020; (b) projected demand by fuel in 2020 relative to 2019 [10]

It is therefore interesting to study the variation in energy demand in March and April, a period marked by a total lockdown and we will do so by reporting an analysis conducted by the *IEA* [10]. The data observe that in this period the share of energy exposed to containment

measures to slow down the virus represents 50% of the total. This analysis shows that countries in total lockdown have experienced an average weekly drop of 25% in energy demand. It is clearly visible from figure 1.10 that periods of economic crisis correspond to a decrease in global energy demand. All of this leads to a decrease in energy demand for all sources except renewable technologies, which were the only ones to record growth, driven by increased installed capacity and priority dispatch, as can be seen in figure 1.10.

1.3.1 CO_2 emission

The dramatic fall in energy demand in the first quarter of 2020 has led to a significant decrease in global CO_2 emissions, overcoming any previous decline (figure 1.11). Global CO_2 emissions were more than 5% lower in the first quarter of 2020 than in the first quarter of 2019, mainly due to a drop of 8% in coal emissions, 4.5% in oil and 2.3% in natural gas. CO_2 emissions fell more than energy demand, as more carbon-intensive fuels experienced the biggest drop in demand in the first quarter of 2020. CO_2 emissions decreased most in the regions that suffered the first and greatest impacts of Covid-19; China (-8%), the European Union (-8%) and the United States (-9%) [10]. Global CO_2 emissions are expected to fall even faster in the remainder of the year, to exceed 30.6 Gt by the end of 2020, almost 8% less than in 2019. This would be the lowest level since 2010. This shows a serious fact: we were able to reduce CO_2 emissions only by reducing production activities. Technological progress towards a decarbonised society has still a long and difficult task ahead of us.

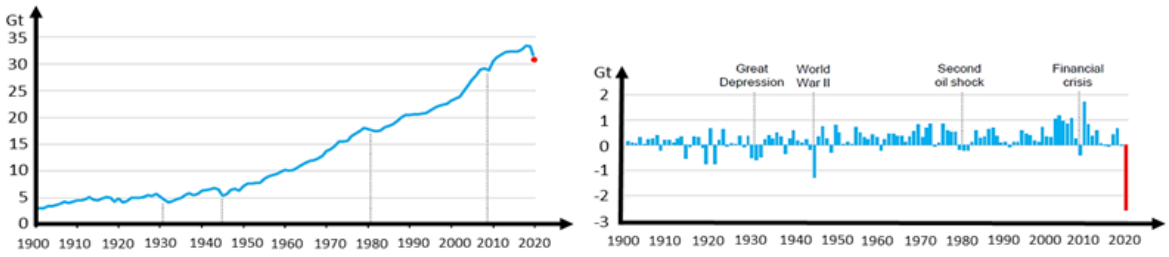

Figure 1.11 Global energy-related CO2 emissions and annual change, 1900-2020 [10]

1.3.2 Oil

As a result of lockdown, mobility (57% of global oil demand) has experienced an impressive decline. Road transport in regions where blocking measures are in place fell between 50% and 75%, with average global road transport activity decreasing to almost 50% of its 2019 level by the end of March 2020. Air transport in some regions has almost stopped, with aviation activity in some European countries falling by more than 90%. Following the drop in mobility, in March, world demand for oil fell by 10.8 mb/d year on year. Activity in China showed a slight recovery compared to the minimum levels at the end of February, as the lockdown were slightly mitigated.

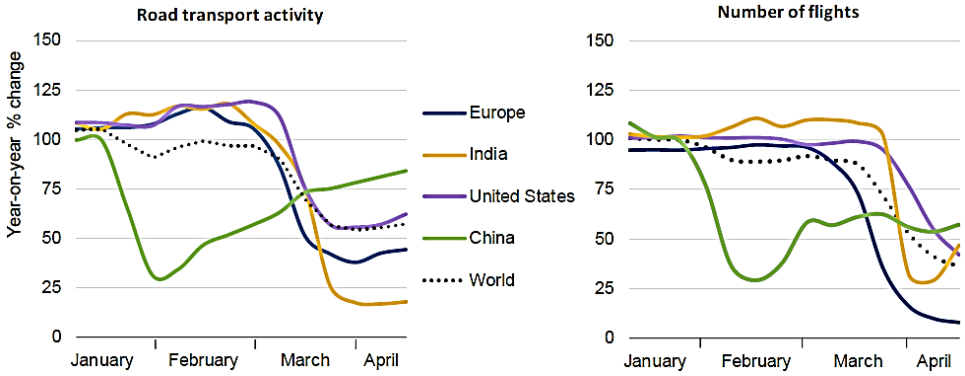

Figure 1.12 Evolution of road transport and aviation activity in 2020 relative to 2019 [10]

Gasoline is the fuel with the greatest absolute drop in demand related to the Covid-19 measures to contain it. In the days following the introduction of lockdown road traffic decrease dramatically (figure 1.12). In France and the UK, for example, demand for petrol fall down by 70% during the lockdown. Similarly, diesel also sufferes a decrease of 1.5 mb/d due to lower economic activity and restrictions on rail and bus transport. The Covid-19 containment measures also reduce demand for other oil products, such as LPG, ethane, naphtha and residual fuel, but the impact will probably be less acute than for petrol, diesel and jet fuel. All this lead to a change in price that become for the first time negative. Demand for some petrochemical products is increased due to increased demand for packaging and personal protective equipment. Finally, it is important to point out that, despite the recent COVID-19 epidemic, the oil sector will continue to be importance in the world economy in the coming years. As underlined by a survey conducted by *McKinsey "However, under most scenarios, oil and gas will remain a multi-trillion-dollar market for decades. Given its role in supplying affordable energy, it is too important to fail"* [9].

1.4 Conversion process

Refining processes are important to convert high-energy crude oil into a cleaner and more exploitable resource. Crude oil is separated into finished or into intermediate products for the petrochemical industry. In this conversion, primary energy is needed to operate almost all the refinery plants and conduct the transition of raw materials to final products. Part of the whole energy content of the crude oil is then used to obtain the required energy and consequently part of the input charge is not converted into final output. The first phase consists of charge processing operations such as desalination of the crude oil and preheating of the charge and removal of the water content. Only at this point the incoming charge is ready to be processed in the main unit of the plant. In the atmospheric crude oil distillation unit the mixture is distilled into lighter and heavier fractions depending on the final volatility of the compounds. Subsequently, the different oil fractions obtained are treated in specific plants, which allow the crude oil yield to be modified both in quantity and quality according to the different market requirements. Support operations are useful to guide the entire conversion system even if they are not directly involved in the main conversion process.

Electricity, high or low pressure steam, process heat and many different resources required by the refinery facilities are provided by the support operating units. Different kinds of refineries will be discussed in section 1.6.

1.5 European refining sector

Considering the latest statistical report of the *FuelsEurope* website [15], figure 1.13 shows where the main European mainstream refineries with a capacity above 30 000 bbl/d are located. They are 81 with a total refining capacity of about 681.5 million tonnes per year. In the last decade, many European refineries have been phased out due to the contraction of oil demand in the country. Having a production of refinery products of 642 million tons per year against a demand of 639 million tons per year, the market balance in Europe is satisfied by exporting refined products.

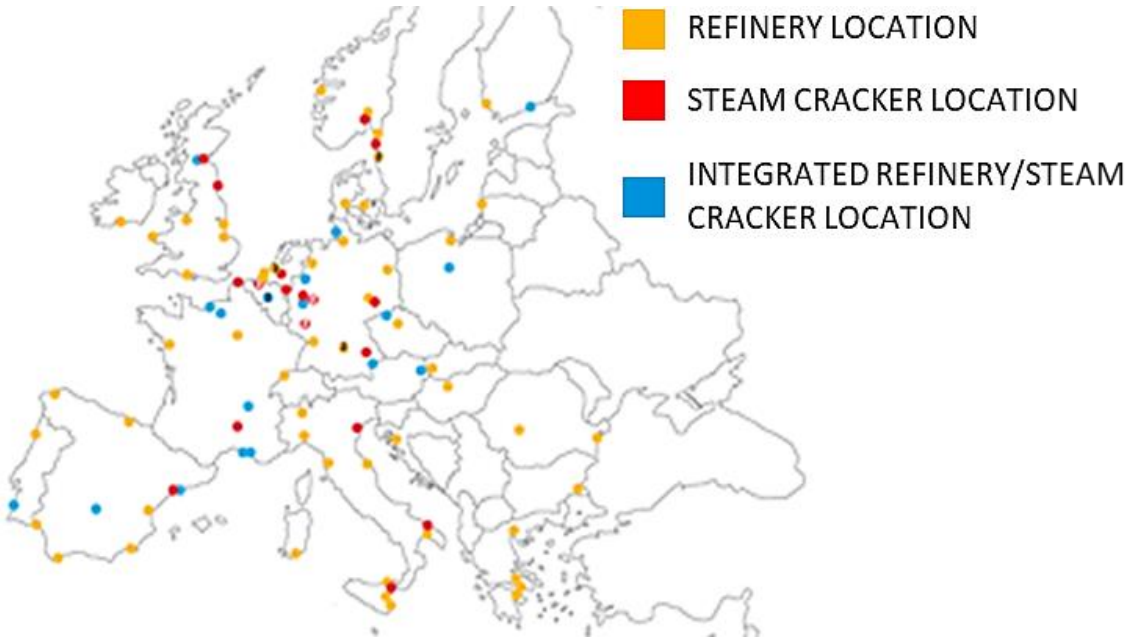

Figure 1.13 Refinery/Steam Cracker sites in Europe [15]

Figure 1.14 shows the main European refineries with a capacity exceeding 30 000 bbl/d classified for distillation capacity. It can be observed that most of the oil refining plants are of average size of about 200 000 bbl/d.

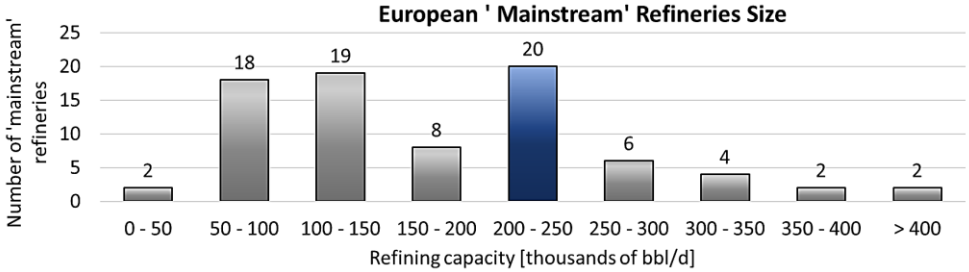

Figure 1.14 European average refineries size. [15]

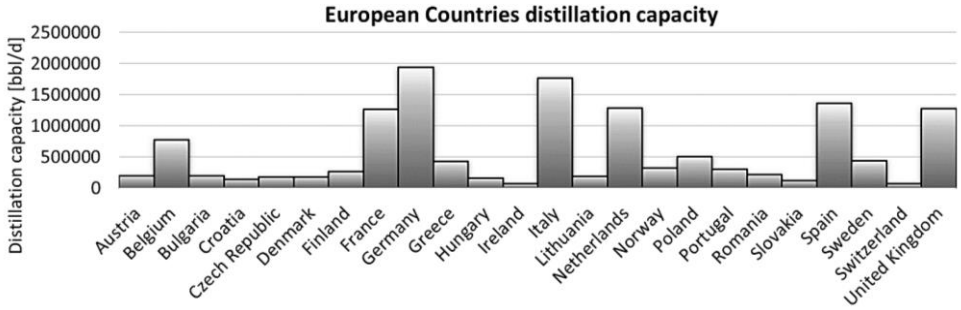

Figure 1.15 European Countries average refineries distribution [15]

Refineries with a medium/high distillation capacity are usually located along the coastal areas of the North Sea or the Mediterranean Sea because the refining activities require a lot of cooling or process water to function properly; moreover they must be built in sites where you can have a good supply of raw materials and you can easily export the refined products. Figure 1.15 shows how refining capacity is distributed in European countries.

1.6 Refineries technology

Going into the detail, we will illustrate the main plant schemes in which refineries can be classified and we describe the main process units of the plant

1.6.1 Refineries type and complexity

In the world there are different types of refineries with different grades of complexity according to different levels of conversion and precise specifications. A generic refinery plant is characterized by several units called process units that can be divided into [16]:

- Separation Unit (Distillation)
- Conversion Unit (Cracking)
- Units to improve the quality of some fractions
- Undesirable components removal unit
- Lubricant oil production unit

All refinery facilities have at least one atmospheric distillation column (CDU). This unit treats all the crude oil in feed and divides it into various fractions according to the different boiling temperatures. It is a very complex unit since it generally also includes the desalination of crude oil and has a series of thermal recoveries. In addition to the atmospheric distillation column there is also a vacuum distillation column (VDU) in order to fractionate also the heavy residue coming from the CDU without a further increase in temperature that would cause an uncontrolled breaking of the heavy hydrocarbon molecules (Cracking). Below we describe the main refinery processes. First of all, we underline how the conversion units are typically both thermal (Visbreaking, Coking and Thermal cracking) and catalytic

(Catalytic cracking and Hydrocracking). Both have the purpose to treat the heavier fractions obtained from vacuum distillation to transform them into higher quality fuels and mixtures.

Catalytic Reforming (CRF) is the best known process to improve the quality of distillates; it essentially serves to improve the octane number of the heavier fractions of gasoline such as Virgin Naphtha heavy thanks to the increase of aromatic and isoparaffinic hydrocarbons (branched paraffins).

Isomerisation (ISO) has always the purpose to transform hydrocarbons into isoparaffins but also treats light Virgin Naphtha (C_5 and C_6).

The Alkylation process (ALK) deals with the treatment of Olefins (C_3 and C_4) by transforming them into C_7 and C_8 components branched with a higher octane number. Regarding the removal of undesirable components such as salts, sulfur compounds, nitrogen compounds and metals there is the desalination process for the salts usually placed in the atmospheric distillation column.

Hydrodesulfurization (HDS) operates on both sulfur and nitrogen eliminating them from hydrocarbons and forming hydrogen sulfide (H_2S) which in turn is sent in a Claus process for final conversion into hydrogen. Finally, there is a hydrogen treatment of light distillates to convert mercaptans into less corrosive mixtures.

Lubricant oil production unit are not present in all refineries because their demand is lower than the other products. The purpose of these units is to treat some lateral cuts and vacuum distillation residue with the aim of improving their viscosity, high and low temperature behavior, color and stability.[16]

Considering the work done by *IEAGHG* on refineries [14], in this section will be proposed four basic plant configurations that represent in a simple and schematic way the complexity and types of the most common plants in Europe and in the world. The aim is to illustrate the great diversity existing without referring to a specific case because in reality each refinery is different and its configuration depends on many factors such as process integration, raw materials and their flexibility, products and their mix, unit size, design and control systems.[17] A classification of the plants can be the following:

- Hydroskimming refinery
- Catalytic cracking refinery
- Coking refinery
- High grade conversion refinery

1.6.1.1 Hydroskimming refinery

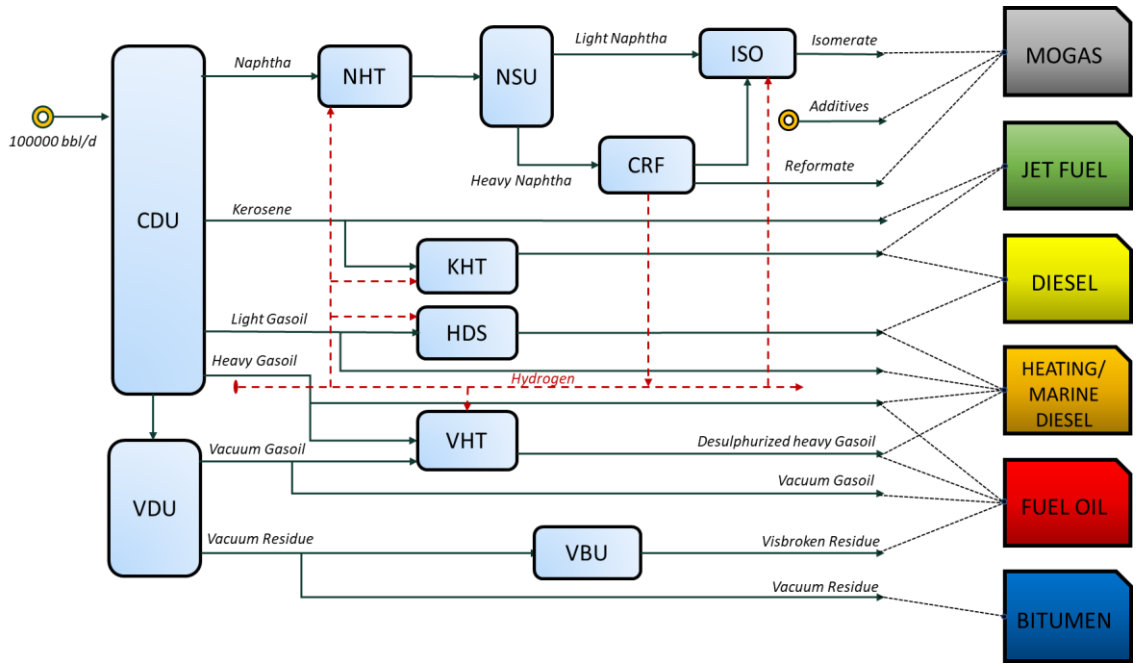

Figure 1.16 Hydroskimming refinery: 100000 bbl/day adapted from CONCAWE - Understanding the cost of retrofitting CO2 capture in an integrated oil refinery [14]. Hydrogen stream red line

Hydroskimming is the simplest type of refinery. It is not very flexible because the production is hardly influenced by the operating conditions of the processing units and the final fuels are mainly fixed by the type of crude oil processed. This type of refinery has been built since the 1950s and 1960s because of the significant increase in fuel demand, low oil costs and huge demand for heavy oils. In the 1970s and 1980s a cracking process was added to many Hydroskimming refineries. Figure 1.16 shows the solution of a Hydroskimming plant proposed by *IEAGHG* [14]. It requires 100 000 bbl/d of raw material entering an atmospheric and vacuum distillation unit respectively CDU and VDU where the crude oil is fractionated into aerial products such as Naphtha, Kerosene, Light and Heavy Diesel. Unstabilized Naphtha is passed into an NHT hydrotreatment unit to make it suitable for downstream catalytic reforming (CRF). The hydrotreated flux is divided into a light and a heavy fraction. Concerning the light fraction there is an isomerisation unit (ISO) that increases the octane number by 20 - 25 times, compensating the loss due to lead elimination; while the heavy fraction is enhanced in the Catalytic Reformer and the H_2 of the reformer is exploited for the desulfurization of Diesel and Naphtha. Saturated light hydrocarbons from CDU, ISO and CRF are sent to the gas plant. The straight cycle kerosene is treated in a hydrotreatment unit (KHT) and is used as jet fuel and a part of the kerosene treated with hydrogen is used as a blending component for the diesel pool. The fuel is in turn desulfurized by an HDS process. Mixing the desulfurized diesel fuel with domestic diesel fuel produces heating fuel oil and marine diesel fuel. Finally, the heavier fractions from the VDU are processed in a VBU Visbreaker unit which allows the structure of the hydrocarbons to be modified in order to control the viscosity to produce fuel oils. [17]

1.6.1.2 Catalytic cracking refinery

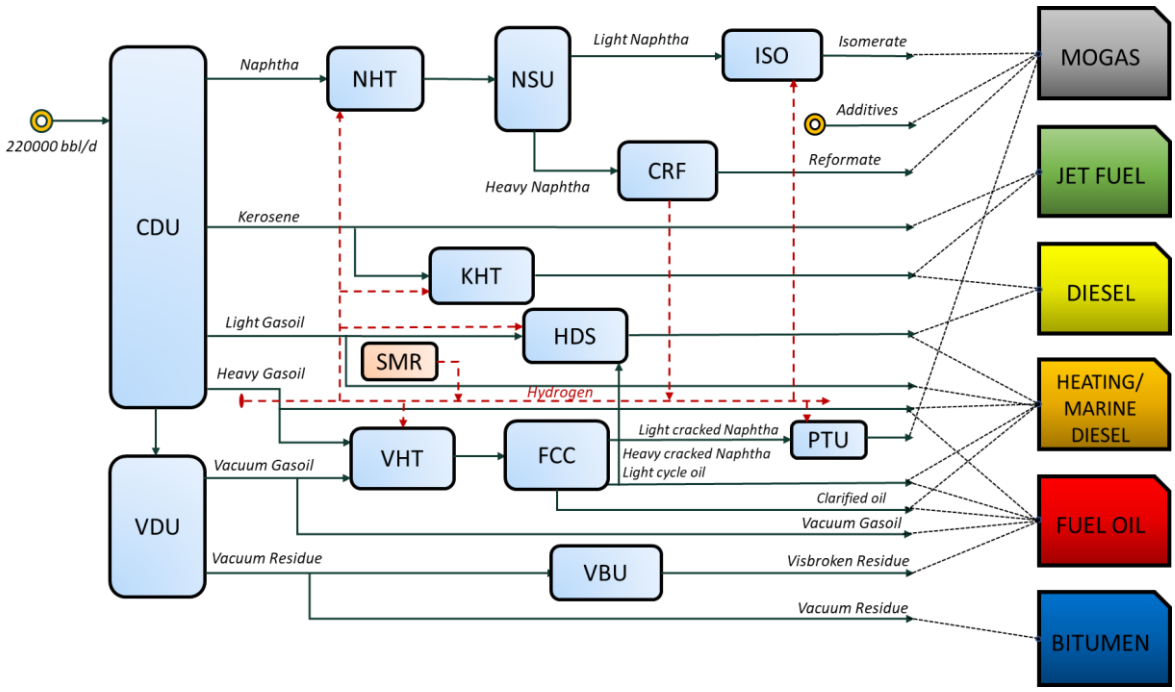

Figure 1.17 Catalytic cracking refinery: 220000 bbl/day adapted from CONCAWE - Understanding the cost of retrofitting CO2 capture in an integrated oil refinery [14]. Hydrogen stream red line

The catalytic cracking refinery is the most present type of refinery in Europe and is the evolution of a hydroskimming refinery. In fact, this last configuration in the 70s and 80s was extended with a fluid catalytic cracking (FCC) unit. In this refinery configuration, much of the atmospheric residue is converted into lighter fuel components, thus reducing fuel oil production. The FCC unit was introduced to increase the production of gasoline and middle distillates. This type of plant has greater flexibility than Hydroskimming because fuel production can be affected by changing operating conditions of the different units [17]. The typical refinery layout is shown in figure 1.17. Unlike Hydroskimming, the VHT product is no longer used completely to make middle distillates but undergoes a cracking process in which long hydrocarbon molecules are broken to form new lighter molecules by means of a fluid catalyst flowing between the reactor and the regeneration zone. After the fluid catalytic cracking, the light naphtha produced is sent to the PTU post treatment unit to reach the sulphur concentration constraints without lowering its quality and the heavy naphtha from the cracking is sent to HDS as a component of the medium distillate or blended with light cracking oil. Due to the high number of processes using hydrogen and the larger size it was necessary to introduce a steam methane reforming SMR to meet the H_2 demand of the plant.

1.6.1.3 Coking refinery

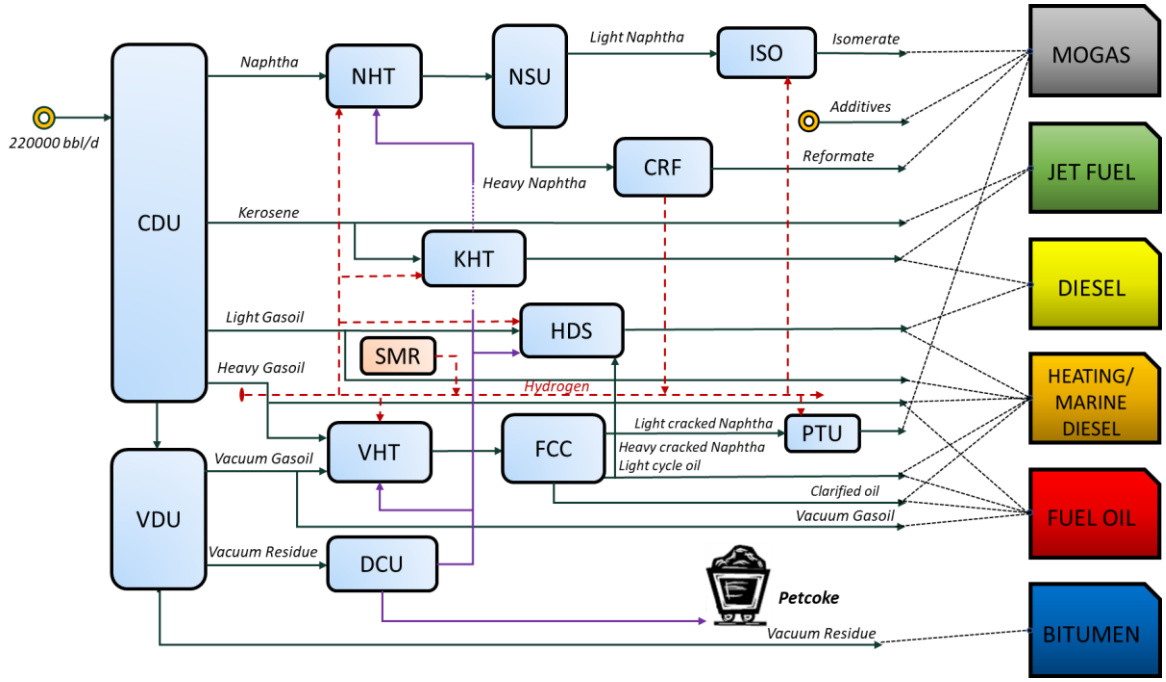

Figure 1.18 Coking refinery: 220000 bbl/day adapted from CONCAWE - Understanding the cost of retrofitting CO2 capture in an integrated oil refinery [14]. Hydrogen stream red line

Concerning Coking refinery, it is basically a catalytic cracking plant and the addition of a delayed coker unit (DCU) to better treat the vacuum residue and recover even more light compounds together with a reduced production of residual fuel oil. Figure 1.18 shows the typical layout of a coking refinery with 220 000 barrels of treated crude oil per day. The coking process is basically a thermal cracking with a longer residence time of the products before cooling: in fact the term “delayed” is attributed to the fact that the coking reaction is delayed until the heated charge is transferred to the appropriate chambers, where the necessary residence time for the reactions is provided.[18] The DCU then converts the heavy residues into lighter fractions and produces petroleum coke. The last product is sold because, depending on its quality, it is used in cement works, steel mills or in the aluminium industry. [17] This type of refinery is more flexible in relation to the maximum production of gasoline or middle distillates, while in contrast to a catalytic cracking plant it is focused only on the increase of gasoline. From DCU the lighter products, except coke, are sent to other processes such as VHT which produces light middle distillates, HDS which produces marine and transport diesel and NHT which produces light distillates and gasoline. Also, in this case it becomes necessary to have a conspicuous production of H_2 for all the treatments and therefore the plant is supported by an SMR.

1.6.1.4 High grade conversion refinery

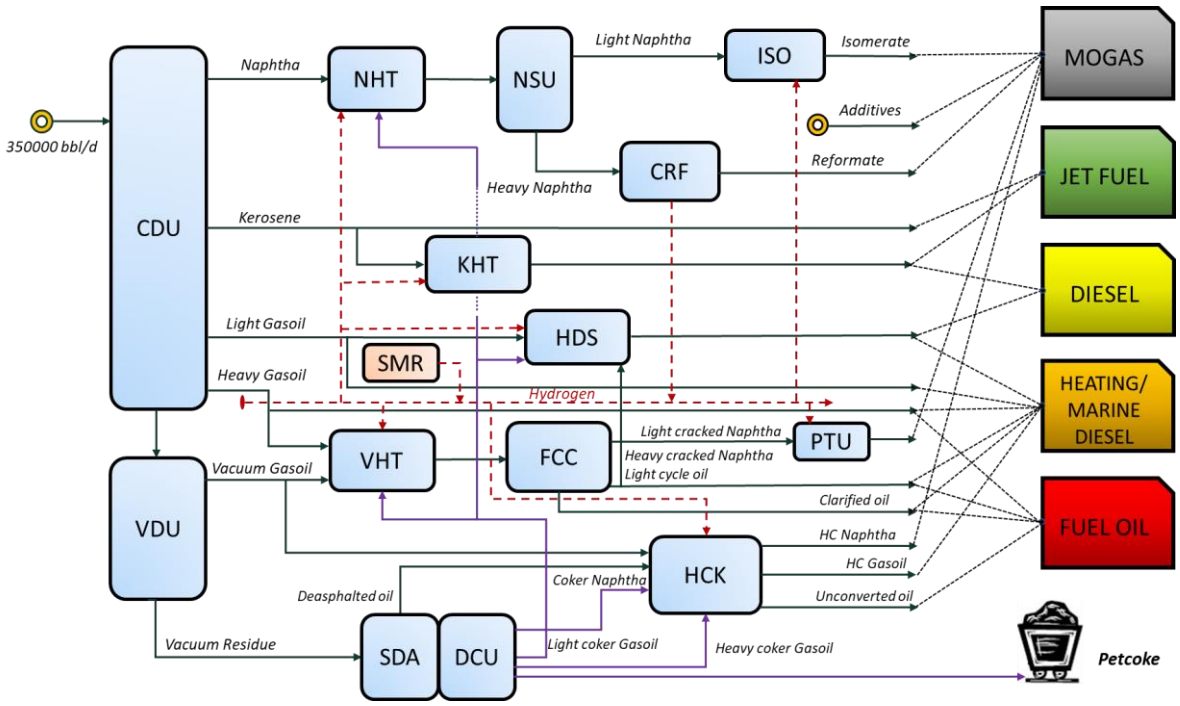

Figure 1.19 High grade conversion refinery: 350000 bbl/day, adapted from CONCAWE - Understanding the cost of retrofitting CO2 capture in an integrated oil refinery [14]. Hydrogen stream red line

High grade conversion refinery is the one that allows the highest conversion of vacuum residue into light products. The flexibility is very high, however, due to a higher complexity of the plant. Figure 1.19 shows the layout of a high conversion refinery with the capacity to process 350 000 barrels per day of oil. This type of plant is characterized by the presence of two additional treatment units compared to a Coking refinery; a solvent deasphaltation unit (SDA) to increase the production of nobler light distillates and the hydrocracker unit (HCK) that helps to break the long hydrocarbon molecules by making them react with hydrogen from an SMR plant. HCK is mainly supplied with deasphalted products, heavy coker naphtha, heavy coker gasoil and a part vacuum gasoil and, once the lighter products are treated, they increase the production of Mogas, marine diesel and fuel oil. SDA is a separation process of hydrocarbons based on their different solubility in solvents which are usually light paraffinic molecules from propane C_3 to pentane C_5. The choice of solvent depends on how many light products you want to separate, usually the solvent with lower molecular weight dissolves less residue because it dissolves only those substances with the lowest boiling temperature; to push more the conversion instead you have to use solvents with a higher molecular weight such as pentane.[19] In this configuration the consumption of H_2 and electrical energy is increased compared to the simpler plant for this reason some high conversion refineries adopt the gasification of coke and waste components of the vacuum residue integrated with a combined cycle. [17]

1.7 Refinery greenhouse gases emissions

Considering *Concawe* article of 2017 [20] European refineries produce about 7% of CO_2 emissions in Europe, emitting 130 million tons of CO_2 per year against 1.8 billion tons of CO_2 per year produced by all other industrial sectors. Concerning the US situation, from the graph of figure 1.20, in 2017 American refineries produce 6.1% of the country's GHG emissions.

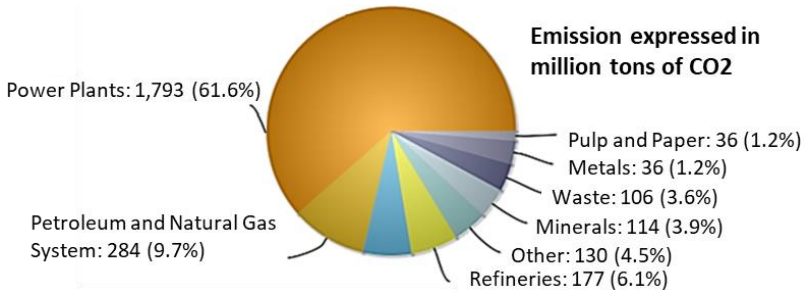

Figure 1.20 U.S. GHG emissions by industrial sector for US situation [21]

Globally, it has been estimated that refineries produce about 6 % of global stationary emissions. It is sufficient to consider that a large-scale refinery (300 000 bbl/day capacity) produces between 0.8 and 4.2 million tons per year. Although it is difficult to have precise estimates because emissions depend on several factors such as the quality of the processed crude oil, the amount of processing, the quality and composition of the product mix [22]. It can be observed that GHG emitted to this type of sector are still quite relevant in the industrial landscape. The graph from *Concawe* [20] (figure 1.21) shows that over the years European CO_2 emissions due to this sector have decreased by 20% since 2007 and this may be associated with the closure of some plants and the improvement of existing ones.

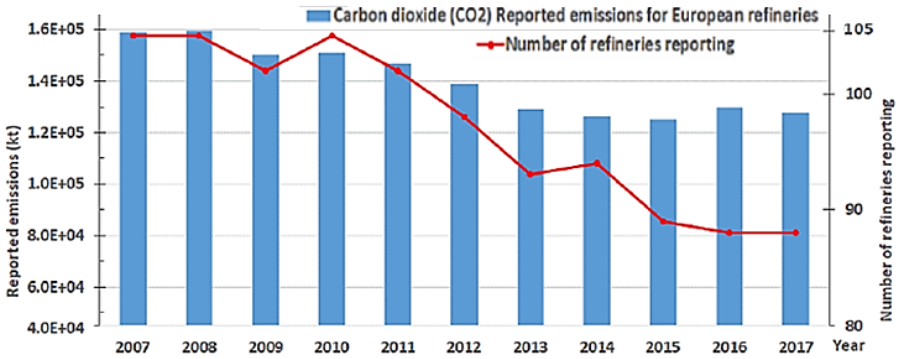

Figure 1.21 Trends of CO_2 emissions reported for European refineries, during 2007-2017, data from E-PRTR [20]

The refining industry has many distributed sources of CO_2, each flow of flue gas arriving from the process units has a substantial climate altering impact. Table 1.1 lists the unit refinery processes and how they produce emissions. Gas or oil heaters are applied in almost all refinery process units in order to preheat the incoming charge or provide thermal energy for distillation columns, boilers or chemical reactors.

CO_2 Refinery Emitters	
Unit Processes	CO_2 Source
Power and Steam unit	Refinery Fuel Gas Heater
Steam Methane Reformer	PSA Offgas + Natural Gas Heater
Fluid Catalytic Cracker	Coke burn off for catalyst regeneration
Crude Distillation Unit	Refinery Fuel Gas Heater
Vacuum Distillation Unit	Refinery Fuel Gas Heater
Catalytic Reformer	Refinery Fuel Gas Heater
Hydrocracker	Refinery Fuel Gas Heater
Delayed Coking Unit	Refinery Fuel Gas Heater
Solvent Deasphalting	Refinery Fuel Gas Heater
Vacuum Hydrotreater	Refinery Fuel Gas Heater
Diesel Hydrotreater	Refinery Fuel Gas Heater
Naphtha Hydrotreater	Refinery Fuel Gas Heater
Kerosene Hydrotreater	Refinery Fuel Gas Heater
Sulphur Recovery Unit	Refinery Fuel Gas Heater
Flaring System	Safety Release of Flue Gases
Auxiliary system	Indirect Emitters
Storage and Equipment	Leakages of Fuel of Flue Gases

Table 1.1 CO2 emission sources [14]

In order to operate all process units in the best possible way, a refinery needs the continuous supply of energy and heat. The necessary energy is given directly or by burning fuel through burners or indirectly through steam. The low, medium and high pressure steam is generated by a power and steam production unit (POW) that is suitably integrated to meet part of the refinery's energy needs, limiting external consumption for the other units, and even selling the surplus energy produced on the grid. Some refineries, however, depend on external power generation plants but still in the vicinity for the import of steam and electricity.[17] Another type of steam and power generation can be a cogeneration cycle (CHP) which, thanks to the increased efficiency of the plant, is able to centralize emissions as much as possible leading to enormous advantages in terms of post-combustion capture.[22] The POW or CHP unit, having therefore an important energy role, are usually the main emitters of CO_2. Another important source of carbon dioxide is the SMR unit to which heat must be supplied to activate the reforming reaction; it uses as fuel either natural gas or offgas from PSA, whose combustion releases a substantial amount of GHG into the environment.

Concerning the fluid catalytic cracker not all refineries have it, but if it is present the emissions of this component can reach even 50% of those of the plant. Differently from the emissions of the other components the production of CO_2 in this case is not related to a real combustion but to the process; in fact, the peculiarity of this cracker is the use of a catalytic converter that during the processing is poisoned by a carbon deposit. In order to regenerate the catalyst, the deposited coke must be oxidized by the air emitting about a concentration of CO_2 in the flue gas that goes from 10% to 20%. [22]

Finally, it is necessary to talk about the flaring system in a refinery. Its purpose is to guarantee both the safety in every dangerous operation of the plant and to discharge the gas that cannot be sold for technical and economic reasons. This process occurs in case of fire, valve breakage or compressor failure or whenever the pressure increases uncontrollably; in this case the system burns and expels the gas to dampen the pressure and ensure safe operations. Flaring represents an inevitable source of CO_2 released with exhaust gases. [23]

Indirect emitters, on the other hand, are auxiliary systems of the refinery that require electrical or primary energy supplied by external suppliers; these systems emit carbon dioxide that is always attributable to the refinery. Finally, there are the emissions derived from the infiltration towards the environment of gases and carbon dioxide due to the leakage of the containers where the gaseous and liquid fuels are stored due to the huge pressure difference between internal and external. The figures below have been adapted from the data of the IEAGHG report [14] and are useful to show the distribution of emission sources in a refinery. In the Hydroskimming refinery the POW unit is the main emitter with 356.2 kton of carbon dioxide emitted per year, or 48.8% of the total emissions of the refinery of 729.4 kton per year. Then the other main emitters are the CDU with 198.1 kton per year, corresponding to 27.2% of total emissions and the CRF with 74.9 ktonn per year with a percentage of 10.3% of the total. Catalytic Cracking Refinery is characterized by higher emissions of 2162.3 kton of carbon dioxide due to the increased distillation capacity and the introduction of FCC and SMR. FCC produces 371.8 kton per year corresponding to 17.2% of the total, CDU 279.4 kton or 12.9% and steam reforming 163 kton per year corresponding to 7.5% of the total.

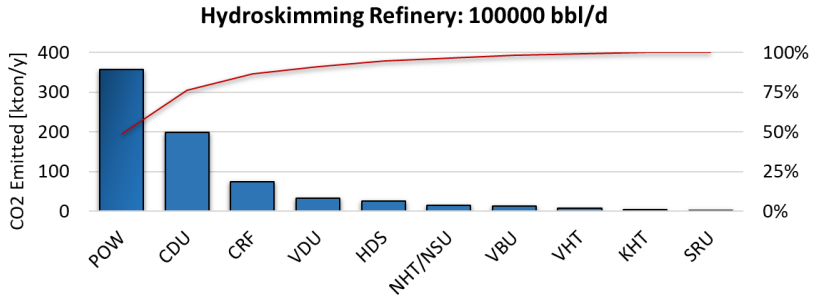

Figure 1.22 Hydroskimming Refinery's unit processes emission, adapted from [14]

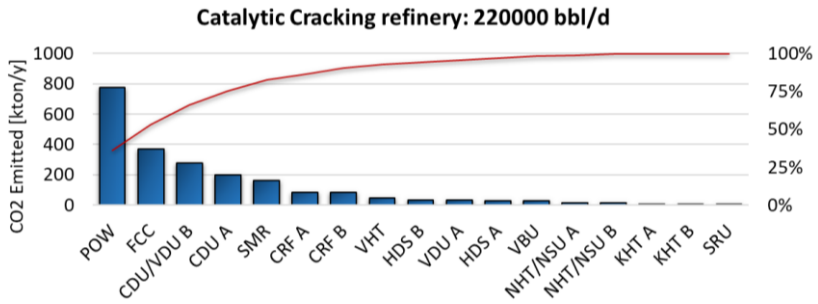

Figure 1.23 Catalytic Cracking Refinery's unit processes emission, adapted from [14]

As regards the coking refinery with the same distillation capacity as the catalytic cracking refinery but with a higher complexity, in this case there is a higher conversion of heavy distillates into light fractions and this inevitably leads to higher emissions of 2334.8 kton per year with a percentage difference of 7.388% compared to the previous case. POW, FCC and SMR emit respectively 667.7 (28.6%), 446.2 (19.1%) and 262 (11.3%) kton of carbon dioxide per year. The emissions of the power plant are lower than the case with catalytic cracking (777 kton per year); this is due to the introduction in the POW of a gas turbine with an HRSG recovery steam generator with an additional flaring system. Part of the electric power is then produced by a 38.3 MW GT and the high-pressure steam is generated by HRSG. Natural gas is fed only to the gas turbine, thus lowering specific CO_2 emissions and increasing the electrical efficiency of the plant [14]. Finally, compared to the previous case, the nominal capacities of FCC and SMR have increased respectively from 50000 bbl/d to 60000 bbl/d and from 22500 Nm^3/h to 350000 Nm^3/h with a consequent increase in emissions. [14]

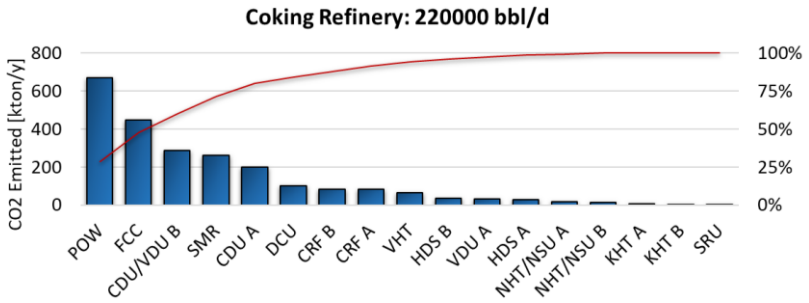

Figure 1.24 Coking Refinery's unit processes emission, adapted from [14]

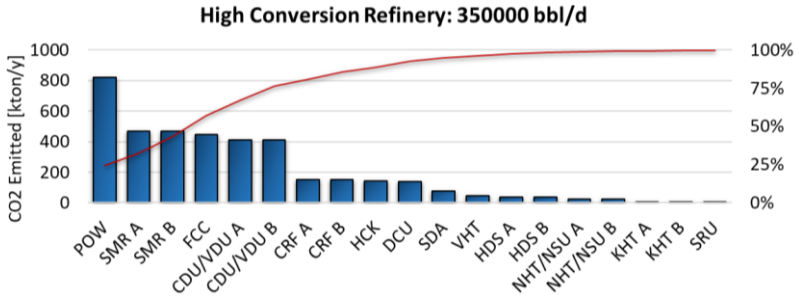

Figure 1.25 High Conversion Refinery's unit processes emission, adapted from [14]

The high conversion refinery with 3870.5 kton per year is the configuration that emits the most carbon dioxide among the four cases. The power generation unit is much larger than the previous configuration, in this case three 45 MWe gas turbines (ISO conditions) operating at 69% load [14] are expected to consume more natural gas producing 18.51% more emissions. Finally, the greater quantity of crude oil treated (350 000 bbl/d) involves a greater quantity of H_2 thus introducing a second steam reforming plant equal to the pre-existing one which in turn produces 467.9 kton of carbon dioxide emitted per year and each unit corresponds to 12.073% of the total.

1.8 European refinery in 2050 – A possible scenario

In this paragraph we present a scenario made by *Concawe* [11]. The European petroleum refining industry is facing a challenging future and action to mitigate climate change is required. The refining industry has started an evolution in order to match this aim but at the same time this industry must continue to satisfy needs of consumers and needs of industries related to its products.

Accordingly, with the report of *Concawe*, the refinery of future will increasingly use new feedstock, such as renewables, waste, and captured CO_2. Also the use of renewables on-site will be maximise and will be an integration with cross-sectoral industries in order to create a cluster. This will be possible thanks to flexibility of refinery infrastructures and this sector will process a variety of feedstocks and deliver a range of products. For example new low-carbon products will serve the main related industrial and civil sector and this fact, accordingly to *Concawe* report, can enhance the competitiveness of the EU economy.

The evolution in refineries will be based on the combination of a wide range of options technically available with the potential to reduce the CO_2 intensity of refinery products. The preferred strategy will to a large extent depend on each individual site because the difference between one each others is very large. Refineries it must be also able to manage the transition and the fuel flexibility where it is limited (e.g. in heavy-duty transport) or high (e.g. for passenger vehicles).

Now we resume the potential pathways toward the transition of the EU refining system. Refineries will find ways to reduce CO_2 emissions through a combination of some possible measures. These can be categorised into three group.

The first group is related to the measures able to reduce the GHG intensity of the production cycle in refineries. These can be energy efficiency, reduction in the burning of liquid fuel, reduction of routine flaring in refineries, use of low-grade heat resulting from refinery operations to produce electricity for internal and external use and closer integration with other industries such as petrochemicals.

The second group is related to external contributions to reduce the GHG intensity of refining. For example, a progressive decarbonisation of electricity system can reduce carbon emission of refinery, this fact can be enhanced with low-carbon production within the refinery. For this fact, some projects can be pursued. For example, the replacement of steam-driven rotating machines and fired heaters with electric ones or the production of hydrogen with electrolysers (green hydrogen) or with carbon capture and storage. Also, can be a valid solution the integration of refineries with the local community, in particular with regard of export steam for district heating. Finally, CCS (Carbon Capture and Storage) and CCU (Carbon Capture and Use) applied to refinery flue gas are valid methods in order to mitigate carbon footprint of sector.

The last group is related to opportunities to reduce feedstock and product with high GHG emission. For example, biomass is recognised as carbon neutral. This offers new potential to process low-carbon feedstocks either in dedicated process units or in combination with fossil feedstocks. The end-products would be high-quality, renewable hydrocarbons, fully running with conventional diesel and gasoline and suitable for use in engines without blending limits. This also make possible the reduction of carbon emissions from road transportation through the quality of fuels and the reduction of carbon emissions by processing waste to produce fuels and feedstock. The waste materials can be also plastic waste and this represents an new opportunity. Figure 1.26 provides a conceptual overview of the refinery of the future.

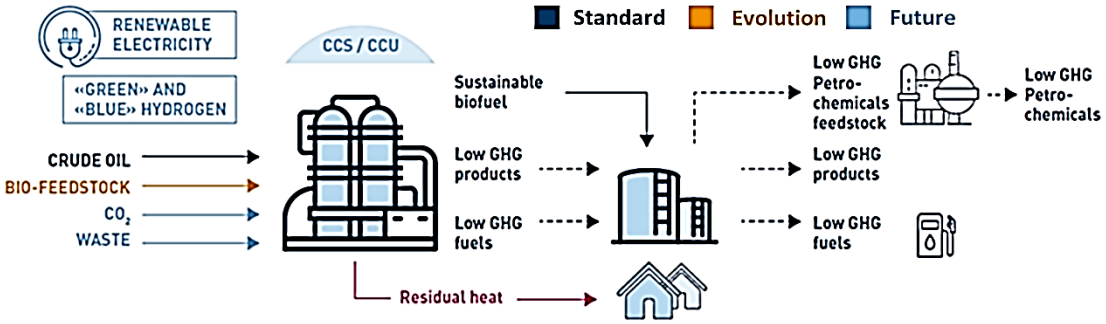

Figure 1.26 Refinery of the future [11]

The EU refining system continues to evolve driving by three different steps.

- Early-stage (low-emission operation): Product mix is oil-based with some low-carbon content in order to meet renewable energy or GHG regulations.
- Evolution (progressive introduction of low-emission components): Progressive transformation of the refinery co-processing low-carbon feedstock or blending higher ratios of new low-emission products.
- Future-stage (hub for production and distribution of low-emission products and raw materials): The refinery of the future will be a very efficient manufacturing center, potentially integrated in a cluster of industries processing and exchanging a variety of feedstocks and semi-finished products. Within these clusters, CCS is foreseen to play a major role to capture and storage remaining CO_2 emissions effectively.

Finally, we report a figure 1.27 that shows how different kinds of waste can be feed into refinery.

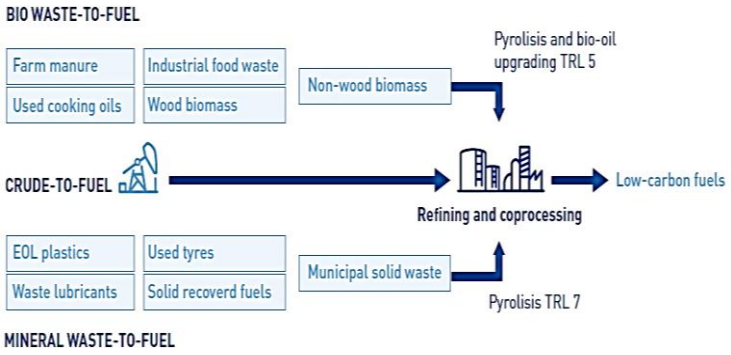

Figure 1.27 Feedstock for refinery of the future [11]

Doing so a CO_2 reduction can be achieved by replacing a share of the crude as feedstock in refineries. For example, using EOL (End Of Life) plastics we avoid emission for incinerator. In addition swapping part of the long-distance crude supply with local transport of plastic waste and residues there is less CO_2 related to transport. Another kind of advantage due to this fact is the low cost and local raw material which implies an easy purchasing. Indeed, availability of plastic waste and residues is about 30.8% of plastics that are sent to landfill.

1.9 Purpose of the thesis

As explained in the paragraph 1.8, refining industry is facing a challenging future and action to mitigate climate change is required. Our purpose is to study an integration system in order to perform a CO_2 capture from SMR and enhance blue hydrogen production. Indeed, as evident in the previous analysis (figures from 1.22 to 1.25) this process is one of the main emitter of GHG in the plant. We analyse a capture system that use molten carbonate fuel cell for carbon dioxide separation and a cryogenic section for the capture. Three different plant layout are under examination: the first assume to feed the cell with natural gas, while the second has offgas of FTR as fuel in anode side and the last, feeding with natural, has fuel recirculation at anode side. Main performance indexes are calculated for the three configuration and a techno-economic sensitivity analysis on cell operating condition is performed in order to assess the best on-design configuration.

At the end, only for the case that guarantee more flexibility a technoeconomic off-design evaluation is made in order to simulate its flexible operation in the production of variable quantities of H_2. The scope is to analyse how this system can be used in order to produce blue hydrogen for market purpose in variable quantities depending on the demand that may have seasonal fluctuations.

Our purpose is to understand how much this retrofit is applicable for decarbonization of the process of hydrogen production.

Hydrogen production 2

This chapter discusses the technologies available today to produce hydrogen from fossil fuels or from renewable sources. As already specified in figure 1.3, most of hydrogen comes from fossil fuels, with over 90 % of the total. Hydrogen is the most abundant element in the universe but it is not present on earth in a significant measure pure and it is found bound either with oxygen atoms to form the H_2O molecule or with carbon atoms in fossil fuels or biomass; for this reason it is necessary to spend energy to make it available.

2.1 Background

Refinery use is one of the two main uses of H_2 in the world. It is largely provided by internal production. However, quick growth requires ever greater quantities obtained from other processes. The other main use of H_2 is the production of ammonia, used for fertilisers, explosives and plastics (polyurethanes, polyacrylates) and methanol (CH_3OH) used for the production of plastics but also for energy purposes (e.g. production of MTBE, used as an additive in petrol to increase its octane number). An analysis conducted by the *IEA* [26] assert how the demand for H_2, which has grown more than three times since 1980 (figure 2.1), continues to grow and consequently its production is responsible for CO_2 emissions of about 830 million tonnes of CO_2 per year, equivalent to the CO_2 emissions of the United Kingdom and Indonesia combined (year 2018).

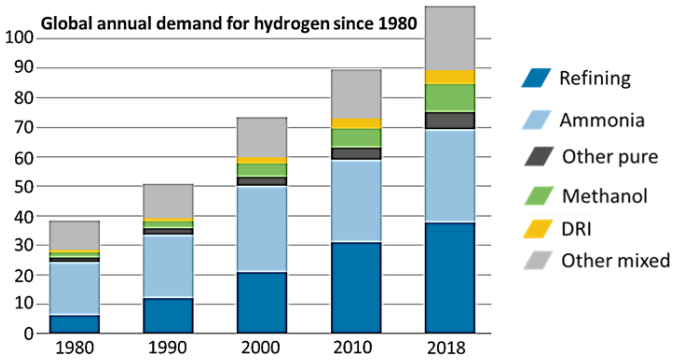

Figure 2.1 Global demand for pure hydrogen, 1980-2018 [26]

This trend is expected to continue in the next years thanks to the use of the energy vector in sectors where it still has very few applications today, such as vehicle power supply (FCEV), hydrogen injection into the gas pipeline, use as a cleaner input for industrial processes, electricity storage and the production of synthetic fuels.

Therefore, the development of technologies to produce low emission hydrogen becomes essential for it to play a leading role in the current energy transition. Currently the reference technology is the reforming of natural gas with high emission intensity, but this path should be abandoned in favour of two main solutions that would allow to reduce the carbon footprint of the process. Coupling of conventional technologies with CCS (Carbon Capture and Storage) or production by water electrolysis. The first solution seems to be the most promising in the short and medium term thanks to the lower costs compared to the second alternative, even if there is a strong interest and research trend on the latter.

2.2 Processes for hydrogen production

Hydrogen can be produced using several different processes that are classified in figure 2.2.

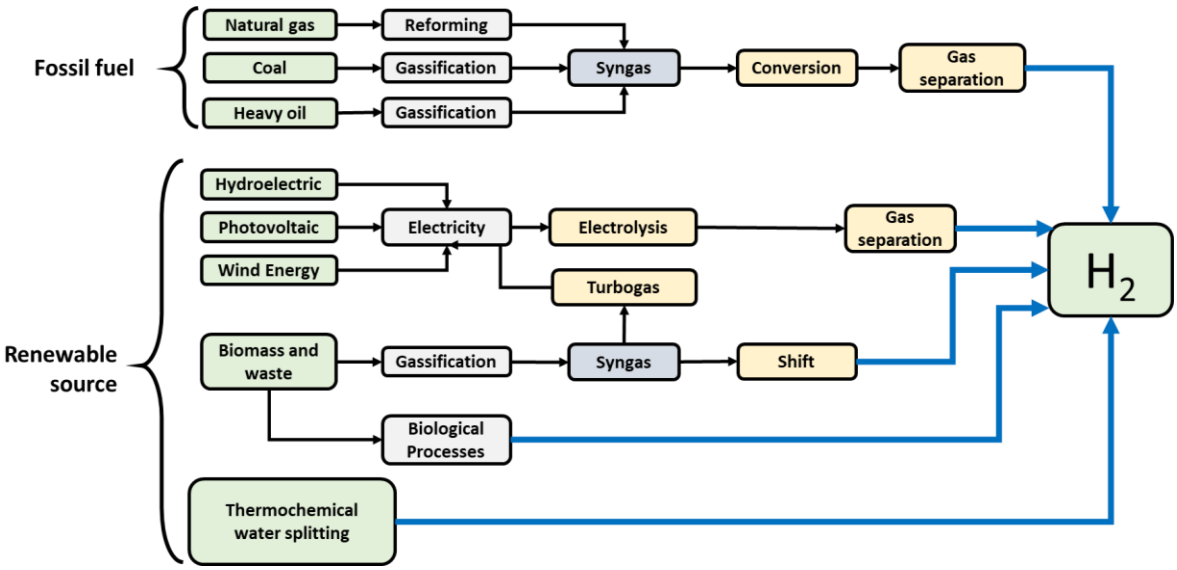

Figure 2.2 Most commonly used methods for the production of hydrogen [30]

Thermochemical processes use heat and chemical reactions to release hydrogen from organic materials such as fossil fuels and biomass. Water (H_2O) can be divided into hydrogen (H_2) and oxygen (O_2) using electrolysis or solar energy. Microorganisms such as bacteria and algae can produce hydrogen through biological processes.

More in detail you have:

Thermochemical processes: some thermal processes use the energy of various resources, such as natural gas, coal or biomass, to release hydrogen from their molecular structure. In other processes, heat, in combination with closed chemical cycles, produces hydrogen from raw materials such as water. They can for example be divided into:

- Natural gas reforming
- Carbon or biomass gasification
- Liquid reforming derived from biomass
- Solar Thermochemical Hydrogen (STCH) [28].

Electrolytic processes: electrolysers use electricity to split water into hydrogen and oxygen. This technology is well developed and commercially available.

Direct solar water splitting processes:[29] direct solar water splitting processes, or photolytic processes, use the energy of sunlight to split water into hydrogen and oxygen. These processes are currently in the very early stages of research but offer long-term potential for sustainable hydrogen production with low environmental impact.

Biological processes: [29] microbes such as bacteria and microalgae can produce hydrogen through biological reactions using sunlight or organic matter. These technological pathways are at an early stage of research, but in the long term they have the potential for sustainable and low-carbon hydrogen production.

The topic of hydrogen production is in itself very wide and complex and a detailed treatment would be beyond the scope of this thesis, so we will describe only the technology of production from natural gas by thermochemical process (in particular reforming with FTR, section 2.3). To understand why reforming hydrogen production technology is the most commonly used, the levelized cost of hydrogen (LCOH) expressed here in €/MWh is reported (table 2.1).

Levelized cost of hydrogen for different technologies		
Technology	LCOH [€/MWh_{H2}]	Reference
FTR + CCS	47.76	[48]
FTR	36.01	[45]
Coal gasification + CCS	68.7	[46]
ATR membrane assisted	46.52	[47]
Biomass gasification	53.1 – 61.5	[49]
Methane pyrolysis	47.72 – 51.2	[49]
Methane decomposition	65.02	[45]
Solar PV Electrolysis	173.5 – 711.3	[49]
Solar Thermolysis	239.5 – 252.1	[49]
Wind Electrolysis	176.8 – 180.9	[49]

Table 2.1 LCOE for hydrogen production

It is therefore clear that FTR technology without CCS is the most cost-effective. In fact, the levelized cost of hydrogen represents the minimum value that the hydrogen produced must have in order to be cost sustainable. Unlike the electricity market, there is not yet a well-formed market for hydrogen that can give an idea of its price. In Italy, for example, the only sales station for H_2 is located in Bolzano where the price is around 11 €/kg_{H2} or a value that corresponds to approximately 330 €/MWh_{H2}. It is true that in such a price includes possible taxes and expenses for transport and storage (in fact H_2 should be stored in liquid form reaching pressures around 70 MPa) but this is useful to make the idea of how FTR+CCS could be convenient when the hydrogen market becomes something well structured.

2.3 Hydrogen production from natural gas

For the production of H_2 from natural gas, mainly steam reforming is used. The technologies to perform it are the following:

- Fired tubular reformer (FTR)
- Auto-thermal reformer (ATR)
- HESR (Heat Exchange Steam Reforming)
- Other technologies (CPO, membranes)

FTR process is considered the main one for the production of hydrogen, in particular for refineries and its production is currently about 200 billion cubic meters per year of hydrogen, of which 35% is used in oil refining (i.e. in hydrotreating, hydrocracking and hydrodesulfurization processes) and 50% for ammonia production, while the remaining 15% is used in methanol synthesis and other industrial processes [14]. So, in this work we will only describe this process for reforming. ATR is an alternative technology to FTR. Usually the discriminating one is the size. The FTR has a more expensive reactor but has no ASU (air separation unit) costs unlike ATR; moreover the reactor is modular, if you want to make a bigger FTR system you have to make more reactors. Cryogenic air separation units that may constitute up to 40% of the plant investment and since they present a sharp scale economy up to 90 000 Nm3/h, it makes the ATR technology convenient for plants with H_2 output greater than 250 000 Nm3/h [35]. In ammonia plants, where air is used as oxidant, ATR may compete also at lower sizes.

Before the introduction of the technologies, we briefly describe natural gas composition and the two main reactions that transform the hydrocarbon into H_2, which are steam reforming and water gas shift.

2.3.1 Steam reforming

It is the main reaction of catalytic reforming and consists of decomposition of hydrocarbons according to the following reaction:

$$C_nH_m + n\,H_2O \rightarrow n\,CO + \left(n + \frac{m}{2}\right)\,H_2 \qquad (2.1)$$

We consider, for simplicity, in our treatment only methane (the most present species inside natural gas). The reaction we have is the following:

$$CH_4 + H_2O \rightarrow CO + 3H_2 \qquad (2.2)$$

It is strongly endothermic (ΔH (298 K) = 206 kJ/mole). It is necessary to provide heat to allow it to react; this heat may come from the oxidation of part of the incoming charge. Being an endothermic reaction, steam reforming is promoted at high temperatures; at atmospheric pressure and with a H_2O/CH_4 = 1/1 ratio at equilibrium, complete conversion is achieved at 900°C. The reaction presented is never totally complete but tends to reach a condition of equilibrium as a function of temperature and pressure. The influence of pressure is well evident by expressing the equilibrium coefficient K_P and remembering that steam reforming takes place with an increase in number of moles.

$$K_P(T) = \frac{P_{CO}\,P_{H_2}^3}{P_{H_2O}\,P_{CH_4}} = \frac{x_{CO}\,x_{H_2}^3}{x_{H_2O}\,x_{CH_4}}\,P^2 \qquad (2.3)$$

Conversion is therefore promoted at low pressure but operating under pressure is necessary to reduce the volume of the equipment and, above all, because many applications require that the gas be pressurized.

2.3.2 Water gas shift reaction

In order to allocate the heating value of CO to H_2, a shift reaction with water is carried out downstream of steam reforming. It can be expressed generically as:

$$CO + H_2O \rightarrow CO_2 + H_2 \qquad (2.4)$$

The reaction is slightly exothermic (ΔH (298 K) = - 41 kJ/mole) and therefore promoted at low temperatures. The pressure has no influence on the process that is equimolar, i.e. the equilibrium coefficient K_P does not depend on it.

2.3.3 Natural gas composition

The raw material used is natural gas, which is a mixture of gaseous hydrocarbons that originate under the earth's surface. NG is considered the cleanest fossil fuel and is a safe source of energy when transported, stored and used. The primary constituent of NG is methane (CH_4) but it also contains other components (HC_{2+}, N_2, CO_2, H_2S, etc.) in variable quantities depending on the area where the fossil fuel is extracted. Below we report a generic mixture of natural gas.

Typical Composition of Natural Gas		
Constituents	Formula	Composition (vol%)
Methane	CH_4	96
Ethane	C_2H_6	2
Propane	C_3H_8	0.6
Butane	C_4H_{10}	0.18
Pentane	C_5H_{12}	0.12
Carbon dioxide	CO_2	0.14
Hydrogen sulphide	H_2S	0.06
Nitrogen	N_2	0.1
Helium	He	0.8

Table 2.2 Natural gas composition. Adapted from Natural gas origin, composition, and processing: a review. [31]

As can be seen in the table, natural gas contains sulphur, the value of which may vary depending on the composition of the material and its mixing with this compound in the distribution pipeline in order to smell it for safety reasons. Although the quantity is very low in absolute terms (about 150 mg/m^3), it must be removed because it would damage the catalysts that are present. For charge purification, it is first hydrogenated so that all the sulphur present is reallocated to hydrogen sulphide (H_2S), such as the reaction below:

$$COS + H_2 \rightarrow H_2S + CO \qquad (2.5)$$

H_2S will be removed from the stream using a zinc oxide catalytic bed, operating at temperatures around 340 - 390 °C (figure 2.3). This operation makes it possible to obtain sulphur concentrations below 10 ppb [32], which is an acceptable target (catalyst poisoning does not occur). The sulphur removal reaction used is as follows:

$$H_2S + ZnO \rightarrow H_2O + ZnS \qquad (2.6)$$

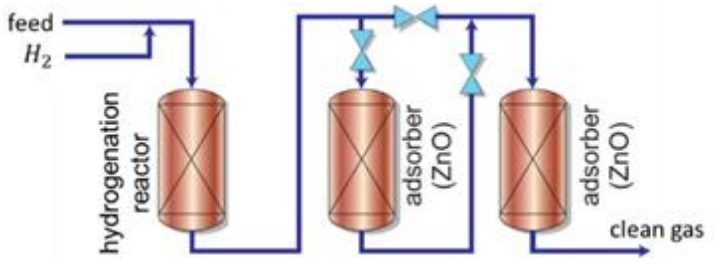

Figure 2.3 Typical scheme for the desulphurization of a gas with a relatively high S concentration.[32]

At the end of desulphurization process, pre-reformer reactor is needed to conclude the charge preparation track. Pre-reforming action is aimed at preventing the thermal cracking of long hydrocarbon molecules (HC_{2+}) into the reformer reactors, this is a trouble situation due to coke deposition on catalyst surface. We want to feed reformer reactor with a homogeneous charge in which CH_4 is the only hydrocarbons molecule. Pre-reformer reactor is adiabatic and operates at relatively low temperature to avoid coke deposition, alumina-supported Ni-based catalyst is then needed to support reaction kinetics and convert the hydrocarbon gas stream to simple compounds as CH_4, H_2O, CO and H_2.

2.3.4 Fired tubular reformer (FTR)

We now begin the treatment of the heart of the process: the reactor to carry out the steam reforming reaction that is FTR. It is endothermic and therefore requires heat input. We supply this heat with the combustion of part of the charge coming in, mixed with the off-gas output from PSA (system for the purification of the syngas stream, downstream of WGS and for the separation of H_2). CO_2 emissions are associated with fluegas, since the other two outputs of the plant (hydrogen and condensate) are carbon-free.

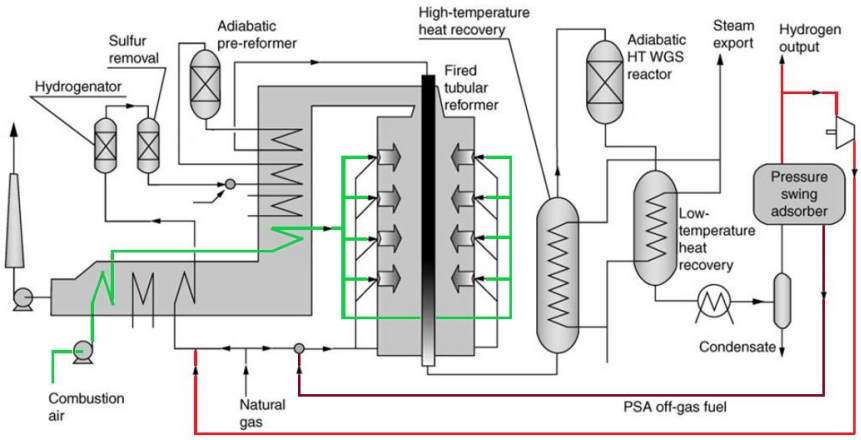

Figure 2.4 Scheme of a mid-size plant for high-purity hydrogen production from natural gas based on a direct flame tubular reformer [35]

The reactor is tubular (made of alloy steel to have a good creep resistance) and a catalyst (usually Nickel based) is dispersed inside to promote the reaction. Most of the heat is provided by irradiation of the flame on the reactor wall. The residual heat from the furnace exhaust gases is used to preheat the charge, while the reformed syngas is a mixture of CO and H_2, with some unconverted CH_4, some excess H_2O (and already present for the next WGS) and all other inert materials entering with the charge. The water must be feed with a certain excess to promote reaction in the direction of the products. In this kind of reactor, it is important to choose carefully the three parameters that determine the operating conditions:

1. Steam to carbon ratio
2. Operating temperature and pressure

2.3.4.1 Steam to carbon ratio

The steam to carbon ratio is the ratio of moles of steam to moles of carbon in the reformer feed. Typical operating values are in the range between 2 and 5 [33].

Upper boundary S/C < 5

This limit is due to thermodynamic reasons. If we increase the amount of steam that we introduce into the charge, a little more H_2 is produced, thus favouring the conversion. Expressing the production efficiency of hydrogen with the following formula

$$\eta_{H_2} = \frac{\dot{m}_{H_2} LHV_{H_2}}{\dot{m}_{NG} LHV_{NG}} \qquad (2.7)$$

η_{H_2} decreases if S/C increases over upper boundary because excess H_2O behaves like an inert that must be heated between input and output. If an inert must be heated, more fuel is consumed, penalising η_{H_2}. For this reason S/C < 5, since the quantity of steam introduced is sufficient for a good H_2 conversion. Figure 2.5 shows the beneficial effect of the increase in the S/C ratio: at the same operating temperature, if the amount of steam increases, the converted fraction of methane increases accordingly.

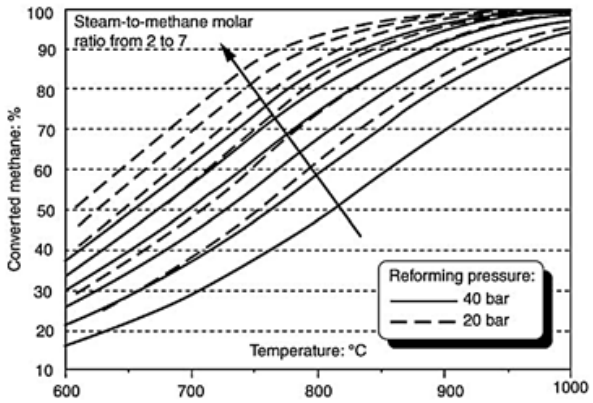

Figure 2.5 Effect of the S/C ratio on the conversion of methane as a function of temperature and pressure [35]

Lower boundary S/C > 2

It is dictated by technical problems. If S/C is too low you may have a solid carbon deposit inside the reactor, giving problems with mechanical and thermal stress. Consider the tubular reactor, heat is introduced inside mainly by irradiation. If carbon is deposited on the catalyst, it is deactivated and the endothermic reaction can no longer absorb heat with the danger that the temperature of the wall will rise above the maximum permitted limit. Furthermore, the deposits on the walls behave as thermal resistance, at equal T_{syngas}, T_{out} must increase causing once again resistance problems as shown in figure 2.6.

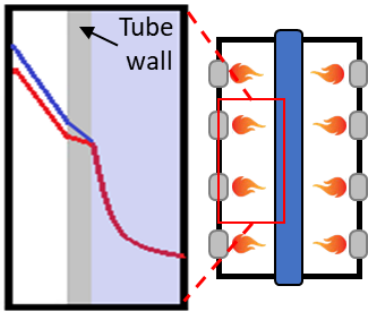

Figure 2.6 Scheme of heat transfer in FTR. Red line: without carbon deposition. Blue line: with carbon deposition

Also in the next WGS reactor you want to maintain a high steam/dry gas ratio because if it is not high the reactor, in addition to the water gas shift, could activate other reactions, such as the Fischer-Tropsch (linear formation of HC molecules), not wanted; so it is convenient to introduce all the steam you need at the beginning (before pre-reforming) in order to be advantageous for the whole process.

2.3.4.2 Operating temperature and pressure

The other operating variables of the reactor are temperature and pressure. As said, they have an effect on the advance of the reaction, so below we see how they influence the sizing of the reactor. FTR has external metal temperatures of about 1050 °C and the stresses it has to resist are essentially high T creep. To remain within the permissible stress range, the pressures must be low with maximum values around 30 bar. If the pressure increases, then the wall thickness should also be increased and therefore the outside temperature should be higher, beyond the permissible limits. To conclude, the usual operating limits of a FTR with Nickel catalyst are:

- Steam to carbon ratio: 3 – 4
- T_{syngas}: 870 – 920 °C
- P_{max}: about 30 bar

2.3.5 Water gas shift reactor

At the outlet of the reforming reactor, independently if it is FTR or ATR (the second reference technology for the production of hydrogen from methane), the syngas has a high concentration of carbon monoxide: to increase the value of the H_2/CO ratio, the water gas shift reaction, already illustrated above, takes place. Thanks to this process it is possible to reallocate the heating value of the syngas from carbon monoxide to hydrogen. The aim is to convert as much carbon monoxide as possible, creating a flux composed mainly of hydrogen, CO_2 and steam. If the reaction is carried out at temperatures around 1000 °C, it reaches equilibrium very quickly without requiring the use of catalysts; however, given the exothermicity of the reaction, the equilibrium achieved is not particularly advantageous for the components and therefore the conversion of carbon monoxide is poor.

In order to promote conversion, it is necessary to lower the inlet temperatures by carrying out a conversion in two stages: one of "high temperature" and one of "low temperature". [34] Below (figure 2.7) we can observe the conversion graph of the syngas, which uses the percentage of carbon monoxide output as an index, which explains in more detail why two stages are necessary.

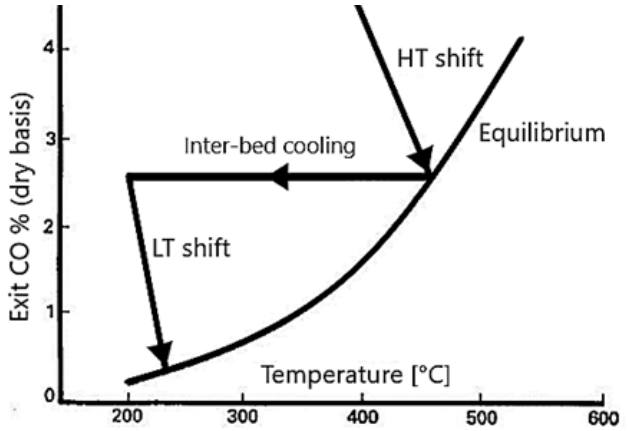

Figure 2.7 Trend of the shift reaction in a system with two adiabatic reactors and one inter-cooling system [36].

High temperature stage (T = 380 - 450 °C): iron-based catalyst. These catalysts show a good sulphur tolerance but are rapidly deactivated when used with a low steam to carbon ratio because it promotes the formation of iron carbides.

Low temperature stage (T = 180 - 330 °C): copper-based catalyst. They are more sensitive to sulphur poisoning which causes the deactivation of the catalyst by sulphurisation of the copper surface. A flux with a sulphur concentration below 10 ppb is required. In addition, it is important to remember that the syngas contains a significant fraction of water in form of steam, whose saturation temperature is generally close to the operating temperature range of the LT-WGS: so it is necessary to foresee an inlet gas temperature at least twenty degrees higher than the saturation temperature in order to avoid condensation on the catalysts.

At the end of this operation, approximately 96% of the carbon entering the natural gas flow was reallocated to CO_2.

2.4 Hydrogen purification process

Downstream of the chemical processes of conversion of natural gas into syngas there is the charge purification section, which has the task of obtaining a flow of pure hydrogen. The technologies most used today are PSA systems, which, however, do not operate selective capture, but merely separate hydrogen from other chemical species.

2.4.1 PSA

Pressure swing adsorption (PSA) is the preferred option to purify syngas stream generated by reforming of light charges. The technique is based on the selective concentration of gaseous species at the surface of microporous solid adsorbents (such as zeolites, silica gel and activated carbons) that have a higher surface/volume ratio. In particular, the materials adopted for hydrogen purification present the capability to adsorb species different from hydrogen and helium, showing an impurity loading proportional to partial pressure of contaminants. We can classify the components according to their adsorption affinity in PSA: H_2 and He species not adsorbed, N_2, O_2 and Ar species slightly adsorbed, CO, CH_4, C_2H_6, C_3H_8, CO_2 species medium adsorbed and H_2O, HC_{4+}, H_2S highly adsorbed species.

PSA operates at constant temperature 'swinging' between two pressures, adsorbing impurities at the higher one and releasing them at the lower one. Since the operating cycle is composed of at least two phases (production and regeneration), in theory a minimum of two beds in parallel are needed to ensure continuous operations. In industrial practice PSA plants are arranged on a higher number of beds (typically 8–12) [35] in order to reduce the consumption of high-pressure, high-purity hydrogen during the repressurization phase. The resulting process produces hydrogen at a pressure slightly lower than the feed stream (less than 1 bar drop), with a purity higher than 99.9% and with a recovery efficiency in the range 80–92% (evaluated as the flow rate of hydrogen separated with respect to the one contained in the syngas). The residual fraction of H_2 is included together with all the impurities in the off-gas stream, leaving the PSA at nearly ambient pressure.

2.5 CO2 capture by solvents

Capturing CO_2 downstream of the water gas shift reactor is advantageous in order to make the process low carbon. In figure 2.8 is one conceptual schemes of how plants with FTR could change to become carbon-free.

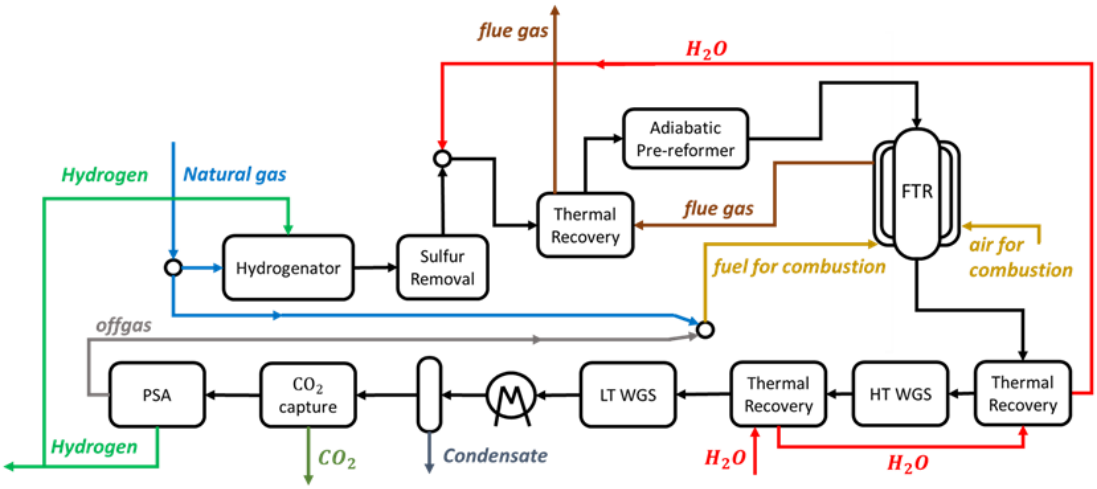

Figure 2.8 Conceptual scheme of FTR

The section AGR (Acid Gas Removal) with MDEA chemical solvent will be treated in detail below. It is necessary to underline that in this thesis work a further capture method will be proposed: through a MCFC fuel cell CO_2 is separated from the flue gas obtaining a syngas flow rich in carbon dioxide that once reformed will be purified in a cryogenic section.

At the exit of the WGS section, syngas from light charges has a hydrogen content of about 70–75% (molar, dry basis), 17–20% of CO_2 and few percent of CH_4, CO and other contaminants. To increase CO_2 capture efficiency, you could do so: instead of feeding the reactor burners with a part of natural gas coming out of the PSA, it is fed with the purge-gas flow coming out of the AGR which is mainly H_2

2.5.1 Physical and chemical solvents for CO_2 removal

The removal of CO_2 from a gaseous stream is usually carried out by means of selective solvents which have a much higher affinity for acidic species (such as CO_2 and H_2S) than the others. The processes can be divided into two categories according to the nature of the interactions between solvent and absorbed species.

Physical absorption: is where the components to be removed are more soluble in the liquid absorbent than the others, but do not react chemically with the solvent. The Rectisol and Selexol processes, which use methanol and a mixture of polyethylene glycol dimethyl ethers as a solvent respectively, are examples of this category.

Chemical absorption: involves a reversible reaction between the species to be removed and the solvent to form weakly bound compounds. All processes using amines, such as monoethanolamine (MEA) or methyldiethanolamine (MDEA), and alkaline salt solutions belong to this category.

The choice is made according to the concentration (and therefore the partial pressure) of the charge. A graph (figure 2.9) illustrating the different capture potential of the solvents according to the partial pressure of CO_2.

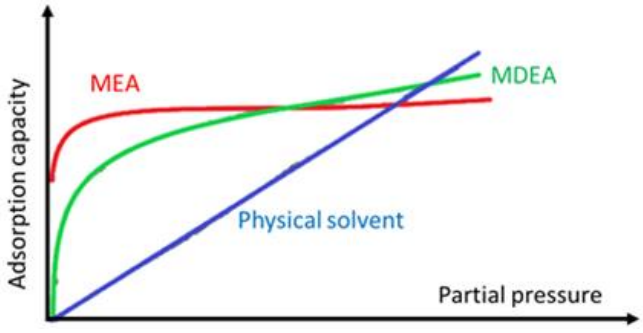

Figure 2.9 Comparison between physical and chemical solvents

Chemical solvents (MEA and MDEA) have a good capture capability for low partial pressure values, which then remains practically constant as the pressure increases; on the other hand, physical solvents are characterised by a linear trend in absorption capacity. In general, for high values of partial pressure, physical absorption systems are preferred (i.e. from the intersection point of the curves), while for lower partial pressures, chemical absorbers are preferred. In FTR systems, the partial pressure of CO_2 output is low for two reasons:

- The steam reforming process is carried out at relatively low pressures in order to preserve the kinetics of the process.
- The high H/C ratio of natural gas (for methane it is four) means that the CO_2 concentration is limited.

A chemical solvent is used: the two most used are mono ethanol amine (MEA) and methyl ethanol amine (MDEA). Chemical solvents, unlike physical solvents, require heat for regeneration, as it is necessary to break the bonds formed with the species to be removed. The necessary thermal power is generally obtained by condensing the steam produced in the plant and this necessity leads to a drop in the overall process efficiency.

The choice of one type of solvent over the other depends on CO_2 concentration in the gases to be purified. Usually if the purification is done on the tail gas of the PSA a MDEA solvent is used, while if it is done in the flue gas coming out from the FTR burner, MEA is used because the concentration is lower. Moreover, MEA has a more aggressive behaviour that requires its dilution in water (with a maximum of 30 % solvent).

Molten carbonate fuel cell and carbon capture

3

In this section, we will describe the operating principles of a fuel cell with particular reference to the technology of MCFC or Molten Carbonate Fuel Cell, together with its advantages and disadvantages. Following the main methods of CCS will be discussed.

3.1 Fuel cells technology

The fuel cell is an electrochemical device that is able to produce electricity through the oxidation of a fuel, without the use of a thermodynamic cycle, i.e. avoiding the combustion process which is the most irreversible passage, limiting the efficiency achievable by the entire process. This procedure allows to exceed the limits imposed by the second principle of thermodynamics. Even in the most efficient thermal machines, such as combined cycle gas turbines, given the maximum temperatures imposed by technological limits of resistance of materials, the maximum efficiency is around 60% - 65% for plants of the new generation. In the internal combustion engines of the most modern cars, the efficiency is much lower, around 40% - 45%. Not passing through thermodynamic cycles, energy production can reach significantly higher efficiencies up to 60% (figure 3.1), which is the reason why fuel cells are highly studied in both scientific and industrial fields.

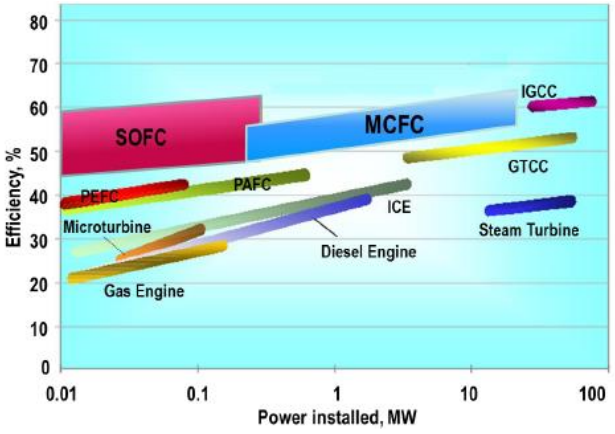

Figure 3.1 Comparison of electric efficiency vs. power installed for combustion-based systems and fuel cell systems [42]

The operation of a fuel cell is based on oxidation reactions on the anodic side and reduction reactions on the cathodic side (different depending on the technology considered). However, the global reaction is the same for all of them and coincides with the oxidation of hydrogen to form water. This is a great advantage compared to conventional thermal engines due to the low emissions and therefore a lower environmental impact. The so-called high temperature fuel cells also have the advantage, given the high operating temperatures, to make available a quantity of heat that can be exploited by thermodynamic cycles placed downstream. A useful classification can be made according to the type of electrolyte and operating temperature distinguishing low temperature cells operating at T below 200°C and high temperature cells with temperatures above 500°C as shown in the figure 3.2.

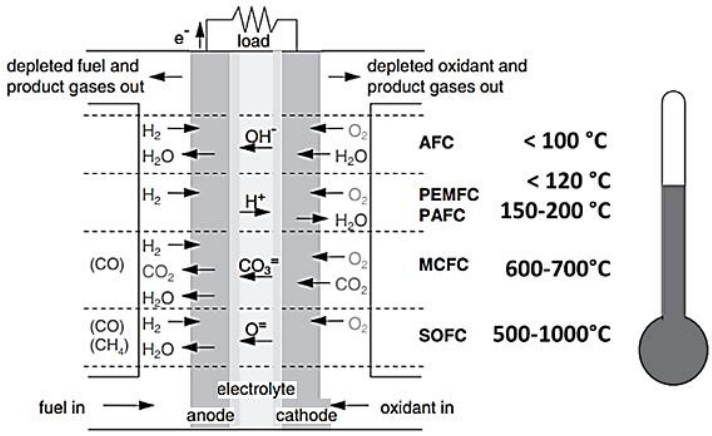

Figure 3.2 Schematic comparison between different fuel cells [40]

3.2 Molten carbonate fuel cell analysis

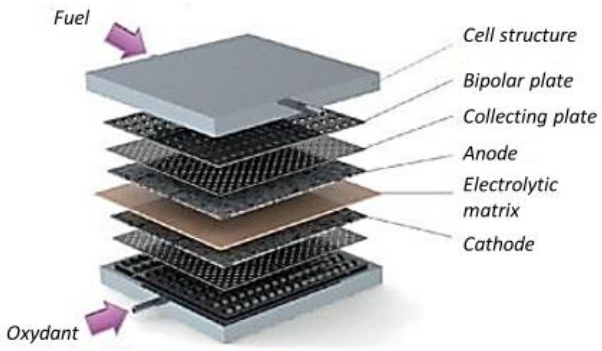

Figure 3.3 MCFC Structure adapted by [44]

MCFCs use as electrolyte a mixture of alkaline-lithium carbonates (Li_2CO_3) potassium (K_2CO_3) and sodium (Na_2CO_3) maintained in the liquid state by the high operating temperature of the cell around 600 - 650 °C and stored inside a ceramic matrix.

Due to the high temperature there is the advantage that the electrodes, Ni-Cr/ Ni-Al based for the anode and NiO lithium based for the cathode[40], do not have catalysts made of noble

metals like Pt and Pd; besides this aspect, the operating conditions of this cell allow to use a fuel that is not pure hydrogen but other compounds like methane because they can be easily reformed inside the cell.

However, working at such high temperatures causes stress on materials that suffer differential thermal expansion, thus reducing their useful life and causing more start-up transients. Besides the fact of being intolerant to sulphur limited to 0.5 ppm by mass[43], the critical aspects concerning this type of cells are corrosion and chemical stability of the materials because the liquid electrolyte is very aggressive towards the electrodes.[43] The electrolyte is able to transfer the ion $CO_3^{=}$ and it is therefore necessary to feed CO_2 on the cathodic side together with the oxidizer; on the anode side instead there is a net transfer of CO_2 which is then released together with H_2O. This peculiarity allows the MCFC to be a very congenial system for the separation of CO_2 from flue gas and then store it in CCS viewpoint. [40] [41]

The main reactions (figure 3.4) that take place inside the cell are:[40]

Anode: $H_2 + CO_3^{=} \rightarrow H_2O + CO_2 + 2e^-$ Cathode: $\frac{1}{2}O_2 + CO_2 + 2e^- \rightarrow CO_3^{=}$

Overall reaction: $H_2 + \frac{1}{2}O_2 + CO_2 \rightarrow H_2O + CO_2$

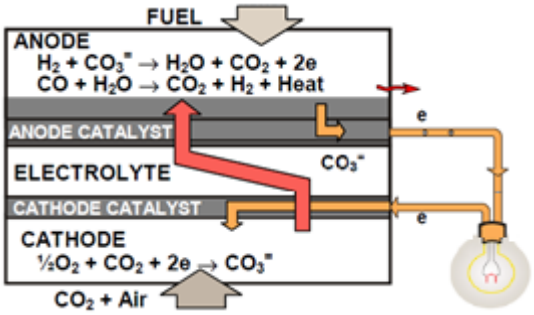

Figure 3.4 Conceptual structure of a molten carbonate fuel cell [40]

The reversible potential for an MCFC is the maximum potential that the cell can reach from the ideal point of view; it considers the transferred CO_2 and is expressed by Nernst's law:[40]

$$E_{rev} = E_0 + \frac{RT}{n_e F} \ln\left(\frac{P_{H_2,a}\, P_{O_2,c}^{0.5}\, P_{CO_2,c}}{P_{H_2O,a}\, P_{CO_2,a}}\right) \qquad (3.1)$$

Where:

- a: anode, c: cathode
- E_0 is the potential under conditions of referment to P_0 or atmospheric pressure
- F Faraday's constant
- P_i partial pressures

By equation 3.1 it can be easily noticed that the potential strongly depends on the ratio between the partial pressures of CO_2 at the cathode and at the anode and the more this difference is marked the more the potential is influenced accordingly [40].

3.2.1 Real potential – polarization curve and losses

In order to produce more power, the goal is to have the highest possible efficiency while minimizing losses in the cell. To achieve this purpose, several operating parameters can be optimized, such as high temperature, high pressure and lower concentration of pollutants, as well as having more performing and thinner materials inside the cell.[41] Concerning the potential it cannot be in fact equal to the ideal one defined by Nernst's equation (E) because, as in any real process, there is a certain irreversibility that we have to take into account that generally tends to decrease the actual voltage. In particular, it is possible to verify that the tension between the electrodes is reduced as the current density (current per unit area of the electrolyte) at which the cell operates increases. The polarization curve (figure 3.5) represents the voltage trend as a function of current density and is typically the most frequently used electrochemical technique to characterize the performance of the fuel cell. It provides a picture of the different types of losses that occur in a cell and are usually called polarization losses. The actual potential is always lower than the ideal one, due to the losses, and the difference between the two (ideal and real) is called overpotential. [43]

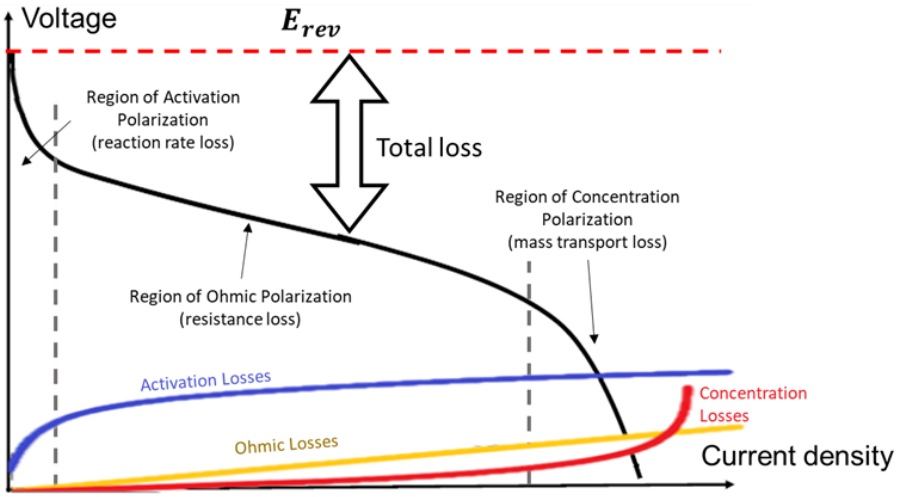

Figure 3.5 Polarization curve adapted from Fuel Cell Handbook [40]

The curve is divided into three main regions of losses as shown in figure 3.5.

- **Activation polarization [43]**

At low current densities, the voltage drop is essentially connected to the activation of the reactions that take place in the cell due to the slow kinetics of the reactions on the electrode. The phenomena of reagent adsorption and desorption of gas phase products to the electrodes, the transfer of electrons between electrodes and electrolyte, contribute to this loss.

- **Ohmic polarization** [43]

As the current density increases, the polarization by activation stabilizes and the loss caused by the resistance to the flow of ions in the electrolyte and the flow of electrons through the electrodes becomes more important. This loss is called ohmic polarization and is related to ohmic losses. The losses in the electrolyte are greater than those in the electrodes; the first ones can be reduced by minimizing the thickness of the electrolyte (which must however maintain a sufficient value to avoid reagent by-pass to the opposite electrode), bringing the two electrodes closer together and thus increasing the ion conductivity. Ohm's law can be used to quantify the loss:

$$\Delta V_{ohm} = j\ R \tag{3.2}$$

As can be observed, this loss is proportional to the current density and varies with it in a linear way, determining the linear profile of the central section of the characteristic curve of a fuel cell.

- **Concentration polarization** [43]

At high current density, to the polarizations already mentioned is added a third one (whose effect in this region is predominant) linked to the high concentration gradients that occur due to the fact that the reagents are consumed rapidly by the reactions of the cell. The concentration of the reagents at the reaction point is in this case significantly lower and not sufficient compared to the flow fed to the cell (bulk phase), causing a sudden drop in voltage when the phenomenon appears.

3.2.2 Power of cell

The power that can be extracted from a fuel cell can be calculated as the product between the actual voltage, current density and the cell surface, according to the expression:

$$W_{el} = (E - \Delta V_{activation} - \Delta V_{ohm} - \Delta V_{concentration})\ j\ A_{cell} \tag{3.3}$$

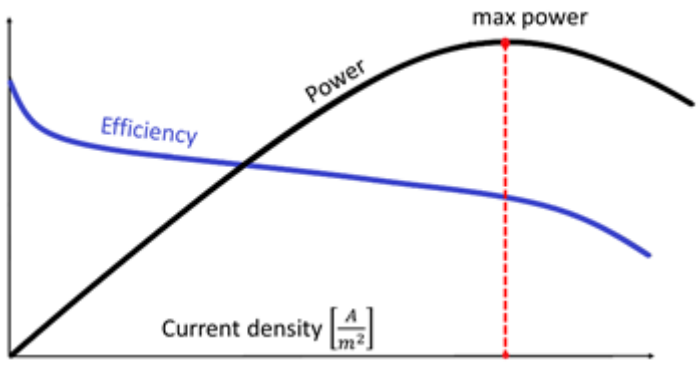

Figure 3.6 Cell power and efficiency adapted from Fuel Cell Handbook [40]

As can be observed in figure 3.6 the point at maximum power density is normally considered the nominal operating point of a cell since it is the one that minimizes the specific cost expressed as €/kW. Moreover, it is substantially counterproductive to operate at higher current densities since the same potential can be obtained at lower current values. Finally, it is possible to observe that the maximum power point does not coincide with the maximum efficiency point. Keep in mind, however, that since the potential generated by a single cell (of the order of 1 Volt) is not sufficient for a satisfactory electrical generation usually we use stacks of cells or a sequence of several MCFC modules connected in series through a bipolar plate to increase the potential produced and thus the power.[40]

3.2.3 Effects of pressure

Concerning the pressure, it has a significant effect on the potential. Rewriting the equation of Nernst we can see how a change of it, from P_1 to P_2, leads to a variation of the reversible potential ΔV_P:[40]

$$\Delta V_P = \frac{RT}{2F}\, ln\frac{P_{1,anode}}{P_{2,anode}} + \frac{RT}{2F} ln\frac{P_{2,cathode}^{3/2}}{P_{1,cathode}^{3/2}} \qquad (3.4)$$

Keeping in mind that the pressure at the anode is equal to that in the cathode ($P_1=P_{1,cathode}=P_{1,anode}$ and $P_2=P_{2,cathode}=P_{2,anode}$) equation 3.4 can be reformulated in this way:

$$\Delta V_P = \frac{RT}{4F}\, ln\frac{P_2}{P_1} \qquad (3.5)$$

By increasing the operating pressure of the MCFC it results that the cell potential rises because an increment of pressure leads to a higher partial pressure of the reagents, an increase in the solubility of the gases, an improvement in the kinetics of the reactions due to the higher density of the reagents on the electrodes, an increase in the mass transport resulting in a decrease in polarization losses and an increment of the current generated. [43] In spite of these benefits increasing pressure leads, in addition to structural problems and containment of liquid electrolytes, to chemical instability and the formation of undesirable and counterproductive reactions such as Boudouard's reaction, methanation reaction and methane decomposition.[40]

- Boudouard: $2CO \rightarrow C + CO_2$
- Methanation: $CO + 3H_2 \rightarrow CH_4 + H_2O$
- CH_4 decomposition: $CH_4 \rightarrow C + 2H_2$

Thus, raising the pressure increases the carbon deposit on the catalysts [40] and this must be absolutely avoided because it obstructs the passage of gases to the anode. For this reason, despite the obvious benefit on the reversible potential (especially at high temperatures) the pressures inside the cell are usually slightly higher than atmospheric pressure.

3.2.4 Effect of temperature

The influence of temperature on the reversible cell potential depends on several factors, one of which concerns the equilibrium composition of the combustible gas. In fact, increasing the temperature will disadvantage the reaction of WGS that produces less H_2. Moreover, from the Nernst equation we can deduce that an increment of temperature corresponds to a diminution of the reversible potential because E_0 reduces with increasing temperature as shown in figure 3.7.[43] In the equation below is reported the term $E_{0.}$

$$E_o = \frac{-\Delta\widetilde{G_O}}{2F} \qquad (3.6)$$

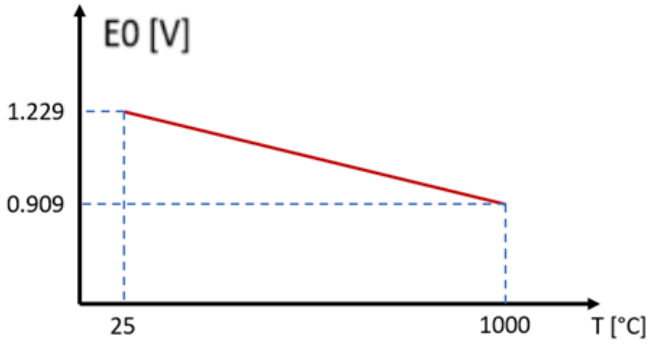

Figure 3.7 Reversible potential in function of temperature [43]

Due to the increase in temperature in addition to the reduction in reversible E, however, there is also a positive effect because the polarization losses decrease. Thus, as a result of this, the ΔV of an MCFC cell usually is between 0.6 and 0.8 similar to all other cell types.[43]

Most MCFC cells currently operate at an average temperature of 640-650 °C. Most carbonates do not remain fused below 520 °C and, as written before, the increase in temperature improves cell performance. Above 650 °C, however, the gains are smaller with increasing temperature. In addition, there is greater loss of electrolyte through evaporation and greater corrosion of the material. An operating temperature of 645 °C therefore offers a trade-off between high performance and cell life.[40]

3.2.5 Reagents utilization factor

As mentioned before, the fact that the cell potential decreases at a limited concentration of reagents at the reaction point places an additional constraint on the system's operation. A limited concentration of reagents may be present in the bulk phase due to excessive consumption of the same reagents along the electrode. To avoid this negative phenomenon it is appropriate that the reagent concentration is sufficiently high in the fluxes leaving the cell. In order to avoid a reduction in voltage on the cell, the reagent concentration should not fall below a minimum threshold. The parameter that defines the limit is the reagent utilization factor expressed as fuel, CO_2 and O_2 utilization factor.[43] The fuel utilization

factor (FU) is evaluated as the ratio between the amount of H_2 converted by the electrochemical reactions and the amount of H_2 equivalent, that is the amount of hydrogen that the fuel can generate through the reaction of steam reforming and water gas shift supplied at the cell inlet, both are expressed in molar quantities, according to the following formula:[43]

$$FU = \frac{\dot{N}H_{2,IN\ Anode} - \dot{N}H_{2,OUT\ Anode}}{\dot{N}H_{2,IN\ Anode}} \quad (3.7)$$

To avoid a lack of reagents this parameter is usually limited to a maximum of 0.75-0.80. [43]

Can be useful to operate the cell with lower fuel utilization factor because it behaves like a reformer for blue hydrogen production. Moreover, matching this technology with industrial process exhaust gas rich in CO2, it permits to make carbon capture

The use factor of CO_2 and O_2 are expressed as:

$$U_{CO2} = \frac{\dot{N}co_{2,IN\ Cathode} - \dot{N}co_{2,OUT\ Cathode}}{\dot{N}co_{2,IN\ Cathode}} \quad (3.8)$$

$$U_{O2} = \frac{\dot{N}o_{2,IN\ Cathode} - \dot{N}o_{2,OUT\ Cathode}}{\dot{N}o_{2,IN\ Cathode}} \quad (3.9)$$

3.2.6 Fuel flexibility

MCFCs have a high tolerance to carbon monoxide and therefore there is no obligation to directly introduce pure H_2 but to be able to use natural gas. Thanks to the high temperatures it is possible to convert the fuel directly inside the device, producing the necessary H_2 thanks to a steam reforming (endothermic reaction), followed by a water gas shift reaction that maximizes the production of hydrogen. There are two ways to perform internal reforming:

Direct: it takes place directly on the anode and in the case of MCFCs Nickel is used as a catalyst, already present for electrochemical reactions. The fact that reforming and WGS take place directly promotes the conversion because the hydrogen generated reacts instantly to form H_2O as a cell product which in turn is a WGS reagent maximizing its advancement. The disadvantage of this configuration is the poor control of the internal temperature because to the electrochemical cell reactions are added the reforming reaction (endothermic) and the water gas shift (weakly exothermic). Finally, at the same potential difference there is a lower current density due to the lower kinetics of reforming that limits H_2 production compared to pure hydrogen powered cells.[43]

Indirect: this configuration is the most used one because it consists in having the reaction of reforming and water gas shift separated from the electrode and just before it, continuing to use the supplied heat of the cell but without the disadvantages of a direct reforming.[43]

3.3 Carbon capture and storage

CCS means "Carbon Capture and Storage (or Sequestration)" and identifies all those processes that involve the capture and storage of carbon dioxide. They consist in the production of decarbonised energy vectors (i.e. such that they do not cause GHG emissions during their use) by capturing, concentrating and compressing CO_2 to make it available for permanent storage. Today's efforts by the scientific community to implement this technology at all industrial and energy levels are remarkable. Now we introduce an overview of all possible CCS systems. It is useful to distinguish the system into two parts, capture phase and storage phase.

3.3.1 Capture phase

The CO_2 capture phase can be done according to three different plant types:

- Pre-combustion capture
- Post-combustion capture
- Oxy-fuel combustion capture

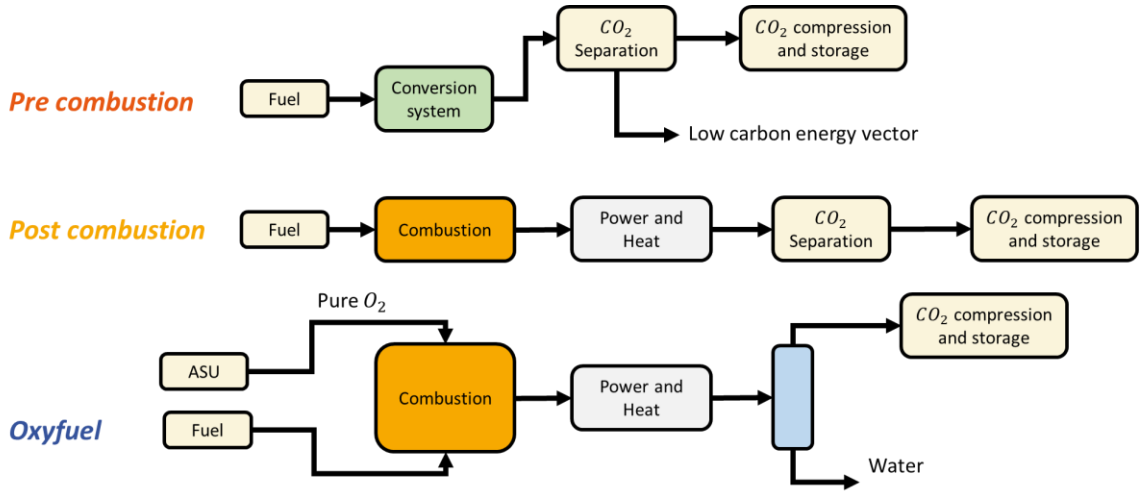

Figure 3.8 CO2 capture systems, adapted from Carbon dioxide capture and storage. IPCC [39]

3.3.1.1 Capture from industrial process streams

Although fossil fuel power plants are the largest emitter of CO_2, some industrial sectors also contribute to CO_2 emissions, and as noted in the first chapter (figure 1.1) they account for about 20 % of total emissions. Therefore, innovative systems are currently being studied to integrate CO_2 capture into these processes, minimising the impact on the cost of the final product. The sectors most under investigation are the waste to energy plants, pulp and paper plants, integrated steel mills, cement plants, oil refineries and steam methane reformers.

The techniques used for CO_2 removal are those described below (pre, post or oxy).

3.3.1.2 Pre-combustion capture

Pre-combustion capture refers to the removal of CO_2 from fossil fuels before combustion has taken place. For example, in a gasification process a fossil raw material (such as coal) is transformed into a synthesis gas. This synthesis gas, or syngas, is a mixture of hydrogen, carbon monoxide, CO_2, and smaller amounts of other gaseous components, such as methane. The syngas can then undergo other reaction, such as the water-gas shift reaction to convert CO and water (H_2O) to H_2 and CO_2, producing a H_2 and CO_2 rich gas mixture. The concentration of CO_2 in this mixture can range from 15-50%. CO_2 can then be captured and separated, transported and finally sequestered, and the H_2-rich flow is available for future applications. Absorption methods using chemical or physical solvents are mostly used to separate CO_2, as described in section 2.5.1.

3.3.1.3 Post-combustion capture

Post-combustion capture refers to the capture of carbon dioxide from exhaust gases after the fossil fuel (e.g. coal, natural gas or oil) has been burned. It is the system that requires the least change in the upstream system, where the section remains more or less unchanged: this solution is best suited for retrofitting existing systems. Usually the molar fraction of carbon dioxide is relatively low and therefore the best method for separation is by means of a chemical solvent, as already described in paragraph 2.5 above, where in figure 2.9 it was highlighted that at low partial pressures of the species to be removed it is necessary to use a solvent of type MEA or MDEA. Capture levels of 90% are reached but some problems are present:

- The solutions used have an amine concentration of 20 – 30%. This is a low percentage due to the corrosive nature of the substance and only by adding suitable corrosion inhibitors is it possible to increase the concentration to higher levels, limiting the circulating flow rates and allowing good energy savings.
- If this solution is applied to exhausted gases with a high concentration of oxygen, such as gases coming out of a combined cycle, the amines tend to degrade, making it necessary to replace them periodically.
- Amines in contact with a flow rich in nitrogen tend to form nitrosamines, removing the possibility of their reaction and forming a carcinogenic compound that requires further treatment.

In addition, as mentioned in paragraph 2.5, chemical solvents require heat for regeneration, resulting in additional energy expenditure to make this thermal power available; there is a loss of efficiency of the entire process. Therefore, in this thesis work we will explore the possibility of making a post combustion capture by means of an MCFC that, as mentioned above, performs the function of separating CO_2 from the flue gas; moreover, through this system it will be possible to produce electricity and hydrogen, both useful products in an oil refinery.

3.3.1.4 Oxy-combustion capture

Oxy-combustion is realized burning fuel with pure oxygen rather than air. In this way water and carbon dioxide are the only products present in the flue gases and can be easily separated as a consequence of different volatility. In these systems the energy consumption is represented by the ASU (air separation unit) which must provide high purity oxygen used as oxidiser. Once the water fraction has been separated by condensation, CO_2 capture can take place through cryogenic separation and the resulting compressed liquid flow can be stored. Carbon dioxide removal efficiencies can be very high, reaching levels of over 98%, and there would be no emissions of other pollutants as they would remain in solution in the liquid CO_2 stream (often for storage in saline aquifers or EOR applications, further cryogenic purification of the carbon dioxide stream is required to remove the few remaining impurities).

3.3.2 Storage phase

Once the flow of compressed and liquefied carbon dioxide has been obtained, appropriate storage solutions must be found; they depend on the geological conformation of the site where the plant is located. At the moment the research is moving in different directions, here reported and analysed briefly.

Geological storage: the storage of carbon dioxide in the underground layers of the earth's crust is a natural process that produces a class of minerals, called carbonates, or deposits of CO_2 in the pure gaseous state or in a mixture. It is therefore possible to think of creating artificial deposits of carbon dioxide. The EOR technique (Enhanced Oil Recovery) identifies the most profitable solution in this field: by injecting the flow of CO_2 into oil fields, in addition to further pressurising the well, part of the carbon dioxide dissolves in the oil making it more fluid and facilitating its extraction. Once depleted, the oil or natural gas field has excellent geological characteristics to allow permanent storage of the injected carbon dioxide.

EBCM system: ECBM (Enhanced Coal Bed Methane) systems exploit the excellent affinity characteristics between CO_2 and coal: by injecting the flow of carbon dioxide into economically unexploitable carboniferous veins, it can move between the cracks and be adsorbed inside the porosity of the coal, favouring the release of less similar gaseous substances, such as methane.

Ocean storage: the seas and oceans are natural absorbers of carbon dioxide: every year the balance between the surface sea layers and the atmosphere causes an absorption of about 7 billion tons of anthropic CO_2. This has led to a progressive increase in the concentration of dissolved carbon dioxide and a consequent acidification of the oceans. It is possible to foresee the release at high depths (typically over 1000 metres) where water movements due to currents are very limited. However, this would be a temporary solution: over the centuries,

the diffusive movements due to a situation of imbalance between the areas where CO_2 would be injected and the surrounding environment would cause it to rise to the surface.

Saline aquifers capture: saline aquifers are water-saturated rock formations in which high quantities of salts are dissolved. They are usually covered by one or more layers of impermeable rock called "caprock". They are characterised by high geological stability, good permeability such as to allow the injection of CO_2 flow and have adequate thicknesses and porosity to guarantee large storage capacities. These aquifers are generally found at depths between 800 and 1000 metres where pressures are close to 100 bar.

3.3.2.1.Potential storage locations in Europe

From the *Concawe* report [50] it is possible to estimate the potential of some European reservoirs that could be suitable from a geological point of view for a possible storage. In the *Getsco* project it was seen that these reservoirs, if fully exploited, could collect the CO_2 emitted for the next 100 years. However, the survey carried out has been done only from a geological point of view and does not concern the real feasibility which foresees higher surveys to verify the safety for possible earthquakes or geological instability. Below are the main countries that joined the survey for the *Getsco* project. [50]

Country	Storage capacity (Mt CO_2)		Emission (Mt CO_2/a)	Potential storage (years)		
	Oil & Gas fields	Saline aquifers	All sources (Based on ETS report)	Oil and Gas fields	Saline aquifers	Total
Germany	2500	33000	474	5	70	75
Denmark	800	16000	26	31	615	646
France	800	27000	131	6	206	212
UK (North Sea)	10000	15000	251	40	60	100
Greece	-	2500	71	-	335	35
Norway	12500	12700	113	111	112	223
Netherlands	11000	2000	80	138	25	163
Total	37600	108200	1146	31	94	127

Table 3.1 Estimated storage in Oil, Gas and Saline Aquifers in Some European Countries [50]

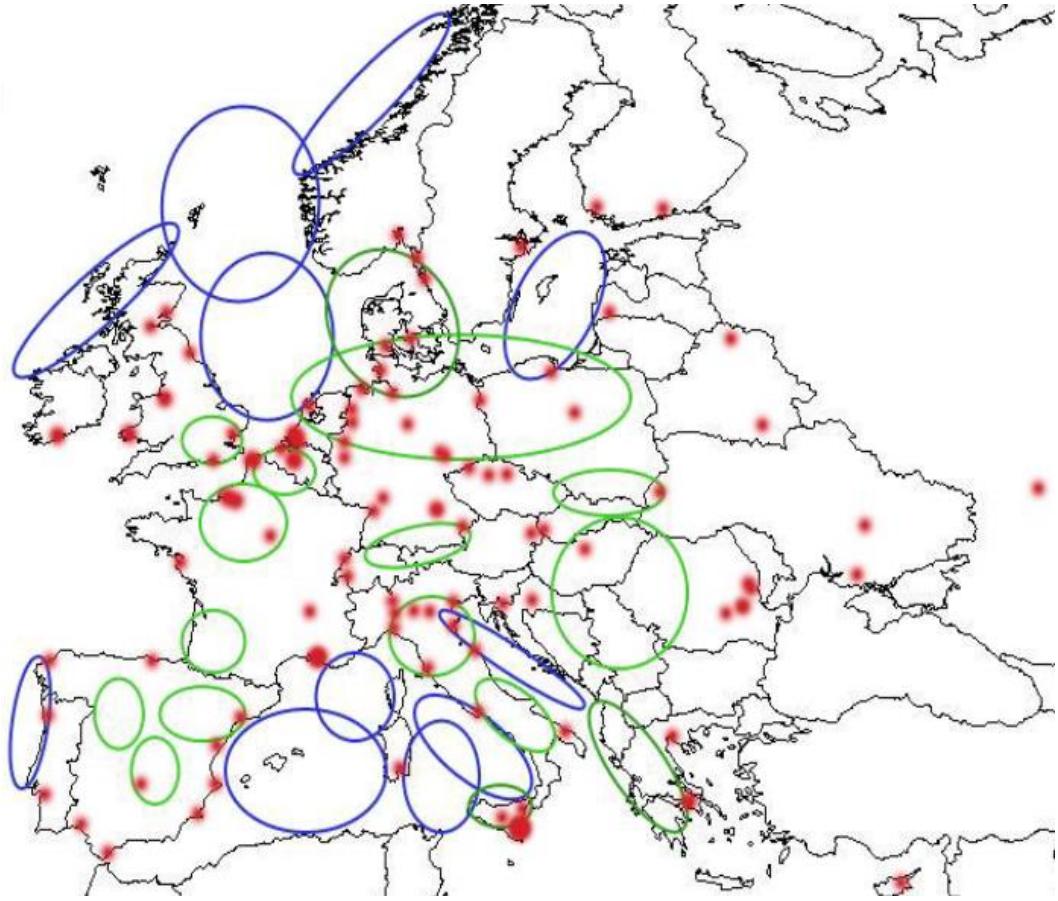

Figure 3.9 Location of EU Refineries and Potential CO2 Storage Areas [50]

Figure 3.9 instead shows the main locations of the basins that geologically would be suitable for a possible storage without including a feasibility study due to instability risks. It is useful to get an idea of the European storage potential and to see that these areas are, in an area of about 500 km, close to the refineries and this allows to lower CO_2 transport costs. The main refineries are shown in red, the geologically suitable areas for on-shore storage are shown in green and those for off-shore storage are shown in blue [50].

Plant description

4

This chapter of the thesis will describe the main assumptions in order to design the system, the methodology used and a detailed description of it. A comparison will then be presented both between the different plant types and with respect to absorption with MEA, the current reference technology for CO_2 post-combustion capture from exhausted gases with a low CO_2 partial pressure. The main purpose of our work is to analyse a possible retrofit plant through an MCFC (Molten Carbonate Fuel Cell) to separate and remove CO_2 from the flue gas of a SMR, one of the main greenhouse gas emitters in a refinery.

The plant was entirely modelled with *Aspen Plus V10.1* commercial software, a calculation program created by *AspenTech* [51] for the modelling and simulation of unitary operations of industrial plants in stationary mode. *Aspen Plus* makes possible to iteratively solve the mass and energy balance in all the points of plant in order to achieve stable convergence at every point of the entire system. Although *Aspen Plus* is a powerful software capable of simulating very complex systems, achieving convergence at a consistent operating point is not a simple conclusion. In fact, in order to achieve it, it is fundamental to know and select suitable operating hypotheses and it is necessary to know in depth the functioning of the various system components and the program itself. In addition, many components are not present in *Aspen Plus* (such as the fuel cell module) but must be modelled through a series of unitary operations, which makes it even more evident that in-depth knowledge of the operation of the components is necessary.

4.1 FTR plant base description

As regards the starting data of the SMR system to be retrofitted, we have referred to the FTR system without capture (Base Case) present in the *Demoys* [52]. The reforming plant is fed with a charge of natural gas with the composition described in table 4.1. It was taken from the above mentioned file which itself follows the guidelines of the *EBTF (European Benchmarking Task Force)* report [52].

Natural gas composition		
Specification	Unit	Value
Natural gas composition		
CH_4 - Methane	%	89.00
C_2H_6 - Ethane	%	7.00
C_3H_8 - Propane	%	1.00
C_4H_{10} - Butane	%	0.10
C_5H_{12} - Pentane	%	0.01
CO_2	%	2.00
N_2	%	0.89
Molar mass	kg/kmol	18.018
Lower Heating Value	MJ/kg	46.482
Higher Heating Value	MJ/kg	51.454
CO_2 specific emission	g_{CO2}/MJ_{LHV}	56.99

Table 4.1 Specification of the natural gas considered for performance evaluation

The incoming air is considered in ambient conditions and assumed with the composition expressed in table 4.2.

Air composition		
Specification	Unit	Value
Air composition		
Ar	%	0.92
CO_2	%	0.03
H_2O	%	0.96
N_2	%	77.34
O_2	%	20.75

Table 4.2 Specification of air considered for performance evaluation

For simplicity we report in table 4.3 the ambient condition:

Ambient condition		
Parameter	Unit	Value
Temperature °C	°C	15
Pressure Bar	bar	1.013
Relative humidity %	%	57

Table 4.3 Ambient condition

In table 4.4 there are the main operating hypotheses used for the FTR system, they are chosen by previous simulations with the same components [52] or according to the literature and our precise design decisions.

Parameter	Unit	Value
Natural gas pre-treating		
Sulphur absorption temperature, °C	°C	365
Pressure drop of natural gas $\Delta P/P_{in}$	%	2
Adiabatic pre reformer		
Inlet temperature	°C	490
Adiabatic pre-reformer S/C ratio	-	3.4
Pressure drop $\Delta P/P_{in}$	%	3
Fired Tubular Reformer		
Heat losses	% of heat transferred	0.2
Inlet temperature	°C	620
Outlet temperature	°C	890
Pressure drop $\Delta P/P_{in}$	%	7
Outlet pressure	bar	32.7
Combustor		
Outlet temperature	°C	1010
Pressure drop ΔP/Pin	%	7
High temperature WGS		
HT-WGS inlet temperature	°C	330
Pressure drop ΔP/Pin	%	2
Flue gas recovery heat exchangers		
Heat losses	% of heat transferred	0.7
Min ΔT gas-gas	°C	25
Min ΔT gas-liquid	°C	10
Subcooling ΔT	°C	5
Pressure drop ΔP/ Pin water phase	%	-
Pressure drop ΔP/ Pin gas phase	%	2
Pressure drop ΔP/ Pin air cold side	%	1
Syngas cooler section heat exchangers		
Heat losses	%	0.3
Min ΔT gas-gas	°C	25
Min ΔT gas-liquid	°C	10
Subcooling ΔT	°C	5
Pressure drop liquid phase ΔP/ Pin	%	-
Pressure drop gas phase ΔP/ Pin	%	1.5
HP & LP Steam Turbines		
Isentropic efficiency	%	87
Mechanical efficiency	%	99.6
Water pump		
Pump hydraulic efficiency	%	70
Pump mechanical efficiency	%	84
Outlet pressure of water	bar	100
Hydrogen compressor		
Isentropic efficiency	%	84
Mechanical efficiency	%	94
Outlet pressure for hydrogen export	bar	39
Miscellaneous		
Electric auxiliaries for heat rejection % of heat rejected	%	1
Electrical efficiency for turbomachinery	%	98.5
PSA		
Hydrogen separation efficiency	%	89
Operating temperature/ Rigeneration pressure	°C/bar	31/1.3
Pressure drop hydrogen ΔP/ Pin	%	3

Table 4.4 Operative assumptions and parameters utilized in the plant simulations

The Fired tubular reforming plant proposed by us wants to reproduce a conventional plant based on the production of 30 000 Nm^3/h of H_2 installed in refineries.

Referring to figure 4.1, the natural gas charge is introduced into the plant at 70 bar [52] (stream 1). It is split because the part not needed for the reforming reaction is sent, together with the offgas coming from the PSA, into the burners to have the necessary heat to support the endothermic reaction in the reactor. The natural gas to be reformed splitted is mixed with compressed H_2 coming from PSA at a pressure of 39 bar, necessary to have the right exit pressure from the reforming by 32.7 bar [52]. The quantity of H_2 mixed is linked to the necessity to have the correct quantity of hydrogen for the hydrogenation and desulphurisation reactions downstream of a first regenerative heating that brings the charge to the operating T for sulphur removal equal to 365°C; these two reactors (beds) are necessary because sulphur is highly dangerous for the FTR catalysts as well as being highly polluting and can be tolerated only if in quantities lower than 100ppb (see chapter 2.3.3). So, the correct molar fraction of H_2 was fixed at 2.10 % in stream 3 [52]. The desulphurised charge before entering the main reforming reactor is mixed with steam from the discharge of the high-pressure steam turbine to obtain the correct steam to carbon ratio of 3.4 for downstream reactions and is pre-reformed by means of an adiabatic pre-reforming at 490 °C necessary to equalise the hydrocarbon components of the natural gas flow and to have a composition at the inlet of FTR mainly composed by CH_4.

Before entering the reactor, the charge is heated up to 620°C in the flue gas recovery, a network of regenerative heat exchangers that use the heat from the burners. The reformed charge exits at 890 °C and is introduced into an syngas cooler to cool it by producing steam, with the aim to obtain a temperature of 330 °C to activate the catalysts of the high-temperature water gas shift reaction that shift the energy quantity from the very abundant CO to the output of the reforming to the H_2, a useful product. Usually to enhance the conversion of CO into hydrogen two WGS reactors are used, one at high temperature and one at low temperature, but in our case we have put only one because the outgoing offgas is sent into the burner with the aim of taking as few natural gas as possible and therefore there is no need of a very high conversion.

The H_2-rich syngas is then cooled and after removing the condensed water it is sent to a PSA (more detailed description in chapter 2.4.1) which separates the H_2 under pressure at 29.5 bar to be sent for export from the outgoing offgas at 1.3 bar, bed regeneration pressure. The outlet offgas is sent entirely into the burners to reduce the quantity of incoming natural gas. In figure 4.1 it is possible to observe that the offgas coming out from the PSA (stream 14) can actually be split if a retrofit with an MCFC fed offgas is required, a case that we will discuss later in section 4.3.

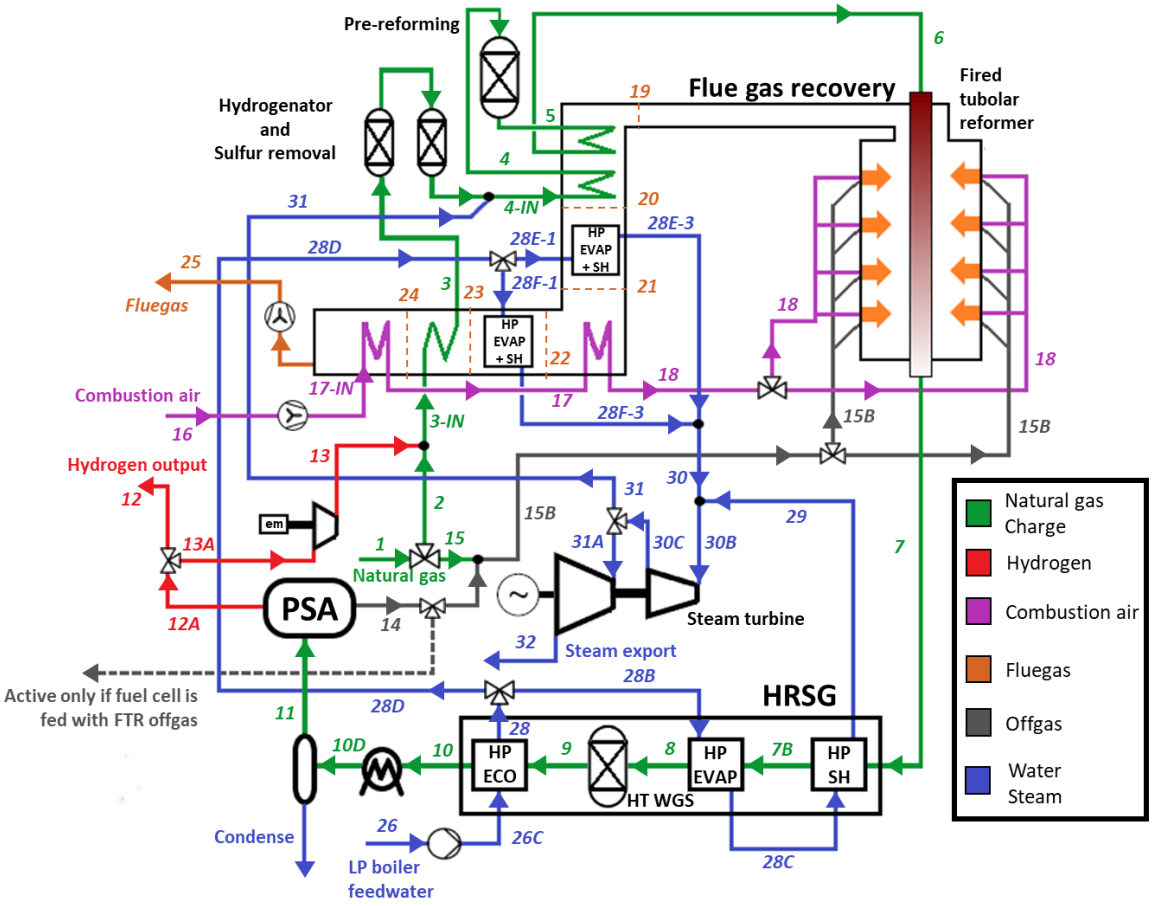

Figure 4.1 FTR plant layout adapted from Demoys [52]

The water required for the steam to carbon ratio and to run two steam turbines is taken from a refinery boiler at 150.8 °C and 6 bar, heated and evaporated in the syngas cooler section using the heat of the reformed charge and in the flue gas recovery through two evaporators and high pressure superheaters. Syngas cooler section is necessary to avoid the problem of metal dusting; in fact, it affects all configurations that adopt a heat exchanger with process gas and is due to the carburization of the metal when it comes into contact with a CO rich flow, especially in the temperature range between 400 and 800°C. The fast cooling of the process gas flow by means of steam generation therefore allows the metal to be kept at temperatures outside the critical range, thus reducing the costs associated with the application of coatings and surface treatments to mitigate this harmful phenomenon [52].

Finally, all the steam produced is sent directly to the turbine group to generate 1.74 $MW_{el,net}$. The steam coming out of the low-pressure turbine is sent in export for refinery use. The air required for combustion is taken at ambient conditions, pressurised through a fan and heated through regenerative heat exchangers exploiting the heat of the flue gases coming out of the combustor. The outgoing flue gases are sent to the stack or, if it exists, to the retrofit capture plant as we will analyse later. Table 4.5 shows the compositions and main thermodynamic conditions of the FTR system flows.

#	T	P	m	N	Q_{LHV}	Mole fraction								
	°C	bar	kg/sec	kmol/hr	MW	Ar	CH_4	CO	CO_2	C_2+	H_2	H_2O	N_2	O_2
1	15.0	70.00	2.63	526.0	122.4	-	89.00	-	2.00	8.11	-	-	0.89	-
2	15.0	70.00	2.18	436.1	101.5	-	89.00	-	2.00	8.11	-	-	0.89	-
3	365.0	38.20	2.19	445.4	102.1	-	87.14	-	1.96	7.94	2.09	-	0.87	-
3-IN	- 1.7	39.00	2.19	445.4	102.1	-	87.14	-	1.96	7.94	2.09	-	0.87	-
4	490.0	35.75	10.09	2.023.7	102.1	-	19.18	-	0.43	1.75	0.46	77.99	0.19	-
4-IN	349.3	37.35	10.09	2.023.7	102.1	-	19.18	-	0.43	1.75	0.46	77.99	0.19	-
5	439.2	34.75	10.09	2.102.9	103.2	-	20.19	0.02	2.27	-	6.02	71.31	0.18	-
6	620.0	35.10	10.09	2.102.9	103.2	-	20.19	0.02	2.27	-	6.02	71.31	0.18	-
7	890.0	32.70	10.09	2.825.0	122.5	-	2.25	8.87	5.62	-	46.75	36.38	0.14	-
7B	764.7	32.20	10.09	2.825.0	122.5	-	2.25	8.87	5.62	-	46.75	36.38	0.14	-
8	330.0	31.70	10.09	2.825.0	122.5	-	2.25	8.87	5.62	-	46.75	36.38	0.14	-
9	405.0	31.00	10.09	2.825.0	120.3	-	2.25	1.98	12.51	-	53.63	29.49	0.14	-
10	170.2	30.50	10.09	2.825.0	120.3	-	2.25	1.98	12.51	-	53.63	29.49	0.14	-
10D	31.0	30.50	10.09	2.825.0	120.3	-	2.25	1.98	12.51	-	53.63	29.49	0.14	-
11	31.0	30.50	5.96	2.000.2	120.3	-	3.18	2.80	17.66	-	75.74	0.42	0.19	-
12	31.0	29.50	0.75	1.339.0	89.9	-	-	-	-	-	100.00	-	-	-
12A	31.0	29.50	0.76	1.348.4	90.5	-	-	-	-	-	100.00	-	-	-
13	61.3	39.00	0.01	9.3	0.63	-	-	-	-	-	100.00	-	-	-
13A	31.0	29.50	0.01	9.3	0.63	-	-	-	-	-	100.00	-	-	-
14	31.0	1.30	5.20	651.8	29.7	-	9.76	8.60	54.20	-	25.57	1.28	0.60	-
15	15.0	70.00	0.45	89.9	20.9	-	89.00	-	2.00	8.11	-	-	0.89	-
15B	23.3	1.30	5.65	741.7	50.7	-	19.37	7.56	47.87	0.98	22.47	1.12	0.63	-
16	15.0	1.01	18.15	2.263.5	-	0.92	-	-	0.03	-	-	0.96	77.34	20.75
17	270.0	1.08	18.15	2.263.5	-	0.92	-	-	0.03	-	-	0.96	77.34	20.75
17-IN	22.6	1.09	18.15	2.263.5	-	0.92	-	-	0.03	-	-	0.96	77.34	20.75
18	425.0	1.07	18.15	2.263.5	-	0.92	-	-	0.03	-	-	0.96	77.34	20.75
19	1010.0	0.99	23.80	2.898.1	-	0.72	-	-	19.71	-	-	17.49	60.57	1.51
19-B	862.4	0.97	23.80	2.898.1	-	0.72	-	-	19.71	-	-	17.49	60.57	1.51
20	748.5	0.95	23.80	2.898.1	-	0.72	-	-	19.71	-	-	17.49	60.57	1.51
21	644.0	0.91	23.80	2.898.1	-	0.72	-	-	19.71	-	-	17.49	60.57	1.51
22	543.5	0.89	23.80	2.898.1	-	0.72	-	-	19.71	-	-	17.49	60.57	1.51
22A	508.8	0.88	23.80	2.898.1	-	0.72	-	-	19.71	-	-	17.49	60.57	1.51
23	392.9	0.86	23.80	2.898.1	-	0.72	-	-	19.71	-	-	17.49	60.57	1.51
24	314.1	0.84	23.80	2.898.1	-	0.72	-	-	19.71	-	-	17.49	60.57	1.51
24B	142.7	0.83	23.80	2.898.1	-	0.72	-	-	19.71	-	-	17.49	60.57	1.51
25	191.8	1.18	23.80	2.898.1	-	0.72	-	-	19.71	-	-	17.49	60.57	1.51
26	150.8	6.00	11.19	2.236.3	-	-	-	-	-	-	-	100.00	-	-
26C	152.8	100.00	11.19	2.236.3	-	-	-	-	-	-	-	100.00	-	-
28	275.0	100.00	11.19	2.236.3	-	-	-	-	-	-	-	100.00	-	-
28B	275.0	100.00	7.59	1.516.3	-	-	-	-	-	-	-	100.00	-	-
28C	310.2	100.00	7.59	1.516.3	-	-	-	-	-	-	-	100.00	-	-
28D	275.0	100.00	3.60	719.9	-	-	-	-	-	-	-	100.00	-	-
28E-1	275.0	100.00	1.53	305.1	-	-	-	-	-	-	-	100.00	-	-
28E-2	310.2	100.00	1.53	305.1	-	-	-	-	-	-	-	100.00	-	-
28E-3	485.0	100.00	1.53	305.1	-	-	-	-	-	-	-	100.00	-	-
28F-1	275.0	100.00	2.08	414.8	-	-	-	-	-	-	-	100.00	-	-
28F-2	310.2	100.00	2.08	414.8	-	-	-	-	-	-	-	100.00	-	-
28F-3	485.0	100.00	2.08	414.8	-	-	-	-	-	-	-	100.00	-	-
29	485.0	100.00	7.59	1.516.3	-	-	-	-	-	-	-	100.00	-	-
30	485.0	100.00	3.60	719.9	-	-	-	-	-	-	-	100.00	-	-
30B	485.0	100.00	11.19	2.236.3	-	-	-	-	-	-	-	100.00	-	-
30C	348.1	40.00	11.19	2.236.3	-	-	-	-	-	-	-	100.00	-	-
31	348.1	40.00	7.90	1.578.3	-	-	-	-	-	-	-	100.00	-	-
31A	348.1	40.00	3.29	658.0	-	-	-	-	-	-	-	100.00	-	-
32	159.7	6.00	3.29	658.0	-	-	-	-	-	-	-	100.00	-	-
CON	31.0	30.50	4.13	824.8	-	-	-	-	-	-	-	100.00	-	-

Table 4.5 Operative condition of fired tubular reforming plant

4.1.1 Modelling of FTR in Aspen Plus

In this section we present the modelling in *Aspen Plus* in more detail. Throughout the system (both FTR and retrofit) the Peng-Robinson state equation has been used. It is able to model quite effectively the real gas behaviour with regard to the hydrocarbon molecules present in the input fuel. To achieve the operating conditions described above, it is necessary to use numerous calculators and design specs, i.e. objective functions calculated iteratively until convergence.

The several DS used make the system very difficult to converge and for this reason it was necessary to analyse the calculation sequences and identify the tear streams, i.e. flows within the system that carry out recirculation and need input parameters not far from the point of convergence. In addition to this, we had to analyse and choose the correct components for the modelling of the various parts of the plant that will be described below. All the reactors used are RGibbs type because it calculates the reactions up to equilibrium.

Fired Tubular Reforming Reactor: as shown in figure 4.2 it was modelled with an RGibbs reactor set to equilibrium at a temperature of 890°C with a pressure drop of 7.00%. All molecules of the pre-reformed charge are allowed to react, keeping only Ar and N_2 as inert. The incoming heat, modelled as a heat stream, comes from the combustor.

Combustor: it is still an RGibbs reactor. In this case you have as input flows the air coming from the preheating zones (stream 18) and the mix of natural gas and offgas (stream 15B) coming from the PSA let it react up to the equilibrium where once again the only inerts considered are nitrogen and argon. In this case there is a pressure drop about 7.00% and we considered the outlet temperature of the flue gas equal to 1010°C. As shown in figure 4.2. three heat flows start from this reactor: Q_2 to the FTR, Q_{LOSS} simulates the heat losses imposed by a calculator equal to 0.2% of Q_2 and the last Q_{RES} is a trick created specifically to model the correct operation through a Design Spec. Thanks to this DS we have changed the amount of natural gas split in the flow 15 (see figure 4.1) so that the Q_{RES} is zero modelling the FTR component. The amount of air entering for the correct combustion reaction was also decided by a DS; in fact, the mass flow rate of air inlet to the system was varied until the molar fraction of O_2 in the flue gas (flow 19) is 1.50% [52], in order to have the right excess of air for a complete combustion.

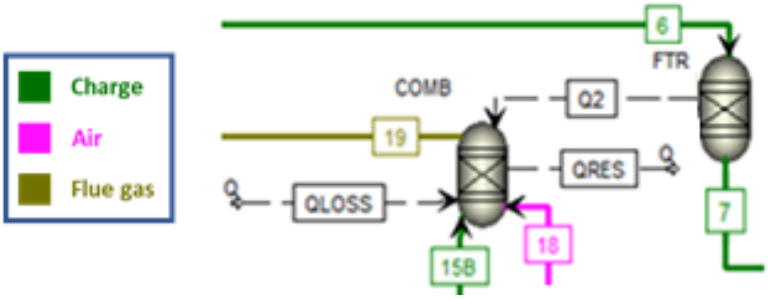

Figure 4.2 Fired Tubular Reforming reactor modelling in Aspen Plus

Pre-reforming reactor: it is an RGibbs reactor carried to equilibrium by imposing adiabaticity and a pressure drop of 3.00% as input data. Also in this case all molecules react except N_2 and Ar, the only inert ones.

Hydrogenator and sulfur removal: these two components, present in a real plant, have not been modelled as reactors for simplicity because the composition found in the literature and as a reference from the *Demoys* [52] does not consider sulfur within the composition of natural gas as it is a very low quantity. Therefore, these two components have not been modelled but we have considered and kept constant the operating conditions for their correct functioning as if they were in the system. In fact, we have set the flow temperature 3 at the outlet of the exchanger to 365°C necessary for charge pre-treatment. Through a Design Spec we decided the amount of H_2 splitted in the flow 13-A in order to have in flow 3 a molar fraction of hydrogen equal to 2.1% [52] in order to simulate the amount of H_2 needed for the pre-treatments; finally we imposed a pressure drop in the next mixer with the steam equal to 2.00%.

Air and flue gas fans: the fans are operated in isentropic mode at the operating conditions expressed in table 4.3 and have been modelled with the *Aspen Plus* compressor model. Both have an output pressure such as to overcome pressure losses: air is compressed up to 1.09 bar and flue gas up to 1.18 bar.

H_2 compressor: it is modelled as an isentropic compressor at operating conditions as in table 4.4 at a discharge pressure of 39 bar such as to have a correct charge pressure at the outlet of the FTR of 32.7 bar considering all the pressure drops.

PSA, cooler and water separator: PSA has been modelled in a very simplified way using the *Aspen Plus* separator model in order to separate the right amount of H_2 from the incoming charge of high temperature WGS.

The operating conditions are described in table 4.4; the output offgas pressure after bed regeneration is 1.3 bar. The right amount of H_2 to be sent for export is decided by means of a DS on the incoming natural gas mass flow rate so that 0.75 kg/s of hydrogen is produced [52]. The PSA operates at a temperature of 31°C and for this reason the incoming flow from the syngas cooler section is cooled via the *Aspen Plus* cooler, a generic heat exchanger that has no cooling flow specification. In reality it is assumed that there is water that cools the gas flow and that it needs the auxiliary pumps for circulation in the heat exchanger. We have taken this fact into account considering an electrical consumption of the auxiliaries equal to 1% of the thermal load as shown in table 4.4. Moreover, the condensed water coming out of the cooler is separated through a separator.

Flue gas recovery heat exchangers

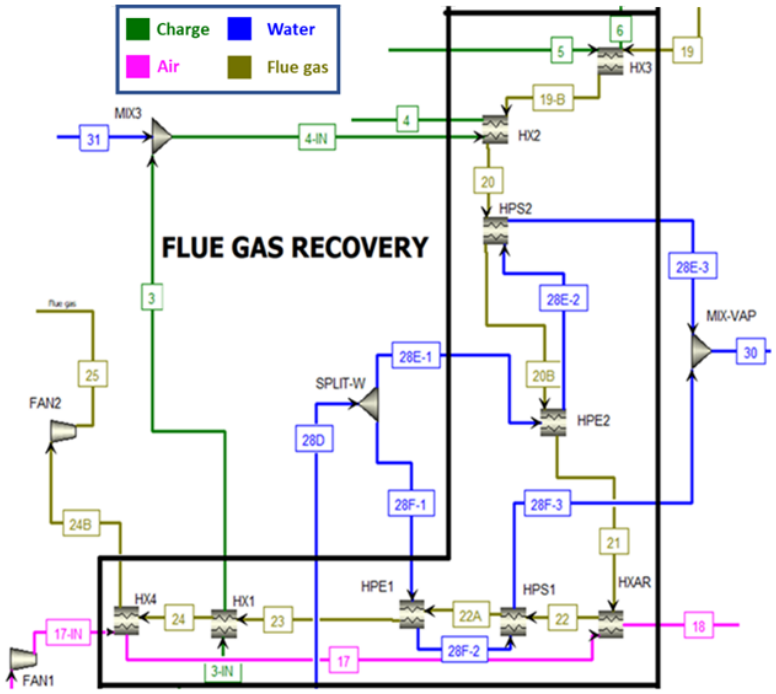

Figure 4.3 Flue gas recovery Aspen Plus section

As you can see from figure 4.3 all heat exchangers have been modelled with the MHeatX model. This allows the calculation of the two heat and cold flows separately in order to facilitate the convergence of the system. For all heat exchangers the operating conditions in table 4.4 have been used. The two evaporators (*HPE1*, *HPE2*) and the high pressure superheaters (*HPS1*, *HPS2*) have the function of generating steam for the right inlet conditions at the high pressure turbine: a temperature of 485 °C and a pressure of 100 bar [52]. The evaporators have been modelled with an input of 0.1 °C superheating to ensure that there is saturated steam at the outlet. The right amount of water from the syngas cooler section economiser (stream 28D) is split by the *splitw* in figure 4.3. To do this, a Design Spec was used on the *splitw* in order to divide the water mass flow rate in order to have a cooling of the flue gas coming out of the second evaporator (stream 21) at 644 °C [52].

In order to find the right amount of water to be sent throughout the recovery section (stream 28D) it was necessary to use another DS to control the amount of H_2O entering the system until the temperature of stream 23 is equal to 393 °C as reported by Demoys [52]. The output temperatures from the heat exchangers are verified in order to respect the operating limit parameters in table 4.4.

Below is the T-Q diagram for the flue gas recovery section.

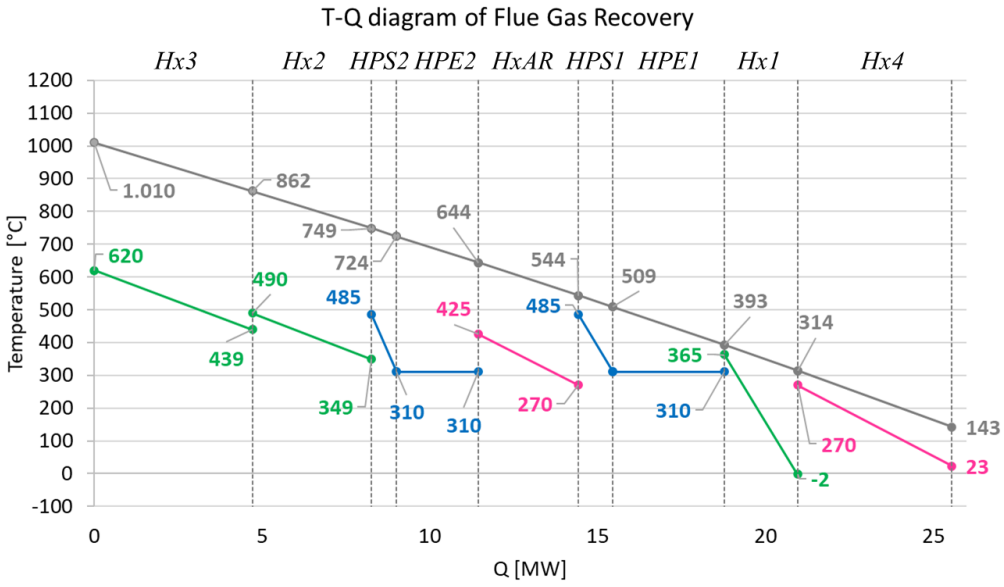

Figure 4.4 T-Q diagram of Flue gas recovery of Aspen Plus section

WGS reactor: water gas shift reactor was modelled with RGibbs set to equilibrium and adiabatic. In order to reach the optimal temperature of 330 °C at the reactor inlet (stream 8) it is necessary to use another DS that controls the amount of water split by the *splitWGS* in figure 4.5.

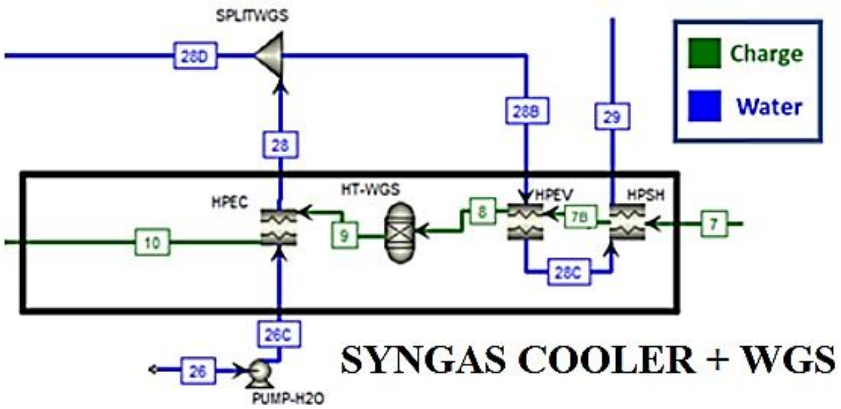

Figure 4.5 Syngas cooler section +WGS Aspen Plus section

Also in this section the heat exchangers are modelled with a MHeatX for the same reasons described above; also in this case the evaporator is set to 0.1 °C superheating condition and the output temperatures of the superheater and economizer have been set to 385°C and 275°C respectively as per *Demoys* [52].

By means of the following T-Q diagram it is possible to see how also in this case the minimum ΔT are satisfied and the gas cooling line has been optimised.

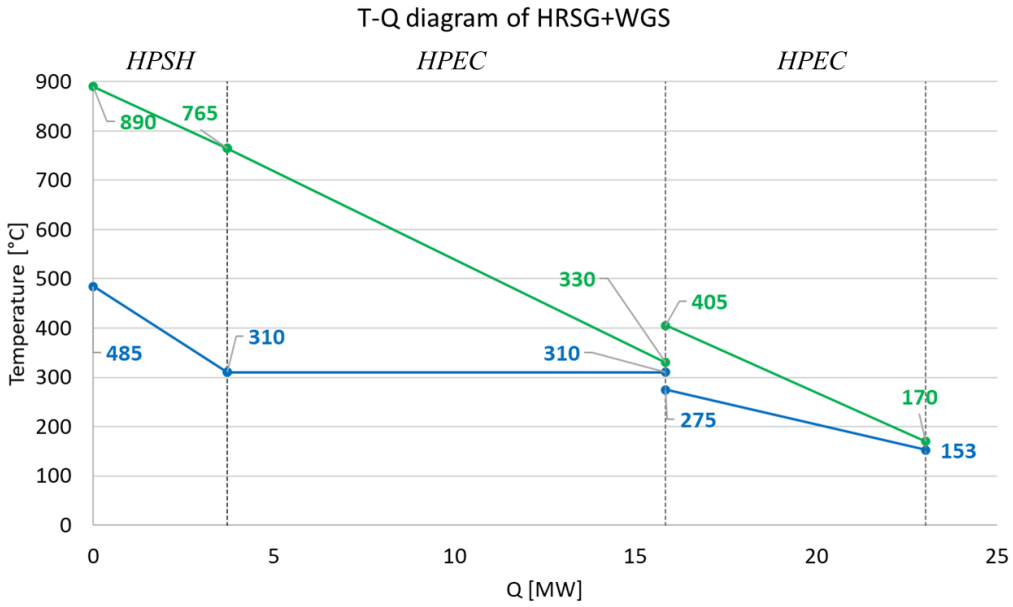

Figure 4.6 T-Q diagram of syngas cooler section in Aspen Plus

HP and LP turbines: both turbines are modelled with the turbine model in isentropic mode at the operating conditions shown in Table 4.4. Based on *Demoys* [52] the exhaust pressures are set at 40 bar and 6 bar respectively for the high and low pressure turbine. As can be seen from figure 4.7 at the high pressure turbine exhaust, through a calculator, part of the steam has been split by the splitter *splistc* to obtain the necessary quantity to be mixed with natural gas to have the right steam to carbon ratio set at 3.4 [52].

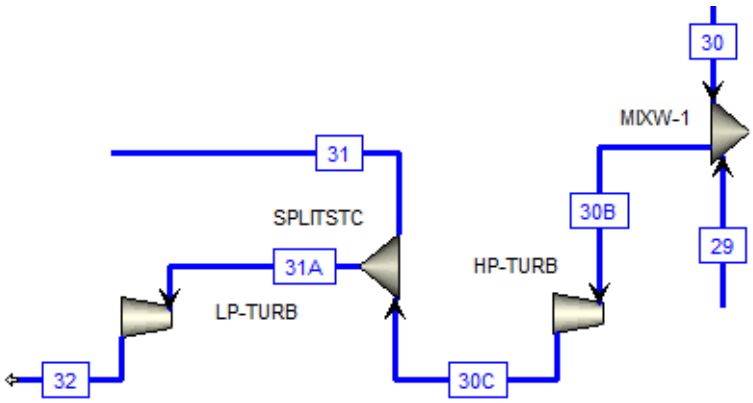

Figure 4.7 Power production Aspen Plus section

4.2 Case A – Base case for retrofit with post-combustion capture

The plant, as we have previously mentioned, is based on the use of molten carbonate fuel cells (MCFC) for the post-combustion capture of CO_2 from the exhaust gases of one of the most emissive processes in a refinery (e.g. the production of hydrogen from steam reforming). As shown in table 4.6 [54], most of the CO_2 emissions derive from fuel combustion in process heaters, utility boilers and power generation plants, followed by FCC and hydrogen plant.

Relevant streams	CO_2 concentration, %v/v	Other component and impurities	% of total emission
Process heaters and utilities flue gas	Gas-fired: 3-6 Oil fired: 7-12	O_2 (2-6%v/v), SO_2 (gas-fired: 10-20 ppmv, oil-fired: 50-600 ppmv), SO_3, NO_x	Process heaters: 30-60 Utilities: 20-50
Fluid catalytic cracker flue gas	8-12	O_2 (1-2%v/v), SO_2 (1000-15000 ppmv), catalyst dust, CO, SO_3, NO_x	20-35
H_2 production plants Syngas PSA off-gas Regenerator off-gas FTR furnace flue gas	 15-35 (@ 20-30 bar) 40-50 95-99 5-20	 H_2, CO, CH_4, N_2 H_2, CO, CH_4, N_2 Traces O_2 (2-6%v/v), NO_x	 - - - 5-20

Table 4.6 Characteristics of the refineries streams relevant for CO2 capture. [54]

The application of post-combustion capture, compared to other capture strategies, has the advantage of requiring limited changes to the upstream process layout. This makes it easy to retrofit the existing plant. On the other hand, the CO_2 concentration in the exhaust gases is rather low (see table 4.6) and conventional post-combustion capture concepts typically require the adoption of chemical solvents (amines MEA type, paragraph 2.5.1) to absorb carbon dioxide. As mentioned in the cited paragraph, the adoption of such "passive" carbon capture processes has removal efficiencies of up to 90% but has the disadvantage of considerably reducing plant efficiency due to the huge amount of thermal energy required to regenerate chemical solvents. In fact, the installation of additional plants to produce steam must be taken into account (this not be feasible without a retrofit of the site utility system [54]) and, depending on the fuel used, this entails additional GHG emissions that would only partially offset the CO_2 reduction obtained.

The use of MCFCs for CCS applications in the energy sector (*Chiesa et al.* 2010 [57]). in the cement sector (*Romano et al*. 2014 [59]) and in the steel sector (*Mastropasqua et al*. 2019 [55]) has already been discussed in previous work carried out by the *GECoS* research group [58]. As far as CO_2 capture is concerned, MCFCs have a rather unique feature among the proposed technologies because they allow, in addition to capture, to generate electricity and hydrogen (which requires a moderate fuel utilisation factor); they represent useful products in a refinery.

Three different plant solutions for CO_2 capture have been proposed:

- Case A: natural gas fuel cell supply
- Case B: fuel cell supply with FTR offgas
- Case C: fuel cell supply with natural gas but without H_2 production

This is useful to verify the best on-design condition when the fuel utilization factor and cell ΔV change. Finally, we presented case D that wants to investigate the off-design behaviour of the cell in case A. In this case we assume to be in a context of strong decarbonisation of the industrial system, where refinery methane reforming also actively participates in hydrogen production for market purpose.

4.2.1 MCFC section description

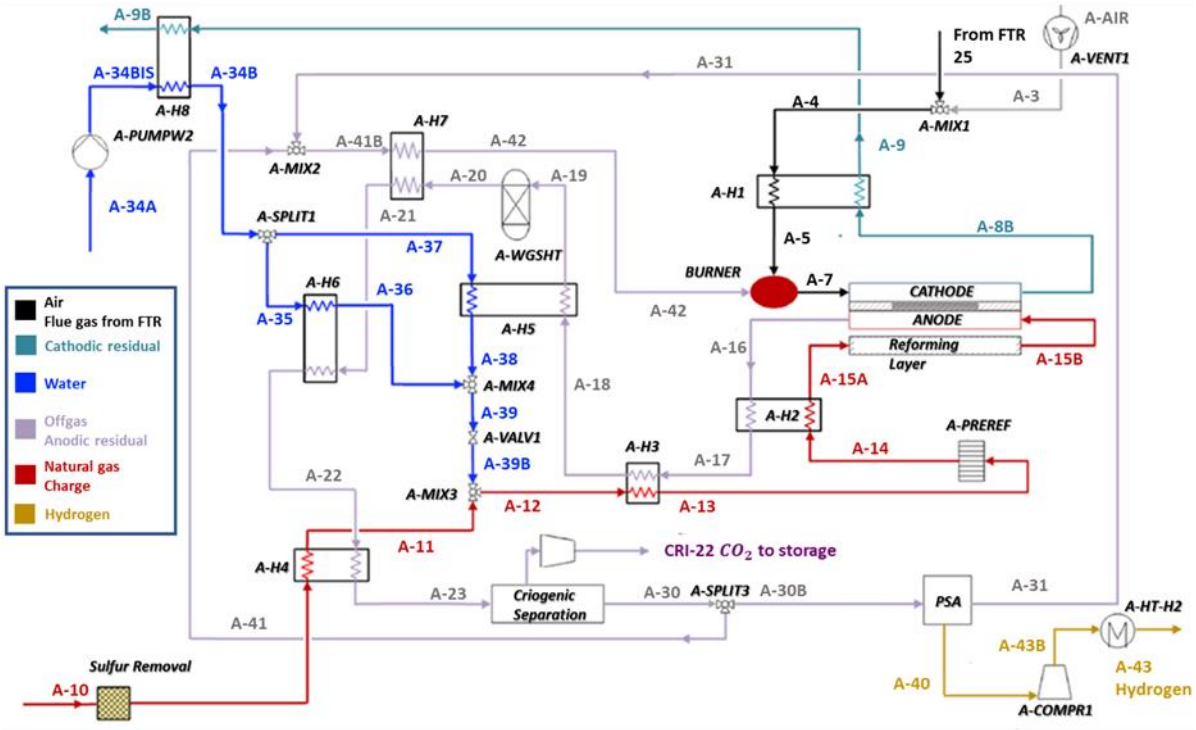

Figure 4.8 MCFC plant with natural gas alimentation - Base case A

We have chosen the plant configuration shown in figure 4.8 with a fuel utilisation factor of 0.75 as the basis for our analyses. A sensitivity analysis will then be carried out, making it change between 0.67 and 0.75.

Below is the flow table with the thermodynamic conditions in the base case.

#	T	P	m	N	QLHV	Mole fraction								
	° C	bar	kg/sec	kmol/hr	MW	Ar	CH_4	CO	CO_2	C_2+	H_2	H_2O	N_2	O_2
A-3	31	1.18	57.9	7.227.4	-	0.92	-	-	0.03	-	-	0.96	77.34	20.75
A-4	80.7	1.18	81.7	10.125.5	-	0.86	-	-	5.66	-	-	5.69	72.54	15.24
A-5	530	1.16	81.7	10.125.5	-	0.86	-	-	5.66	-	-	5.69	72.54	15.24
A-7	575.1	1.12	82.8	10.237.0	-	0.85	-	-	6.46	-	-	6.17	71.76	14.75
A-8A	575.1	1.10	73.4	9.387.6	-	0.93	-	-	1.01	-	-	6.73	78.26	13.07
A-8B	645	1.10	73.4	9.387.6	-	0.93	-	-	1.01	-	-	6.73	78.26	13.07
A-9	153.6	1.08	73.4	9.387.6	-	0.93	-	-	1.01	-	-	6.73	78.26	13.07
A-9B	142.6	1.06	73.4	9.387.6	-	0.93	-	-	1.01	-	-	6.73	78.26	13.07
A-10	15.0	1.17	0.9	181.3	42.19	-	89.00	-	2.00	8.11	-	-	0.89	-
A-11	140	1.15	0.9	181.3	42.19	-	89.00	-	2.00	8.11	-	-	0.89	-
A-12	127.2	1.15	2.9	586.5	42.19	-	27.51	-	0.62	2.51	-	69.09	0.28	-
A-13	450.0	1.13	2.9	586.5	42.19	-	27.51	-	0.62	2.51	-	69.09	0.28	-
A-14	246.0	1.09	2.9	657.8	43.52	-	23.91	0.02	5.95	-	19.09	50.78	0.25	-
A-15A	450	1.07	2.9	657.8	43.52	-	23.91	0.02	5.95	-	19.09	50.78	0.25	-
A-15B	600	1.07	2.9	972.5	52.09	-	-	12.59	7.62	-	65.04	14.58	0.17	-
A-16	645	1.05	12.4	1.538.8	13.41	-	-	4.14	45.44	-	8.14	42.18	0.10	-
A-17	565.7	1.03	12.4	1.538.8	13.41	-	-	4.14	45.44	-	8.14	42.18	0.10	-
A-18	446.4	1.01	12.4	1.538.8	13.41	-	-	4.14	45.44	-	8.14	42.18	0.10	-
A-19	330	0.99	12.4	1.538.8	13.41	-	-	4.14	45.44	-	8.14	42.18	0.10	-
A-20	361.7	0.96	12.4	1.538.8	12.82	-	-	0.77	48.81	-	11.50	38.82	0.10	-
A-21	338.9	0.94	12.4	1.538.8	12.82	-	-	0.77	48.81	-	11.50	38.82	0.10	-
A-22	176.4	0.92	12.4	1.538.8	12.82	-	-	0.77	48.81	-	11.50	38.82	0.10	-
A-23	160.7	0.90	12.4	1.538.8	12.82	-	-	0.77	48.81	-	11.50	38.82	0.10	-
A-26B	160.7	0.90	12.4	1.538.8	12.82	-	-	0.77	48.81	-	11.50	38.81	0.10	-
A-30	30	22.36	1.1	263.3	12.56	-	-	4.22	29.12	-	66.09	-	0.57	-
A-30B	30	22.36	0.9	201.5	9.61	-	-	4.22	29.12	-	66.09	-	0.57	-
A-31	30	1.18	0.8	83.0	1.65	-	-	10.24	70.72	-	17.66	-	1.39	-
A-34A	15	1.01	2.0	405.2	-	-	-	-	-	-	-	100.00	-	-
A-34B	106.8	2.00	2.0	405.2	-	-	-	-	-	-	-	100.00	-	-
A-34BIS	15	2.00	2.0	405.2	-	-	-	-	-	-	-	100.00	-	-
A-35	106.8	2.00	1.2	232.0	-	-	-	-	-	-	-	100.00	-	-
A-36	121.8	2.00	1.2	232.0	-	-	-	-	-	-	-	100.00	-	-
A-37	106.8	2.00	0.9	173.3	-	-	-	-	-	-	-	100.00	-	-
A-38	121.8	2.00	0.9	173.3	-	-	-	-	-	-	-	100.00	-	-
A-39	121.8	2.00	2.0	405.2	-	-	-	-	-	-	-	100.00	-	-
A-39B	120.1	1.15	2.0	405.2	-	-	-	-	-	-	-	100.00	-	-
A-40	30	21.36	0.1	118.5	7.96	-	-	-	-	-	100.00	-	-	-
A-41	30	22.36	0.3	61.9	2.95	-	-	4.22	29.12	-	66.09	-	0.57	-
A-41B	28.5	1.18	1.1	144.8	4.60	-	-	7.67	52.95	-	38.35	-	1.04	-
A-42	300	1.16	1.1	144.8	4.60	-	-	7.67	52.95	-	38.35	-	1.04	-
A-43	31	29.50	0.1	118.5	7.96	-	-	-	-	-	100.00	-	-	-
A-43B	65.2	29.50	0.1	118.5	7.96	-	-	-	-	-	100.00	-	-	-
A-AIR	15	1.01	57.9	7.227.4	-	0.92	-	-	0.03	-	-	0.96	77.34	20.75
A-PERMEA	575.1	1.10	9.4	849.4	-	-	-	-	66.68	-	-	-	-	33.32

Table 4.7 Case A – Operative conditions of MCFC section

Here we report the main assumptions used in the modelling of the system.

Parameter	Unit	Value
Pump, fan and compressor		
Pump hydraulic efficiency	%	70
H2 compressor isentropic efficiency	%	84
Outlet pressure for hydrogen export	bar	29.5
Blower isentropic efficiency	%	80
Mechanical efficiency	%	94
Electrical efficiency	%	98.5
Reactor		
HT-WGS inlet temperature	°C	330
Adiabatic pre-reformer inlet temperature	°C	450
Internal reformer inlet temperature	°C	450
Pressure losses	%	3
Adiabatic pre-reformer S/C ratio	-	2.1
Adiabatic pre-reformer ethane conversion	%	100
Adiabatic pre-reformer methane conversion	%	2.5
Molten carbonate fuel cell		
Cathode inlet temperature	°C	575
Anode inlet temperature	°C	600
Cell operating temperature	°C	645
Cathode inlet pressure	bar	1.12
Anode inlet pressure	bar	1.07
Maximum cathodic ΔT across cell	°C	70
Minimum xO2 cathode outlet	%	2.5
Minimum xCO2 cathode outlet	%	1
Minimum cell voltage	mV	600
Air/fuel channels pressure losses	%	2
DC/AC electrical efficiency	%	94
Heat loss	%LHV	1
Heat exchangers		
Heat losses	% of heat transferred	1
Min ΔT gas-gas	°C	30
Min ΔT gas-liquid	°C	10
Min ΔT liquid-liquid	°C	10
Subcooling ΔT	°C	15
Pressure drop liquid phase	%	-
Pressure drop gas phase	%	2
Miscellaneous		
Electric auxiliaries for heat rejection	% of heat rejected	1
PSA		
Hydrogen separation efficiency	%	89
Operating temperature	°C	30
Pressure drop hydrogen	%	4
Rigeneration pressure	bar	1.18

Table 4.8 Main assumption for MCFC section

In the proposed cycle arrangement (figure 4.8), the process exhaust gases (stream 25) are used directly as a supply to the cathode of the cell, where CO_2 permeates through the electrolyte to the anode, concentrating the carbon dioxide to the exhaust of the latter (stream A-16).

Before entering the fuel cell, the gases from the FTR are mixed with ambient air (stream A-AIR, forced by a fan, *A-VENT1*, in order to overcome pressure drops) to provide sufficient oxygen for cathodic reactions and to control the cell temperature.

This mixture then enters a Ljungstrom regenerative heat exchanger (*A-H1*) where it heats up, cooling the hot cathodic residue (stream A-8B), until cold stream reaches a temperature of 530 °C; in this way it is possible to use less fuel at the burner and to reduce the second principle losses at the stack due to outgoing exhaust gases.

The oxidant mixture then enters a catalytic burner. This is fed by the flow coming out of the cryogenic section (stream A-41) which contains oxidisable species such as CO and H_2 and by the PSA offgas (stream A-31); this mixture before being oxidized is preheated to a temperature of 300 °C in the exchanger *A-H7* cooling the hot anodic residue coming out of the high temperature WGS reactor. The fuel flow temperature of 300 °C is set in order to respect the ΔT at the heat exchanger; in fact the operating temperature of the WGS reactor is 330 °C, therefore not knowing a priori the temperature at the outlet (because the reaction is endothermic) we try to maintain at least the temperature difference of 30 °C.

This combustor, in addition to providing the necessary heat for the correct cathode inlet temperature (set at 575 °C), oxidises the carbon monoxide present in the offgas flow, increasing the concentration of CO_2 at the inlet. As suggested in a previous study of the steel mill [55], it is assumed that the sulphur content of the exhaust gases is low enough (less than 1 ppm) to avoid further off-gas cleaning sections. Otherwise multi-stage wet scrubbers or other desulphurisation systems are required [55].

The fuel cell operates at approximately atmospheric pressure and is supplied with natural gas. The fuel (stream A-10) is preheated and desulphurised in advance if necessary (by means of ZnO beds) as MCFC does not tolerate the presence of sulphur compounds.

The external pre-reformer (which requires an input temperature of 450 °C) converts all hydrocarbons above methane and part of it. As the endothermic reaction, this component lowers the exit temperature (stream A-14), thus requiring an additional heat exchanger to reach an inlet temperature of 450 °C at the anode side (stream A-15A).

In the diagram in figure 4.8 the discharge flow from the anode, at a temperature of 645 °C, is cooled by preheating the charge, producing the steam necessary to obtain the correct steam to carbon ratio: the quantity of water necessary for the process enters with the flow A-34A at ambient conditions. It is first pumped up to 2 bar by means of a centrifugal pump in order to overcome the pressure drops in the following exchangers and to allow an optimization of the heat recovery from the anodic residue thanks to a higher evaporation temperature. This also makes it possible to have smaller evaporator ducts.

The water is then preheated to 107 °C (maintaining a sub-cooling ΔT of 15 °C) in an economiser (*A-H8*) that uses the heat from the hot cathodic residue. This sub-cooling ΔT has been chosen so that there is enough flexibility in the operation of the off-design system.

In some configurations, on the other hand, the anodic residue is used to economise water but in the basic case proposed here, this solution cannot be pursued in order to respect the minimum ΔT in the subsequent exchangers; moreover, decreasing the temperature of the stream A-9 allows lower second principle losses to the stack.

It can be an equivalent solution to use the anodic residue as a hot fluid in the economiser, while in the natural gas preheater (*A-H4*) the cathodic fluid can be used. However, this solution was avoided in order to prevent safety problems in the system in the case of natural gas leaks, which would then escape with the cathodic residue. This problem does not exist in the first case because water leaks in the cathodic residue do not give any safety problems, as well as natural gas leaks in the anodic residue because it will be subsequently processed in the cryogenic section for CO_2 separation.

The amount of water divided between flow A-35 and A-37 via the splitter (*A-SPLIT1*) is set with a Design Spec so that the correct operating temperature (330 °C) is present at the WGS-HT inlet. The water evaporation process is divided between two evaporators that recover the available heat in the anodic exhausts. The saturated steam produced at T_{sat} = 122 °C (streams A-36 and A-38 mixed in the mixer *A-MIX4*) is mixed with natural gas (stream A-11) in the mixer (*A-MIX3*). The flow of natural gas to be mixed is first heated (in the exchanger *AH-4*) from the inlet conditions to a sufficient temperature so as not to cause condensation of the steam flow during mixing.

The presence of the WGS reactor is necessary in order to allocate the calorific value from CO to H_2 and increase the concentration of carbon dioxide before the cryogenic section. In this study it is assessed whether a low-temperature shift reactor is also required. Since the concentration of carbon monoxide leaving the high-temperature reactor is very low (0.77% for the base case, but also in other plant configurations it is always very low, around 1%) the additional cost of this component does not justify the advantages that can be obtained.

The anodic flow out of the last heat exchanger (*A-H4*) is processed in the GPU (gas purification unit) which has the task of obtaining a stream of pure CO_2 to be sent to storage and a stream of hydrogen-rich to be purified in a PSA.

Single MCFC

We have chosen to use a single MCFC and not two stacks in series because the CO_2 concentration coming out of the SMR is not too concentrated in CO_2. The operating conditions of the cell are fixed referring to the work carried out by *Mastropasqua et al* [55]. The cathode inlet temperature is set at 575 °C in order to minimize the input air flow, while the cell outlet temperature is 645 °C and is within the operating range of an MCFC cell as described in paragraph 3.2.4. The CO_2 concentration at the exit from the cathode is set at the minimum possible value in order to maximize the separation efficiency of the cell as reported by Spinelli et al [62]. The minimum value is 0.5 – 1 %. For oxygen exit from the cathode a concentration higher than 2.5 % is also required. These limits are due to the fact that if the concentration of reactants at the outlet is too low, diffusion losses would increase severely the MCFC resistance, and the efficiency would decrease more rapidly as a function of the current density value. The cell voltage is imposed at the value of 0.7 V even if it does not coincide with the point of maximum power density. As will be clear in the sensitivity analysis on the ΔV, a higher value of it guarantees a higher capture efficiency but a lower power density with, therefore, a larger area with the same power. In our opinion, 0.7 V is a good compromise value for the base case.

TQ diagram of heat exchangers

We discussed the heat recovery line. Its correct design is important to maximize the thermal efficiency of the system. An optimal profile can be achieved in the heat exchanger network avoiding heat waste but also respecting the ΔT_{min} of the different types of heat exchangers. In the design procedure the layout of the heat exchangers is set with the optimal positioning for each component in order to recover heat efficiently. The operating temperatures of the WGS reactors, the temperature drop of the pre-reformers and the optimal thermal condition of the fuel cells influence the thermal profiles and consequently the positioning procedure of the heat exchangers. It is worth noting that the heat output exchanged by the cathodic air-residue preheater is very high and will therefore require the use of an exchanger with a high surface area; as we will see later in the economic analysis this exchanger will be the one with the highest costs.

We report the T-Q diagrams of the anodic residue and cathodic residue (figure 4.9). As can be seen, between evaporator *A-H5* and preheater *A-H7* the temperature of the exhausted anodic flow increases thanks to the presence of the WGS reaction which, being exothermic, causes an increase in temperature between inlet and outlet.

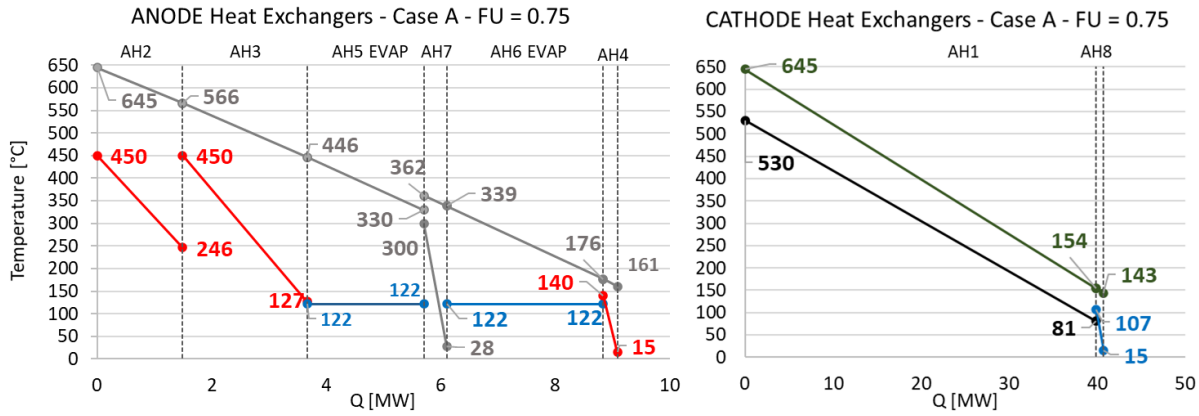

Figure 4.9 T-Q diagram Case A – FU fuel = 0.75

As can be seen from the T-Q diagrams, the minimum ΔT is always satisfied.

4.2.2 Cryogenic section description

The discharge from the shift reactor has a CO_2 concentration (about 80 % on a dry molar basis) that does not allow a purity corresponding to the standards required for transport and pipeline storage (CO_2 purity greater than 96 % [56]). In addition, the exhaust gas from the anode contains a significant amount of unreacted H_2 and CO. This requires a gas processing unit (GPU) to generate high purity CO_2 (stream CRI-22) and pure H_2 (stream A-40).

This separation should be carried out by cryogenic techniques, where the temperature is made low enough so that most of the CO_2 is condensed and separated by gravity from the combustible gaseous species included in the mixture which have a much lower boiling point. Various solutions can be adopted to organise the layout of this process, especially with regard to:

Internal vs. external cooling

The aim is to evaluate whether it is more convenient to reach the required low temperatures by throttling the separate CO_2 flow in a self-cooled cycle or by removing the heat by means of an external chiller. It is useful to remember the behaviour of a flow subject to lamination by introducing the Joule-Thomson effect "*In thermodynamics, the Joule-Thomson effect is a phenomenon in which the temperature of a real gas increases or decreases as a result of compression or expansion conducted at constant enthalpy. i.e. an adiabatic transformation from which no work is extracted*". We express the Joule-Thomson coefficient as

$$u_{JT} = \left(\frac{\partial T}{\partial P}\right)_H \qquad (4.1)$$

The value of u_{JT} depends on the gas under examination, as well as on its temperature and pressure before expansion.

For all real gases, this value is equal to zero at the inversion point, while for ideal gases u_{JT} = 0 for any condition because it depends on interactions between molecules. The liquid phase separated from the drum contains almost pure CO_2 and this component in the thermodynamic conditions considered has a positive u_{JT} value; so, if $\partial P < 0$ then $\partial T < 0$ and the system is self-cooled.

Liquid vs. gaseous CO_2 compression

The aim is to evaluate the convenience of reaching the pressure required for transport (which must be higher than the critical value, 73.8 bar) by pumping liquid CO_2 at low temperature or by compressing CO_2 in the gaseous phase. In the former case the compression work is reduced but the unfavourable heat balance in the exchangers requires additional energy consumption in the cooling process. This is because higher is the pressure, higher is the average temperature of the heat absorbed by the flow of liquid CO_2 (which circulates on the cold side of the heat exchangers) during the evaporation phase. In this case external chillers must be added to cool the flow circulating on the hot side. In our work, we are based on the scheme proposed in the article "*CO_2 cryogenic separation from combined cycles integrated with molten carbonate fuel cells*" by Paolo Chiesa et al. [57] which will be described below. Figure 4.10 shows the plant layout.

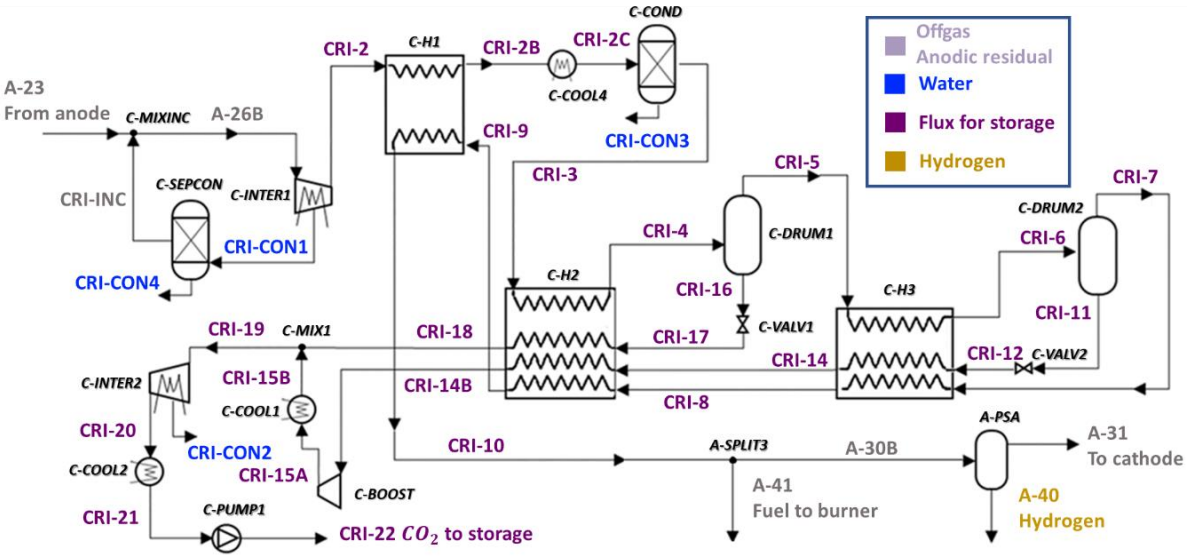

Figure 4.10 Cryogenic section

The table below shows the thermodynamic conditions for the case with fuel utilization factor equal to 0.75.

#	T C	P bar	m kg/sec	N kmol/hr	QLHV MW	Mole fraction								
						Ar	CH_4	CO	CO_2	C_2+	H_2	H_2O	N_2	O_2
CRI-2	104.9	24.16	9.40	945.0	12.82	-	-	1.26	79.47	-	18.73	0.37	0.17	-
CRI-2B	100.4	23.86	9.40	945.0	12.82	-	-	1.26	79.47	-	18.73	0.37	0.17	-
CRI-2C	30.0	23.86	9.40	945.0	12.82	-	-	1.26	79.47	-	18.73	0.37	0.17	-
CRI-3	30.0	23.86	9.39	941.5	12.82	-	-	1.27	79.77	-	18.79	-	0.17	-
CRI-4	-33.0	23.56	9.39	941.5	12.82	-	-	1.27	79.77	-	18.79	-	0.17	-
CRI-5	-33.0	23.56	3.54	461.4	12.65	-	-	2.47	59.26	-	37.93	-	0.33	-
CRI-6	-53.0	23.26	3.54	461.4	12.65	-	-	2.47	59.26	-	37.93	-	0.33	-
CRI-7	-53.0	23.26	1.13	263.3	12.56	-	-	4.22	29.12	-	66.09	-	0.57	-
CRI-8	-45.0	22.96	1.13	263.3	12.56	-	-	4.22	29.12	-	66.09	-	0.57	-
CRI-9	10.1	22.66	1.13	263.3	12.56	-	-	4.22	29.12	-	66.09	-	0.57	-
CRI-10	30.0	22.36	1.13	263.3	12.56	-	-	4.22	29.12	-	66.09	-	0.57	-
CRI-11	-53.0	23.26	2.41	198.1	0.09	-	-	0.16	99.34	-	0.48	-	0.02	-
CRI-12	-55.9	7.03	2.41	198.1	0.09	-	-	0.16	99.34	-	0.48	-	0.02	-
CRI-14	-38.9	6.73	2.41	198.1	0.09	-	-	0.16	99.34	-	0.48	-	0.02	-
CRI-14B	27.0	6.43	2.41	198.1	0.09	-	-	0.16	99.34	-	0.48	-	0.02	-
CRI-15A	91.0	13.64	2.41	198.1	0.09	-	-	0.16	99.34	-	0.48	-	0.02	-
CRI-15B	30.0	13.64	2.41	198.1	0.09	-	-	0.16	99.34	-	0.48	-	0.02	-
CRI-16	-33.0	23.56	5.84	480.1	0.17	-	-	0.10	99.48	-	0.41	-	0.01	-
CRI-17	-36.0	13.94	5.84	480.1	0.17	-	-	0.10	99.48	-	0.41	-	0.01	-
CRI-18	27.0	13.64	5.84	480.1	0.17	-	-	0.10	99.48	-	0.41	-	0.01	-
CRI-19	27.9	13.64	8.25	678.2	0.26	-	-	0.12	99.44	-	0.43	-	0.02	-
CRI-20	111.3	80.00	8.25	678.2	0.26	-	-	0.12	99.44	-	0.43	-	0.02	-
CRI-21	25.0	80.00	8.25	678.2	0.26	-	-	0.12	99.44	-	0.43	-	0.02	-
CRI-22	39.1	150.00	8.25	678.2	0.26	-	-	0.12	99.44	-	0.43	-	0.02	-
CRI-23A	30.0	22.36	1.13	263.3	12.56	-	-	4.22	29.12	-	66.09	-	0.57	-
CRI-CON1	30.0	2.03	2.97	593.8	0.00	-	-	0.00	0.00	-	0.00	100.00	0.00	-
CRI-CON2	0.0	-	-	-	-	-	-	-	-	-	-	-	-	-
CRI-CON3	30.0	23.86	0.02	3.5	-	-	-	-	-	-	-	100.00	-	-
CRI-CON4	30.0	2.03	2.97	593.8	-	-	-	-	-	-	-	100.00	-	-
CRI-INC	30.0	2.03	0.00	0.0	0.00	-	-	0.01	99.65	-	0.34	-	0.00	-

Table 4.9 Case A – Operative conditions of cryogenic section

The main assumptions of calculation for the cryogenic section are as follows

Parameter	Unit	Value
CO_2 liquid pump		
Hydraulic efficiency	%	80
Mechanical efficiency	%	84
Electrical efficiency	%	98.5
Liquid CO2 conditions at pump inlet	°C / bar	25 / 80
Outlet pressure	bar	150
Booster compressor		
Isentropic efficiency	%	84
Mechanical efficiency	%	94
Electrical efficiency	%	98.5
Intercooled compressor		
Isentropic efficiency	%	84
Mechanical efficiency	%	94
Electrical efficiency	%	98.5
CO2 compressor stage pressure ratio	-	2.5
Inter-coolers outlet temperature	°C	30
Inter-coolers pressure losses	%	2
Heat exchangers		
Minimum separation temperature	°C	-56
Minimum ΔT in the exchangers	°C	3
Heat loss	% of heat transferred	0.3
Pressure drop liquid phase	%	2
Pressure drop gas phase	%	2

Table 4.10 Main assumption for cryogenic section

The stream A-23 (anodic residue) is first compressed in a four-stage intercooled compressor (*C-INTER1*) at the pressure required to guarantee a CO_2 purity over 99%; we impose this condition through the use of a DS in *Aspen Plus*.

Considering figure 4.11, remember that at the same temperature if the pressure increases then xCO_2 in the liquid phase decreases while xCO_2 in the gas phase increases and we send to storage a flow less pure CO_2 but the gas phase contains a greater amount of the other components and therefore we lose less CO_2 in the vent. So the capture efficiency increases with pressure.

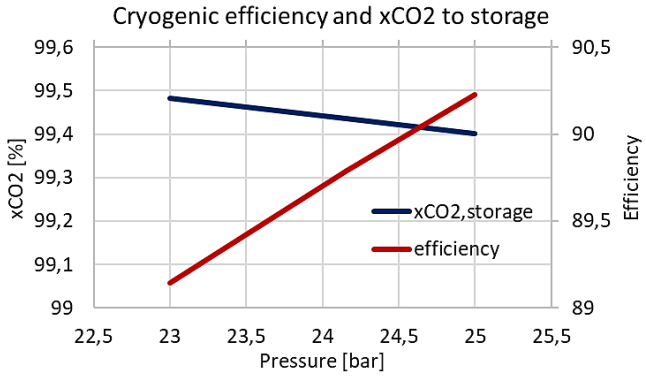

Figure 4.11 Cryogenic efficiency and xCO_2 to storage with respect pressure

The condensates are recirculated at the compressor inlet after separation from water, which is removed by a sour water stripper (which has a negligible influence on global energy processes). Stream CRI-2 is cooled by heating the charge to the PSA (stream CRI-9) up to 30 °C (process operating temperature), then it is cooled again to ambient temperature and enters a separator that removes all the water present; therefore, stream CRI-3 is dry.

The temperature at the hot side outlet of the heat exchanger *C-H2* (stream CRI-4) is an important parameter for the operation of process. Lowering this temperature facilitates condensation and reduces the mass flow rate sent to the *C-DRUM2* and therefore the mass flow rate condensate by the second drum (stream CRI-11) circulated to the CO_2 re-booster compressor (*C-BOOST*) and the associated power. On the other hand, lowering the temperature at point CRI-4 increases the duty of heat exchanger *C-H2*, requiring a greater pressure drop in the valve (*C-VALV1*) to maintain a given minimum temperature difference within *C-H2*; this reduces the pressure of the combined flow (CRI-19) entering the second intercooled compressor (*C-INTER2*), increasing the required power.

In order to find a compromise between these opposite effects, a sensitivity analysis is carried out on the temperature of the hot flow inlet to the first knockout drum so as to minimize the compression work demand of the entire cryogenic section (which includes the two intercooled compressors, the booster compressor and the liquid CO_2 pump). The sensitivity analysis carried out for case A with fuel utilization factor 0.75 is shown in figure 4.12.

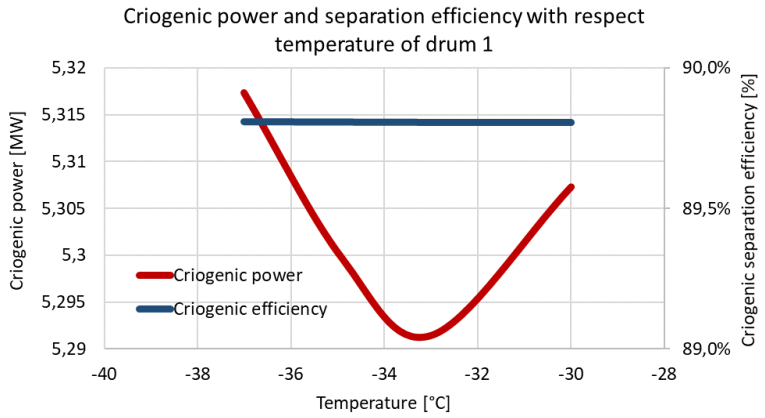

Figure 4.12 Sensitivity analysis of the cryogenic CO_2 separation island: effect of knockout drum temperature on power consumption and separation efficiency

The temperature of stream CRI-4 is set at -33 °C, a value that minimizes the overall compression power and satisfied the minimum ΔT at the heat exchangers.

Additionally, we have carried out a sensitivity analysis on the CO_2 capture efficiency trend when the temperature of the first knockout drum (*DRUM1*) changes, obtaining that there is no remarkable dependence between the two parameters; this is due to the presence of the second separator (*C-DRUM2*) which works at temperatures close to those of the triple point (-56.6 °C). The latter temperature was chosen because the separation efficiency increases

monotonically as the temperature decreases. As a result, the steam fraction coming out of the first knockout drum is further cooled to -53 °C by the heat exchanger *C-H3* (stream CRI-6). This value is chosen to ensure that the inlet temperature of cold side flow of heat exchangers *C-H3* (stream CRI-12) is slightly above (+ 0.6 °C) the CO_2 freezing point after being throttled by a valve (*C-VALV2*) which requires a cooling of - 3 °C (to achieve this we have imposed a DS in *Aspen Plus*).

The liquid of stream CRI-16, separated in the first knockout drum, is throttled through a valve (*C-VALV1*) and introduced into the cold side of the heat exchanger (*C-H2*) where it is heated and evaporated. The pressure drop in *C-VALV1* is set by means of a DS in order to guarantee a minimum ΔT of 3 °C inside *C-H2*. Since the knockout drums are isothermal, stream CRI-7 enters at the same outlet temperature as the hot flow and will therefore start exchanging heat in an intermediate part of the heat exchanger.

The separate liquid flows in the drums and evaporated in the heat exchangers are set to the same pressure. The booster compressor is used to send the liquid coming out from the second knockout drum at the same pressure as the liquid coming out from the first knockout drum (they are not liquid at the compressor inlet because they were heated in a heat exchanger before); in this way stream CRI-18 is not laminated and more duty is not required to the next intercooled compressor. This compressor brings the pressure of the mixed flow (CRI-19) up to 80 bar, which is then pumped in the liquid phase up to 150 bar for long-range transport. According to the calculation made, the process achieves CO_2 separation efficiencies around 89% (base case) and provides a storage flow whose purity is close to 99.5% (molar base).

The steam fraction coming out of the second drum (stream CRI-7) is heated in *C-H3*, *C-H2* and *C-H1* up to a temperature of 30 °C. Before entering the PSA, the A-30 flow is separated and part of it is sent as fuel to the catalytic burner. This avoids the use of pure H_2 at the burner, which not only reduces the efficiency of hydrogen production, but also requires an unnecessary additional load on the PSA. The remaining flow enters the separation beds (A-30B); they have efficiencies around 89 %, while the offgas (stream A-31) produced during system regeneration (which takes place at 1.18 bar) are also sent to the combustor to oxidise the carbon present in the form of CO.

4.2.3 Capture section modelling in Aspen Plus

Below is a brief description of the steps performed in *Aspen Plus* modelling of the capture section including fuel cell and cryogenic separation. In this section we have also chosen a Peng-Robinson as the equation of state for the reasons explained above. Numerous design specs and calculators have been imposed to find the correct operating conditions. It is important to underline that for each splitter a DS has been imposed, as well as for natural gas, water and air inlet flows. For example, the input air flow controls the cell conditions such as to obtain a certain ΔV of the cell as output parameter or there is a DS on the water

splitter at the evaporators input to ensure that the hot anodic residue at the high temperature WGS has the correct operating temperature of 330 °C.

4.2.3.1 Modelling of fuel cell

In *Aspen Plus* software there is no fuel cell and so it is modelled through a series of unitary operations as described in figure 4.13.

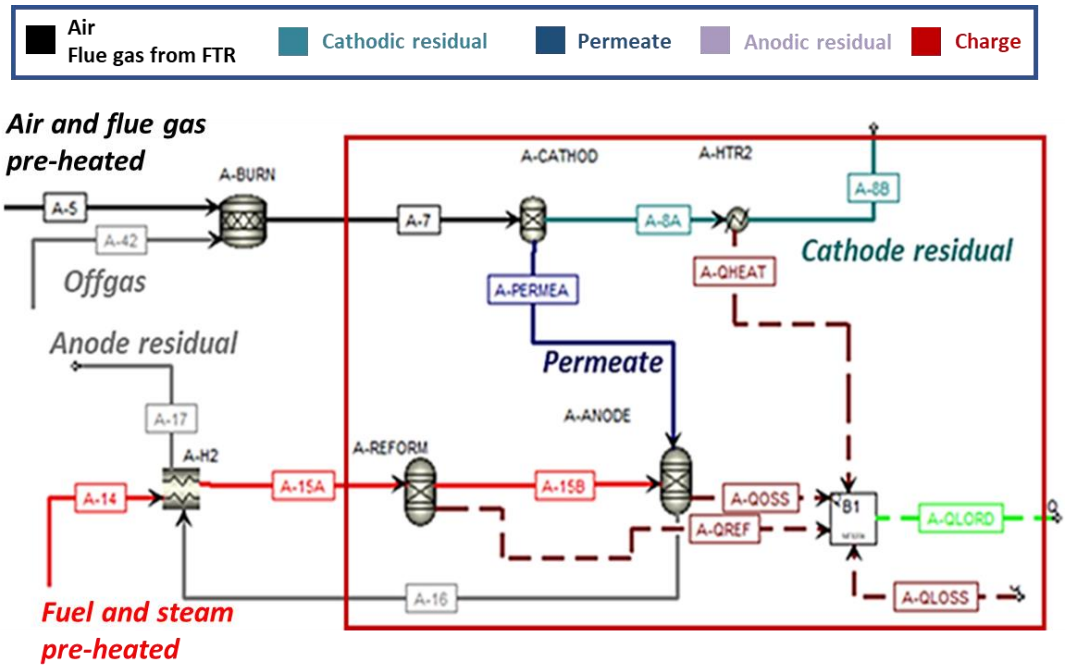

Figure 4.13 Modelling scheme of MCFC in Aspen Plus

Catalytic burner: the RStoic model has been chosen, in which we impose a complete combustion. The incoming oxidisable species are CO and H_2. As a result, we will have the following reactions:

Carbon monoxide oxidation $$CO + \frac{1}{2}O_2 \rightarrow CO_2$$

Hydrogen Combustion $$H_2 + \frac{1}{2}O_2 \rightarrow H_2O$$

It is required that the reactor is adiabatic and the outlet temperature of 575 °C will be controlled by a design spec on the recirculated fuel flow (stream A-41).

Heat exchangers: the MHeatX model is chosen for the same reasons already described for the FTR.

Anode: the RGibbs model is chosen with an output temperature of 645 °C equal to that of the cathodic side.

Internal reforming: the RGibbs model is chosen with an output temperature of 600 °C [55]. It is important to remember that, given the high operating temperatures of molten carbonate fuel cells, it is possible to make an internal reforming.

Cathode: To model the cathode of the cell, remember what happens in this section. There is the reaction $CO_2 + \frac{1}{2}O_2 + 2e^- \rightarrow CO_3^=$ and so a permeate stream of $CO_3^=$. Moreover, at the exit from the cathode, the mass flow rate will not be equal to the input value precisely because part of CO_2 and part of O_2 permeates the anode. We model this permeation by means of a separator Sep. Finally, a reaction takes place at the cathode. The heat is modelled by means of a heat exchanger Heater that is used to increase the inlet flow temperature from the value of A-7 (575 °C) to the outlet temperature of the cathode, i.e. the flow A-8B equal to 645 °C; in this case the cell is exothermic.

This model was first validated starting from the one proposed by *Mastropasqua et al.* [55], after all the functional parameters and plant layouts is modified to adapt it to our specific case.

4.2.3.2 Modelling of anode residual cooling

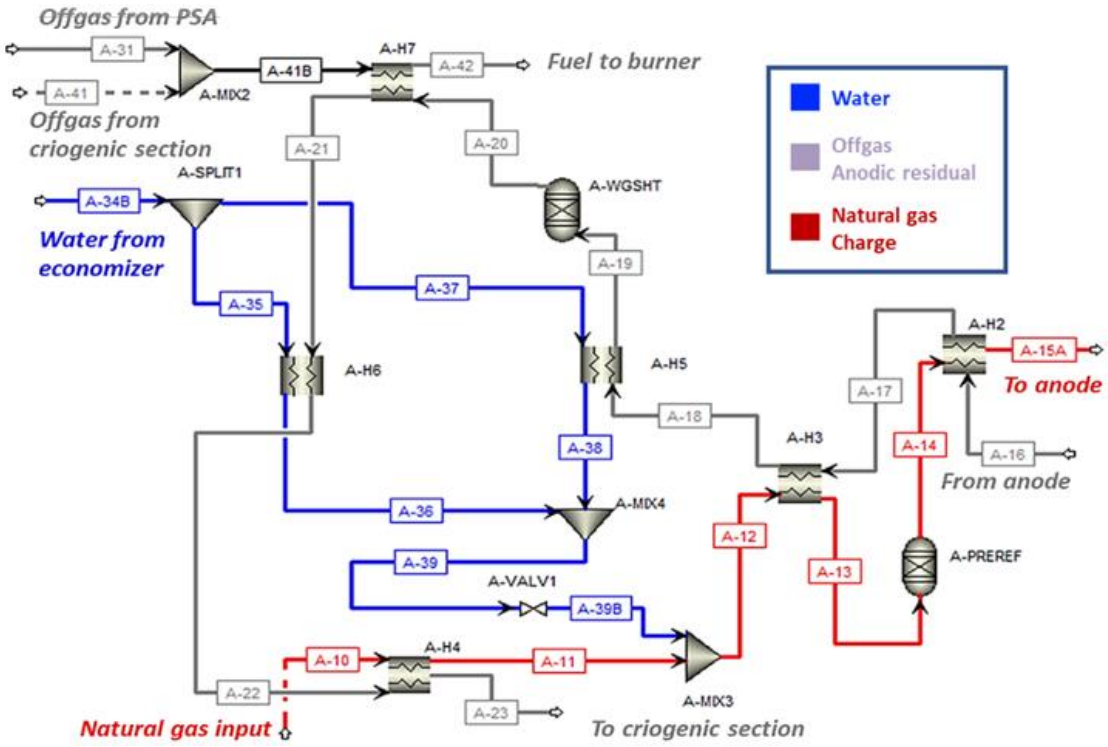

Figure 4.14 Modelling scheme of anode residual in Aspen Plus

The anodic residue cooling system has been modelled as follows.

External pre-reforming: the RGibbs model is chosen, requiring it to be adiabatic, i.e. with zero heat duty. We put CH_4 inert with a fraction equal to 0.975 because only 2.5% of methane reacts by assumptions described in table 4.8.

Water gas shift reactors: the RGibbs model is chosen and the reaction is set to equilibrium. So, pressure and zero duty are imposed as specifications because the reactor is adiabatic.

4.2.3.3 Modelling of cryogenic section

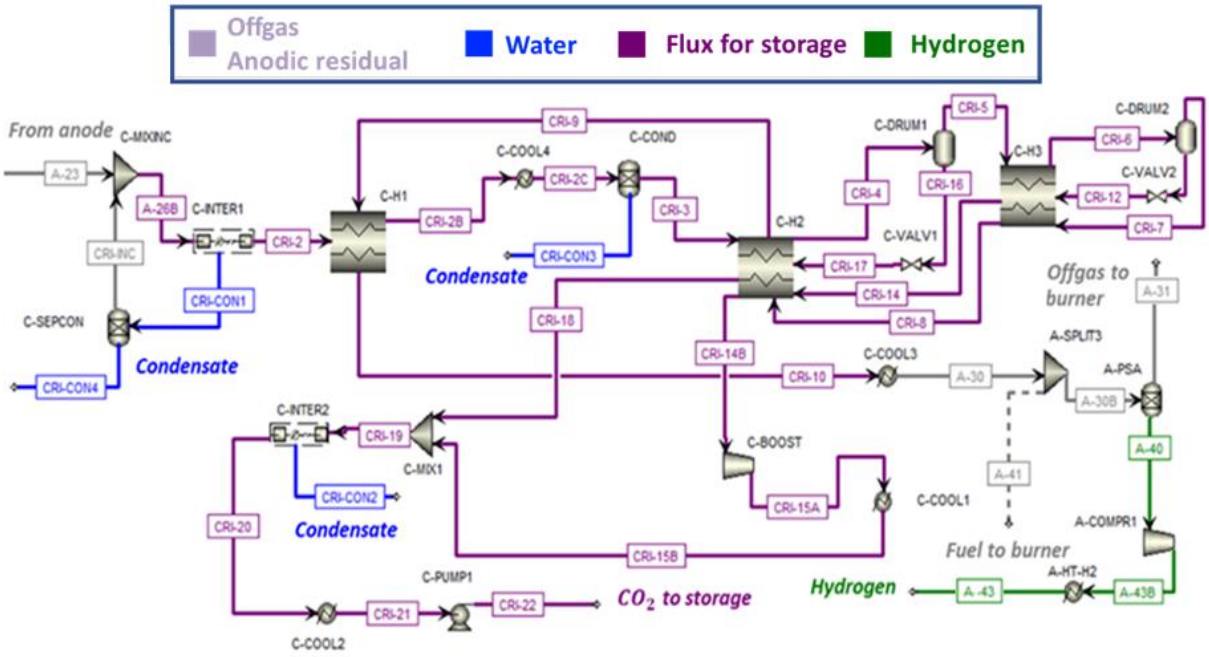

Figure 4.15 Modelling scheme of cryogenic section in Aspen Plus

The cryogenic section in figure 4.15 is modelled according to the specifications below.

Booster compressor: Compr model is chosen. In contrast with the cooled model, here it is not possible to choose number of stages, neither the cooling nor any condensation. This means that it is used when the required pressure increasing is limited.

Intercooled compressors: MCompr model is chosen. It allows to set the number of compressor stages, the cooling between one stage and the next, the removal of condensates and the performance parameters of the component.

Water separators: Sep model is chosen. In this case the outlet water fraction (CRI-CON4 and CRI-CON3) is set as a unit.

Drum: model Flash2 is chosen. The knockout drum is adiabatic and the pressure drops inside it is neglected.

PSA: as in the FTR, it is not modelled in detail but the unitary operation Sep is used. A split fraction of H_2 equal to 0.89 is imposed in the A-40 current, that is the value of the purification efficiency of PSA. Considering that the off-gas are the product of the regeneration of the beds of PSA, an operation normally done in depression is expected a pressure of the flow A-31 lower than the flow A-40. It is required among the specifications of the flash outlet that flow A-31 has a lower pressure.

Valves: Valve model is chosen. The pressure drop is regulated by means of a DS that imposes a ΔT equal to 3 °C with respect the inlet flow to knockout drum.

This model is first validated starting from the one proposed by *Chiesa et al.* [57] after which the functional parameters have been modified to adapt it to our specific case.

4.2.4 Performance and results

The sankey diagram related to carbon (figure 4.16) is created considering the carbon entering the global plant (FTR with capture section) and considering the outgoing one which is divided between the storage one from the cryogenic section and the cathodic residue from the cell.

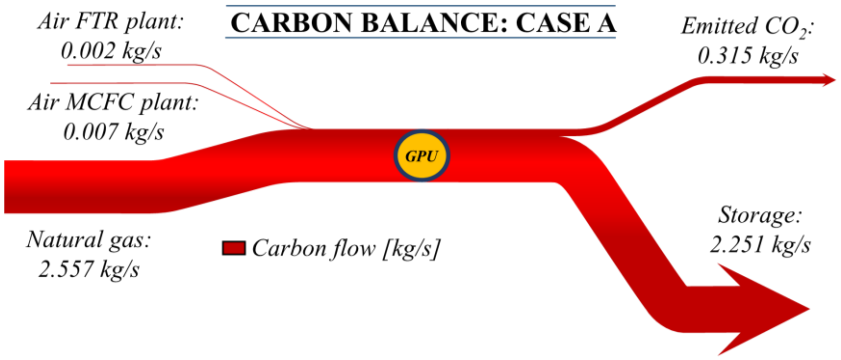

Figure 4.16 Carbon balance – Case A – FU=0.75

As you can realize, almost all of the carbon (99.6%) in the system is due to the natural gas that feeds the cell and the SMR. Of this, about 88% is captured by the cryogenic section and sent to storage, while the remain part is released to the plant stack, representing the only source of greenhouse gas emissions.

Let's consider a study conducted by *IEAGHG* commissioned by *Foster Wheeler* [48] on the capture of CO_2 from the flue gas of a FTR stand-alone (i.e. operating in merchant plant mode) by means of a passive process using a MEA type chemical solvent. In this case it is possible to achieve CO_2 capture efficiencies up to 90% but decreasing the performance of the plant as the efficiency of hydrogen equivalent produced and net electrical power produced. Before discussing this, we define the most important parameters about CO_2 capture.

Carbon capture ratio: It is the ratio between the carbon contained in the stream sent to storage and the carbon contained in the natural gas input.

$$CCR = \frac{N_{C,storage}}{N_{C,in}} \tag{4.2}$$

CO_2 avoided with respect no capture case: is the ratio between the CO_2 equivalent avoided (g_{CO2}/MJ_{H2}) using the retrofit system compared to the one emitted in the case without capture.

$$CA = \frac{E_{CO_2,eq}^{conv} - E_{CO_2,eq}^{ccs}}{E_{CO_2,eq}^{conv}} \tag{4.3}$$

This value is lower with respect CCR because the plant with carbon capture has a lower equivalent hydrogen efficiency e so requires more fuel at inlet to produce the same quantity of hydrogen.

Equivalent hydrogen production efficiency: the plant considered is designed for the production of hydrogen but also produces export steam and electricity. Therefore, in order to compare homogeneously the performances of the plants, this index is calculated as follows

$$\eta_{H_2,eq} = \frac{m_{H_2}^{out}\, LHV_{H_2}}{m_{NG}^{in}\, LHV_{NG} - \frac{Q_{steam}^{export}}{\eta_{th}} - \frac{W_{el}}{\eta_{el}}} \tag{4.4}$$

where:

- $\eta_{th} = \frac{Q_{th}}{Q_{LHV,in}}$ is the reference thermal efficiency of a conventional industrial boiler and it is assumed equal to 90 % [52]
- $\eta_{el} = \frac{W_{el,net}}{Q_{LHV,in}}$ is the electric efficiency of a conventional natural gas fired power plant and it is assumed equal to 58.33 % [52]

SPECCA: this is the Specific Primary Energy Consumption for CO_2 Avoided. This coefficient is used only for plant with CCS and measures the amount of thermal fuel input in terms of primary energy in order to avoid the emission of one kg of CO_2. [52]

$$SPECCA = \frac{\frac{1}{\eta_{H_2}^{ccs}} - \frac{1}{\eta_{H_2}^{conv}}}{E_{CO_2,eq}^{conv} - E_{CO_2,eq}^{ccs}} \tag{4.5}$$

We present a comparison of the variation in system performance between the base case and the respective CO_2 capture retrofits (table 4.11). As can be seen, in the case of amine capture this implies a strong decrease in the electrical power produced and a slight increase in the natural gas required at the input in order to maintain the same production of hydrogen of the base plant. In the case of fuel cell capture, the production of hydrogen increases slightly, while the electricity produced increases by about seven times compared to the initial value;

in this case, the necessary input of natural gas is greater than the previous retrofit, while the CO_2 avoided and the carbon ratio are slightly lower, even if they remain at high values. Instead, we do not make a direct comparison with the *Demoys* research [52], also related to CCS applied to the production of hydrogen, since in that case the capture is done on syngas stream output from the PSA and we obtain lower carbon ratio values, between 65 and 85 %, also characterized by a decrease in the electrical power produced by the plant.

The advantage of a capture with MCFC is that it can produce both electricity and hydrogen at the same time. The former is useful to self-power the auxiliaries of the capture section and the cryogenic section and feed energy into the power grid, while the latter allows to increase the hydrogen production of the plant considered as visible in figure 4.17. Finally, we can see how amine capture leads to a lower equivalent hydrogen production efficiency and a higher SPECCA especially since the system is passive. Instead, capture with MCFC is an active system with an equivalent hydrogen production efficiency equal to 40.8 %. Finally $W_{el,net}$ / $Q_{LHV,in}$ increases using MCFC and decreases using MEA.

IEAGHG - Case 3 [48]		
	FTR base case	FTR+MEA
Hydrogen production [MW_{th}]	299.7	299.7
Electricity to grid [MW_{el}]	9.9	0.4
$W_{el,net}$ / $Q_{LHV,in}$ [%]	2.5	0.1
$\eta_{H_2,eq}$ [%]	79.3	69.2
Feed+fuel [MJ/Nm^3H_2]	14.2	15.6
CO_2 avoided [%]	-	89.2
Carbon capture ratio [%]	-	90
SPECCA [MJ/kg_{CO2}]	-	2.74
Case A - FU = 0.75		
	FTR base case	FTR with capture
Hydrogen production [MW_{th}]	90.0	97.9
Electricity to grid [MW_{el}]	1.8	15.0
$W_{el,net}$ / $Q_{LHV,in}$ [%]	1.4	9.1
$\eta_{H_2,eq}$ [%]	80.6	74.7
$\eta_{H_2,eq}^{MCFC}$ [%]	-	40.8
Feed+fuel [MJ/Nm^3H_2]	14.6	18.0
CO_2 avoided [%]	-	84.8
Carbon capture ratio [%]	-	88.0
SPECCA [MJ/kg_{CO2}]	-	1.50

Table 4.11 Comparison of performance between SMR with CCS using MEA (IEAGHG) or MCFC section (Case A)

From the sankey it is possible to observe the main useful and loss energy outputs, including the steam output produced, which is calculated with reference to ambient conditions.

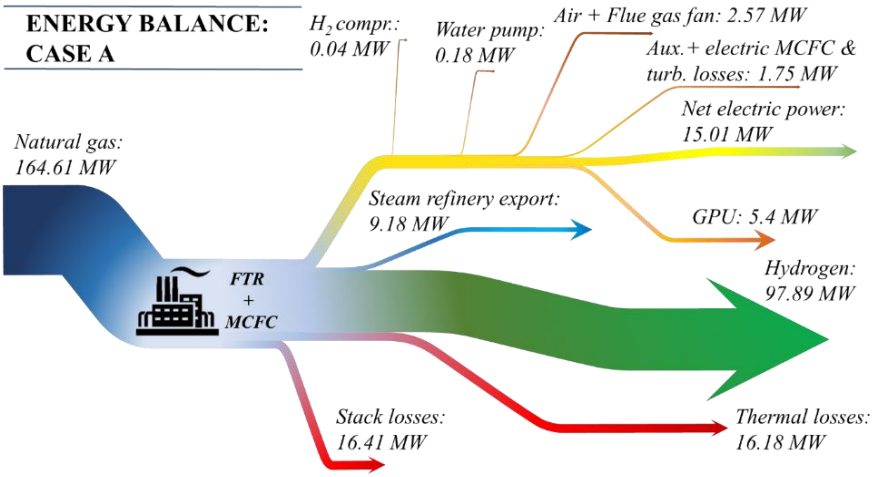

Figure 4.17 Energy balance – Case A – FU = 0.75

4.3 Case B – Feed fuel cell with offgas of FTR

The second configuration analysed assumes that MCFC is no longer fed with natural gas but with the offgas produced by the PSA of FTR. Figure 4.18 illustrates the system layout.

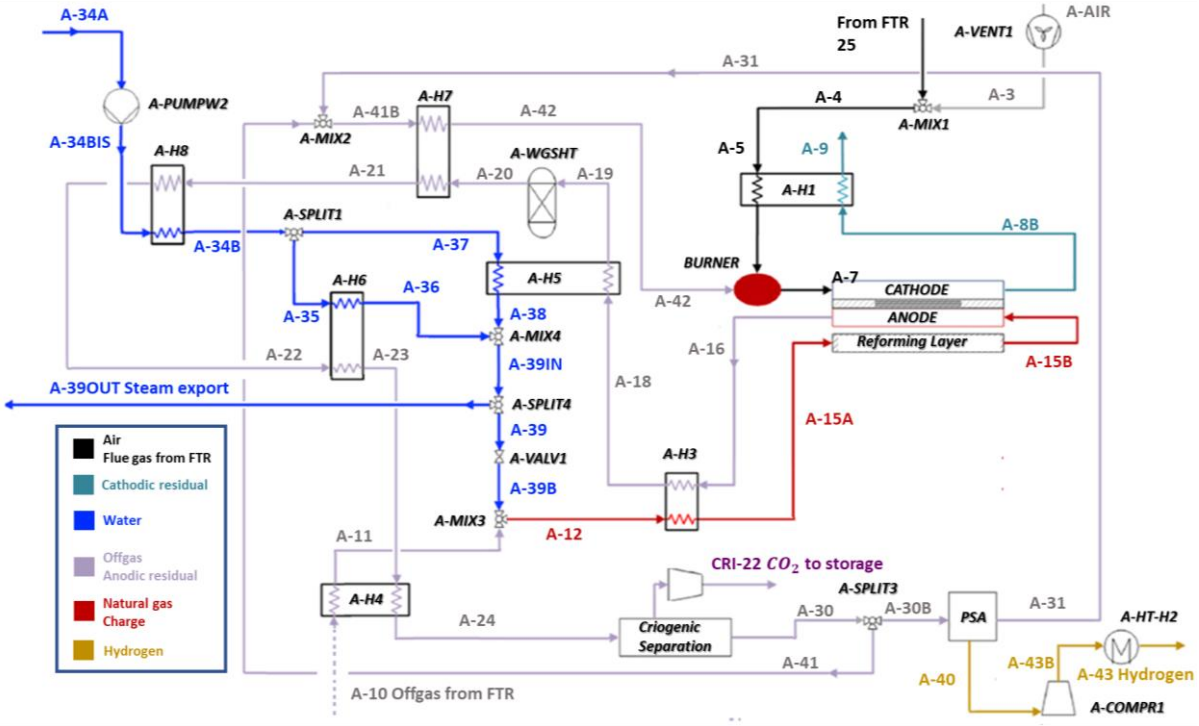

Figure 4.18 MCFC plant with offgas alimentation - Case B

This configuration provides two main advantages:

- We avoid the supply of natural gas to the fuel cell
- Offgas are free of hydrocarbons higher than methane, avoiding the use of pre-reforming

The last advantage is important because in this case the anodic residue coming out of the cell is no longer strongly cooled to heat the charge coming out from endothermic pre-reforming and it is possible to use that heat to produce steam (flow A-39OUT). As we have seen, the FTR produces steam at a pressure of 6 bar and so in this case it is necessary that the pump gives a head to the incoming water (stream A-34A) such as to obtain the value considered. This results in a better and more optimised heat exchange line; in fact, higher is the evaporation temperature lower is the heat exchange ΔT between the hot and cold flow. The minimum ΔT will always be at the natural gas preheater since it also represents the inlet of the cryogenic section.

We report the T-Q diagrams (figure 4.19) of the anodic residue cooling line and the cathodic residue cooling line for the case with a fuel utilization factor equal to 0.75

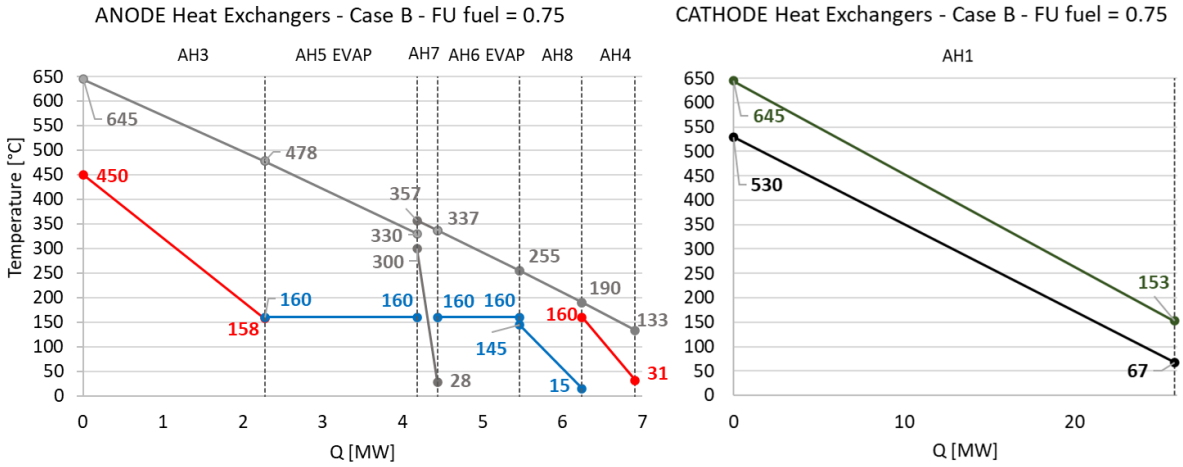

Figure 4.19 T-Q diagram Case B – FU fuel = 0.75

In this case the pre-heating of the water is performed using exhausted anodic gases and no longer exhausted cathodic gases, as in case A. If we propose the solution of base case, the hot cathodic gas enters at a temperature of 153 °C and must heat the water up to 145 °C, i.e. maintaining a sub-cooling ΔT of 15 °C. This solution did not allow a sufficient quantity of water to be introduced into the system even to satisfy the correct steam to carbon ratio, otherwise the T-Q diagrams would be crossed, which was not physically possible and moreover the ΔT_{min} in the economiser could not be respected.

However, this solution also has disadvantages, mainly due to the FTR section. If before the combustor to supply heat to the reforming was fed by the combustion of a mixture of natural gas and offgas, now decreasing the share of offgas that feeds this reactor, it must be replaced by natural gas. This leads to a higher consumption of it in the FTR section. We underline that the totality of the incoming natural gas (i.e. the FTR + capture section) is lower than in case A.

Natural gas compared to offgas has a higher H/C ratio (3.75 compared to 1.28 for offgas) and a higher lower heating value; so at the same thermal power the flow required to the burner decreases. This means that the mass of the flue gas decreases as well as its c_p. In fact if in offgas case it was rich in CO_2 which behaved like a "thermal ballast", in this case the natural gas has less of it and therefore the flue gas is richer in N_2 (but less with respect CO_2) deriving from the air than CO_2. We report mass flow rates, molars and flue gas concentrations in cases A and B with a utilization factor equal to 0.75.

Flue gas	***m*** *kg/sec*	***N*** *kmol/hr*	***Mole fraction***								
			Ar	CH_4	CO	CO_2	C_2+	H_2	H_2O	N_2	O_2
Case A	23.8	2898	0.72	-	-	19.71	-	-	17.49	60.57	1.51
Case B	18.9	2405	0.81	-	-	11.82	-	-	17.73	68.05	1.59

Table 4.12 Comparison of thermodynamic condition of flue gas between case A and case B

Finally, it should be remembered that the c_p of a bi-atomic molecule (N_2) is lower than one of a triatomic molecule (CO_2). Therefore, the thermal capacity in case B is lower than in case A. This means that there is less heat available in the exhaust gases that can be used to produce steam to be expanded in turbines and sent for export. This means that the FTR in case B has a lower electrical and thermal power output. The latter is not compensated by the steam production of MCFC.

4.3.1 Performance and results

Figure 4.20 shows the sankey diagram on the carbon balance at the capture plant. As said before, by feeding the cell with the offgas of the FTR you have a higher expenditure of natural gas at the SMR but nothing at the capture section, obtaining as final result a decrease of the fuel demand. In fact, the incoming total carbon moles are lower than in case A.

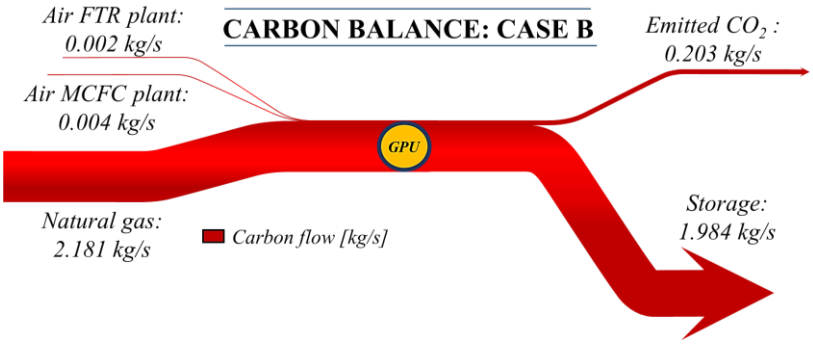

Figure 4.20 Carbon balance – Case B – FU = 0.75

In this case the percentage of carbon entering with natural gas is 99.7 % while the flow of CO_2 in storage represents about 90 % of the total entry. As in case A, also here it seems useful to make a comparison with the analysis performed by *IEAGHG* [48]; the main outputs are shown in the table below.

Before analysing the results, it is necessary to underline that the steam in export in table 4.13 is valued as the extractable quantity bringing this steam from the saturated steam to the saturated liquid conditions at the same pressure because in the refinery processes considered water is used up to the saturated liquid state; therefore this value is different from the one presented in the sankey energy diagram.

In this case the CO_2 capture performance improves to the levels of MEA solvent absorption presented in the IEAGHG paper, while the percentage increase of hydrogen produced and electricity output is lower than in case A for the reasons explained above in the plant description. In addition, if in case A the steam produced by the plant does not change compared to the case without capture, despite additional steam production by the capture section, the total output decreases by about half. Finally, as in case A, the natural gas input increases, but less in percentage. Also, in this case SPECCA with MCFC is lower but with respect case A hydrogen production equivalent efficiency is lower mainly due to a little amount of H_2 produced by capture section.

IEAGHG - Case 3 [48]		
	FTR base case	FTR+MEA
Hydrogen production [MW_{th}]	299.7	299.7
Electricity to grid [MW_{el}]	9.9	0.4
$W_{el,net}$ / $Q_{LHV,in}$ [%]	2.5	0.1
$\eta_{H_2,eq}$ [%]	79.3	69.2
Feed+fuel [MJ/Nm^3H_2]	14.2	15.6
CO_2 avoided [%]	-	89.2
Carbon capture ratio [%]	-	90
SPECCA [MJ/kg_{CO2}]	-	2.74
Case B - FU = 0.75		
	FTR base case	FTR with capture
Hydrogen production [MW_{th}]	90.0	93.26
Electricity to grid [MW_{el}]	1.8	6.7
$W_{el,net}$ / $Q_{LHV,in}$ [%]	1.4	4.8
Heat steam export [MW]	6.99	3.98
$\eta_{H_2,eq}$ [%]	80.6	74.9
$\eta_{H_2,eq}^{MCFC}$ [%]	-	24.17
Feed+fuel [MJ/Nm^3H_2]	14.6	16.1
CO_2 avoided [%]	-	89.7
Carbon capture ratio [%]	-	90.9
SPECCA [MJ/kg_{CO2}]	-	1.4

Table 4.13 Comparison of performance between SMR with CCS using MEA (IEAGHG) or MCFC section (Case B)

It is important to remember that, for the same total steam required in the refinery, a decrease here considered would lead to an additional demand for POW with higher indirect CO_2 emissions and a higher supply of natural gas. Assuming the boiler has a production efficiency of 90 % and assuming it is supplied with natural gas whose carbon is fully oxidised to CO_2, then there is an additional demand to the POW of 0.07 kg/s of natural gas with an additional CO_2 emission of 0.19 kg_{CO2}/s. However, we do not consider these values in the sankey

diagrams because they refer only to the section of hydrogen production with capture, while their valorisation will be necessary in the economic analysis.

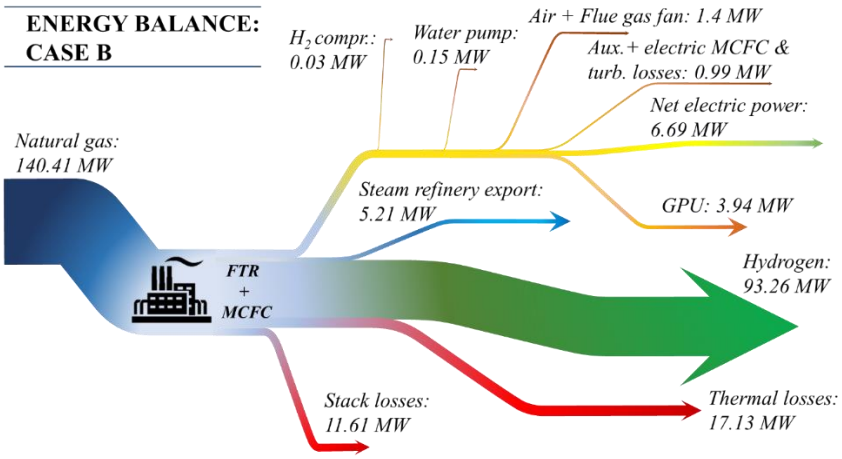

Figure 4.21 Energy balance – Case B – FU = 0.75

4.4 Case C – Without hydrogen production

In this paragraph we will describe a retrofit plant with an MCFC that only involves the capture of CO_2 and not the production of H_2. The plant under consideration was modelling in *Aspen Plus* based on the model A described above and with the same operating conditions (described in table 4.8) as regards the fuel cell, reactors and heat exchangers. FTR is not considered since it has already been described in detail in paragraph 4.1.

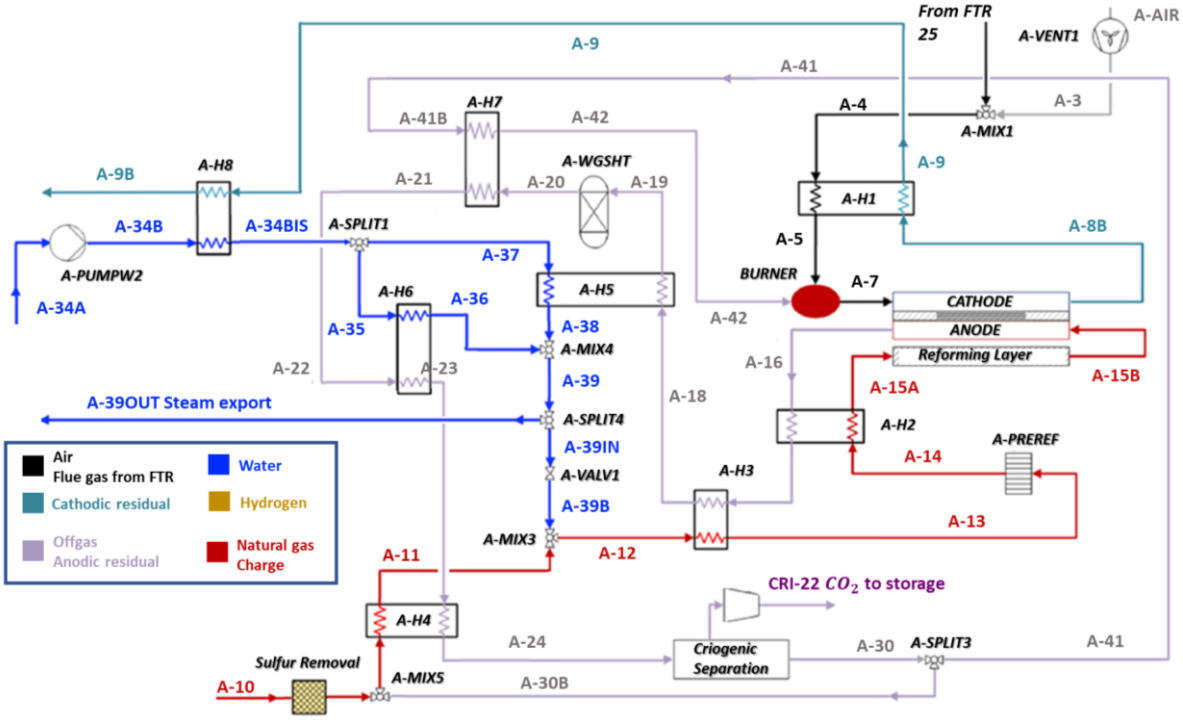

Figure 4.22 MCFC plant without hydrogen production – Case C

According to figure 4.22 it can be seen that, unlike in case A, there is no PSA at the cryogenic section output; in fact the offgas are divided and partly sent to the cathodic burner so a temperature equal to 575°C is provided at the cell input; the remaining part is sent as fuel at the anode input. This makes possible to require less natural gas and therefore, as will be seen later, a lower cost related to the fuel compared to case A.

However, the system configuration is different with respect case A; in fact, a charge richer in offgas and less in natural gas implies a higher H/C ratio. It also means less heavy hydrocarbons in the charge and consequently less heat necessary for pre-reforming to uniform it. The anodic exhaust leaves the exchanger with a temperature higher than 15.85 °C compared to case A. This means that the anodic and cathodic exchanger section must be optimised again, as can be seen in the T-Q diagram in figure 4.23.

Another difference compared to case A, also taken into consideration in the case with offgas supply, is the increase of pressure up to six bar in order to optimize the evaporators. In this way the evaporation temperature increases to 160 °C and steam is produced under the same thermodynamic conditions as the FTR.

The flow rate of water entering the system has been optimised in order to cool as much as possible the anodic residue coming out from the evaporator (*A-H6*) and meet ΔT_{min} at the next exchanger (*A-H4*) by 30 °C. In this case the steam to carbon ratio of 2.1 has been imposed by changing the quantity split in the splitter (*A-SPLIT4*); the excess steam is exported as a useful product.

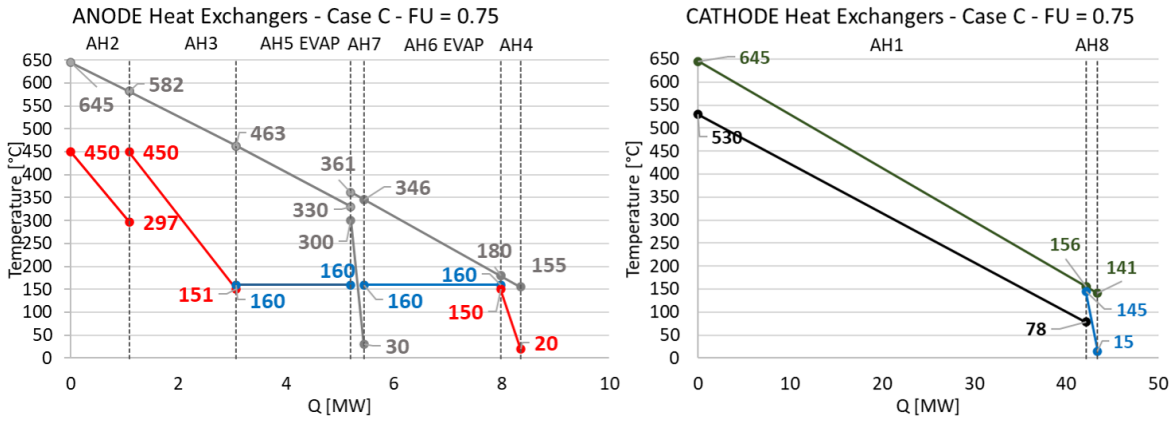

Figure 4.23 T-Q diagram Case C – FU fuel = 0.75

From figure 4.23 it can be seen that also in this configuration both exchanger lines have been optimised and the ΔT_{min} respected.

The further advantage of case C is obtained by recirculating the offgas flow rate at the outlet of the cryogenic section: this flow is rich in H_2 and this allows, at the same utilization factor at the single passage (0.75), to decrease the flow rate of incoming natural gas. The advantage is more evident going to calculate the global fuel utilization factor. To do this it is necessary

to know the moles of reacted H_2, which are equal to $N_{CO_3^=}$ permeate and calculate the equivalent hydrogen in input with the natural gas known that the charge is subjected to a reforming reaction and a shift reaction. So, we obtain:

SR $$C_nH_m + n\,H_2O \leftrightarrow n\,CO + \left(n + \frac{m}{2}\right) H_2 \qquad (4.6)$$

WGS $$n\,CO + n\,H_2O \leftrightarrow n\,CO_2 + n\,H_2 \qquad (4.7)$$

Combining the two reactions you get

$$C_nH_m + 2n\,H_2O \leftrightarrow n\,CO_2 + \left(2n + \frac{m}{2}\right) H_2 \qquad (4.8)$$

In case of absence of hydrogen production, it is useful to feed the cell with less natural gas as possible. The recirculation is a winning solution because FU at the single pass remains equal to the maximum allowed value of 0.75 under penalty of losses due to lack of reagents, while the global one becomes 0.88 leading to a saving of the fuel consumed globally.

4.4.1 Performance and results

As in previous cases, the sankey diagram (figure 4.24) on the carbon balance of the entire plant is shown.

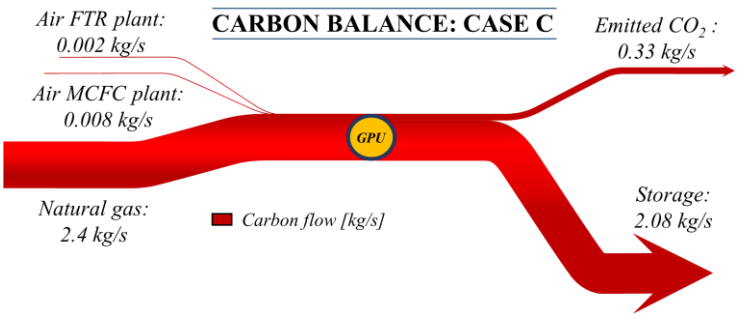

Figure 4.24 Carbon balance – Case C – FU = 0.75

In this case, as mentioned above, natural gas feeds both SMR and the capture section but the value for the latter is lower with respect to case A because here a CO and H_2 rich flow out of the cryogenic section is recirculated. The CO_2 capture from the cryogenic section represents about 86% of the total input, being from this point of view the worst solution among the three cases presented.

It is useful to make a comparison with the plant studied in the work of *IEAGHG* [48] and for this reason we report the table 4.14. Compared to case A, the amount of natural gas input decreases, but since there is no hydrogen production, the share related to Nm^3 produced is

higher. It improves steam production, thanks to the fact that, as said, pre-reforming is less stressed. This quantity produced is higher than case B; if we want to do the same analysis on POW as the previous case, here we would have a saving on natural gas flow rate of 0.025 kg/s and a lower CO_2 emitted by the same unit of 0.07 kg/s. The SPECCA is again lower with respect to the MEA plant.

IEAGHG - Case 3 [48]		
	FTR base case	FTR+MEA
Hydrogen production [MW_{th}]	299.7	299.7
Electricity to grid [MW_{el}]	9.9	0.4
$W_{el,net}$ / $Q_{LHV,in}$ [%]	2.5	0.1
$\eta_{H_2,eq}$ [%]	79.3	69.2
Feed+fuel [MJ/Nm^3H_2]	14.2	15.6
CO_2 avoided [%]	-	89.2
Carbon capture ratio [%]	-	90
SPECCA [MJ/kg_{CO2}]	-	2.74
Case C - FU = 0.75		
	FTR base case	FTR with capture
Hydrogen production [MW_{th}]	90.0	90.0
Electricity to grid [MW_{el}]	1.8	13.3
$W_{el,net}$ / $Q_{LHV,in}$ [%]	1.4	8.6
Heat steam export [MW]	6.99	8.03
$\eta_{H_2,eq}$ [%]	80.6	73.21
$\eta_{H_2,eq}^{MCFC}$ [%]	-	-
Feed+fuel [MJ/Nm^3H_2]	14.6	18.4
CO_2 avoided [%]	-	82.4 %
Carbon capture ratio [%]	-	86.4 %
SPECCA [MJ/kg_{CO2}]	-	1.96

Table 4.14 Comparison of performance between SMR with CCS using MEA (IEAGHG) or MCFC section (Case C)

Finally, as for the case with offgas supply, we do not consider these values in the sankey diagrams because it is referred only to the section of hydrogen production with capture, while their valorisation will be necessary in the economic analysis.

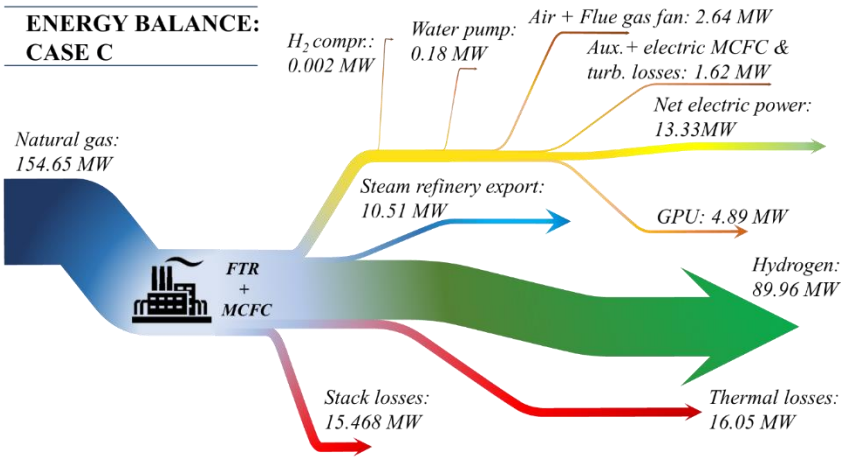

Table 4.15 Energy balance – Case C – FU = 0.75

4.5 Modelling of polarization curve

This paragraph focuses on the development of a correlation between cell voltage and current density using a simplified lumped parameter approach. The parameters under examination have not been calibrated through laboratory work and the data of the polarization curves of various operating conditions are difficult to know because they represent an industrial secret. For this reason, the polarization curve present here only approximates the actual cell trend. We referred to the study performed by *Lukas et al.* [63], adopted by several other papers such as ours.

It is known that the potential decreases as the current density increases from an initial value, the Nernst Voltage (E_{rev}), according to the following relationship

$$\Delta V = E_{rev} - \eta_{act} - j\, R_{ohm} - \eta_{conc} \qquad (4.9)$$

The expressions presented here are based on the ideal gas assumption and considering the operating temperature of the cell, it seems to be an excellent hypothesis. Here are the equations used

Nernst voltage: we report the equation 3.1:

$$E_{rev} = E_0 + \frac{RT}{n_e F} \ln\left(\frac{P_{H_2,a}\, P_{O_2,c}^{0.5}\, P_{CO_2,c}}{P_{H_2O,a}\, P_{CO_2,a}}\right) \qquad (4.10)$$

The partial pressures (normalized to atmospheric pressure) depend on the pressure and composition of the anodic/cathodic gas, while the standard potential depends on temperature. Polarization losses of fuel cells generally depend on partial pressures, temperature and current density and are distributed space-wise in a real cell. The study by *Lukas et al.* is a lumped parameter model, CSTR type, where the output properties are equal to the average properties. Therefore in the presented equations it is considered that:

- The temperature used, expressed in Kelvin, is the arithmetic average between the input and output temperature of the cathode.
- The partial pressures at the cathode and at the anode are the arithmetic average between the inlet and the outlet condition, where for the anodic side the composition downstream of the internal reforming is considered in order to take into account the variation of the gas composition inside the reforming unit.

Standard potential: for the calculation of this term, an expression as a function of temperature is used.

$$E_0 = \frac{4184 * \left[58.3 - T\,(0.0113 + 9.6 * 10^{-7}\, T)\right]}{2F} \qquad (4.11)$$

Activation losses: they are calculated according to the following formula

$$\eta_{act} = \frac{RT}{2F}\left[-21 - 0.31\ \ln\left(P_{H_2,a}\right) - 0.24\ \ln\left(P_{CO_2,a}\right) - 0.95\ \ln\left(P_{H_2O,a}\right) + 0.86\ \ln\left(P_{CO_2,c}\right) - 1.8\ \ln\left(P_{O_2,c}\right) + \frac{7050}{T} - 2.6\ \ln(j)\right] \quad (4.12)$$

Ohmic loss: as reported in M. Spinelli's PhD thesis [64], the composition of the reagents does not influence the MCFC intrinsic resistance. As a consequence, ohmic losses can be expressed as a function of operating temperature such as

$$R_{ohm} = 0.4\left[-2870\ \left(\frac{1}{923} - \frac{1}{T}\right)\right] \quad (4.13)$$

In addition, in the doctoral thesis cited above [64] is mentioned an experimental activity carried out at the laboratories of Fuel Cell Energy, Inc., a leader in the field of MCFCs, which asserts that for ohmic losses, the value obtained from the calibration of experimental data is the same as that obtained with the expression proposed by Lukas et al. [63], information that makes the effectiveness of this model more valid.

Concentration losses: concentration losses, as seen in chapter 3, have an effect on the potential only at high current density or if the molar fraction of reagents leaving the cell is below certain limits. As described in section 4.2.1, the concentration of CO_2 and O_2 always remains above the minimum value, as well as H_2, being the single pass fuel utilization factor limited to 0.75. We report the expression used

$$\eta_{conc} = -1.22\ \ln\left(1 - \frac{j}{0.64}\right) \quad (4.14)$$

Consider for example the polarization curve obtained in the case with a utilization factor of 0.75 in case A.

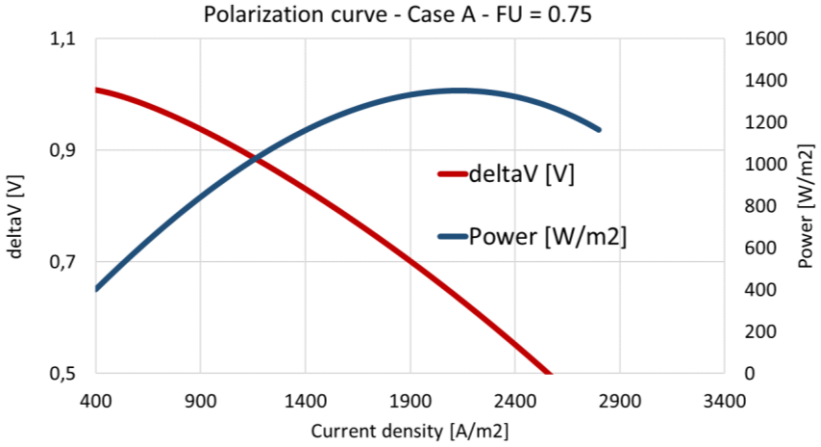

Figure 4.25 Polarization curve and power density – Case A – FU fuel = 0.75

The linear trend of ΔV is a function of current density, in the area of polarization losses. It is also possible to observe that the point of maximum power density matches a ΔV of about 0.65.

It is necessary to remember that a direct comparison between the polarization curves is not part of this work and it is not even possible because they have not been drawn either with the same fuel utilization factor or with the same CO_2 utilization factor. The latter varies in order to keep the cathode output CO_2 concentration constant at 1%. In the *Aspen Plus* model, we used a DS imposing an output CO_2 concentration of 1% by varying the amount of permeated CO_2. This imposition is used to find the value of the CO_2 utilization factor that maximizes the separate flow rate to the cathode; ideally you want all the incoming CO_2 with the flue gas to be permeated to the anode, but this is not technically possible because at the exit section of the cathode there would be losses of concentration due to lack of reagents. If we express the CO_2 utilization factor by reporting equation 3.8 we have that:

$$U_{CO_2} = \frac{N_{CO_3^=}}{N_{CO_2}^{in}} \tag{4.15}$$

The value of CO_2 at the inlet $N_{CO_2}^{in}$, for the same amount of exhausted gas coming from the FTR, remains more or less constant, because the contribution of air and offgas at burner can be considered negligible with respect the total amount of CO_2 at cathode inlet. The value changing is the carbon dioxide concentration at the cathode inlet, $x_{CO_2,c}^{in}$. Indeed it can be expressed as:

$$x_{CO_2,c}^{in} = \frac{N_{CO_2,c}^{in}}{N_c^{in}} \tag{4.16}$$

Where N_c^{in} depends on the quantity of air at the inlet. We express $N_{CO_3^=}$ as:

$$N_{CO_3^=} = N_{CO_2,c}^{in} - N_{CO_2,c}^{out} = N_c^{in}\ \frac{x_{CO_2,c}^{in} - x_{CO_2,c}^{out}}{1 - x_{CO_2,c}^{out}} \tag{4.17}$$

Using equation 4.16 and 4.17, we obtain:

$$N_{CO_3^=} = \frac{N_{CO_2,c}^{in}}{x_{CO_2,c}^{in}}\ \frac{x_{CO_2,c}^{in} - x_{CO_2,c}^{out}}{1 - x_{CO_2,c}^{out}} \tag{4.18}$$

By performing a few simple numerical steps finally you get:

$$N_{CO_3^=} = \frac{N_{CO_2,c}^{in}}{1 - x_{CO_2,c}^{out}}\ - \frac{1}{x_{CO_2,c}^{in}}\ \frac{N_{CO_2,c}^{in}\ x_{CO_2,c}^{out}}{1 - x_{CO_2,c}^{out}} \tag{4.19}$$

$\frac{N_{CO_2,c}^{in}}{1-x_{CO_2,c}^{out}}$ e $\frac{N_{CO_2,c}^{in}\ x_{CO_2,c}^{out}}{1-x_{CO_2,c}^{out}}$ can be consider more or less costant with the assumptions done before. So the variation of quantity of $N_{CO_3^=}$ depends on the carbon dioxide concentration at cathode inlet but not on the flow rate in the case in which flue gas from FTR remain constant (as in

case A and C). At the end the carbon dioxide utilization factor depends on air flow rate: higher is this value, lower is the CO_2 concentration at cathode and so lower is U_{CO2}.

The method for modelling the polarization curve is useful for fuel cell cost estimation, expressed as €/m^2. We verify the correspondence between the cost calculated referring to power or to active area and this is matched. At the end, seems useful to evaluate the active area of fuel cell in off-design condition, situation in which it must be taken constant. We remind that an analysis in the laboratory for the realization of a more detailed polarization curve remains necessary, even if the model adopted here does not compromise the validity of our analysis.

4.6 Results and comparisons

In this paragraph the results and performances for the three cases are presented, after which a comparison between them is presented. Table 4.16 shows the main differences in plant design between the three cases.

Plant configuration overview				
Case	Fuel for MCFC	MCFC steam production	Pre-reformer	PSA for MCFC
A	Natural gas	Absent	Present	Present
B	Offgas of FTR	Present	Absent	Present
C	Natural gas with MCFC offgas recirculation	Present	Present	Absent

Table 4.16 Overview of the differences between the three plant configurations

Comments on them have already been included in the descriptions of the systems and will therefore not be repeated here.

4.6.1 Fuel cell performance

For each configuration a polarization curve has been created using the procedure described in paragraph 4.5. As said, they are not comparable because the utilization factor of CO_2 and O_2 is not the same. However, results are useful for a calculation of current density and cell active area. The operating conditions of the cell are the same for the three cases and here we do not resume them because they are shown in table 4.8. Instead, we report the final cell performance.

Fuel cell performance														
Case	ΔV V	j A/m^2	A_{stack} m^2	U_{CO_2} %	U_{O_2} %	$x_{O_2,in}^{cathode}$ %	$N_{CO_2,in}^{flue\ gas}$ kmol/s	$Offgas_{in}$ kg/s	NG_{in} kg/s	$H_{2,out}$ Nm^3/h	Q_{steam} MW	$W_{cell\ DC}$ MW	$W_{el,net}$ MW	η_{el} %
A	0.7	1732.6	17533	85.7	18.74	13.07	0.159	-	0.9	2677.4	-	21.3	18.6	44.2
B	0.7	1475.4	10292	82.1	16.54	11.68	0.078	4.1	-	1109.3	0.7	10.5	9.2	39.3
C	0.7	1730.0	15667	83.4	15.58	13.73	0.159	-	0.7	-	1.0	19.0	16.5	51.1

Table 4.17 Overview of fuel cell performance

As you can see from the above table the amount of carbon dioxide input with fluegas coming from the FTR in case B is reduced by 50% compared to case A for what said in paragraph 4.3. Therefore, the permeated CO_2 is lower considering that the contribution on carbon dioxide of air and offgas to the burner is almost negligible. We express the cell current as:

$$I\ [A] = 2FN_{CO_3^=} \tag{4.20}$$

Looking the table, it is possible to observe how I decreases in case B. We report then the formula for the gross cell power

$$W_{cell\ DC}[W] = I \cdot \Delta V \tag{4.21}$$

ΔV is constant and equal to 0.7, so the power decreases. Also the active area of MCFC decreases because carbon dioxide permeation is less. The hydrogen production by fuel cell in case B is less with respect case A because, considering the same fuel utilization factor, if $N_{CO_3^=}$ decreases the equivalent hydrogen in input decreases.

Different is the situation in case C when the carbon dioxide flow rate to cathode can be considered almost constant because FTR system does not change. Processing equation 4.19 and writing $\frac{N_{CO_2,c}^{in}}{x_{CO_2,c}^{in}}$ as $N_{air}^{in} + N_{fluegas}^{in} + N_{offgas}^{in}$ we obtain:

$$N_{CO_3^=} = \frac{N_{CO_2,c}^{in}}{1-x_{CO_2,c}^{out}} - N_{air}^{in}\ \frac{x_{CO_2,c}^{out}}{1-x_{CO_2,c}^{out}} - \frac{N_{fluegas}^{in}\, x_{CO_2,c}^{out}}{1-x_{CO_2,c}^{out}} - N_{offgas}^{in}\ \frac{x_{CO_2,c}^{out}}{1-x_{CO_2,c}^{out}} \tag{4.22}$$

For the reasons explained before, in this case $N_{CO_3^=}$ depends almost on air flow rate. The fuel feeding fuel cell is no more only natural gas, but a mixture of natural gas and retentate at the outlet of cryogenic section. This last stream is H_2 rich due to the absence of PSA. So, the ratio CH_4/CO_2 feeding to fuel cell is less and this fact implies less heat absorbed by reforming reaction. If the reforming absorbs less heat, this means that for control the temperature, more air has to be fed at the cathode side. Looking equation 4.22, $N_{CO_3^=}$ decreases and at the same ΔV also cell power decreases. Cell active area decreases, driving by the less cell power while current density remains almost constant. Electrical efficiency of MCFC is defined as the ratio between the net electric power of FC, i.e. the gross power of cell minus the power absorbed by auxiliaries (fan and pumps). It increases thanks to offgas recirculation that permits less input of natural gas.

4.6.2 Overall plant performance

We report the results for the global plant (FTR + capture section) after the retrofit in order to evaluate how the performances change with respect the different layout possibilities.

Overall plant performance										
Case	NG_{in} kg/s	$H_{2,out}$ Nm^3/h	CO_2^{out} kg/s	CCR %	CO_2 avoided %	E_{CO_2} $\frac{g_{CO_2}}{MJ_{H_2}}$	$W_{el,net}$ MW	Q_{steam} MW	η_{H_2} %	SPECCA $\frac{MJ}{kg_{CO_2}}$
No capt	2.63	30258.9	6.98	-	-	77.61	1.77	6.99	80.60	-
A	3.54	32936.4	1.158	88.0	84.8	11.8	15.01	6.99	74.67	1.50
B	3.02	31368.2	0.745	90.9	89.7	8.0	6.69	3.98	74.89	1.36
C	3.33	30258.9	1.231	86.4	82.4	13.7	13.33	8.03	73.21	1.96

Table 4.18 Overview of overall plant performance

Considering SPECCA, it is clear how case B is the case that:

- require less primary energy for CO_2 capture with respect the two other cases
- has a higher equivalent hydrogen production efficiency with respect the two other cases, mainly due to the lower inlet flow of natural gas despite the quantity of hydrogen produced is lower than in case A and the heat in export is lower than in case C.

Case C is the one characterized by a higher steam production but despite this, the absence of hydrogen produced by the cell penalizes the retrofit in terms of SPECCA and η_{H_2}.

In fact, we have the same amount of hydrogen produced compared to the case without capture but with a higher demand of natural gas to feed the MCFC.

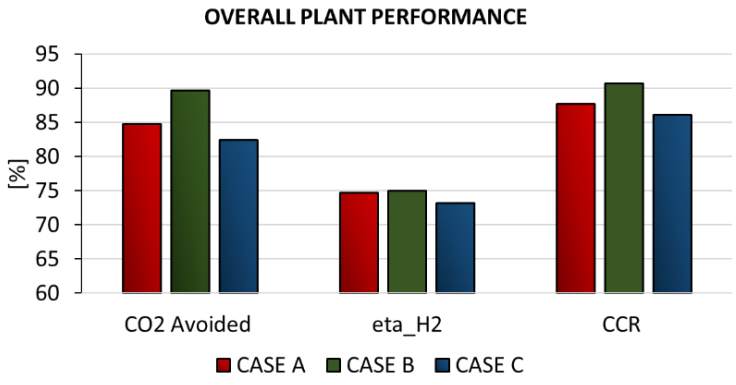

Figure 4.26 Three main performance index of overall plant. CO_2 avoided with respect base case, equivalent hydrogen production efficiency and carbon capture ratio (CCR)

Considering figure 4.26 it is clear how in terms of carbon capture, case B is the best thanks mainly to offgas feeding of fuel cell that gives two main advantages.

- The flue gas of the FTR is less CO_2 rich because the main reforming reactor combustor replaces part of the offgas with natural gas in smaller quantities due to its higher heating value as described in section 4.3.
- The supply to the cell with offgas avoids the necessity to feed natural gas to the capture section.

4.6.3 Carbon performance of retrofit

We explain some results with the following table.

Carbon performance			
Parameter	*Case*		
	A	*B*	*C*
	%	*%*	*%*
% C in with fuel for anode with respect the total amount of carbon inlet at MCFC	25.5	56.5	20.8
% C in with FTR flue gas with respect the total amount of carbon inlet at MCFC	74.2	43.4	78.9
% CO2 out for uncomplete FC separation at cathode with respect the amount of CO2 inlet at cathode	16.5	21.4	17.6
% CO2 out for uncomplete FC separation at cathode with respect the amount of C inlet at MCFC	12.3	9.3	13.9
% CO2 loss by cryogenic section with respect the amount of CO2 inlet at cryogenic section	10.2	7.5	9.9
% CO2 loss by cryogenic section with respect the total amount of C inlet at MCFC	9.9	7.4	9.5

Table 4.19 Overview of carbon performance of overall plant

Case A and case C have the same CO_2 quantity entering the capture section because upstream FTR does not vary. However, in case C, as said, the amount of natural gas at the cell decreases thanks to recirculation and therefore the amount of carbon coming in with the flue gas increases in percentage.

In case B instead, as said several times before, the amount of carbon in the flue gas decreases while the amount of carbon in the anode fuel increases, since the offgas are characterized by a lower H/C ratio compared to natural gas.

The proportion of CO_2 not separated from the cell with respect to the cathode input carbon for case B is higher due to the fact that, as previously explained, the input carbon is much lower for the considerations made on the FTR and consequently with x_{CO2} set at the operating limit the $N_{CO_3^=}$ is permeated is lower. On the contrary, the same parameter compared to the total carbon input in the cell for case B is the lowest because, as previously explained, the carbon inside offgas at the anode is higher.

The last two parameters of table 4.19 analyse the behavior of the cryogenic section. Also in this case it is not possible to obtain a unitary CO_2 purification because a small amount of CO_2 cannot be stored. In addition, as we have seen in figure 4.11, a higher efficiency would result in a less pure storage CO_2 flow. It is lower for case B because being fed by offgas, the flow to the cryogenic section is more concentrated in CO_2, with a higher separation efficiency.

Sensitivity and Economic Analysis

5

In this chapter a technical-economic analysis of the A, B and C systems will be performed as the fuel utilization factor and the cell ΔV vary in order to estimate which is the best on-design condition. For the economic analysis we will briefly summarize the procedure used to estimate the costs, after which only for the most promising case we will examine NPV, payback time and LCOH at the variation of some parameters such as selling price of electricity and hydrogen and carbon tax.

5.1 Sensitivity analysis – Case A

For case A, a sensitivity analysis will be presented to vary the fuel utilization factor, underlining that these are only on-design cases where the surfaces of the components (cell, heat exchangers, reforming, etc.) have not been kept constant. The range of variation is between 0.67 and 0.75. The upper limit is imposed by average literature values beyond which, MCFCs start to have problems due to the lack of reagents in the bulk phase. Below the lower limit the anodic and cathodic cooling section should be further revisited; a lower utilization factor leads to a higher input fuel flow rate and, an equal steam to carbon ratio, a higher water content to evaporate. Moreover, the pre-reforming would absorb more heat for the reaction with a consequent further cooling of the anodic exhaust in order to obtain the correct temperature at the cell inlet.

Table 5.1 shows the cell performance in relation to the fuel utilization factor.

Fuel cell performance – Case A – Sensitivity analysis on fuel utilization factor												
FU	ΔV V	j A/m^2	A_{stack} m^2	$N_{CO_3^=}$ kmol/s	U_{CO_2} %	U_{O_2} %	GN_{in} kg/s	m_{aria} kg/s	$H_{2,out}$ Nm^3/h	$W_{cell\ DC}$ MW	$W_{el.net}$ MW	η_{el} %
0.67	0.7	1719.5	20092	0.179	89.0	26.1	1.16	47.21	5736	24.2	21.5	39.9
0.71	0.7	1730.3	18570	0.167	87.1	21.4	1.02	53.68	4002	22.5	20.8	42.0
0.75	0.7	1732.6	17533	0.157	85.7	18.7	0.91	57.94	2677	21.3	18.6	44.2

Table 5.1 FU sensitivity analysis on fuel cell performance – Case A

As the utilization factor decreases, the input air decreases due to the fact that the internal reforming absorbs more heat at the same CO_2 amount from the flue gas. Resuming equation 4.22 we obtain that the flow rate of $N_{CO_3^=}$ increases to obtain an output CO_2 concentration equal to 1%. This, as mentioned in the previous chapter, implies not only a higher cell power but also a higher active area and a higher cost, which we will evaluate in the economic analysis.

We report two graphs: the first with the trends of CO_2 and O_2 utilization factor and the second with net electrical power and net electrical efficiency considering fans and auxiliary pumps.

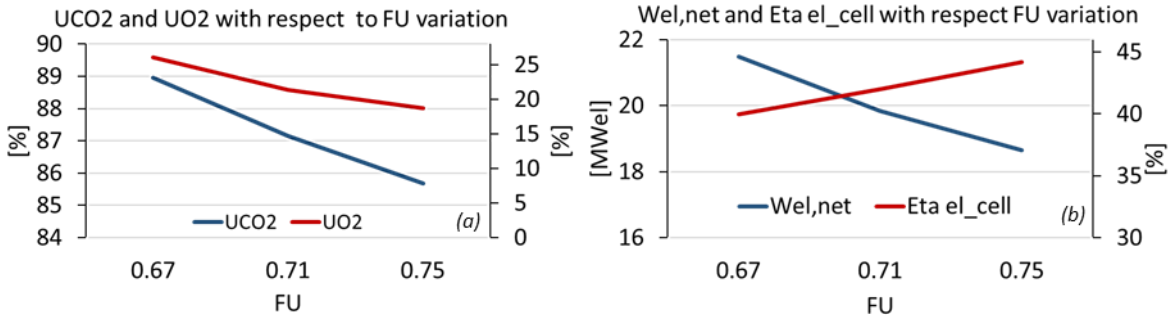

Figure 5.1 Overview of fuel performance with respect FU – Case A. (a) carbon dioxide and oxygen utilization factor with respect fuel utilization factor; (b) net cell electric power and net cell electrical efficiency with respect fuel utilization factor.

The performance of the global plant is shown in table 5.2 below.

Overall plant performance – Case A – Sensitivity analysis on fuel utilization factor

FU	NG_{in} kg/s	$H_{2.out}$ Nm^3/h	CO_2^{out} kg/s	CCR %	CO_2 avoided %	E_{CO_2} $\frac{g_{CO_2}}{MJ_{H_2}}$	$W_{el.net}$ MW	η_{H_2} %	SPECCA $\frac{MJ}{kg_{CO_2}}$
No capt.	2.63	30258.9	6.98	-	-	77.61	1.77	80.60	-
0.67	3.79	35995	0.978	90.55	88.23	9.14	16.73	76.59	0.95
0.71	3.65	34261	1.082	89.14	86.32	10.62	15.71	75.49	1.25
0.75	3.54	32936	1.158	88.02	84.76	11.83	15.01	74.67	1.50

Table 5.2 FU sensitivity analysis on overall plant performance – Case A

By decreasing the utilization factor, the CO_2 capture performance (CCR in figure 5.2a) and also the net power of the system increase, again due to what has been said about the quantity of permeated ion. From this analysis the most performing utilization factor appears to be 0.67 but this must also be confirmed with an economic analysis since a greater cell area corresponds to a greater MCFC cost, as well as a greater input natural gas flow rate corresponds to a greater variable O&M cost.

We report the trends of the main parameters in figure 5.2a and 5.2b.

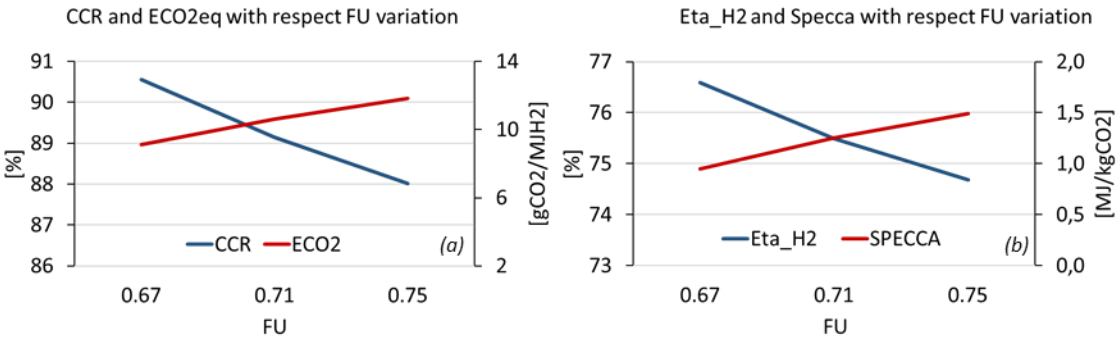

Figure 5.2 Overview of overall plant performance with respect FU – Case A. (a) carbon capture ratio and equivalent CO_2 emission with respect fuel utilization factor; (b) equivalent hydrogen production efficiency and SPECCA with respect fuel utilization factor.

A sensitivity analysis is calculated by varying the ΔV between 0.67 and 0.73 and keeping a constant utilization factor equal to the base case of 0.75. We want to evaluate the effect of the potential on the plant's CO_2 capture and hydrogen production efficiency.

Fuel cell performance – Case A – Sensitivity analysis on cell voltage													
ΔV V	FU	j A/m^2	A_{stack} m^2	$N_{CO_3^=}$ kmol/s	U_{CO_2} %	U_{O_2} %	GN_{in} kg/s	m_{aria} kg/s	$H_{2,out}$ Nm^3/h	$W_{cell\ DC}$ MW	$W_{density}$ W/m^2	$W_{el.net}$ MW	η_{el} %
0.67	0.75	1866	15873	0.153	83.8	15.8	0.89	67.49	2415	19.8	1250	17.2	41.7
0.70	0.75	1733	17533	0.157	85.7	18.7	0.91	57.94	2677	21.3	1213	18.6	44.2
0.73	0.75	1586	19644	0.161	87.6	22.9	0.93	48.35	2943	22.8	1158	20.2	46.6

Table 5.3 ΔV sensitivity analysis on fuel cell performance – Case A

For each case we define the polarization curve by following the procedure described in paragraph 4.5. Given the ΔV we obtain the corresponding current density. We remind that the polarization curves are plotted knowing the temperature, the pressure and the composition of the flows entering and exit from the cell. In this case by varying ΔV the compositions remain about the same while temperatures and pressures are fixed, this means that the relation between voltage and current density remains more or less the same as the relation between power density and current density.

For more clarity we report the polarization curves calculated for the three cases, evidencing the area of our interest, otherwise they would be superimposed and therefore indistinguishable.

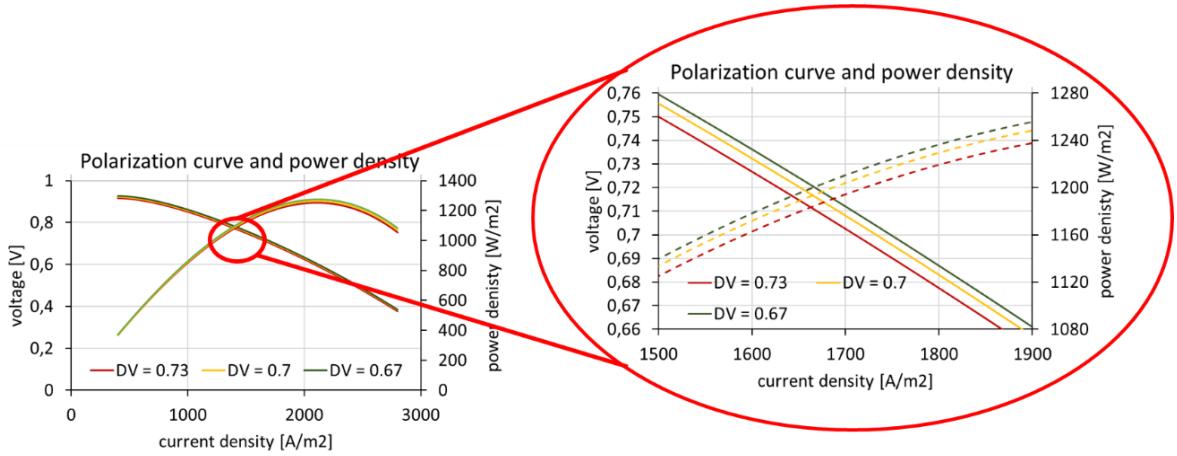

Figure 5.3 Polarization curve sensitivity analysis. Voltage: solid line; Power density: dotted line.

By decreasing the ΔV, the current density becomes higher leading to a high ohmic resistance that penalises the net electrical efficiency of the fuel cell module and therefore that of the MCFC system as illustrated in figure 5.4b.

Due to the increased heat emitted by the electrochemical process, a higher input air flow rate is required. This additional air flow is also due to a lower thermal power absorbed by the internal reforming.

However it increases the power density because, as explained in paragraph 4.2.1, the nominal operating point of the cell is not set for a voltage that maximises the power density but for a higher one to promote the CO_2 capture by the MCFC. Consequently, resuming once again the equation 4.22, results that a lower air flow coincides with a higher permeation of $CO_3^=$ ion; this leads to a higher cell power (figure 5.4b) and a higher CO_2 utilization factor (figure 5.4a).

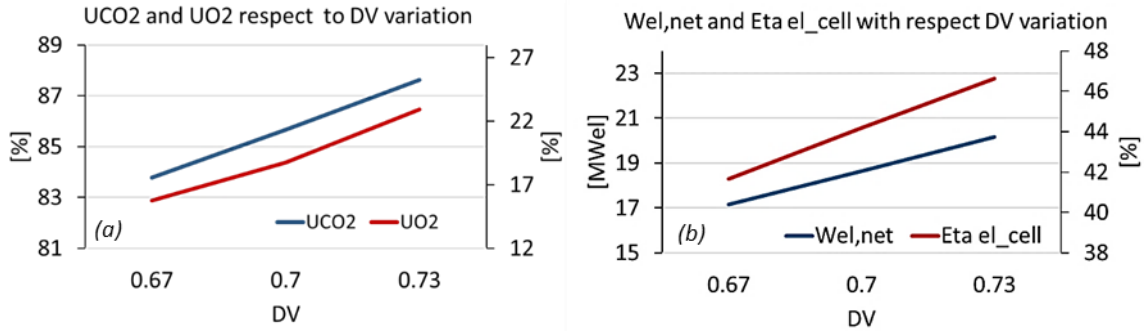

Figure 5.4 Overview of fuel performance with respect ΔV – Case A. (a) Carbon dioxide and oxygen utilization factor with respect cell voltage; (b) net cell electric power and net cell electrical efficiency with cell voltage.

The performance of the global plant is shown below.

Overall plant performance – Case A – Sensitivity analysis on cell voltage									
ΔV V	NG_{in} kg/s	$H_{2.out}$ Nm^3/h	CO_2^{out} kg/s	CCR %	CO_2 avoided %	E_{CO_2} $\frac{g_{CO_2}}{MJ_{H_2}}$	$W_{el.net}$ MW	η_{H_2} %	SPECCA $\frac{MJ}{kg_{CO_2}}$
No capt	2.63	30258.9	6.98	-	-	77.61	1.77	80.60	-
0.67	3.52	32674	1.307	86.40	82.67	13.45	13.68	73.39	1.90
0.70	3.54	32936	1.158	88.02	84.76	11.83	15.01	74.67	1.50
0.73	3.56	33202	1.002	89.70	86.91	10.16	16.41	76.05	1.10

Table 5.4 ΔV sensitivity analysis on overall plant performance – Case A

For what has just been mentioned, a higher ΔV implies a higher CO_2 permeation and therefore a lower CO_2 emission at the output (figure 5.5a). The hydrogen produced increases only slightly because of the slight increase in natural gas. The electrical power increases, despite the lower power density of the cell because this decrease is determined by the greater cell area. Finally, the SPECCA decreases due to lower CO_2 emissions (figure 5.5b).

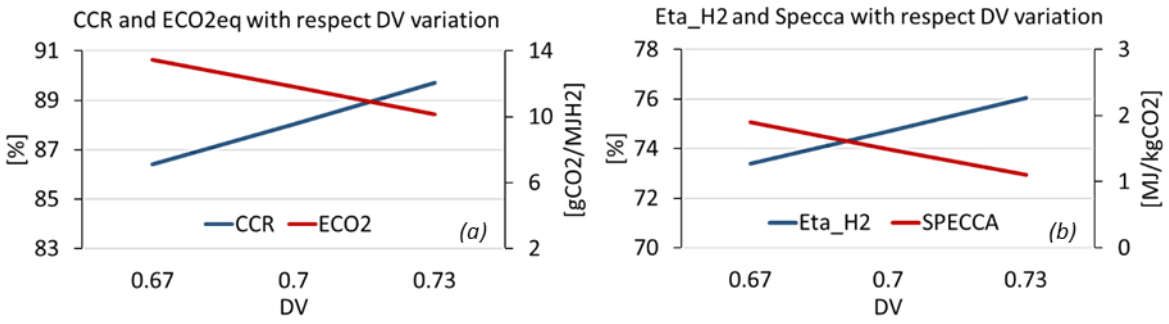

Figure 5.5 Overview of overall plant performance with respect ΔV – Case A. (a) carbon capture ratio and equivalent CO_2 emission with respect cell voltage; (b) equivalent hydrogen production efficiency and SPECCA with respect cell voltage.

5.2 Sensitivity analysis – Case B

Analysing the case with the offgas feed, reducing the utilization factor leads to a decrease in the heat duty that can be exploited by the steam in export. This is because decreasing the utilization factor increases the offgas flow rate split by the FTR system and consequently increases the flow rate of natural gas to compensate for the splitting. The increase in natural gas of FTR does not occur in a proportional manner and this leads to a variation in the flue gases flow rate and their composition, which therefore require less water for cooling and therefore produce less steam in FTR. Electricity production of cell increases, as does the CO_2 utilization factor because $CO_3^=$ permeate increases. The electrical efficiency of cell decreases due to an additional input fuel used by the cell.

Fuel cell performance – Case B – Sensitivity analysis on fuel utilization factor												
FU	ΔV V	j A/m²	A_{stack} m²	$N_{CO_3^=}$ kmol/s	U_{CO_2} %	U_{O_2} %	$Offgas_{in}$ kg/s	$H_{2,out}$ Nm³/h	Q_{steam} MW	$W_{cell\ DC}$ MW	$W_{el.net}$ MW	η_{el} %
0.67	0.7	1447	10463	0.0784	84.8	21.7	4.60	2263	0.66	10.60	9.33	35.49
0.71	0.7	1465	10292	0.0781	83.3	18.7	4.32	1660	0.68	10.54	9.23	37.32
0.75	0.7	1475	10188	0.0779	82.1	16.5	4.08	1109	0.70	10.52	9.15	39.25

Table 5.5 FU sensitivity analysis on fuel cell performance – Case B

The following figure illustrates the trends of the main parameters.

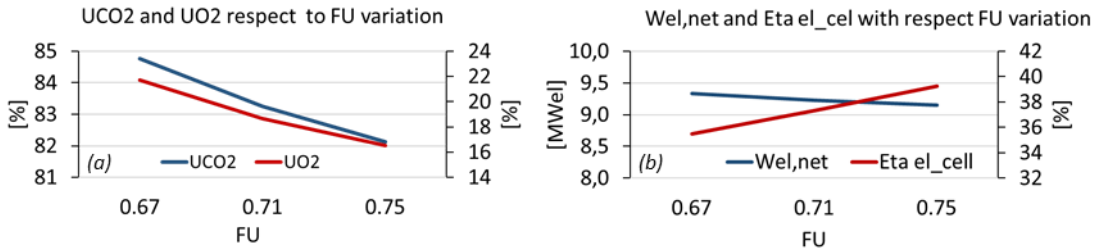

Figure 5.6 Overview of fuel performance with respect FU – Case B. (a) carbon dioxide and oxygen utilization factor with respect fuel utilization factor; (b) net cell electric power and net cell electrical efficiency with respect fuel utilization factor.

The table 5.6 shows once again how lowering the utilization factor leads to an improvement in performance in terms of CO_2 capture, while the decrease in electrical power is not as significant as in the case A.

Overall plant performance – Case B – Sensitivity analysis on fuel utilization factor										
FU	NG_{in} kg/s	$H_{2.out}$ Nm³/h	CO_2^{out} kg/s	CCR %	CO_2 avoided %	E_{CO_2} $\frac{g_{CO_2}}{MJ_{H_2}}$	Q_{steam} MW	$W_{el.net}$ MW	η_{H_2} %	SPECCA $\frac{MJ}{kg_{CO_2}}$
No capt	2.63	30258.9	6.98	-	-	77.61	6.99	1.77	80.60	-
0.67	3.07	32522	0.62	92.60	91.74	6.41	3.38	6.34	75.51	1.17
0.71	3.04	31919	0.69	91.68	90.62	7.28	3.75	6.52	75.21	1.27
0.75	3.02	31368	0.75	90.96	89.70	7.99	3.98	6.69	74.89	1.36

Table 5.6 FU sensitivity analysis on overall plant performance – Case B

For more details we report in figure 5.7 the trend of the main values.

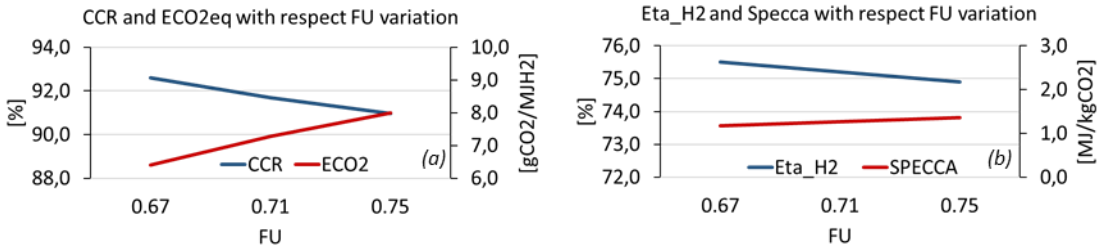

Figure 5.7 Overview of overall plant performance with respect FU – Case B. (a) carbon capture ratio and equivalent CO_2 emission with respect fuel utilization factor; (b) equivalent hydrogen production efficiency and SPECCA with respect fuel utilization factor.

We remind that a sensitivity analysis for case C has not been realized because, by not producing hydrogen and lowering the utilization factor, the cell area increases enormously and is not convenient from an economic point of view. On the contrary, even increasing the utilization factor would have problems due to the lack of anode reagents and higher concentration losses, so we stopped at a FU of 0.75, a literature limit value.

5.3 Economic analysis methodology

Low-carbon technologies designed to reduce the climate impact of the standard installation are usually evaluated through an economic analysis to estimate the increase in costs due to retrofitting. It is in fact obvious that a modification of the upstream plant must be economically competitive so that it can be adopted and not frustrate the efforts towards an increasingly carbon-free production system. For this reason, the analysis considered will be differential type, considering the revenues and costs deriving from the capture section only.

In this paragraph we first describe the methodology used to estimate investment costs considering the main components of the plant. Then we examine the cost of installation of the plant and the costs related to its actual management during the activity. In particular, we focus on fuel cell technology, which is still immature from an economic point of view, and then present a future scenario in which its costs could be reduced by making this retrofit more accessible so as to guarantee its rapid and large diffusion. As will be clear, the competitivity of this capture system is closely linked to the costs of MCFC. After the costs we evaluate the main revenues deriving, in particular from the production of electricity (for sale or for internal self-consumption in the refinery), hydrogen, steam in export and from the non-payment of the carbon tax thanks to this system that allows to reduce greenhouse gas emissions.

5.3.1 Methodology for the cost calculation

The methodology used to calculate the costs of the plant divided into investment costs, fixed O&M costs and variable O&M costs will be briefly presented below.

5.3.1.1 Investment costs

The costs of the plants estimated in this economic analysis include only the installation of CO_2 capture plant emitted by steam methane reforming. First, the calculation of the total investment costs must be defined. Reference is made to the approach followed by *M. Spinelli et al.* [62] in his study on CO_2 capture from cement plants.

The levelized cost of hydrogen (LCOH) is calculated considering a bottom-up approach: the logic behind the model is to divide the costs into different phases, starting from the cost of the devices and progressively applying the additional expenses at each level of the project (as in figure 5.8).

The first step is to determine the total direct cost of the plant (TDPC). It is the sum of all the costs of the system components estimated within the specific cost functions described later in this section. Since it is not possible from this model to calculate the actual initial amount of catalyst for the WGS reactor, sorbents and activated carbon for the purification beds, we assume to take this into account in the TDPC. This cost is only related to initial supply, while any replacements during the useful life of the plant will be considered through operation and maintenance costs.

The second calculation step is the EPC (engineering procurement and construction), i.e. the cost related to engineering services and the construction cost which is determined by adding the cost related to the engineering phase, the site activities and the construction of the plant with all the necessary related services; we will instead neglect the cost related to the acquisition of land for the installation of the new plant as it is assumed that there is enough free space present in a refinery.

The third cost step is the TPC (Total Plant Cost). It considers the additional costs of the owner relating to property taxes and construction and contractual fees.

The Capex calculation is the fourth step of the procedure necessary to actualize the investment cost of the plant according to the discount rate and the inflation rate. The investment cost is divided over a period of three years before the first start-up of the plant [62]. Assume that the costs are allocated at 40% the first year, 30% the second year and 30% the third.

The procedure is schematized in figure 5.8

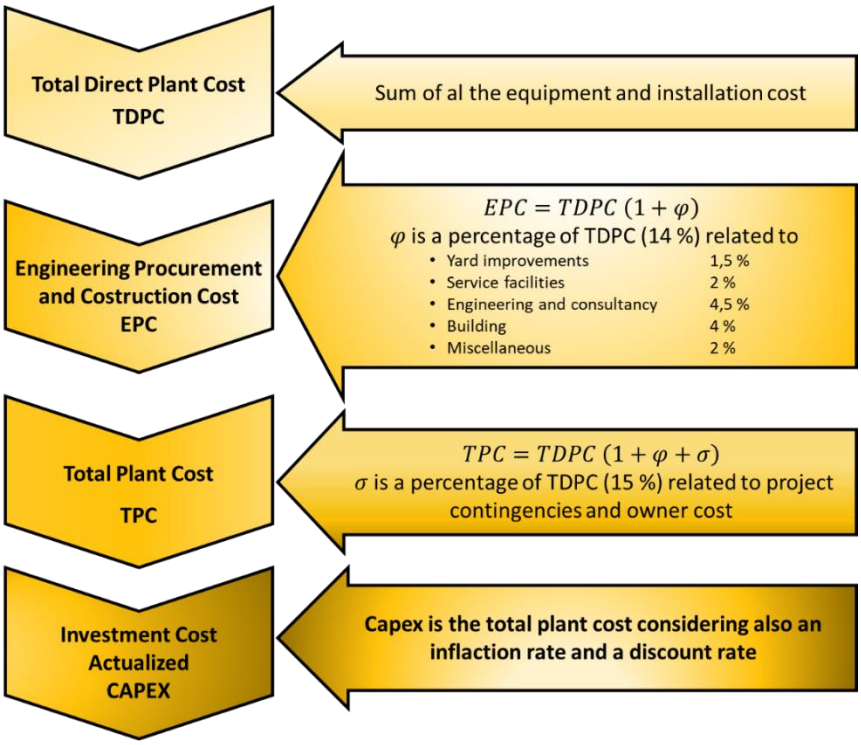

Figure 5.8 Investment cost procedure for CAPEX determination

5.3.1.2 Determination of component costs

Two formulations are adopted for the determination of the costs of the components as shown below:

$$C_{eq} = b\left(\frac{S}{a}\right)^{c} \qquad (5.1)$$

These cost functions are useful for the determination of those components that follow the economy of scale and are generally diffused for each component that is present on the market and has achieved full technological development.

- b: is the basic cost of the unit whose reference is specified in the table below.
- a: is the scaling parameter that is the representative parameter of the component.
- S: is the value of the reference parameter in our specific case.
- c: is a parameter that considers the scaling effect. Components with a value of c close to 1 are slightly affected by the size effect, while those with a value close to zero are strongly affected by the size effect.

Ref.	Component	Parameter	UM	a	b	c	UM of cost
[55]	AH-2 Anode side heat exchanger	Heat transfer surface	m²	63	6640	1	€
[55]	AH-3 Super heater	Heat transfer surface	m²	505	250019	0.74	€
[55]	AH-6 Evaporator	Heat transfer surface	m²	5000	1300000	0.788	€
[55]	AH-5 Evaporator	Heat transfer surface	m²	5000	1300000	0.788	€
[55]	AH-8 Economizer	Heat transfer surface	m²	10000	1070000	0.684	€
[55]	AH-4 Natural gas heat exchanger	Heat transfer surface	m²	63	6640	1	€
[55]	AH-7 Offgas heat exchanger	Heat transfer surface	m²	63	6640	1	€
[68]	Water gas shift reactor high temperature	Outlet flow	m³/s	2.016869	0.175722	0.67	M€
[68]	PSA	Inlet flow	m³/s	4.628549	36.55818	1	M€
[68]	Cooling water system	Thermal power reinject to the ambient	MW	470	25.84	0.67	M€
[67]	Cryogenic separation, turbomachinery and BOP	Compressor power	MW	62.1	78.6135	0.67	M€
[68]	ZnO desulphurization	Natural gas flow	kg/s	17	0.292871	0.67	M€
[72]	Combustor	QPCI	MW	105.058	6.36	1	M€
[68]	Pre-reformer	Inlet flow	kg/s	17.11	1.2447	0.67	M€

Table 5.7 Equipment cost functions of designed plant configurations – Equation 5.1

For the cost of the Ljungstrom recuperative cathode heat exchanger it was decided according to literature data [62] to consider it as 50 €/m² to represent its value more properly. Finally, the costs related to compressors, pumps and fans have been determined in accordance with the following equation:

$$\log(C_{eq}) = k_1 + k_2 \log(S) + k_3[\log(S)]^2 \qquad (5.2)$$

k_1, k_2, k_3 are appropriate tabulated parameters.

Ref.	Component	Parameter	UM	k_1	k_2	k_3	UM of cost
[65]	Air fan	Inlet flow	m³/s	3.5391	-0.3533	0.4477	€
[65]	Flue gas fan	Inlet flow	m³/s	3.5391	-0.3533	0.4477	€
[65]	H2 compressor	Fluid power	kW	2.2897	1.3604	-0.1027	€
[65]	Pump H2O. centrifugal	Shaft power	kW	3.3892	0.0536	0.1538	€

Table 5.8 Equipment cost functions of designed plant configurations – Equation 5.2

The cost of MCFC is not considered in this analysis due to its low market diffusion and its low sales volume which would lead to cost functions with low confidence. However, it should be mentioned that MCFC today is a fully commercial product. The main producer in the sector is *Fuel Cell Energy Inc.* Therefore, for the cost of the stack will be considered two different scenarios, emphasizing that knowing with precision the costs of an MCFC is not easy and therefore we refer to literature values [62].

- The first scenario (scenario 1) is characterized by a cost of the stack about the current one, assumed 1200 €/kW_{el}. Since the maintenance costs due to the replacement of the stack are influenced by the cost of materials, it is considered as an equivalent cost of the equipment. In particular, it is assumed that the maintenance cost is 50% of the initial cost (i.e. 600 €/kW_{el}), with a total equivalent cost of 1800 €/kW_{el}. This value includes the replacement of the stack every 7 years, for the whole life of the plant.
- The second scenario (scenario 2) represents an achievable future scenario in case MCFC production becomes significant (more than 200 MW/year [62]). In this case the total cost including maintenance and stack replacement is equal to 610 €/kW_{el}.

To make the cost more evident and since our cell is mostly designed for capture and not for power generation, we have chosen to report the cost based on the m^2 of active cell area. This procedure consists in initially considering the specific cost to the power and, once noted the polarization curve and the power density curve, report the specific cost to the active cell area assuming that it is calculated at the point of maximum power density. It is a necessary procedure to consider the fact that the cell is not operated at the point of maximum power but at a higher ΔV because this leads to a higher CO_2 permeation in the electrolyte.

5.3.1.3 Total plant cost for the three different plant configurations

We report below the investment costs for the three plants in the base case with utilization factor 0.75 and 0.67 and cell potential 0.7 V. Two possible scenarios will be distinguished, scenario 1 and scenario 2, depending on the cost of the fuel cell. In this way we want to underline how decreasing the utilization factor leads to better capture efficiency, hydrogen production and lower SPECCA but also to greater investment costs.

Investment cost for three different plant configurations										
	FU = 0.75						FU = 0.67			
	A		B		C		A		B	
Cost Item	Sc.1 M€	Sc.2 M€	Sc.1 M€	Sc.2 M€	Sc.1 M€	Sc.2 M€	Sc.1 M€	Sc.2 M€	Sc.1 M€	Sc.2 M€
MCFC stack	39.92	13.31	20.87	6.96	35.63	11.88	45.49	15.16	21.19	7.06
Heat exchangers	1.26		0.76		1.38		1.25		0.68	
Pre-reforming	0.38		-		0.38		0.45		-	
WGS HT	0.91		0.72		0.86		1.05		0.77	
Balance of plants	0.9		0.51		0.84		1.5		0.81	
Criogenic separation	13.83		11.22		12.99		15.61		11.91	
TDPC	**57.21**	**30.60**	**34.08**	**20.17**	**52.08**	**28.32**	**65.35**	**35.02**	**35.35**	**21.23**
Yard improvement	0.86	0.46	0.51	0.30	0.78	0.42	0.98	0.53	0.53	0.32
Service facilities	1.14	0.61	0.68	0.40	1.04	0.57	1.31	0.70	0.71	0.42
Engineering & consultancy	2.57	1.38	1.53	0.91	2.34	1.27	2.94	1.58	1.59	0.96
Building	2.29	1.22	1.36	0.81	2.08	1.13	2.61	1.40	1.41	0.85
Miscellaneous	1.14	0.61	0.68	0.40	1.04	0.57	1.31	0.70	0.71	0.42
EPC	**65.22**	**34.88**	**38.85**	**22.99**	**59.37**	**32.29**	**74.50**	**39.93**	**40.30**	**24.20**
Other Owner's costs	9.78	5.23	5.83	3.45	8.91	4.84	11.18	5.99	6.04	3.63
TPC	**75.00**	**40.11**	**44.68**	**26.44**	**68.27**	**37.13**	**85.68**	**45.91**	**46.34**	**27.83**

Table 5.9 Investment cost for three different plant configurations

If the utilization factor is lower so both the costs and the percentage weight of MCFC on the overall cost increases (figure 5.9). Therefore, it is evident that the investment cost of the plant is intrinsically related to the cost of the fuel cell.

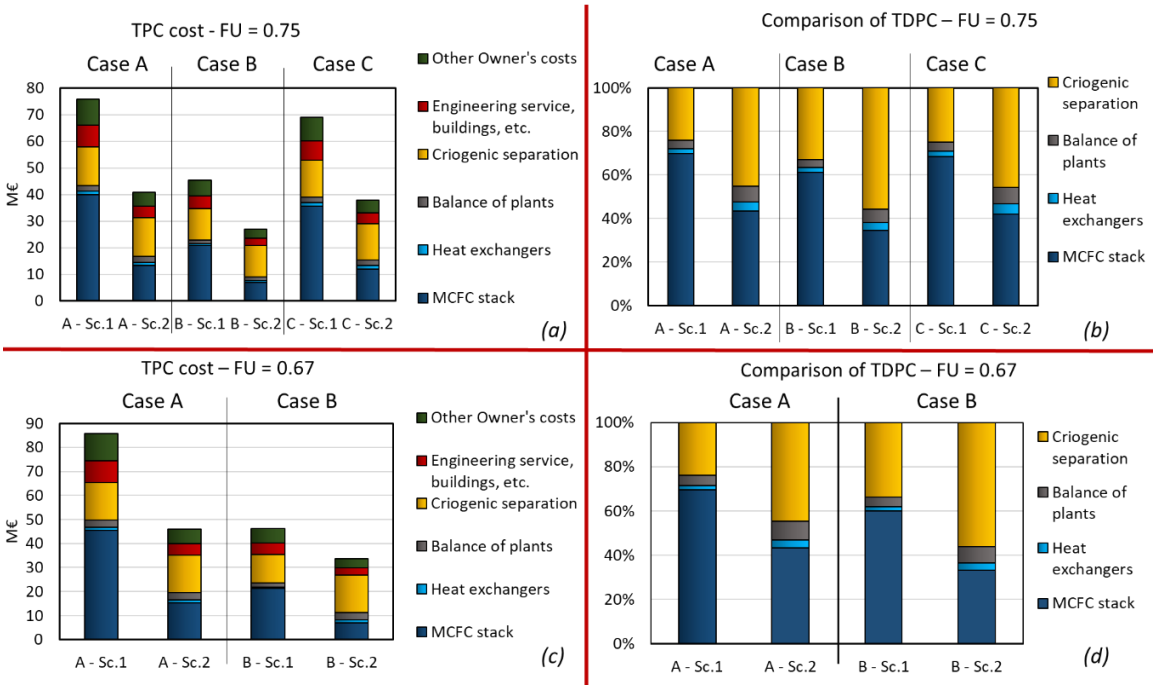

Figure 5.9 Comparison of TDPC and TPC for different case and different FU. In the figure balance of plants also includes the cost for WGS and pre-reforming. (a) TPC with fuel utilization factor equal to 0.75 and different MCFC cost scenarios; (b) TPC in percentages with fuel utilization factor equal to 0.75 and different MCFC cost scenarios; (c) TPC with fuel utilization factor equal to 0.67 and different MCFC cost scenarios; (d) TPC in percentages with fuel utilization factor equal to 0.67 and different MCFC cost scenarios

It is interesting to compare case A and case C, both fed by natural gas. With the same utilization factor, case C allows a lower investment cost, it has no hydrogen production but produces more steam in export. Therefore, it is not possible to evaluate which of the two can be the most profitable and NPV will have to be calculated considering O&M costs and gains. The cost of cryogenic capture, after the cell cost, is the most relevant in all types of plants, it may even become more predominant in the second scenario. From the graph it can be observed that case B with the same utilization factor (equal to 0.67) is the most economical one; this is essentially because the stack area is about 7345 m^2 smaller with respect case A.

5.3.2 Determination of operation and maintenance costs

The second type of cost to analyse are the expenses related to operating and maintenance costs. Each component requires a periodic control during the useful life of the plant in order to ensure its correct operating conditions. For this reason, we consider these fixed O&M costs as a percentage (2.5% of TPC) of the initial investment cost. It is also important to underline that materials such as catalysts, sorbent and activated carbon for PSA are considered in the fixed O&M costs although they are subject to periodic replacements as expressed above. This hypothesis is not dramatic from the point of view of the levelized cost

of hydrogen because the equivalent annual operating hours of the plant are extremely high as it is typical for refinery applications where plant shutdowns are not frequent.

Other fixed operation and maintenance costs that we consider are relative to insurance (2 % of TPC) and labour costs, expressed as 1.8 k€/MW/year as mentioned by literature references [55] [62]. The cost instead of clean process water is usually related to the recirculation and purification systems of it that we assume are included in the operating cost of the component. Otherwise, raw water is widely used in the refinery plant and therefore its inclusion in O&M costs is not necessary. We report the fixed operation maintenance costs in case of utilization factor 0.75.

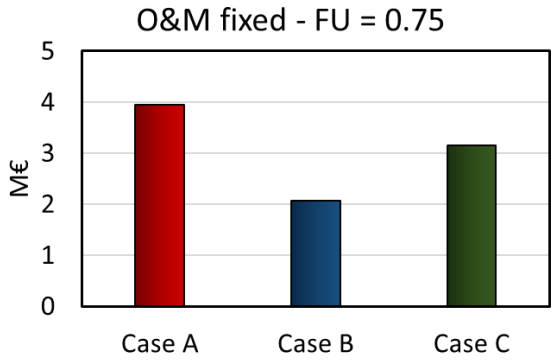

Figure 5.10 Fixed operation and maintenance cost for FU = 0.75 for different plant configuration

The cost of natural gas is included in the variable O&M. It is assumed as base value a cost of 6 €/GJLHV. The estimate of the range of variation of it comes made referring to the data provided from the *GME* [73] (Gestore Mercati Elettrici) and from the observation made on the diagram of figure 5.11. It is well to remember that the precise cost of natural gas is not something easily predictable due to the influence of socio-political factors whose characterization is beyond the scope of our work. Viewing the statistics of previous years compiled by the Italian energy market manager, it seems appropriate to make an analysis between 4 €/GJLHV and 8 €/GJLHV to give the reader an idea of how this value can influence the convenience of the retrofit. It will be done only for the case of off-design where it shows a real variation of natural gas input to meet the demand for hydrogen in output.

To give an idea of how variable the price of natural gas is, we want to report in a summary way the variation of the price in the TTF market (figure 5.11).

The TTF (Title Transfer Facility) is a virtual marketplace in which natural gas is traded on the Dutch platform and thanks to its central location allows a transfer of gas between the markets of Norway, Germany, France, Italy and Great Britain.

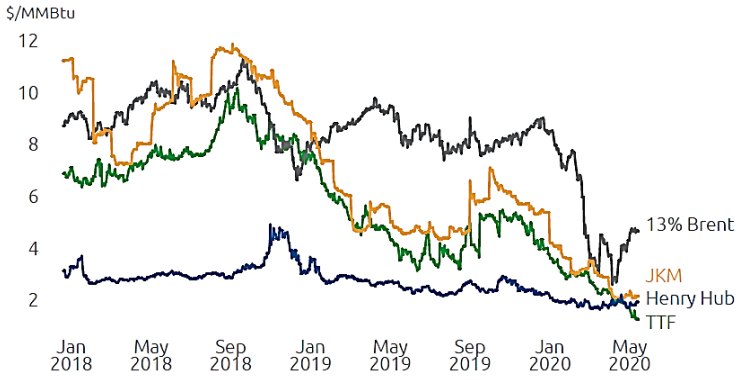

Figure 5.11 Trend of gas price in TTF market [70]

It is interesting to note that the price of natural gas in North America (Henry Hub) has been much lower than in other countries in the past. This is due to the production of shale gas which is now an economical and reliable technology. In contrast, North East Asia (represented by the JKM or Japan-Korea marker market) has geographical problems in natural gas supply, so high demand can only be met with imported natural gas transported in liquid phase through special tankships. When the gas arrives at the place of use, it is regasified and introduced into the gas network. As a result, the entire transport process from the well is energy intensive and, for this reason, the prices of liquefied natural gas are higher than the traditional natural gas transported in the pipelines. However, it should be highlighted that the Asian price has also dropped dramatically in recent years.

Finally, it is interesting to mention the effect of the recent and current coronavirus pandemic. In chapter 1 we have discussed how it has greatly reduced energy consumption in the months of full lockdown, while here we observe how commodity prices have been affected; they have been drastically reduced even if, as reported in the *Snam* report, gas prices had started to fall even before this, driven by a surge in LNG supply and lower demand.

We evaluate the last variable O&M cost, which is the cost of CO_2 transport and storage. We have already discussed, in chapter 3, the possible methods for storage, and therefore here we do not consider a precise one, but we will assume a constant average value equal to 7 €/tonnCO_2.[62]

Finally, we neglect disposal costs and do not consider them in the cash flow statement. This hypothesis is very frequent in the literature at these levels of analysis. In fact, the value of the recovery of components and materials is assumed to be equal to the cost of disposal and rehabilitation of the site, resulting in a net zero cost.

5.3.3 Evaluation of parameters for sensitivity analysis

As mentioned above we will analyse sensitivity for the most promising case to the variation of electricity price, hydrogen sales value and carbon tax. Therefore, here below is a detailed description to define the possible sales ranges of them.

Electricity selling price:

Thanks to the utilization of the MCFC system for the capture, it is also possible to produce electricity, which represents an alternative source of income that can partially compensate the costs due to the retrofit. This output allows to decrease the energy taken from the grid by refinery, bringing a gain due to the non-purchase of electricity. Looking at the purchase prices on the electricity market from the statistics published on the *GME* (Gestore Mercati Elettrici) website, a range between 30 and 80 €/MWh_{el} is analysed.

Hydrogen selling price:

The sensitivity analysis will be performed in a range between 1.5 and 4 €/kg_{H2}. The justification of the minimum value investigated is that conversion of natural gas into hydrogen through conventional reference technology such as steam reforming would lead to a hydrogen production cost that can be evaluated by the following equation

$$c_{H_2,prod} = c_{GN} \frac{PCI_{H_2}}{\eta_{SMR}} \qquad (5.3)$$

Assuming that $\eta_{SMR} = 60\%$ and knowing that PCI_{H_2}= 119.95 MJ/kg and PCI_{GN} = 46.5 MJ/kg is obtained, with a natural gas price of 8 €/GJ, a value of $c_{H_2,prod}$ equal to 1.5 €/kg_{H2}.

Carbon tax value

In the Italy there is no tax on emissions and even today it remains a practice not unanimously adopted by all European countries. Therefore, to give a correct value is not possible, but only to define a range of variation. We do this by referring to the main European countries and consider two different cases:

- Spain: carbon tax value equal to 15 €/$tonn_{CO2eq}$
- Sweden: carbon tax value equal to 112 €/$tonn_{CO2eq}$

Therefore, the sensitivity analysis will be done by varying the tax between 0 and 100 €/tonnCO_2.

It is important to remind that the products and sectors of application of the tax vary from country to country and also that it is different from the price attributed to carbon dioxide through the so-called ETS (Emission Trading System), whose value is much lower, is the result of market dynamics and market share trading.

5.3.4 Resume of the procedure for estimation of NPV and LCOH

In the economic evaluation the main indices of economic engineering have been considered. They are able to evaluate the profitability of the investment. The considered indices are presented below.

Net Present Value (NPV) is defined as:

$$NPV = \sum_{i}^{plant\ life} DCF_i = \sum_{i}^{plant\ life} \frac{CF_i}{(1+d)^i} \qquad (5.4)$$

It is the sum of the future cash flows of an investment discounted to year zero (i.e. the present) using an appropriate discount rate d, that is useful to actualize the cost over the whole useful life of the plant. The minimum acceptable value is an NPV ≥ 0. If this value is negative it would mean that the revenues obtained from the investment are not able to repay the costs.

Internal Rate of Return (IRR) is defined as:

$$IRR \rightarrow \sum_{i}^{plant\ life} \frac{CF_i}{(1+IRR)^i} = 0 \qquad (5.5)$$

It is the discount rate for which the Net Present Value is zero and represents, in technical terms, the return on an investment. In order to obtain its value, it is necessary to use an iterative procedure. The calculation of the internal rate of return is used to evaluate the convenience or not of an investment: IRR is compared with a limit rate of return, so-called acceptance rate or cut-off rate that in this analysis is assumed to be equal to the discount rate supposed. It is worth making the investment if IRR is higher than the cut-off value.

If the NPV function has more than one zero, the IRR calculation may generate errors. If the IRR can be calculated, it is preferable to NPV because it is a non-dimensional index, so it is independent of the size of the plant. The NPV on the contrary is not suitable if it is not compared with the value of the investment: at equal NPV obtained, the economic quality of the project is very different depending on the initial investment required.

Payback time is the period of time necessary for the discounted cash flows from the revenues obtained to equal the initial investment. Lower PBT periods are preferable because they allow you to pay back your investment more quickly, while longer PBTs coincide with a riskier investment. This index is more a performance of time risk return than a performance of financial return on the project.

It is necessary that this return period is limited to a maximum acceptable value set by the company, which, in any case, must be lower than the overall financial cycle regarding the investment. The maximum acceptable recovery period set by the firm, also known as the

cut-off period, represents the upper limit beyond which the investment proposal will be rejected. In the hypothesis of alternative projects, similar in terms of useful life, the one with a shorter recovery time will be preferred. In our analysis, no cut-off period has been considered even if, with payback time longer than about 12 years, no investment is recommended despite an acceptable NPV and IRR.

We report below the assumptions used during the economic analysis.

Type of assumption	***Value***
Power plant operating life, years	20
Construction period, years	3
Operating hours first year, h	5700
Operating hours after first year, h	7500
Tax-rate	Pre-taxation
Depreciation time	No depreciation
Inflaction rate	0%
Construction inflaction	0%
Discount rate	8%
Capital expenditure during construction	
Year -3	40%
Year -2	30%
Year -1	30%

Table 5.10 Long-run profitability analysis assumption

Depreciation is not considered in the discounted cash flow analysis. The results presented in this study is reported on Earnings Before Interest, Taxes, Depreciation and Amortization (EBITDA) basis.

We now illustrate in a schematic way the procedure followed for the calculation of LCOH. For simplicity we will indicate with:

- *ccs*: the FTR system plus the capture section
- *conv*: the basic FTR system without capture
- *capt.*: the capture section only

Resume of economic calculation procedure

Investment cost calculation: $IC_i \left[\frac{M€}{y}\right] = \%\ allocation\ of\ investment\ cost_i * TPC^{capt}$ where i is the specific year considered

Total cost: $Ex_i \left[\frac{M€}{y}\right] = IC_i + O\&M_{fix,i} + O\&M_{var,i} + O\&M_{TeS,i} + C_{tax,i}$

where

$$O\&M_{var,i} = m_{GN} * 3600 * h_{eq} * c_{GN}$$
$$O\&M_{TeS,i} = m_{CO_2} * 3600 * h_{eq} * c_{TeS}$$
$$C_{tax,i} = \left(m_{CO_2}^{ccs} - m_{CO_2}^{conv}\right) * 3600 * h_{eq} * c_{tax}$$

In this case it is possible to observe how $m_{CO_2}^{ccs} < m_{CO_2}^{conv}$ and therefore the carbon tax from cost becomes a gain

Total revenues: $Rev_i \left[\frac{M€}{y}\right] = RFE_i + RFH_i + RFQ_i + RFQ_{CO_2,i}$

where

$$RFE_i = W_{el,net,year} * price_{el}$$
$$RFH_i = \left(m_{H_2}^{ccs} - m_{H_2}^{conv}\right) * 3600 * h_{eq} * price_{H_2}$$

RFQ_i represents the revenue from the non-payment of natural gas to the power unit boiler that should have produced the same thermal power. Where

$$\eta_{BOILER} = 90\ \% \rightarrow \eta_{BOILER} = \frac{Q}{m_{GN} LHV_{GN}} \rightarrow m_{GN} = \frac{Q}{\eta_{BOILER}\ LHV_{GN}}$$

Therefore $\left(\frac{Q^{CCS} - Q^{CONV}}{\eta_{BOILER}\ LHV_{GN}}\right) = \Delta m_{GN}$ represents the more or less natural gas to be put in comparison to the basic case.

$$RFQ_i = \left(\frac{Q^{ccs} - Q^{conv}}{\eta_{BOILER}\ LHV_{GN}}\right) * h_{eq} * 3600 * price_{GN}$$

In addition, we also consider the gain due to non-payment of the carbon tax to the boiler. It is calculated as:

$$RFQ_{CARBON\ TAX} = \left(\frac{Q^{ccs} - Q^{conv}}{\eta_{BOILER}\ LHV_{GN}}\right) * E_{CO_2}^{boiler} * h_{eq} * 3600 * c_{TAX}$$

$E_{CO_2}^{boiler} \left[\frac{kg_{CO_2}}{kg_{GN}}\right]$ represents the emission of the boiler for kg_{GN} spent that is calculated considering the composition of the natural gas and assuming that the incoming carbon is oxidized all to CO_2.

Calculation discounted cash flow e NPV

$$DCF_i = \frac{Rev_i - Ex_i - IC_i}{(1 + d - If)^i}$$

where d is the discount rate that is useful to actualized the cost over the whole useful life of the plant and If is the rate of inflation

$$NPV = \sum_i^{plant\ life} DCF_i \text{ e}$$

5.4 Economic results and comparison

It is useful to report below the results of the main economic indexes of the plant after the retrofit to determine whether the capture section is profitable or not. Remember that being a differential analysis, it may be that the additional capture section has a negative NPV, which does not necessarily mean that FTR + capture has a negative revenue.

The following basic values are considered for the calculation of the base case:

- Hydrogen price: 2 €/kg_{H2}
- Electricity price: 50 €/MWh_{el}
- Price of natural gas: 6 €/GJ
- Price of carbon tax: 20 €/$tonn_{CO2}$

We now report the outputs for cases A, B and C in the basic configuration.

Minimum value for different case with FU = 0.75						
	A		B		C	
	Sc. 1	Sc. 2	Sc. 1	Sc. 2	Sc. 1	Sc. 2
NPV [M€]	-92.38	-34.31	-57.43	-27.07	-105.24	-53.40
Minimum value for hydrogen price [€/kg_{H2}]	6.87	3.81	9.31	5.45	-	-
Minimum value for electricity price [€/MWh_{el}]	137.96	82.66	197.26	119.42	164.76	108.23
Minimum vale for carbon tax [€/$tonn_{CO2}$]	75.54	40.62	53.26	35.68	83.35	52.14

Table 5.11 Economic results for different case with FU = 0.75

Observing only the NPV, case B would seem the most convenient. As shown in figure 5.9 it is the one characterized by the lower investment cost on components, especially for MCFC and the lower cost for fuel because it is noted in table 4.18 which is the one that requires lower expenses for natural gas. However, this configuration has the disadvantage to produce a much lower quantity of hydrogen and electricity; for this reason, it is obtained that the minimum selling price of hydrogen is higher than in case A, although it has higher investment costs.

If we assume that we are in scenario 2 for the cost of MCFC, projected in the future, where hydrogen has a valorisation around it not only for the self-consumption, but also for the sale, it is clear that system A is cheaper than B. Moreover, the off-gas supply of the cell decreases the flexibility of the MCFC section and forces FTR to operate in off-design because this plant was already existing and programmed to operate with natural gas; otherwise we should provide for retrofitting also the FTR section. Finally it's useful to underline that in the refinery there are other sources of CO_2 emission, as pointed out in table 4.6 and in table 1.1, so in case A we could consider to feed to the cathode these streams to be absorbed while case B remains related to the need to feed to the anode a flow free of hydrocarbons greater than CH_4 because of the absence of pre-reforming. Therefore case A is more flexible facing an inlet flow at cathode of exhaust gases of different refinery processes.

If, on the other hand, we were to consider the carbon tax, plant B would be the preferred one because it is affected by lower CO_2 emissions despite the increase in indirect emissions caused to the POW to produce the difference in steam. Finally, we underline how plant C is the least economically recommended one, a fact that highlights even more how hydrogen production is fundamental to pay back the costs of the capture section.

We evaluate how the parameters of table 5.11 when the utilization factor varies, for cases A and B. This analysis will not be pursued for case C because it is already the most disadvantaged in every condition.

5.4.1 Case A

We report in the table the main values for case A with a variation of the utilization factor.

Minimum value for case A with different fuel utilization factor						
	A - FU = 0.75		A - FU = 0.71		A - FU = 0.67	
	Sc. 1	Sc. 2	Sc. 1	Sc. 2	Sc. 1	Sc. 2
Total Plant Cost [M€]	76.00	41.11	80.59	43.67	86.81	47.05
NPV [M€]	-92.38	-34.31	-87.43	-25.98	-80.84	-14.65
Minimum value for hydrogen price [€/kg$_{H2}$]	6.87	3.81	5.09	2.92	3.99	2.36
Minimum value for electricity price [€/MWh$_{el}$]	137.96	82.66	129.05	73.49	118.10	62.34
Minimum vale for carbon tax [€/tonn$_{CO2}$]	75.54	40.62	71.88	35.42	67.14	28.54

Table 5.12 Economic results for case A with different fuel utilization factor

It is possible to observe that a decrease of the utilization factor leads to higher investment costs, whose driving force is the largest active area of MCFC and therefore the higher stack cost but the additional revenues due to the higher hydrogen production and higher electricity sales fully compensate the higher plant cost.

In order to understand how these values can influence the parameters examined, we observe the economic results when the prices of the main outputs of the plant vary. This is done only for the most promising case, the one with the lowest NPV i.e. FU = 0.67 and scenario 2 (figure 5.12).

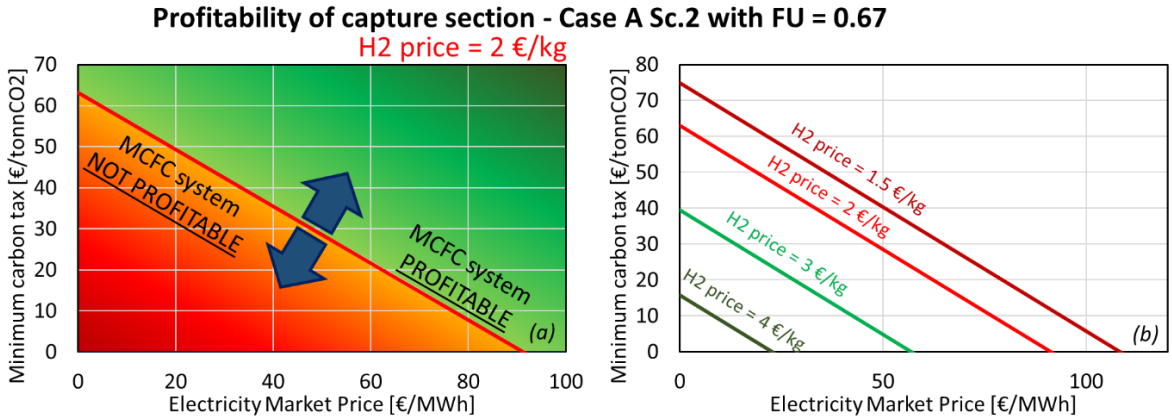

Figure 5.12 Minimum carbon tax value that justifies the MCFC system installation, plotted as function of electricity market price. (a) with a given hydrogen price; (b) varying hydrogen price

The red curve of the graph in figure 5.12 (a) represents the electricity market price and the minimum carbon tax value where NPV is equal to zero for a given hydrogen price. Its slope depends therefore on the electric power produced and CO_2 avoided compared to the base case while its location in the plan depends on the quantity of hydrogen extra produced at the same selling price. The more hydrogen is produced the more the red curve is lowered making the positive profit zone greater. This will be more evident in case B, where the quantity of H_2 produced is less than in case A where the not profitable area is wider.

We now show in figure 5.13 the NPV value at the last year of lifetime for different hydrogen price values, first by varying the carbon tax with the electricity price fixed at the base value (a), then by varying the electricity price with the carbon tax fixed at the base value (b).

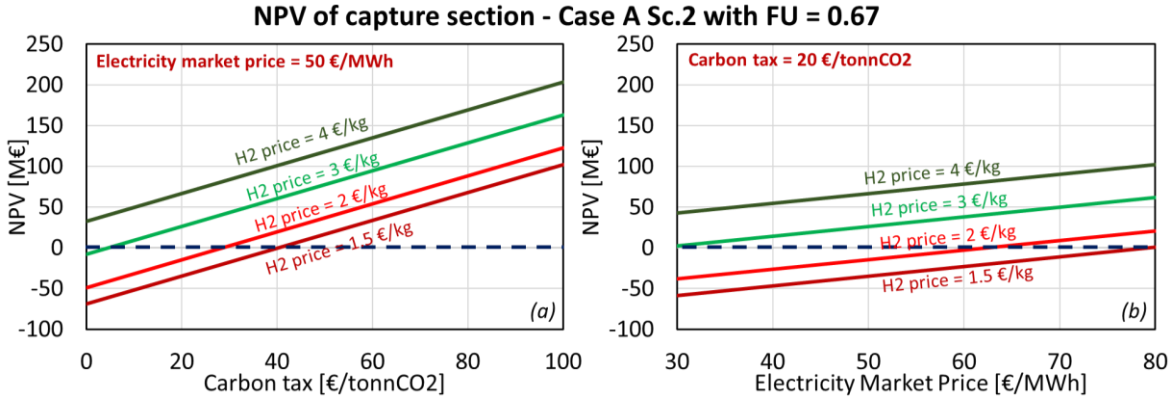

Figure 5.13 NPV of capture section – Case A Sc.2 with FU 0.67 plotted as function of (a) carbon tax and hydrogen price (b) electricity market price and hydrogen price

It is possible to observe how the slope of the curves in figure (a) is greater than that of figure (b) which indicates how a variation of the carbon tax influences the retrofit more than a variation of the electricity market price.

We want through a simple analysis to try to explain the greater slope of the curve dependent on carbon tax compared to the electricity market price. To get this, it is useful to observe table 5.2 and make a comparison between case 0.67 and the base case without capture. The revenue from carbon is defined as:

$$\left(m_{CO_2}^{ccs} - m_{CO_2}^{conv}\right)\frac{tonn_{CO_2}}{y} * C_{tax}\frac{€}{tonn_{CO_2}} \tag{5.6}$$

while the revenue from the sale of electricity as:

$$\left(W_{el,netta}^{ccs} - W_{el,netta}^{conv}\right)\frac{MWh}{y} * P_{el}\frac{€}{MWh} \tag{5.7}$$

We calculate these values and we get that

- $m_{CO_2}^{ccs} - m_{CO_2}^{conv} = -162123.46\ \frac{tonn_{CO_2}}{y}$
- $W_{el,netta}^{ccs} - W_{el,netta}^{conv} = 112220.0\ \frac{MWh}{y}$

Therefore, the value that multiplies the carbon tax is greater, in absolute terms, than the value that multiplies the net electrical power.

Finally, we report in table 5.13 the payback time in function of carbon tax and hydrogen price (a) and electricity market price and hydrogen price (b)

(a)

Case A Sc.2 with FU = 0.67 - Payback time with respect carbon tax and hydrogen price with constant electricity market price equal to 50 €/MWh$_{el}$

Carbon tax [€/tonn$_{CO2}$]	H_2 price = 1.5 €/kg$_{H2}$	H_2 price = 2 €/kg$_{H2}$	H_2 price = 3 €/kg$_{H2}$	H_2 price = 4 €/kg$_{H2}$
0	NO PBT	NO PBT	NO PBT	9
20	NO PBT	NO PBT	10	6
40	NO PBT	11	6	4
60	9	6	4	3
80	6	5	3	3
100	4	3	3	2

(b)

Case A Sc.2 with FU = 0.67 - Payback time with respect electricity market price and hydrogen price with constant carbon tax equal to 20 €/tonnCO2

Electricity market price [€/MWh$_{el}$]	H_2 price = 1.5 €/kg$_{H2}$	H_2 price = 2 €/kg$_{H2}$	H_2 price = 3 €/kg$_{H2}$	H_2 price = 4 €/kg$_{H2}$
30	NO PBT	NO PBT	19	8
40	NO PBT	NO PBT	13	6
50	NO PBT	NO PBT	10	6
60	NO PBT	NO PBT	8	5
70	NO PBT	15	7	4
80	20	11	6	4

Table 5.13 Payback time of capture section – Case A Sc.2 with FU = 0.67 as function of (a) carbon tax and hydrogen price; (b) electricity market price and hydrogen price

The values in the table confirm the above-mentioned for figure 5.13 plotted as function of (a) carbon tax and hydrogen price (b) electricity market price and hydrogen price. It is also possible to observe how a hydrogen price of 4 €/kg$_{H2}$ and with electricity price and carbon tax equal to the base value (50 €/MWh and 20 €/tonn$_{CO2}$) allows an economic return in only 6 years making the retrofit considerably advantageous.

If we assume a cut-off period about 12 years, not all scenarios considered are good although they are characterized by a positive NPV. Indeed, if the payback period is too long, the investment is riskier.

5.4.2 Case B

From the following table it can be seen that also for case B, to go down with the utilization factor is more convenient in economic terms; in particular we have that the minimum prices analysed decrease because, as already reported in the previous analysis, the useful outputs of the plant increase.

Minimum value for case B with different fuel utilization factor						
	B - FU = 0.75		B - FU = 0.71		B - FU = 0.67	
	Sc. 1	Sc. 2	Sc. 1	Sc. 2	Sc. 1	Sc. 2
Total Plant Cost [M€]	45.49	27.25	46.27	27.92	47.21	28.69
NPV [M€]	-57.43	-27.07	-53.97	-23.42	-50.36	-19.54
Minimum value for hydrogen price [€/kg$_{H2}$]	9.31	5.45	6.59	3.99	5.14	3.22
Minimum value for electricity price [€/MWh$_{el}$]	197.26	119.42	193.28	112.18	188.79	103.85
Minimum vale for carbon tax [€/tonn$_{CO2}$]	53.26	35.68	51.05	33.48	48.75	31.15

Table 5.14 Economic results for case B with different fuel utilization factor

Although decreasing the utilization factor the investment is cheaper at the basic prices of hydrogen, electricity and carbon tax considered previously but it remains not profitable investment. Also, in this case therefore we report an sensitivity analysis with the price variation of the main outputs to better understand in which circumstance the plant with lower utilization factor (the most convenient) is a profitable investment

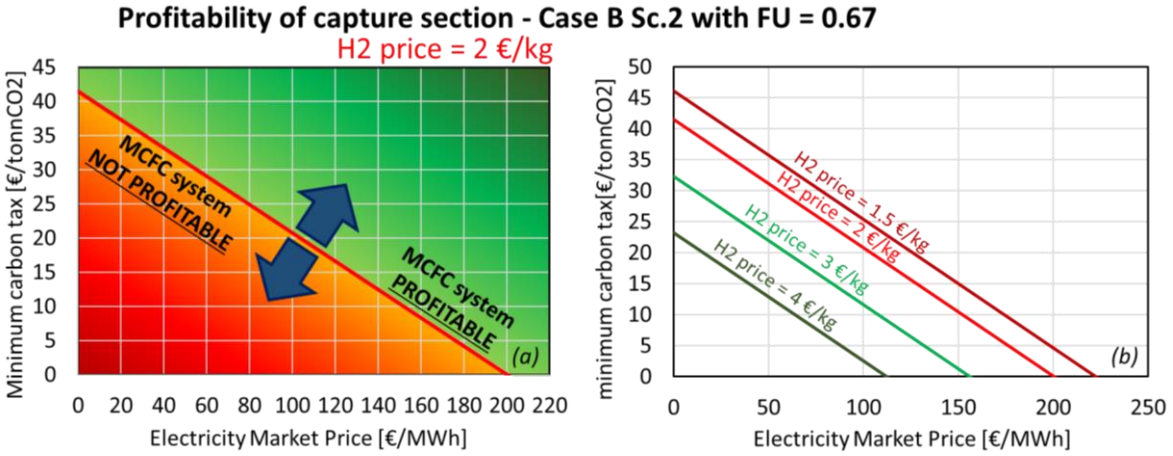

Figure 5.14 Minimum carbon tax value that justifies the MCFC system installation, plotted as function of electricity market price. (a) with a given hydrogen price; (b) varying hydrogen price

Even in this case, the figure 5.14 shows the trend of the carbon tax and the electricity market price, it turns out like that one of case A. In this case (in the figure a) it can be noticed how the electric production is clearly lower in comparison to the case A. In fact consequently this brings to have high prices for the electricity in correspondence of low values of the carbon tax (around 200 euro for MWh), on the contrary in correspondence of a zero price of the

electricity it can be observed how the ability to separate more CO_2 allows to have lower carbon tax at 40 euro per ton of CO_2 in comparison to 67 of the case A.

From graph b it is clear that varying the price of hydrogen the investment is more likely to be positive for very high electricity prices. Hydrogen production plays a determining role for the profitability of the investment. In fact, at the same cost of H_2 the case A, that produces much more of it, becomes much more profitable.

From figure 5.15, comparing the lines between case A and case B it can be observed that the profitability curves of the case with natural gas supply are more inclined than the case with offgas feed. This is essentially because the useful outputs of case A are almost double those of case B while it has the advantage of emitting less emissions. Profitability of case B depends less on electric production with respect case A because, with fixed carbon tax, to reach positive profit a larger variability of the electric price is necessary. For low electricity market price case B is more profitable than case A, while for high electricity price case A is more profitable. The electricity market price that decided this is the one obtained crossing the lines at same H_2 price (points in figure 5.15). This is due to the fact that B produces less electricity but has better CO_2 capture performance compared to case A.

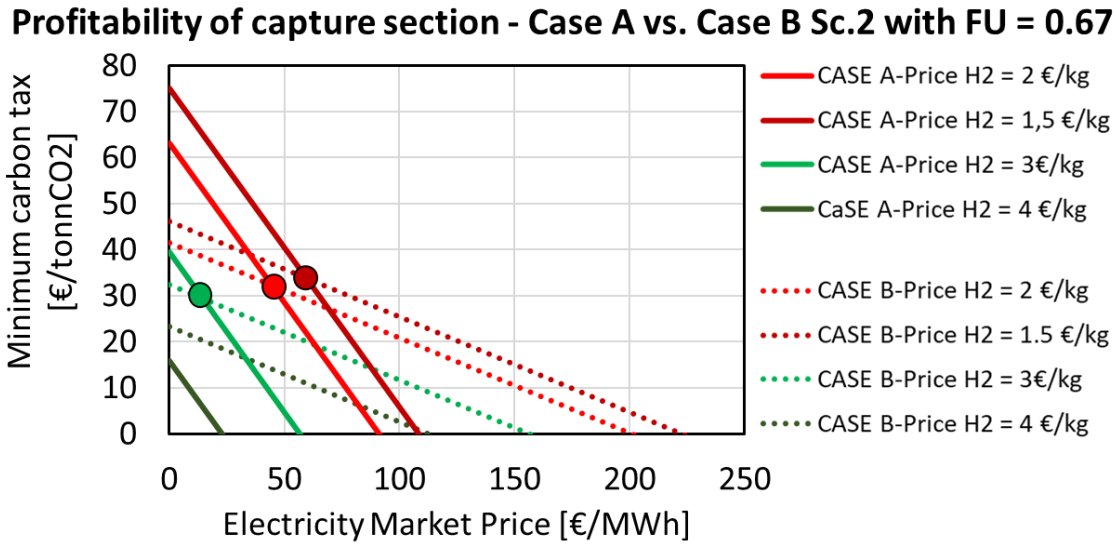

Figure 5.15 Minimum carbon tax value that justifies the MCFC system installation, plotted as function of electricity market price varying hydrogen price. Case A solid line; Case B dotted line

From the graph 5.16a and 5.16b, always referring to the last year of operative life, it is evident that also in case B, the Net Present Value trend is more dependent on the variation of the carbon tax than on the variation of the electric energy. Differently from case A, the dependence from hydrogen is lower and this is visible from the smaller space between the different curves drawn at the variation of €/kg_{H2}; they are more compressed. Moreover, in case B, observing the figure 5.16 b the curve is more flat underlining how the revenue from electric power production is less important.

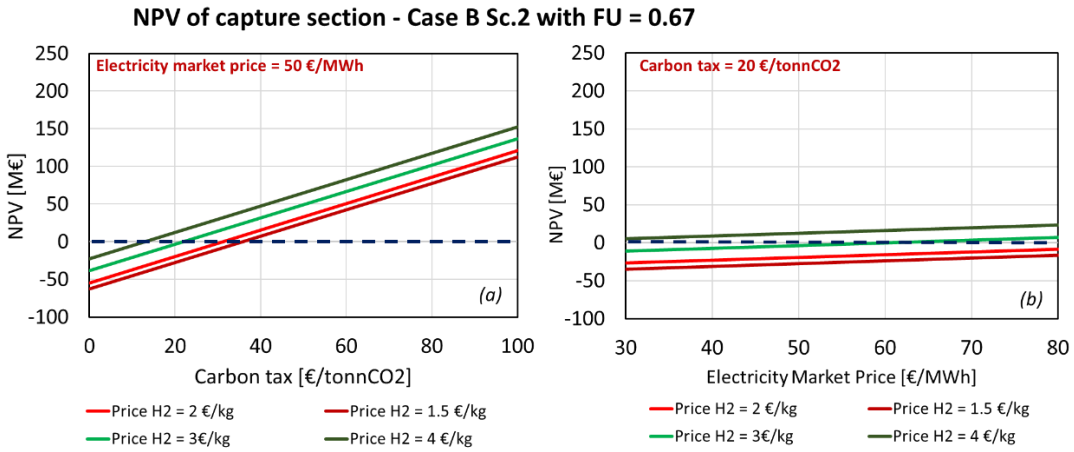

Figure 5.16 NPV of capture section – Case B Sc.2 with FU 0.67 plotted as function of (a) carbon tax and hydrogen price (b) electricity market price and hydrogen price

Finally, in the following two tables we report also for the B plant the payback time with respect the variation of carbon tax, the price of hydrogen and electric power always referred to the fuel utilization factor that gives more advantages.

(a)

Case B Sc.2 with FU = 0.67 - Payback time with respect carbon tax and hydrogen price with constant electricity market price equal to 50 €/MWh$_{el}$

Carbon tax [€/tonn$_{CO2}$]	H_2 price = 1.5 €/kg$_{H2}$	H_2 price = 2 €/kg$_{H2}$	H_2 price = 3 €/kg$_{H2}$	H_2 price = 4 €/kg$_{H2}$
0	NO PBT	NO PBT	NO PBT	NO PBT
20	NO PBT	NO PBT	NO PBT	11
40	13	10	7	5
60	5	5	4	3
80	3	3	3	2
100	2	2	2	2

(b)

Case B Sc.2 with FU = 0.67 - Payback time with respect electricity market price and hydrogen price with constant carbon tax equal to 20 €/tonn$_{CO2}$

Electricity market price [€/MWh$_{el}$]	H_2 price = 1.5 €/kg$_{H2}$	H_2 price = 2 €/kg$_{H2}$	H_2 price = 3 €/kg$_{H2}$	H_2 price = 4 €/kg$_{H2}$
30	NO PBT	NO PBT	NO PBT	15
40	NO PBT	NO PBT	NO PBT	13
50	NO PBT	NO PBT	NO PBT	11
60	NO PBT	NO PBT	20	10
70	NO PBT	NO PBT	16	9
80	NO PBT	NO PBT	14	8

Table 5.15 Payback time of capture section – Case B Sc.2 with FU = 0.67 as function of (a) carbon tax and hydrogen price; (b) electricity market price and hydrogen price

From the table 5.15a it is evident that with a price of H_2 of 4 €/kg$_{H2}$, fixed the value of the carbon tax and the electric energy to the base value, it is possible to obtain an economic return after 11 years, close to half of the plant life. The investment does not result profitable for prices of H_2 below 2 €/kg$_{H2}$ with fixed carbon tax. This leads us to conclude that case B is economically advantageous only in cases where there is the carbon tax and it is very high.

5.4.3 Comparison between Case A and Case B using IRR

From table 5.9 is evident how Case A is characterized by the higher investment cost than case B, while looking the previous analysis is also the case that can obtain highest positive NPV. So, it is important to perform a non-dimensional analysis using Internal Rate of Return (IRR). The study is done considering constant the electricity market price and varying hydrogen price and carbon tax (figure 5.17).

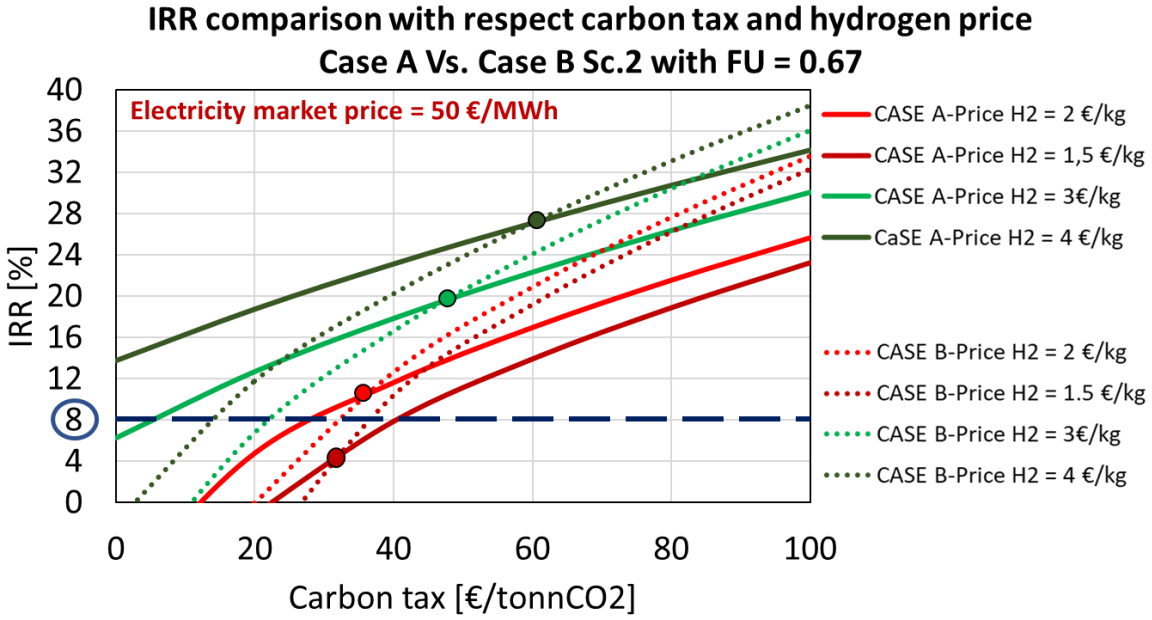

Figure 5.17 IRR comparison with respect carbon tax and hydrogen price with a constant electricity market price equal to 50 €/MWh. Case A solid line; Case B dotted line. FU = 0.67 with scenario 2 for MCFC cost

Considering only the case in which IRR is greater than 8%, i.e. the value assumed for the discount rate. From the diagram in figure 5.17 it is possible to observe how for low hydrogen prices the case B is the one with higher IRR and so it is the preferable one to commit even if it requires a minimum carbon tax value higher than 30 €/tonn$_{CO2}$. At high H_2 prices case A is more convenient up to average carbon tax values because it produces more hydrogen.

It is possible to remark how the break-even point of IRR between the two cases moves to higher carbon tax if the price of hydrogen increases. This means that, in order to have for case B the same investment return as case A, is necessary to have a carbon tax and that it is quite penalizing for the plant that has higher emissions.

With a high value of the hydrogen produced, it is better to choose the solution that allows a higher production of this energy vector, i.e. case A. Instead with low H_2 valorisation case B is preferable because it allows a higher capture, i.e. lower emissions that imply a higher saving for the non-payment of the carbon tax. At the end, the choice between investment A and investment B is dictated by the current and future market conditions in which the plant operates and how this market valorises the useful products of the capture section.

Off-design case 6

The purpose of this chapter is to study the retrofit capture system with MCFC when operating conditions change to analyse in detail how the system behaves and if problems occur due to an off-design condition. Our study wants to simulate the situation in which an operator for market reasons needs to vary hydrogen production. Taking as reference the base case A described in chapter 4 in which the retrofit plant is fed with natural gas, we made an analysis changing the utilization factor in order to simulate the H_2 production variable. The variation has been done in a range from 0.75 in which we consider minimum or absence the hydrogen production to 0.67 in which we consider maximum the quantity produced.

6.1 Method description

After evaluating the sensitivity analysis of the on-design plant (Case A) described in chapter 5, we decide on a configuration with a fuel utilization factor of 0.71 as a base case. This choice has been made because in a refinery the plant works for most of the year in an average production condition and only when necessary it decides to produce more hydrogen.

For example this is due to the fact that the market may require a higher production of light products that need an increase in the availability of this energy vector or in the future MCFC retrofit will produce hydrogen when renewables source surplus for electrolysis production will not be available.

Once the basic case of optimized design has been defined, it is necessary to investigate all the geometries of the most critical components to study their operation more realistically when operating conditions change.

On this retrofit plant the analysis is made only on the heat exchangers for the cooling of the anodic and cathodic side gases and on the stack of MCFC cells, i.e. all those components where the fixed geometry is decisive for the performance of the plant. The cryogenic section, the PSA, the catalytic burner, the water gas shift, and pre-reforming reactor have not been

analysed so in detail because our analysis wants to focus mainly on the fuel cell and its performance.

6.1.1 Heat exchanger modelling

The correct design of anodic and cathodic heat exchangers is important to maximize the thermal efficiency of system. An optimal profile can be achieved avoiding to waste heat but respecting the ΔT_{min} of the different types of components. In the design the layout of the heat exchangers is set considering the optimal positioning for each component to recover heat efficiently. We report the T-Q diagrams in figure 6.1. As can be observed, between evaporator *A-H5* and preheater *A-H7* the temperature of the exhausted anodic flow increases due to the presence of the WGS reaction because it is exothermic.

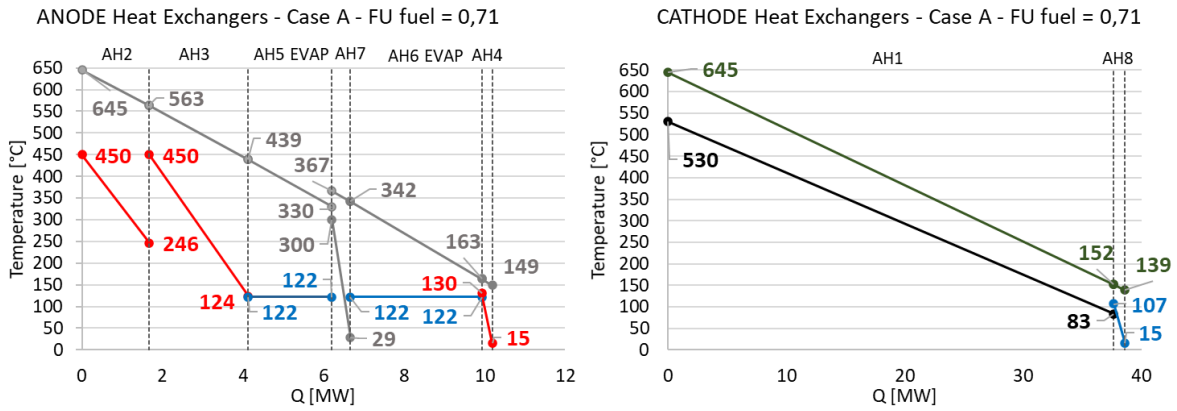

Figure 6.1 T-Q diagram of heat exchangers - Case A/D – FU fuel = 0.71

According to the T-Q diagrams, the heat exchangers have been optimized and the minimum design ΔT (as shown in table 4.8) are respected. The operating temperature of the WGS reactor, the temperature drop of the pre-reformer and the optimal thermal condition of the fuel cells influence the thermal profiles and consequently the positioning sequence of the heat exchangers.

It is important to note from table 6.1 that the heat output exchanged by the *A-H1* cathodic air-residue preheater is very high and will therefore require the use of an heat exchanger with a high surface area; as we will see later in the economic analysis this exchanger will also be the one with the highest costs.

Heat Exchangers	Q [MW]	Surface [m^2]
AH2	1.67	26.6
AH3	2.46	49.8
AH5-EVAP	2.07	16.4
AH7	0.47	11.7
AH6-EVAP	3.26	62.3
AH4	0.26	14.3
AH1	37.64	21002.6
AH8	0.95	305.7

Table 6.1 Heat duty and design surface – Design case with FU = 0.71

For the determination of the overall heat exchange coefficient U we have adopted a simplified approach (electrical analogy) that provides a correct estimation of the heat duty that occurs in a component (figure 6.2). Indeed, convective heat transfer coefficient depends on numerous factors such as the motion of the fluid, its speed, heat capacity, density, viscosity and geometry of the component. Not being able to refer to a precise heat exchanger model as for its geometry and not knowing the motion of the fluid, we assume negligible the conductive resistance of heat exchange and the fouling of the ducts, considering the wall of the pipes thin enough and the thermal conductivity k quite high.

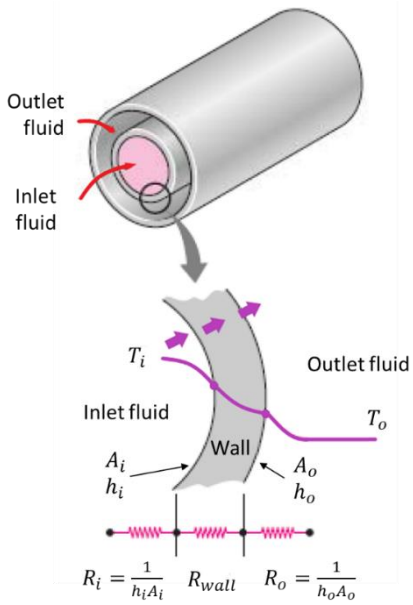

Figure 6.2 Overall heat transfer coefficient scheme [74]

So, overall heat exchange coefficient U can be defined as follows. Thermal power exchanged between the two fluids can be expressed as:

$$Q = UA \cdot \Delta T_{mln} \tag{6.1}$$

Where ΔT_{mln} is expressed as the ratio between the difference of ΔT at the ends of the component and the natural logarithm of their ratio:

$$\Delta T_{mln} = \frac{\left(T_{hot,in} - T_{cold,out}\right) - \left(T_{hot,out} - T_{cold,in}\right)}{\ln \frac{T_{hot,in} - T_{cold,out}}{T_{hot,out} - T_{cold,in}}} \tag{6.2}$$

For the assumptions presented UA is the same and we have that:

$$\frac{1}{UA} = \frac{1}{U_i A_i} = \frac{1}{U_o A_o} = R = \frac{1}{h_i A_i} + R_{wall} + \frac{1}{h_o A_o} \tag{6.3}$$

It is important to mention that for each heat exchanger there are two global heat exchange coefficients U_i and U_o because the areas of the internal and external surfaces are different. Therefore $U_i A_i = U_o A_o$ but $U_i \neq U_o$unless $A_i = A_o$. In our case, having supposed tubes of small thickness and made with materials with a very high thermal conductivity, as occurs in most cases, the R_{wall} resistance becomes negligible and the areas of the internal and external surfaces are almost the same. So, from equation 6.3 it is possible to obtain:

$$U = \left(\frac{1}{h_{inside}} + \frac{1}{h_{outside}}\right)^{-1} \tag{6.4}$$

As far as the convective heat exchange coefficient is concerned, the assumed values aim to represent only a possible order of magnitude. They respect the range of literature and have been inspired by some works previously performed by the *GECoS* research group [58] of Politecnico di Milano.

Fluid type	**h [W/m²K]**
Natural gas	500
Offgas	500
Air	40
Flue gas	40
Saturated steam	5000
Subcooled water evaporator inlet	20000
Water inlet economizer	10000

Table 6.2 Convective heat exchange coefficient

The values resulting from equation 6.4 are as follows:

Component	Type of component	U [W/m^{2}K]
A-H1	Cathode air pre-heater	20
A-H2	Anode pre-heater	250
A-H3	Pre-reformer heater	250
A-H4	Natural gas pre-heater	250
A-H5	Evaporator	487.7
A-H6	Evaporator	487.8
A-H7	Off-gas pre-heater	250
A-H8	Economizer	39.84

Table 6.3 Heat exchangers condition

The design surfaces of the heat exchangers in table 6.1 have therefore been determined as follows:

$$S_{design,i} = \frac{Q_i}{U_i \cdot \ \Delta T_{mln,i}} \qquad (6.5)$$

Once the geometry is determined in the design condition with equal to 0.71, the off-design of the gas-gas heat exchangers was calculated in *Aspen Plus* by using DS on each heat exchanger, changing the temperature of the output cold fluid and assuming constant global heat exchange coefficient so that the surface calculated as in equation 6.5 was equal to the design value.

Particularly challenging was the approach on the *A-H5* and *A-H6* evaporators and the *A-H8* economizer. In fact, in this case there are two constraints to impose:

- the geometry of the heat exchangers.
- the saturated steam condition set at the evaporator outlet because in any off-design condition it is not admissible for the system to exit the fluid in a two-phase state or that the $\Delta T_{sub-cooling}$ to the economizer drops so much to evaporate the water inside the piping.

The second condition is absolutely to be avoided because if the water starts boiling inside the pipes it will cause vibrations and the consequent failure of the system. Another problem concerns the water pump upstream of the economizer. In fact, graph 6.3 shows in a qualitative way the characteristic curve of a centrifugal pump at constant speed. It must always be able to satisfy the volumetric flow rate of water required by the evaporator and therefore in the graph to have the operating point on the right of the maximum flow rate of steam generated by the cylindrical forms. If there was a sudden evaporation inside the economizer, it would increase the pressure drop because the density of the vapor is lower than that of the liquid water.

Increasing the head of the system, the pump could no more guarantee the flow rate required by the evaporator considered as a cylindrical form that would go to empty out causing numerous problems.

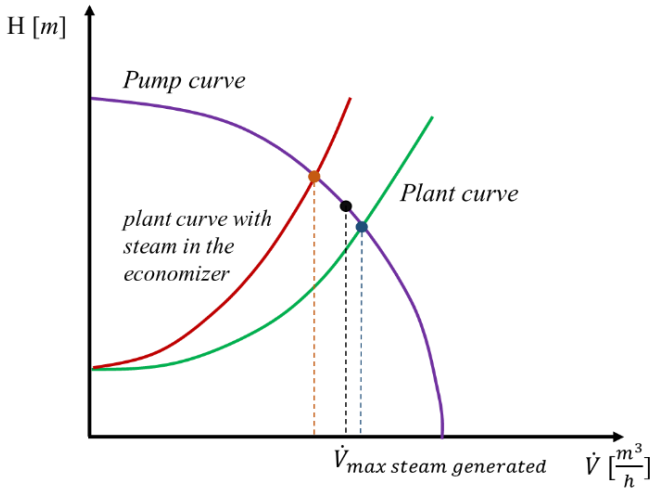

Figure 6.3 Qualitative pump-implant characteristic curve if steam would be generated in the economizer

For this reason it is necessary to have the correct $\Delta T_{sub-cooling}$ so that even under off-design conditions it remains so good to not cause inconveniences to the system. We have decided to adopt, as explained in chapter 4.2.1 of case A, a $\Delta T_{sub-cooling}$ equal to 15°C. The following table shows the variation of $\Delta T_{sub-cooling}$ in off-design condition.

Utilization factor of MCFC	**$\Delta T_{sub-cooling}$ [°C]**
0.75 – no H_2 production	11.844
0.75 – H_2 production	11.84
0.71 – reference design case	15.00
0.67 – maximum production of H_2	13.071

Table 6.4 $\Delta T_{sub-cooling}$ variation during off-design condition

The problems described above have been solved in *Aspen Plus* thanks to DS. The methodology is similar to that used in gas-gas heat exchangers but, as concerns the economizer, a variation has been set on $\Delta T_{sub-cooling}$. Concerning the evaporators, the heat exchanger surface has been set by varying the inlet water flow rate at the evaporators while maintaining the saturated steam condition at the outlet.

Observing figure 6.4 specifically, the inlet flow rate at *A-H5* is decided by the *A-SPLIT1* splitter and the inlet flow rate at *A-H6* has been found by varying the flow rate of the A-34A at the pump inlet.

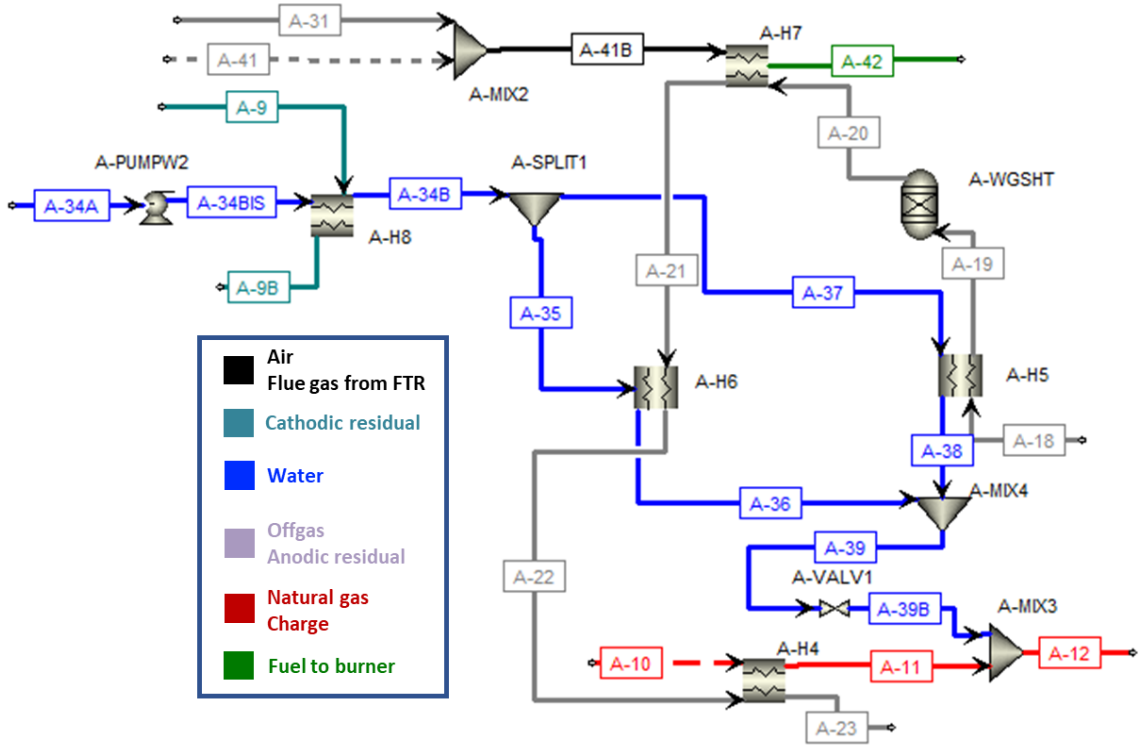

Figure 6.4 Water heating section in Aspen Plus

6.1.2 MCFC active area modelling

Another very relevant aspect to consider in an off-design scenario is the active cell area. It must be kept constant as operating conditions change. We model the polarization curve in FU 0.71 design case using the method described in detail in section 4.5, and by setting the design ΔV to 0.7, the current density *j* and thus the design area of the cell is calculated from it.

$$A_{design} = \frac{W_{cell}}{\Delta V \cdot j} \qquad (6.6)$$

For each variation of hydrogen production (considered with a different cell FU) an iterative process has been used: assumed a first attempt ΔV, we evaluate the input and output parameters of the cell, the stack power and we obtain a polarization curve. From it, given the ΔV we obtain the current density and from equation 6.6 the active area of the stack. We compare the area with the design one and if the difference is less than a certain tolerance (equal to 0.5 %) the cell voltage assumed is correct. In figure 6.5 the algorithm used for the iterative process is described.

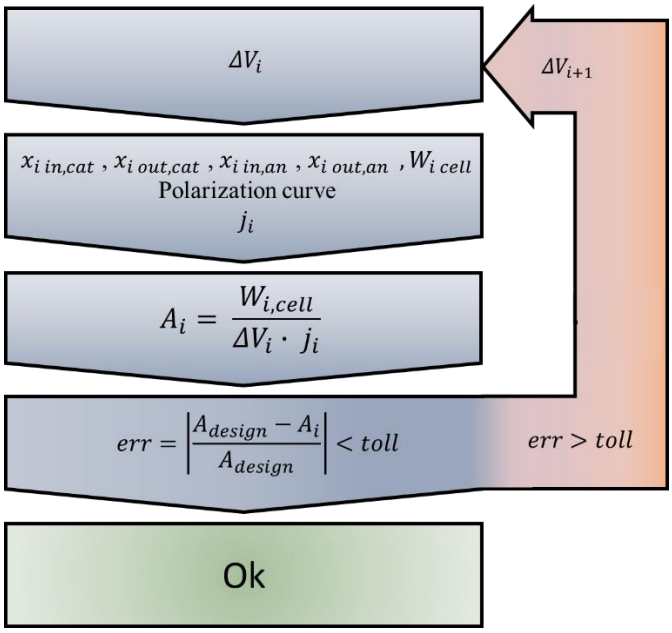

Figure 6.5 Iterative algorithm for cell voltage calculation in off-design condition

6.1.3 Anode inlet temperature modelling

Another important aspect to consider for the correct off-design of the cell is the anode inlet temperature. Indeed, since there is an indirect internal reforming upstream, it is the only one that can vary in an off-design condition because the output temperature (both at the cathode and at the anode) remains optimized at correct value (645 °C) and the input temperature at the cathode is set by the burner (575 °C).

To properly model the temperature variation at the anode input, it is necessary to analyse the upstream internal reforming reaction. It, being endothermic, requires heat from the cell to take place. The input fuel charge therefore undergoes simultaneously a heating and a variation of the composition due to the reaction itself. Both these phenomena cause a variation of the specific heat value and therefore of the thermal capacity that varies with the composition.

A correct modelling is to divide the process in infinite reactors that make an infinitesimal reaction. In this way it is possible to have a correct estimate of the variation of the composition and the thermal capacity. In our Aspen analysis, we have chosen to divide reaction in 10 RGibbs reactors brought to equilibrium (see figure 6.6). In order to have a more reliable estimation of the temperature variation we have considered each reforming reactor as if it is ideally a constant geometry heat exchanger that, in addition to carrying the reaction to equilibrium, exchanges heat with the fuel cell considered as a heat source at a constant temperature equal to 645 °C.

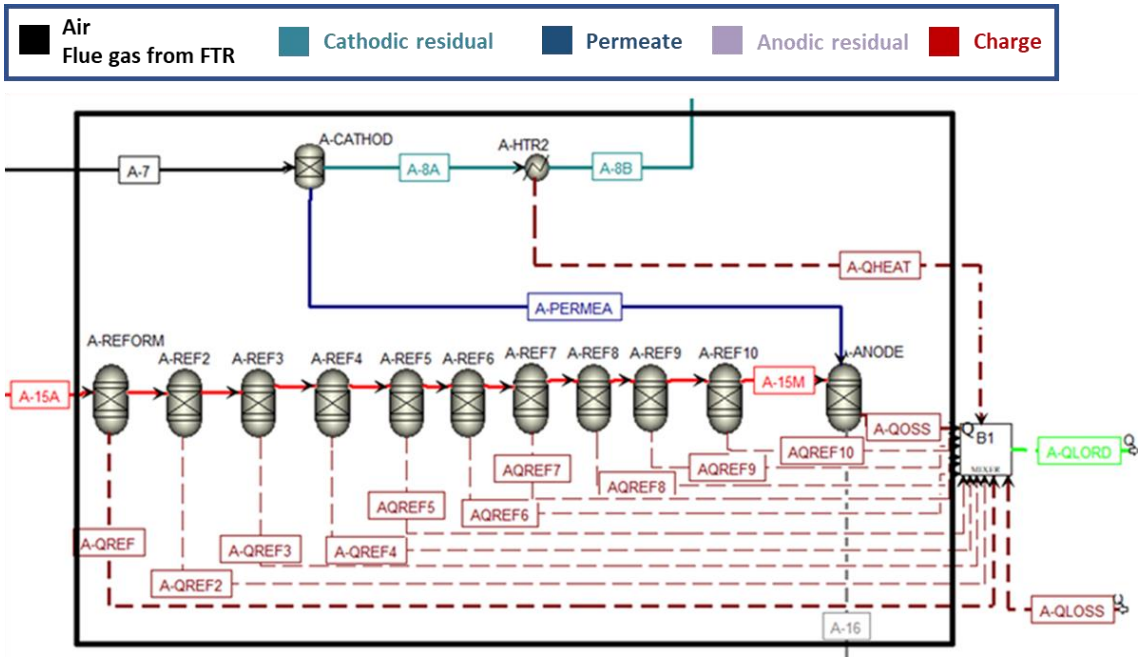

Figure 6.6 MCFC off-design section in Aspen Plus to model internal pre-reforming component

To find the design condition we have considered that each reactor had a constant temperature difference equal to 15°C, dividing the operating temperature gradient of the internal reforming equal to 150°C for the number of reactors and computed with the equation 6.1 the l'$UA_{i,design}$ of each reactor considering a ΔT_{mln} as follows:

$$\Delta T_{mln} = \frac{(T_{cell} - T_{cold,out}) - (T_{cell} - T_{cold,in})}{\ln \frac{T_{cell} - T_{cold,out}}{T_{cell} - T_{cold,in}}} \qquad (6.7)$$

Once the design UA_i has been set, in off-design condition, it has been kept constant to the variation of the equilibrium temperature of each reactor through a DS.

Case D		
FU	T in anode [°C]	T in internal reforming [°C]
0.67	578.6	421.44
0.71 On Design	**600.0**	**450.00**
0.75	610.3	466.81
0.75 no H_2	625.5	480.00

Table 6.5 Temperature inlet and outlet for internal reforming with respect different operation conditions

Table 6.5 shows how at low utilization factor the heat exchangers and the internal pre-reforming are undersized because the quantity of fuel fed is greater, higher is the flow rate and therefore their efficacy decreases. On the contrary to high utilization factors the heat exchangers are oversized, their efficacy increases and consequently they have a lower minimum ΔT.

6.2 Analysis of performance with respect hydrogen production of MCFC

The system operates at nominal load with a utilization factor of 0.71. An operator can decide to vary the flow rate of hydrogen produced by the cell, varying the fuel utilization factor. It is evident, from the sensitivity analysis on FU presented in chapter 5, that a lower value guarantees a higher H_2 production. We study the performance of the system at maximum (FU = 0.67), minimum (FU = 0.75) or zero (FU = 0.75 with PSA valve closed) hydrogen production. We report the main outputs of the plant in table 6.6.

Retrofit section performance									
FU	ΔV	j	U_{CO2}	GN in	Steam to carbon ratio	H_2 out	$W_{cell, DC}$	$W_{el, net}$	η_{cell}
	V	A/m^2	%	kg/s		Nm^3/h	MW	MW	%
0.67	0.655	1934	86.20	1.20	1.98	5250.95	23.60	21.85	36.67
0.71 On Design	**0.70**	**1730**	**87.14**	**1.02**	**2.10**	**4001.97**	**22.49**	**20.82**	**42.01**
0.75	0.719	1642	86.60	0.92	2.20	2837.45	22.02	20.39	45.67
0.75 no prod. H_2	0.752	1475	85.95	0.68	2.75	0	20.66	19.13	50.50

Table 6.6 Overview of fuel cell performance

If the operator increases the production of hydrogen the amount of natural gas fed increases. As explained, the heat exchangers are undersized and therefore the inlet temperature at the internal reforming of the anode decreases (as indicated in table 6.5), as well as the temperature after the reforming because it is kept at constant geometry. The thermal power released from the cell increases due to high current density.

It is therefore important to observe the polarization curve in figure 6.7.

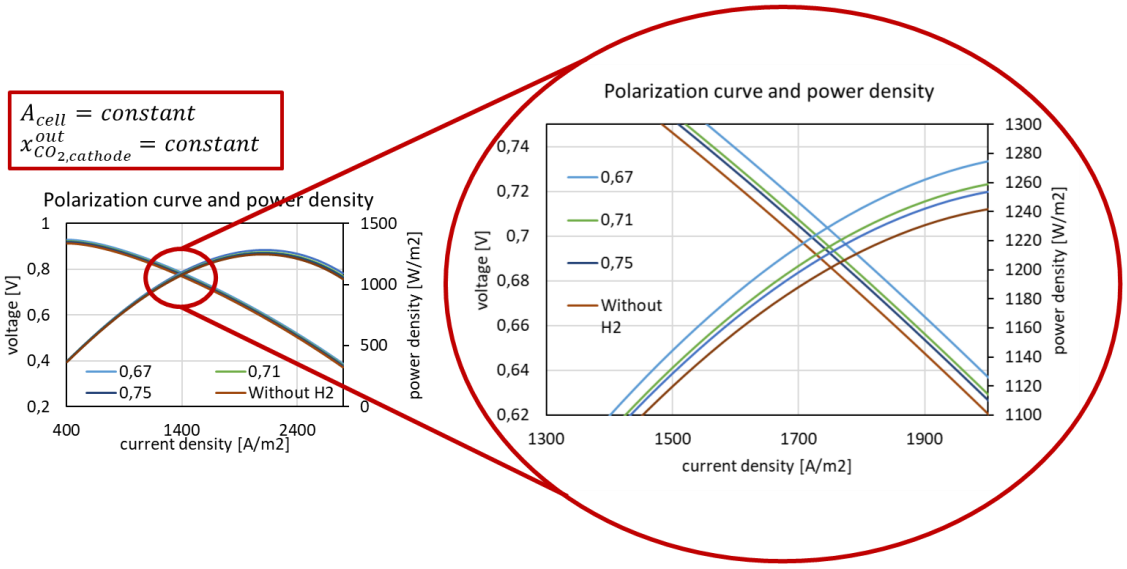

Figure 6.7 Polarization curve and power density in different operating conditions

The heat is inversely proportional to the cell voltage, greater is the heat output and the lower is the ΔV. At the same cell area, if ΔV decreases, the power increases (since we obtain higher power density) and the current density increases. The second fact assumes that at constant active cell area, the amount of $N_{CO_3^=}$ increases.

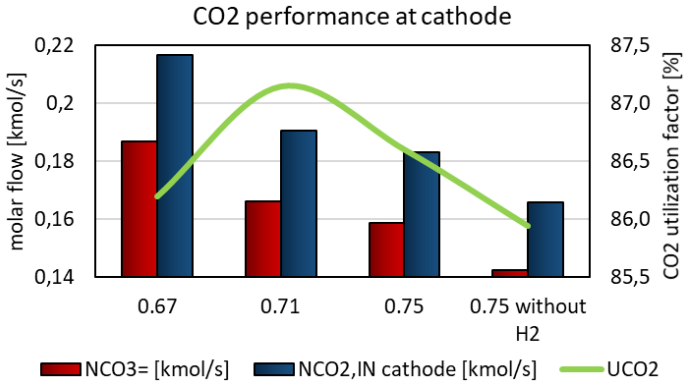

Figure 6.8 CO_2 performance at cathode. CO3 permeation, mole flux of carbon dioxide inlet and carbon dioxide utilization factor

As shown in figure 6.8, the amount of CO_2 entering the cathode increases by decreasing the utilization factor. This trend is justified by two aspects. The first is due to the *A-H1* exchanger which is undersized at low FU and so the input temperature to the catalytic burner is lower, which leads to a higher demand for retentate offgas (rich in CO which is oxidized to CO_2). The second aspect is due to the constraint to keep constant the molar fraction of CO_2 output to the cathode equal to 1%.

The input air flow rate increases as more cooling is required to the cell. At low FU, the steam to carbon ratio decreases but remains at acceptable values. Its decrease, as well as the change in the equilibrium temperatures of the reforming, results in a different composition at the anode inlet compared to the design case.

Finally, the cell efficiency decreases because the higher input natural gas is not proportional to the higher power produced. Decreasing the production of hydrogen (table 6.6), the parameters analysed have a trend opposite to the above but agree with the presented theory.

The performance of the overall plant is presented in table 6.7.

Overall plant performance									
FU	NG in kg/s	H_2 out Nm^3/h	CO_2 out kg/s	CCR %	CO_2 avoided %	E_{CO2} g_{CO2}/MJ_{H2}	$W_{el,net}$ MW	η_{H_2} %	SPECCA MJ/kg_{CO2}
0.67	3.84	35510	1.31	87.45	83.95	12.45	15.74	73.48	1.84
0.71 On Design	**3.65**	**34261**	**1.082**	**89.14**	**86.32**	**10.62**	**15.71**	**75.49**	**1.25**
0.75	3.55	33096	1.079	88.86	85.87	10.97	15.79	75.61	1.23
0.75 no prod. H_2	3.32	30259	1.02	88.69	85.33	11.39	12.76	72.21	2.18

Table 6.7 Overall plant performance

In contrast to what observed with the sensitivity analysis (chapter 5), here the SPECCA is minimal for a utilization factor of 0.75, as well as the efficiency of hydrogen production. A comparison between this case and on design sensitivity analysis is not important. Hydrogen efficiency rises with the increase of the utilization factor for two main factors: the first reason is related to the decrease of natural gas input, while the second is related to the better efficiencies of the heat exchangers that allow to obtain better plant performance.

For the case without production, the plant has worse performances. The efficiency of hydrogen production decreases because the capture section does not produce hydrogen. Consequently, the SPECCA increases.

Finally, regarding the behaviour of the retrofit section for CO_2 capture, the on-design configuration is the best, as shown in figure 6.9a and 6.9b. This trend is due to the higher CO_2 utilization factor.

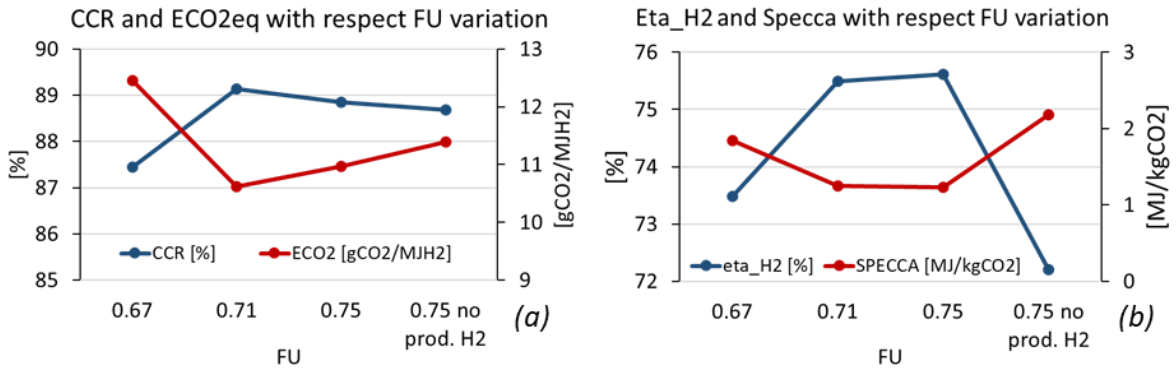

Figure 6.9 Overall plant performance in different condition. (a) Carbon capture ratio and CO2 specific emission in different operating conditions; (b) Equivalent hydrogen production efficiency and SPECCA in different operating conditions

At the end, for CO_2 capture it is better on-design condition, for equivalent hydrogen production efficiency the operating point with FU equal to 0.75 one, for the quantity of hydrogen produced the configuration with the lowest utilization factor while for the lower cost of natural gas the operating point without hydrogen production.

It is not possible to decide only on technical analysis which operating point is the most suitable. For this reason, an economic analysis will be performed.

6.3 Economic analysis

In this paragraph two types of analysis will be discussed:

I. In the first one will be made a comparison between two types of scenario to understand how to allocate correctly the hours of operation between the different configurations: scenario A in which we will consider the hours of operation at various operating points based on the random trend of renewable sources (wind + photovoltaic) to produce more hydrogen when it is not possible to make a storage of energy from RES and scenario B where it is considered only an average operating point.
II. The second analysis is a sensitivity study on scenario B to the variation of the parameter "hours of operation without hydrogen production".

6.3.1 First analysis: variable production vs. fixed production

To make a more detailed analysis, the analysis referred to "variable production" will still be conducted in a differential way but in this case, it is useful to define the hours of operation at each operating point. In this way it is possible to simulate the variable profits and costs due to the variation of the operating points during the year. A precisely determination of the hydrogen demand fluctuation in a refinery is not simple because it depends on many factors such as the demand for a certain product on the market and crude oil quantity and composition. Therefore, we assume that MCFC operating in merchant plant mode as regard hydrogen production.

According to a study performed by Siemens [75] for the integration of fluctuating renewable energies, storage technologies are essential. Large scale storage provides grid stability, which is fundamental for a reliable energy system and the energy balancing in hours to weeks' time ranges to match demand and supply. This study assert that storage needs are in the two-digit terawatt hour and gigawatt range and a report citated in this study claims how starting from 2040, a storage energy equal to 40 TWh would be required.

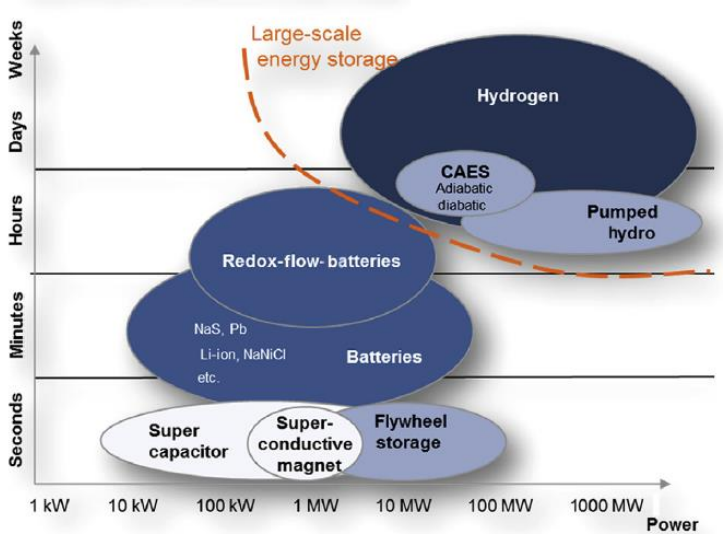

Figure 6.10 Overview of storage technologies and their typical power and capacity ranges. [75]

This paper demonstrates how hydrogen can cover energy capacities up to very large quantity and offers a broad power range too as shown in figure 6.10. This storage is applicable in the distribution grid.

Figure 6.11 shows the possible utilizations of hydrogen produced from a surplus of renewable energy that cannot be dispatched. It can be stored in special geological sites (salt deposit, cavern, etc...), fed into the grid together with natural gas (*Snam* is experimenting since 2019 a mix of hydrogen in volume between 5 - 10% in the Italian national network [76]), used for the Sabatier process ($CO_2 + 4H_2 \rightarrow CH_4 + 2H_2O$) or as a material for fuel cell vehicles, in combined cycles or for some industrial processes.

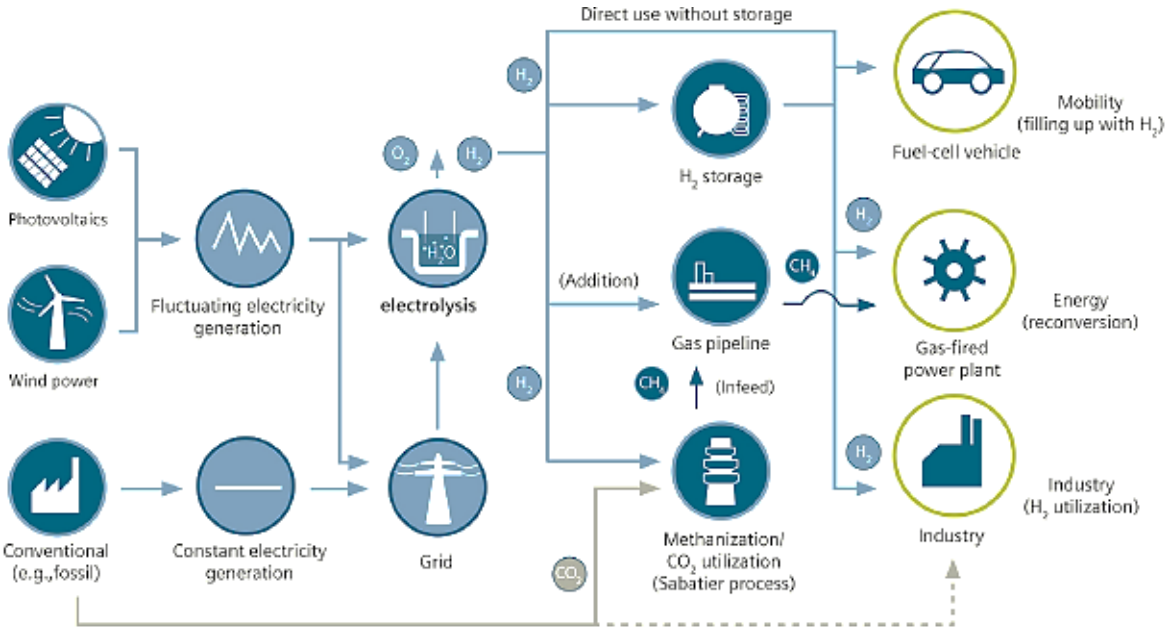

Figure 6.11 Possible hydrogen utilization for storage of power surplus in the electric system [75]

To determine the hours of operation in each configuration we report the trend of electricity production from wind and photovoltaic for the year 2019 in Italy in figure 6.12.

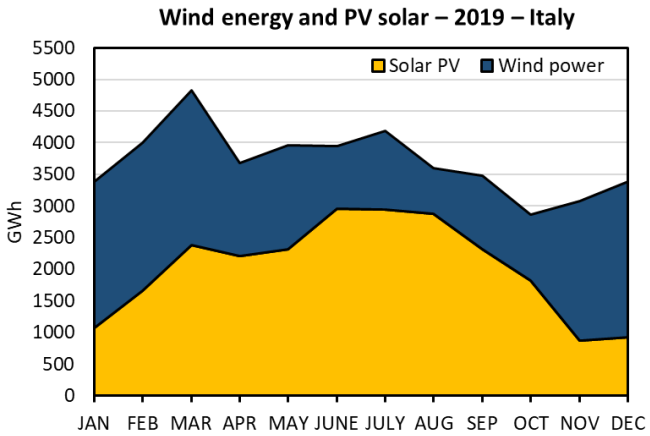

Figure 6.12 Wind energy and solar PV production in Italy in 2019 – Adapted from Terna report [77]

The data reported here are not a forecast of energy production from these sources for the future but we want to provide an idea of which months of the year are affected by a higher production and which by a lower generation.

According to the figure 6.12, we estimate the equivalent hours for each operating point assuming that the hydrogen production of the plant is inversely proportional to the production of electricity from renewable sources that cannot be dispatched. In this way it is possible to guarantee a hydrogen supply even when renewable sources, having no production surplus, cannot produce it through electrolysis. In figure 6.12 there is never surplus, but we believe that in a future scenario, in which the installed capacity is higher, the surplus may occur in the peak months. In fact, to consolidate our hypothesis, from figure 6.13 from the paper by *Zappa et. al* [78], a forecast of installed capacity in 2050 is shown. It is based on data provided by *ENTSO-E* (European network of transmission system operators for electricity) and has been estimated considering the worst weather in 2010 when the electricity supply from solar and wind power was lower. Observing the graph, the European installed capacity expected in 2050 increases enormously compared to the electricity demand and there is a significant increase in the energy volume produced by photovoltaics and wind power. [78]

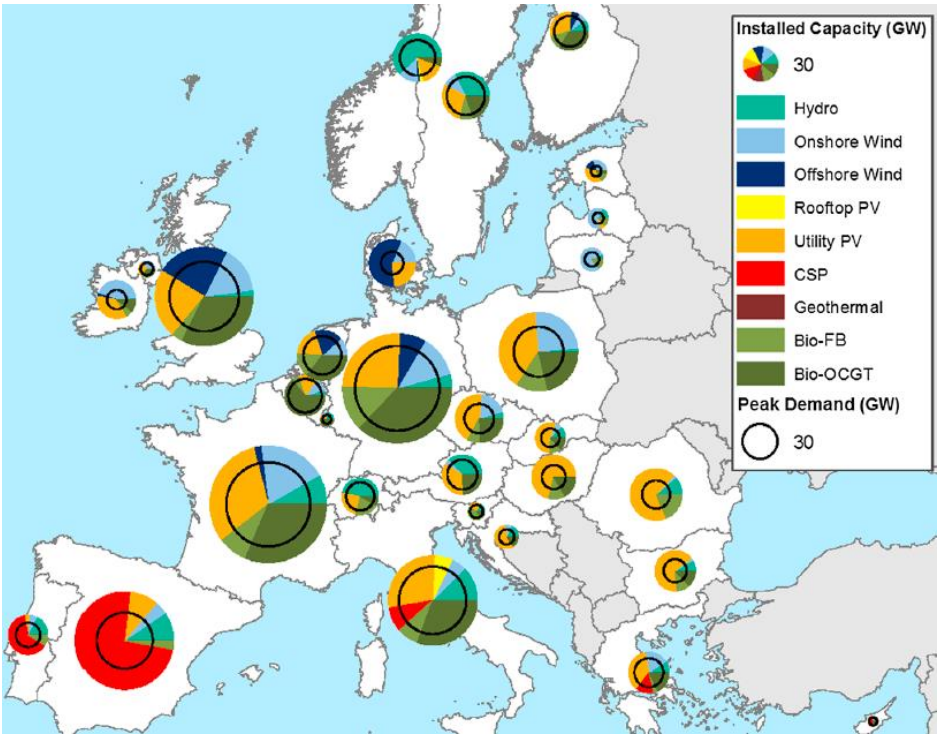

Figure 6.13 Optimized generation capacity per technology in 2050 per country optimized for RES, based on weather year 2010. The pie charts show the share of capacity per generation technology, while the size (area) of the pie chart is proportional to the total installed capacity. The circles within each pie chart show the peak demand per country. [78]

Referring to the trend shown in figure 6.12 we have supposed to divide the operation in the different operating points according to the annual distribution of electricity production from wind and solar power. The table below shows this subdivision:

Equivalent hours for different operating points			
Energy production	Configuration point	Months per year	Share of h_{eq} [%]
GWh < 3400	Max H_2 production	4	33
3400 ≤ GWh < 4000	Medium H_2 production	5	42
4000 ≤ GWh < 4500	Minimum H_2 production	2	17
GWh ≥ 4500	No H_2 production	1	8

Table 6.8 Equivalent hours for different operating points

Concerning scenario B, as from figure 6.14, the parameter that influences the profitability of the plant is the number of hours of operation without production because in the other operating conditions the trends of electrical production, hydrogen production, natural gas request, carbon capture and efficiencies are mostly linear and can be approximated with an average production operation (FU = 0.71). In fact, if on one side decreasing the utilization factor you have more profits for the hydrogen produced on the other side you have a higher cost of natural gas input. The electric power remains almost constant in the three operating conditions.

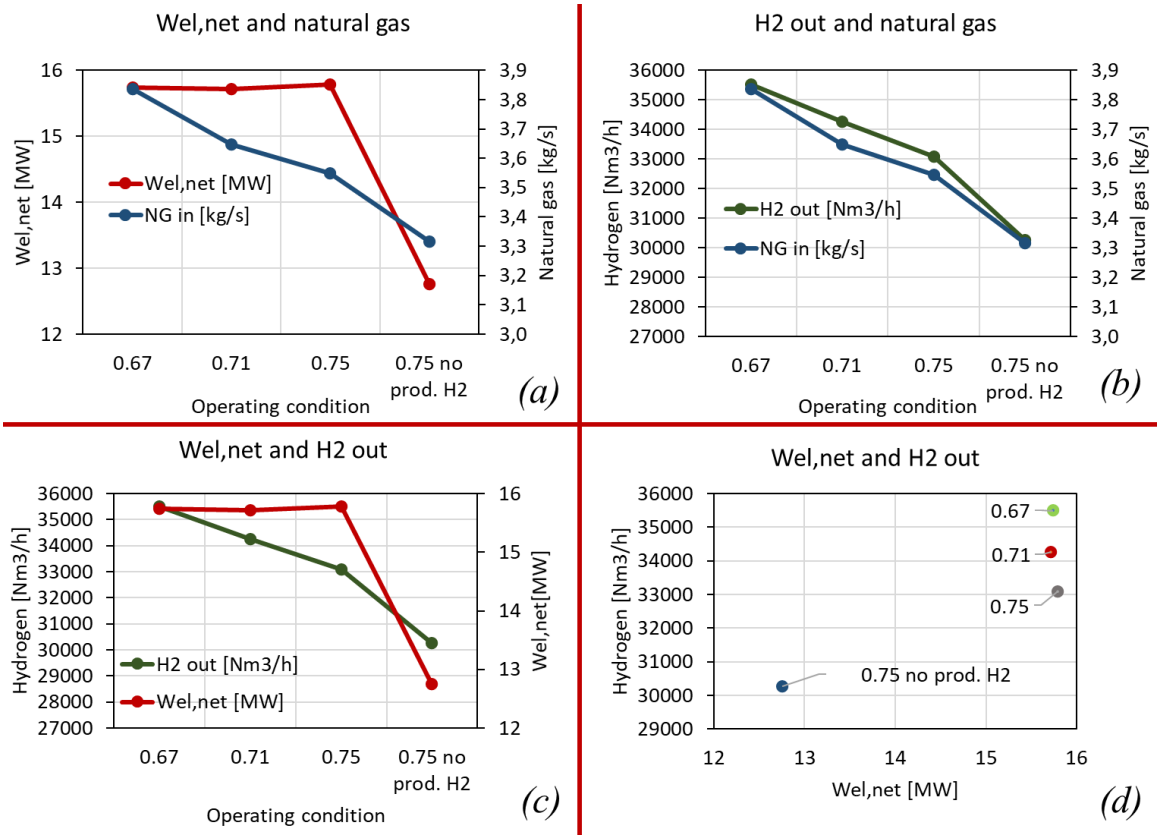

Figure 6.14 Overview of plant performance. (a) Electric power and natural gas input; (b) Hydrogen output and natural gas input; (c) Hydrogen output and electric power; (d) Hydrogen output and electric power

We report the analysis performed that demonstrates the above. The basic parameters used are:

- Electricity market price: 50 €/MWh
- Carbon tax: 20 €/tonn$_{CO2}$
- Price of hydrogen: 2 €/kg$_{H2}$
- Price of NG: 6 €/GJ$_{LHV}$
- Fuel cell cost: scenario 2 (paragraph 5.3.1)

Configuration point	Scenario A	Scenario B
	Share of h_{eq} [%]	Share of h_{eq} [%]
Max H_2 production	33	0
Medium H_2 production	42	92
Minimum H_2 production	17	0
No H_2 production	8	8
NPV [M€]	**-28.0**	**-27.0**

Table 6.9 Comparison between Scenario A and Scenario B with respect variable share of equivalent hours

NPV value is almost the same (table 6.9) and the small difference is due only to the different hydrogen production efficiency. Therefore, for simplicity, we will perform the same analysis made in paragraph 5.4 only for scenario B. For the cost of the cell, we will refer only to a future scenario (see paragraph 5.3.1). As explained in paragraph 5.4, we will perform an analysis when the main outputs change. In this case, we also add the price of natural gas because we want to evaluate its influence on the profitability of the system.

The slopes of the curves (figure 6.15a and 6.15b) are comparable, which shows that it depends only on the carbon tax and the electricity market price. A lower cost of natural gas or a higher price of hydrogen make the system more competitive.

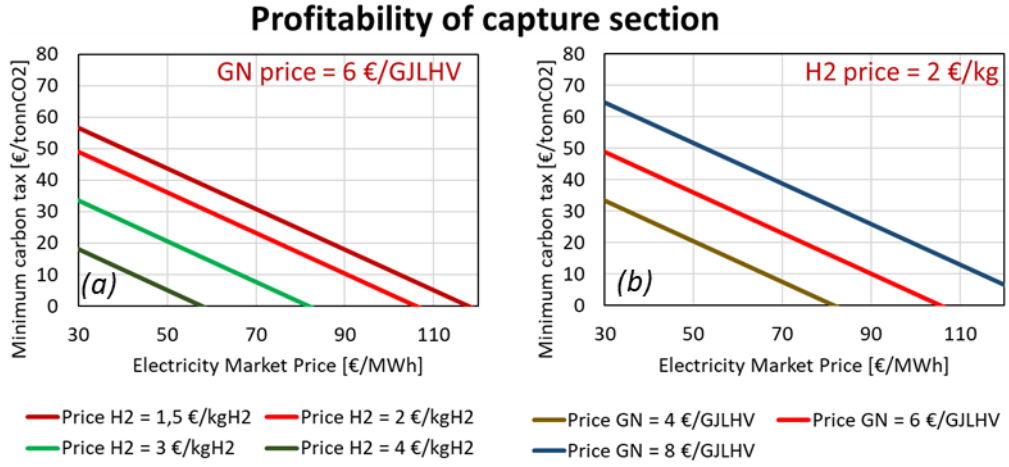

Figure 6.15 Profitability of capture section with respect electricity market price (a) with variable hydrogen price and (b) natural gas price

As mentioned in the previous chapter (see paragraph 5.4.1) the dependence of the NPV on the carbon tax is greater than the dependence on the electricity market price.

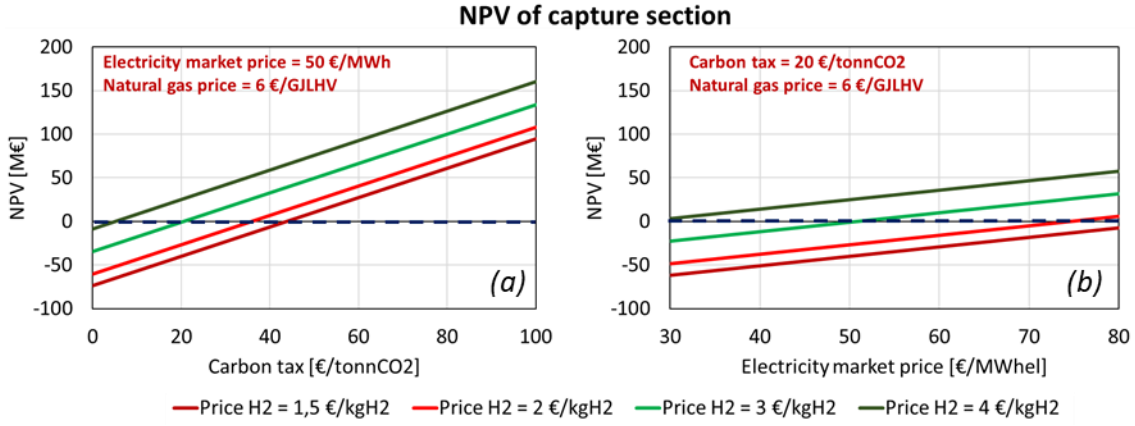

Figure 6.16 NPV of capture section with variable H_2 price (a) with respect carbon tax and (b) electricity market price.

6.3.2 Second analysis: variation of hours without hydrogen production

The purpose of this second analysis is to study the performance of the plant as the hours of operation without hydrogen production vary. We report in table 6.10 an analysis of the maximum possible operating hours without hydrogen at the variation of carbon tax considering the other parameters equal to the base values. Note that to use the plant without hydrogen production the carbon tax must be higher than 34.13 €/tonn$_{CO2}$.

Hours without hydrogen production – Feasible analysis								
P_{H2} = 2 €/kg$_{H2}$, P_{el} = 50 €/MWh, P_{GN} = 6 €/GJ$_{LHV}$								
Carbon tax [€/tonn$_{CO2}$]	0	10	**20**	30	34.13	40	50	60
Maximum share of hour in no hydrogen production [%]	Never feasible	Never feasible	**Never feasible**	Never feasible	0	24.91	67.65	> 100

Table 6.10 Feasibility analysis without hydrogen production varying carbon tax

In table 6.11 we repeat the same analysis shown above about the variation of hydrogen price. A value of it higher than 2.84 €/kg$_{H2}$ gives the possibility of operation without H_2 production.

Hours without hydrogen production – Feasible analysis					
C_{tax} = 20 €/tonn$_{CO2}$, P_{el} = 50 €/MWh, P_{GN} = 6 €/GJ$_{LHV}$					
Hydrogen price [€/kg$_{H2}$]	1.5	**2**	2.84	3	4
Maximum share of hour in no hydrogen production [%]	Never feasible	**Never feasible**	0	6.60	33.72

Table 6.11 Feasibility analysis without hydrogen production varying hydrogen price

In table 6.12 the analysis is performed at the variation of the electricity market price, whose value greater than 71.53 €/MWh allows an operation without hydrogen production.

Hours without hydrogen production – Feasible analysis							
P_{H2} = 2 €/kg$_{H2}$, C_{tax} = 20 €/tonn$_{CO2}$, P_{GN} = 6 €/GJ$_{LHV}$							
Electricity market price [€/MWh]	30	40	**50**	60	70	71.53	80
Maximum share of hour in no hydrogen production [%]	Never feasible	Never feasible	**Never feasible**	Never feasible	Never feasible	0	19.90

Table 6.12 Feasibility analysis without hydrogen production varying electricity market price

From the analysis conducted previously we can observe how the parameters that most influence the profitability of the plant are the carbon tax and the selling price of the hydrogen produced. Therefore, below some studies will be conducted with a variation of these parameters compared to the equivalent hours without hydrogen production keeping the others fixed to the base values.

In table 6.13 we report the case with the lowest selling price of hydrogen, while in table 6.14 the case with the highest selling price.

P_{H2} = 1.5 €/kg$_{H2}$, P_{el} = 50 €/MWh, P_{GN} = 6 €/GJ$_{LHV}$												
% h_{eq} Without H_2	C_{tax} = 0 €/tonn$_{CO2}$		C_{tax} = 20 €/tonn$_{CO2}$		C_{tax} = 40 €/tonn$_{CO2}$		C_{tax} = 60 €/tonn$_{CO2}$		C_{tax} = 80 €/tonn$_{CO2}$		C_{tax} = 100 €/tonn$_{CO2}$	
	NPV	PBT	NPV	PBT	NPV	PBT	NPV	PBT	NPV	PBT	NPV	PBT
0	-71.69	NO PBT	-37.98	NO PBT	-4.28	NO PBT	29.43	9	63.13	5	96.84	4
20	-76.93	NO PBT	-43.15	NO PBT	-9.38	NO PBT	24.39	10	58.18	6	91.93	4
40	-82.16	NO PBT	-48.32	NO PBT	-14.49	NO PBT	19.35	11	53.18	6	87.02	4
60	-87.40	NO PBT	-53.49	NO PBT	-19.59	NO PBT	14.31	12	48.21	7	82.11	4
80	-92.63	NO PBT	-58.67	NO PBT	-24.70	NO PBT	9.27	14	43.23	7	77.20	5
100	-97.87	NO PBT	-63.84	NO PBT	-29.80	NO PBT	4.23	17	38.26	8	72.29	5

Table 6.13 Net present value and payback time of retrofit section with respect equivalent hours without hydrogen production and carbon tax, with hydrogen price equal to minimum value

P_{H2} = 4 €/kg$_{H2}$, P_{el} = 50 €/MWh, P_{GN} = 6 €/GJ$_{LHV}$												
% h_{eq} Without H_2	C_{tax} = 0 €/tonn$_{CO2}$		C_{tax} = 20 €/tonn$_{CO2}$		C_{tax} = 40 €/tonn$_{CO2}$		C_{tax} = 60 €/tonn$_{CO2}$		C_{tax} = 80 €/tonn$_{CO2}$		C_{tax} = 100 €/tonn$_{CO2}$	
	NPV	PBT	NPV	PBT	NPV	PBT	NPV	PBT	NPV	PBT	NPV	PBT
0	-0.86	NO PBT	32.84	8	66.55	5	100.25	4	133.96	3	167.66	2
20	-20.26	NO PBT	13.51	13	47.28	7	81.05	4	114.82	3	148.59	3
40	-39.66	NO PBT	-5.83	NO PBT	28.01	9	61.84	6	95.68	4	129.51	3
60	-59.07	NO PBT	-25.16	NO PBT	8.74	15	42.64	7	76.54	5	110.44	3
80	-78.47	NO PBT	-44.50	NO PBT	-10.53	NO PBT	23.43	10	57.40	6	91.37	4
100	-97.87	NO PBT	-63.84	NO PBT	-29.80	NO PBT	4.23	17	38.26	8	72.29	5

Table 6.14 Net present value and payback time of retrofit section with respect equivalent hours without hydrogen production and carbon tax, with hydrogen price equal to maximum value

From tables 6.13 and 6.14 it is evident how it is important to limit number of hours without hydrogen production of retrofit section works because this leads to a lower return on investment, a higher payback time and therefore it is more risky to start this project.

Finally, it is important to report NPV trends as carbon tax and operating hours vary.

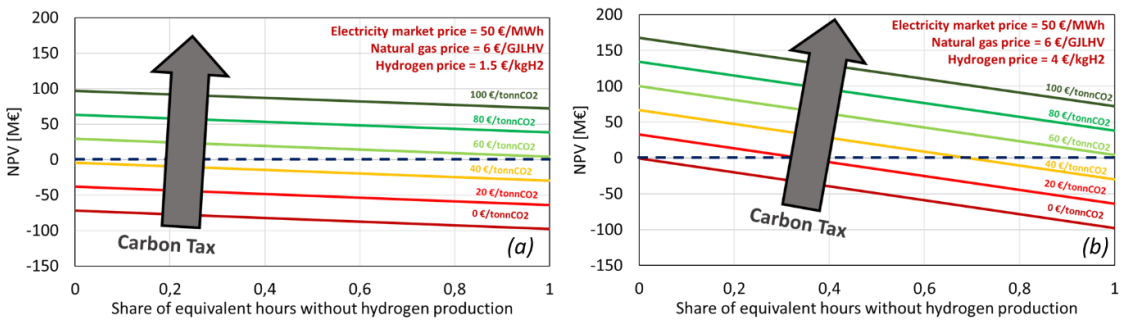

Figure 6.17 Capture section NPV with respect share of h_{eq} without hydrogen, carbon tax and hydrogen price. (a) with H_2 price equal to 1.5 €/kg$_{H2}$; (b) with H_2 price equal to 4 €/kg$_{H2}$

In figure 6.17b the slope of the curves is greater because at a higher price of H_2, if the hours of operation without H_2 production increase, the penalty is more significant. From this we can deduce that it is profitable to produce as much H_2 as possible in case its valorisation is maximum, while an absence of carbon tax does not justify in any case the investment.

For a better analysis, we also perform a study with non-dimensional parameter in order to disconnect this evaluation from plant's size. In figure 6.18 we report IRR analysis.

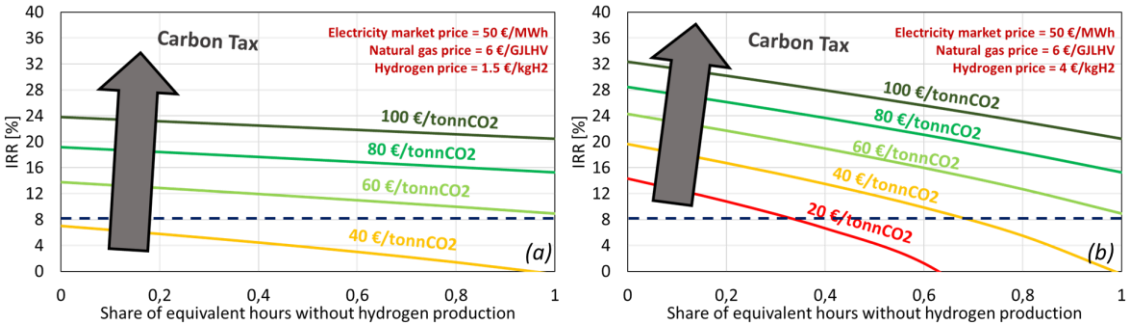

Figure 6.18 IRR comparison with respect Ctax and share of equivalent hours without H_2 production with a constant electricity market price equal to 50 €/MWh and constant NG price equal to 6 €/GJ. (a) with H_2 price equal to 1.5 €/kgH2; (b) with H_2 price equal to 4 €/kgH2

We have not consider the case with a carbon tax < 40 €/tonnCO_2 (for H_2 price equal to 1.5 €/kgH_2) and with carbon tax < 20 €/tonnCO_2 (for H_2 price equal to 4 €/kgH_2) because in this case the value of IRR is negative or it is not possible to calculate. In addition, we consider not useful a calculation of a negative IRR.

It is consistent that the areas of the graph with IRR > 8% correspond in figures 6.17a and 6.17b to the parts of the graph with NPV > 0. If IRR is lower than cut-off rate we will not realize the expected return on investment and we have some options: the first is to reduce the investment in the project for example using some incentives, the second is to increase future cash flow and the last option (the most probable) is not to proceed with this project and invest in other opportunities.

The slope of the lines in figure 6.18b is higher with respect the one in figure 6.18a because the valorisation of H_2 in the case b is higher and so a decreasing in its production penalize more the plant profitability; in addition comparing the two graphs, at the same condition, a higher hydrogen price permits a higher IRR and so a better return on investment. Moreover, increasing the carbon tax, the curves are more flat with a lower slope. This is because a better valorisation of the CO_2 capture compensates the lower hydrogen production.

Considering the natural gas price and the electricity market price equal to the base values, only a carbon tax greater about 60 €/tonnCO_2 permits to run the MCFC without hydrogen production and recirculating the fuel at anode side increasing global FU. This means that a retrofit section, in addition to CO_2 capture, has to produce others useful products to reach the profitability of the plant.

7 Conclusion

Refineries in the future will be becoming an industrial clusters and will need a transformation to become more sustainable. They will be integrated with their surroundings and will not only be used for oil processing but also to provide electric energy, district heating and hydrogen for customers. Hydrogen will play an important role and its production will be done partially through renewable sources, in part with conventional thermochemical technologies with the use of CCS. The MCFC technology as reported in paragraph 4.2.4 results to be more convenient compared to an amine plant allowing to increase considerably both electricity and hydrogen production as well as to do the capture only with a slightly more pronounced increment of natural gas input. From the technical point of view the plants considered have each of the advantages and some disadvantages. The best one depends on the main project purpose. As shown in table 4.18 from the point of view of CO_2 capture the best system is the case B which included the anode feeding with the offgas coming from the FTR, however it is more unfavourable with respect to the production of H_2 and electricity. As concerns the production of hydrogen, the best performing plant is the case A with a low utilization factor; moreover, being powered by natural gas, it is more flexible than the case B even in off design conditions. Case C could be technologically valid only in view of steam production in export and capture although it is lower. In general, a retrofit of existing processes for CO_2 capture leads to a decrease in performance. Therefore, as shown previously, its convenience is obtained only in the case of a carbon tax or an absence of it but with a rather high price mix. This condition can probably be achieved in the future. The most economically advantageous plant therefore depends on market conditions.

This technology can be a valid alternative for CCS and blue hydrogen production operating MCFC as reforming, only when the cost of the cell will be lower than the current value and a carbon tax will be applied to the emissions of industrial processes.

List of Figure

List of Tables

Acronyms and abbreviations

ALK	Alkylation unit
API	America Petroleum Institute
ASU	Air Separation Unit
ATR	Auto Thermal Reactor
Bbl	Billion barrels of petroleum liquids
BEV	Battery electric vehicle
BP	British Petroleum
CAFE	Corporate Average Fuel Economy
CCS	Carbon Capture and Storage
CDU	Crude distillation unit
CHP	Combined heat and power plant
CPO	Catalytic partial oxidation
CRF	Catalytic reformer
CSTR	Continuous Stirred Tank Reactor
DCU	Delayed coker unit
DS	Design Spec
ENTSO-E	European Network of Transmission System Operators for Electricity
EOL	End Of Life
EOR	Enhanced oil recovery
EPC	Engineering Procurement and Construction Cost
E-PRTR	The European Pollutant Release and Transfer Register
ETS	Emission Trading System
FCC	Fluid catalytic cracker
FCEV	Fuel cell electric vehicle
FTR	Fired Tubolar Reformer
FU	Fuel utilization factor
GHG	Greenhouse Gas Emissions
GPU	Gas Processing Unit
GT	Gas Turbine

HCK	Hydro cracker
HDS	Diesel hydro-desulphurisation unit
HRSG	Heat recovery steam generator
ICE	Internal Combustion Engine
IEA	International energy agency
IEAGHG	International energy agency greenhouse gases
IPCC	Intergovernmental Panel on Climate Change
ISO	Isomerization unit
KHT	Kerosene hydrotreater
LCOH	Levelized Cost Of Hydrogen
LHV	Lower heating value
MBDOE	Million oil-equivalent barrels per day
MCFC	Molten Carbonate Fuel Cell
MDEA	Methyl diethanolamine
MEA	Monoethanolamine
MTBE	Metil-t-butil etere
NHT	Naphtha hydrotreater
NSU	Naphtha splitter unit
OPEC	Organization of the Petroleum Exporting Countries
POW	Power/CHP plant
PSA	Pressure Swing Adsorbtion
PTU	Gasoline post-treatment unit
RES	Renewable Energy Source
SDA	Solvent deasphalting unit
SMR	Steam methane reformer
SRU	Sulphur recovery unit
TDPC	Total Direct Plant Cost
Toe	Tonne of oil equivalent
TPC	Total Plant Cost
TPES	Total Primary Energy Supply
U	Global heat transfer coefficient
U_{CO2}	Carbon dioxide utilization factor

U_{O2}	Oxygen utilization factor
VBU	Visbreaker unit
VDU	Vacuum distillation unit
VHT	Vacuum gasoil hydrotreater
WGS	Water Gas Shift

Bibliography

[1] The Oil and Gas Industry in Energy Transitions, IEA report 2018
[2] IEA - Data and statistics
[3] France Strategy - How can we now reduce CO2 emissions from cars?
[4] Hydrogen from renewable power technology – IRENA outlook (2018)
[5] ExxonMobil 2019 – Energy outlook: a perspective to 2040
[6] BP statistical review of world energy (2018).
[7] NOAA – National Oceanic and Atmospheric Administration
[8] IPCC - Climate Change 2014 Synthesis Report
[9] Oil and gas after COVID-19 The day of reckoning or a new age of opportunity. McKinsey
[10] Global Energy Review 2020. The impacts of the Covid-19 crisis on global energy demand and CO2 emissions – IEA
[11] Vision 2050 A pathway for the evolution of refining industry and liquid fuels – Concawe and Fuels Europe – 2019
[12] https://www.fuelseurope.eu/wp-content/uploads/FuelsEurope-Statistical-Report-2019-2.pdf
[13] https://www.concawe.eu/refineries-map/
[14] Damien Valdenaire CONCAWE John Gale IEAGHG, Lily Gray CONCAWE. Understanding the cost of retrofitting CO2 capture in an integrated oil refinery. Technical report, IEAGHG, 2017/TR8, August 2017. Cap 1.1 , pag 104,pag 126,pag 19,pag 25
[15] https://www.fuelseurope.eu/wp-content/uploads/SR_FuelsEurope-_2020-1.pdf pag 1,39,40,41
[16] Enciclopedia Idrocarburi Vol II cap 1.1: pag 3-8
[17] Pascal Barthe et al. Best available techniques (BAT) reference document for the refining of mineral oil and gas. Technical report, DOE/NETL, 2015. Pag72, cap.8.1.1, cap 8.1.2, cap 8.1.3, cap8.1.4, pag 66
[18] Enciclopedia Idrocarburi Vol II cap 5.1: pag 213-214
[19] Enciclopedia Idrocarburi Vol II cap 7.1: pag 301-302
[20] Report European emission refineries Concawe 2017 Rpt_20-4: pag37, pag38
[21] EPA. U.S. - direct GHG emissions of selected gases reported by sector. https://ghgdata.epa.gov/ghgp/main.do# pie sector 2017
[22] DET Norske Veritas- CCS Refineries: pag1, pag 15-16, pag17
[23] Eman A. Emam- GAS FLARING IN INDUSTRY: AN OVERVIEW. Department of Chemical Eng. and Pet. refinery, Suez University, Egypt, pag 1-2.
[24] European Commission. EU crude oil imports and supply cost. https://ec.europa.eu/energy/en/data-analysis/eu-crude-oil-imports, 2018.
[25] Enciclopedia Idrocarburi Vol I cap 1.1: pag 39

[26] IEA - https://www.iea.org/fuels-and-technologies/hydrogen
[27] Use of membranes in systems for electric energy and hydrogen production from fossil fuels, P. Chiesa, M.C. Romano and T.G. Kreutz, in Handbook of Membrane Reactors: Reactor Types and Industrial Applications, 2013
[28] Solar Thermochemical Hydrogen Production via Terbium Oxide Based Redox Reactions Rahul Bhosale, Anand Kumar, and Fares AlMomani
[29] An overview of hydrogen production technologies J.D. Holladay, J. Hu, D.L. King, Y. Wang, pages 244–258, 2008.
[30] Eni, Enciclopedia degli idrocarburi. Volume III, Vettori energetici.
[31] Natural gas origin, composition, and processing: A review. Authors: S. Faramawy, T. Zaki, A.A.-E. Sakr. Page 41.
[32] Eni, Enciclopedia degli idrocarburi. Volume II. Capitolo 10.3 – Idrogeno e gas di sintesi.
[33] Chapter 11 - Hydrogen Production. Mohamed A.Fahim, Taher A.Alsahhaf, Amal Elkilani
[34] Eni, Enciclopedia degli idrocarburi. Volume II. Capitolo 10.4 – Metanolo, dimetiletere, ammoniaca, urea
[35] Advanced technologies for syngas and hydrogen (H2) production from fossil-fuel feedstocks in power plants. Paolo Chiesa – 2010
[36] G.Groppi, «Processi per la produzione di idrogeno».
[37] Pre-combustion CO2 capture from natural gas power plants, with ATR and MDEA processes Matteo C. Romano, Paolo Chiesa, Giovanni Lozza
[38] Hydrogen Separation Membranes of Polymeric Materials. Xiayun Huang, Haiqing Yao Zhengdong Cheng. Pages 85 – 116
[39] Carbon dioxide capture and storage. IPCC 2005
[40] Fuel Cell Handbook (seventh edition) by EG&G Technical service,inc. U.S. Department of Energy.
[41] IEAGHG TECHNICAL REPORT.2019-03 Review of fuel cell technologies with CO_2 capture for the power sector: Pag 40-43-44
[42] Dossier: International status of molten carbonate fuel cells technology 2015. Stephen J. McPhail, Luigi Leto, Massimiliano Della Pietra, Viviana Cigolotti, Angelo Moreno. ENEA: pag 2
[43] Politecnico di Milano: “Sistemi energetici avanzati” by Paolo Chiesa
[44] Master Thesis: “Celle a carbonati fusi per la cattura della CO2 da impianti di grossa taglia ed utilizzo della CO2 come reagente nel processo di produzione di policarbonati” by Federico Pino. Politecnico di Torino. Pag29
[45] Hydrogen and hydrogen-derived fuels through methane decomposition of natural gas – GHG emissions and costs. Sebastian Timmerberg et al.
[46] Techno-economic assessment of combined hydrogen & power co-generation with carbon capture: The case of coal gasification. Ana-Maria Cormos, Calin-Cristian Cormos

[47] Economic assessment of membrane-assisted autothermal reforming for cost effective hydrogen production with CO2 capture. Shahriar Amini et al.
[48] IEAGHG Technical Report 2017-02 February 2017. Techno-Economic Evaluation of SMR Based Standalone (Merchant) Hydrogen Plant with CCS
[49] A comparative overview of hydrogen production processes. Poullikkas et al.
[50] CONCAWE. The potential for application of CO2 capture and storage in EU oil refineries.
[51] Aspen Plus® version V10.1. Aspen Technology. Inc. Cambridge. Massachusetts U.S.A
[52] Demoys. Assessment of performance and thermal balance of plants based on mixed conducting oxygen and hydrogen separation membranes. collaborative project with Politecnico of Milan. Pag 36 to 41-56
[53] IEA – World Energy Outlook 2020
[54] Application of advanced technologies for CO2 capture from industrial sources (Matteo C. Romano and other)
[55] L. Mastropasqua, L. Pierangelo, M. Spinelli, M.C. Romano, S. Campanari, S. Consonni, Molten Carbonate Fuel Cells retrofits for CO2 capture and enhanced energy production in the steel industry, International Journal of Greenhouse Gas Control, Volume 88, 2019, Pages 195-208, ISSN 1750-5836, https://doi.org/10.1016/j.ijggc.2019.05.033
[56] Fout. T.. Herron. S.. 2013. Quality guidelines for energy system guidelines. CO_2 impurity design parameters. NETL Qual. Guidel. Energy Syst. Stud.
[57] CO_2 cryogenic separation from combined cycles integrated with molten carbonate fuel cells. Paolo Chiesa et al.
[58] GECoS (Group of Energy Conversion Systems) is a group of researchers of Politecnico di Milano working in the field of environmentally friendly energy conversion technologies
[59] Application of Molten Carbonate Fuel Cells in Cement Plants for CO_2 Capture and Clean Power Generation. Matteo C. Romano et al.
[60] CO_2 capture from combined cycles integrated with Molten Carbonate Fuel Cells. (Campanari and other)
[61] GS. This tool has been developed since early 90’s at the Energy Department of Politecnico di Milano within a Fortran 90 programming environment.
[62] Spinelli, M. et al. Campanari, S., Consonni, S., Romano, M.C., Kreutz, T., Ghezel-Ayagh, H.,Jolly, S., 2018. Molten carbonate fuel cells for retrofitting postcombustion CO_2 capture in coal and natural gas power plants. J. Electrochem. Energy Convers. Storage 15, 031001. https://doi.org/10.1115/1.4038601.
[63] M. D. Lukas, K. Y. Lee and H. Ghezel-Ayagh, "An explicit dynamic model for direct reforming carbonate fuel cell stack," in IEEE Transactions on Energy Conversion, vol. 16, no. 3, pp. 289-295, Sept. 2001, doi: 10.1109/60.937210
[64] Maurizio Spinelli. Advanced technologies for CO2 capture and power generation in cement plants. PhD thesis. Politecnico di Milano

[65] Turton, R., Bailie, R.C., Whiting, W.B., Shaeiwitz, J.A., Bhattacharyya, D., 2012. Analysis, Synthesis, and Design of Chemical Processes, fourth edition. https://doi.org/10. 1017/CBO9781107415324.004.

[66] ISPRA. Fattori di emissione atmosferica di CO2 e altri gas a effetto serra nel settore elettrico

[67] EBTF. European best practice guidelines for assessment of CO2 capture technologies. 2011.

[68] Riva, L., Martínez, I., Martini, M., Gallucci, F., van Sint Annaland, M., Romano, M.C., 2018. Techno-economic analysis of the Ca-Cu process integrated in hydrogen plants with CO2 capture. Int. J. Hydrogen Energy 43, 15720–15738. https://doi.org/10. 1016/j.ijhydene.2018.07.002.

[69] An Introductory Note on Carbon Taxation in Europe A Vermont Briefing Professor Mikael Skou Andersen, Aarhus University, Denmark & European Environment Agency (EEA), Scientific Committee Vice-Chair

[70] Global Gas Report. 2020. Snam

[71] Miroslav Hájek, Jarmila Zimmermannová, Karel Helman, Ladislav Rozenský, Analysis of carbon tax efficiency in energy industries of selected EU countries, Energy Policy, Volume 134, 2019, 110955, ISSN 0301-4215, https://doi.org/10.1016/j.enpol.2019.110955.

[72] B. D. James, A. B. Spisak, and W. G. Colella, “Manufacturing Cost Analysis of Stationary Fuel Cell Systems,” Strateg. Anal., no. September, pp. 1–143, 2012.

[73] GME (Gestore dei Mercati Energetici)

[74] Cengel, Y: Introduction to Thermodynamics and Heat Transfer.

[75] Erik Wolf, Chapter 9 - Large-Scale Hydrogen Energy Storage, Editor(s): Patrick T. Moseley, Jürgen Garche, Electrochemical Energy Storage for Renewable Sources and Grid Balancing, Elsevier, 2015, Pages 129-142, doi 10.1016

[76] Snam - Press release: “Per la prima volta in Europa fornitura di idrogeno misto a gas naturale su rete di trasmissione a utenti industriali”. https://www.snam.it/

[77] Terna SpA – Rapporto mensile sul sistema elettrico – Dicembre 2019

[78] “Is a 100% renewable European power system feasible by 2050?” William Zappa, Martin Junginger, Machteld van den Broek

Appendix

In this section we present in the next pages the plant layout in Aspen Plus for the cases analysed.

PLANT CONFIGURATION - CASE A

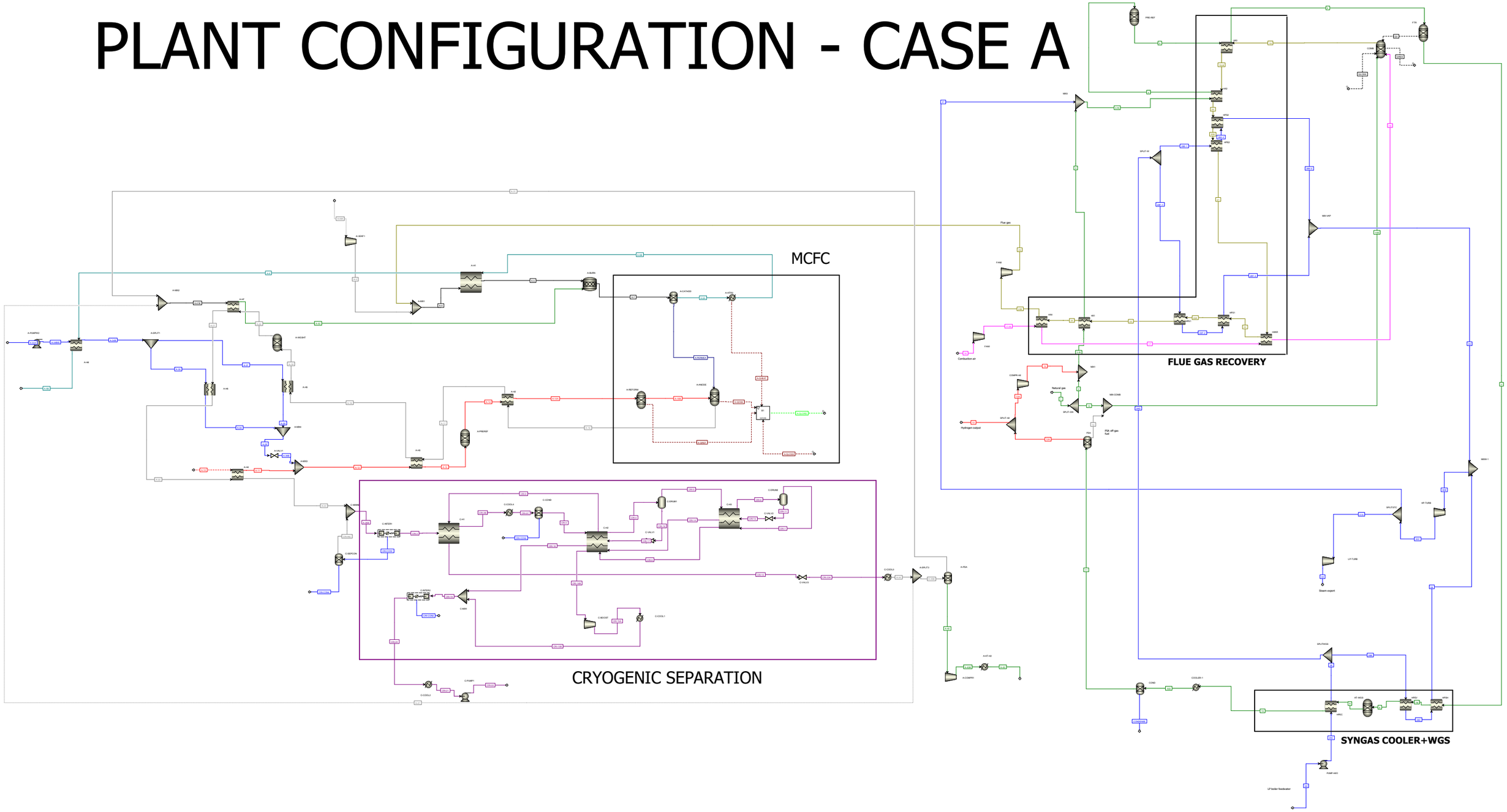

PLANT CONFIGURATION - CASE B

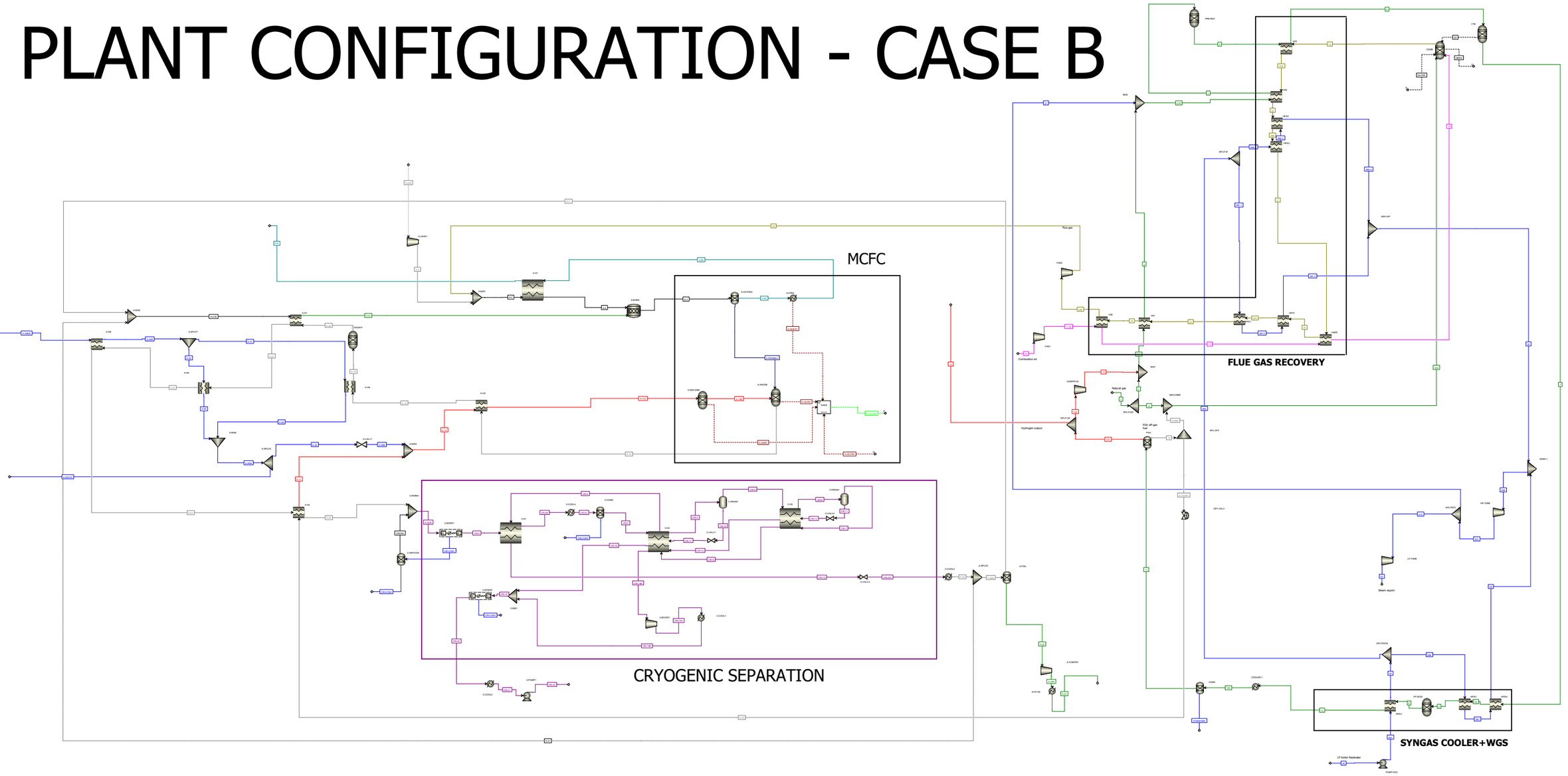

PLANT CONFIGURATION - CASE C

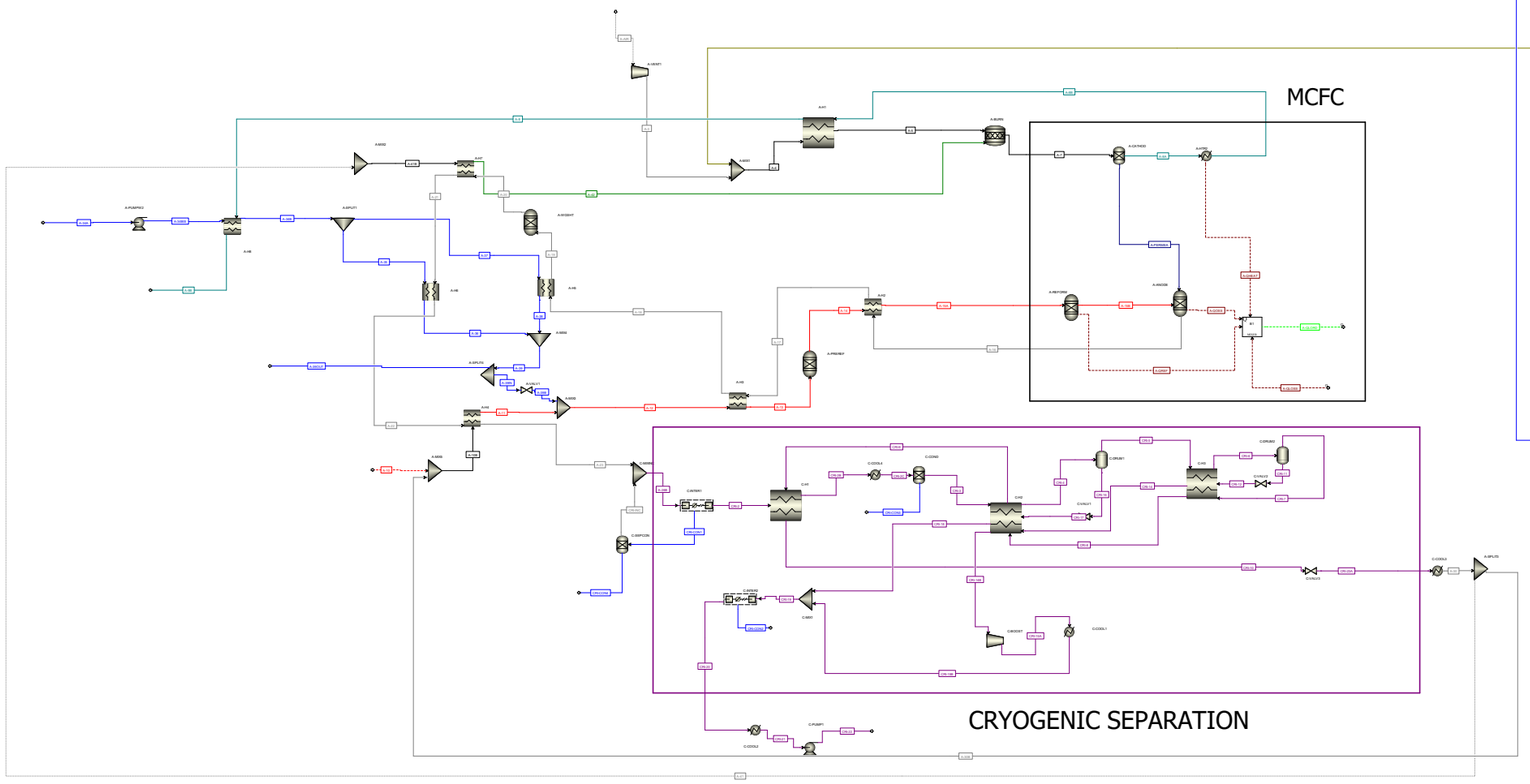

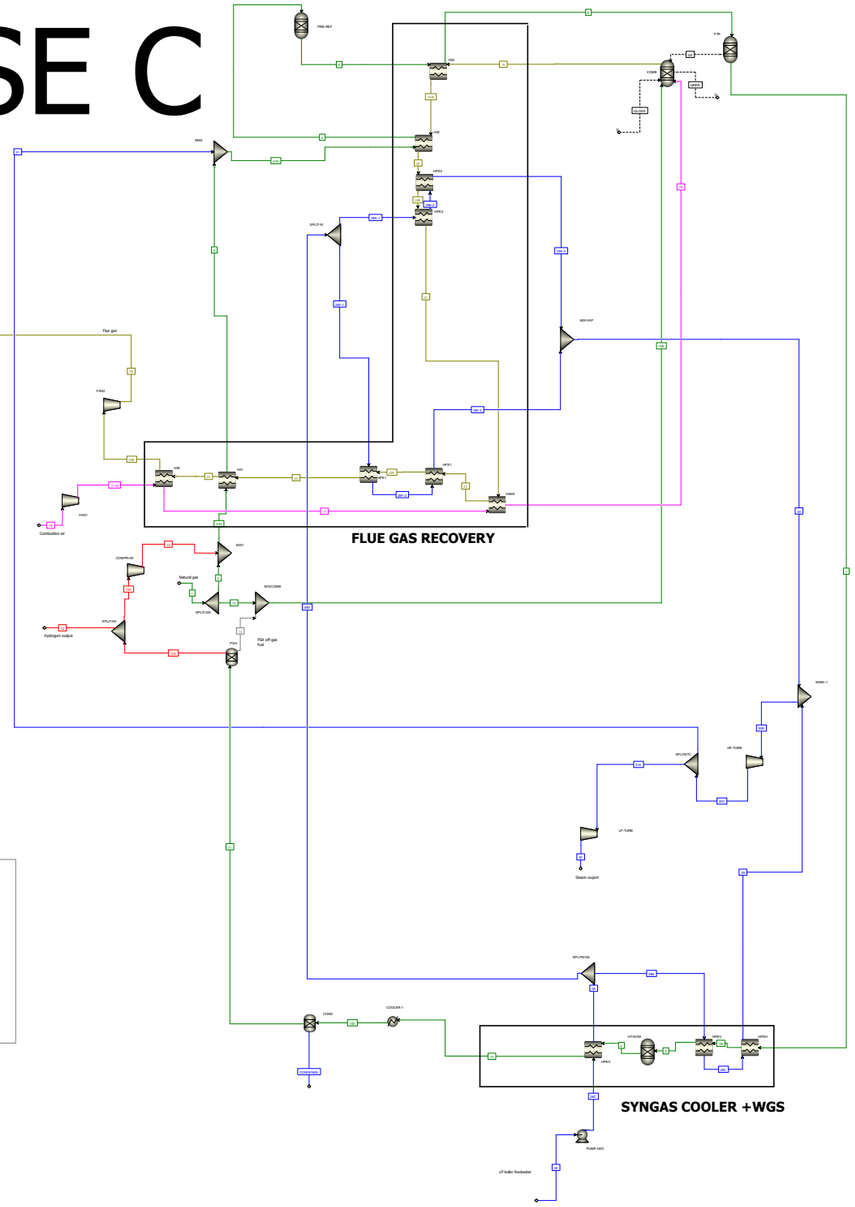

PLANT CONFIGURATION
OFF DESIGN CONDITION
CASE D